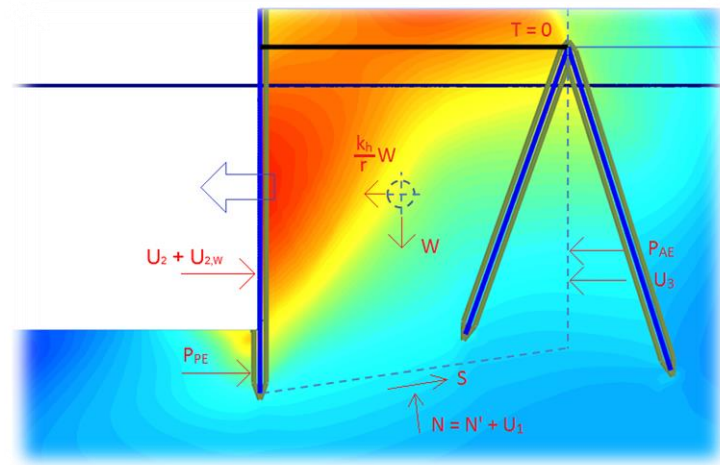


Graduation Thesis: MSc. Hydraulic Engineering (HSFR)

Performance-Based Seismic Analysis of an Anchored Sheet Pile Quay Wall



Date: July 2nd, 2015

Author: Camille Habets

Student number: 1539558

Graduation Committee:

Prof. Dr. Ir. S.N. Jonkman
(Chairman Committee, Delft University of Technology,
Section Hydraulic Engineering)
Dr. Ir. J.G. de Gijt
(Delft University of Technology, Section Hydraulic Engineering)
Prof. Dr. A.V. Metrikine
(Delft University of Technology, Sections Structural Mechanics and Offshore
Engineering)
Ir. D.J. Peters
(Royal HaskoningDHV)

Preface

Dear reader,

In front of you is the result of the final project to complete my MSc. degree in Hydraulic Engineering at Delft University of Technology. I have worked on a topic which I think comprises significant theoretical consideration on the one hand and actual relevance for engineering practice on the other hand. Royal HaskoningDHV offered me the opportunity to work on this topic by means of a graduation internship at their Maritime & Waterways department in Rotterdam. For this opportunity I would like to thank Dennis Broere and Bunno Arends. Other people within the company who I would like to thank especially are John Adrichem for his active involvement and guidance in the seismic and geotechnical part, Jesper van Es for helping me with troubleshooting and understanding PLAXIS, Martin de Kant for more valuable advice on geotechnical content and Albert Wiggers for his participation in defining the scope of my work and his feedback. Last but not least I would like to thank Dirk Jan Peters for his role as one of my committee members on behalf of RHDHV and the inspiring guidance he has provided. And by that I come to thanking the other members of my graduation committee for their supervision and feedback: Bas Jonkman, Andrei Metrikine and Jarit de Gijt. Closing off I definitely want to thank Iris for listening to my continuous contemplations about the content of my graduation thesis and my parents, Werner and Wietske, for their full support during my study time.

Camille Habets
Delft, July 2nd 2015

Abstract

Ports are civil works which have a major societal and economic importance. Quay structures are infrastructural elements of primary significance for the functioning of a port system. The ability to economically design quay structures with sufficient seismic resistance is therefore of great importance when situated in areas that are prone to earthquakes.

Conventional seismic design is force-based i.e. that structures are designed to have sufficient capacity to withstand a pseudo-static seismic design force. This methodology is associated with no insight in the performance of the structure when exceeding the pseudo-static limit equilibrium state and uneconomic design due to the demand that the structure can resist a very high seismic design force without deforming. A more advanced alternative is Performance-Based Design (PBD) methodology. In this methodology the key design parameters for the seismic performance of structures are stress states and deformations of soil and structure, rather than just a seismic design force. Furthermore it recognizes that varying amounts of permanent deformations associated with different degrees of (repairable) damage are allowable.

The present study is embedded in the topic of performance-based seismic design of quay structures. Typical quay types are gravity-based quay walls, sheet pile quay walls and pile-deck structures. The observed trend in seismic quay design is that gravity and sheet pile type structures (i.e. retaining walls) are associated with areas with zero to low seismicity while pile-deck structures are generally the preferred solution in areas with higher seismicity. This can be explained by more favourable seismic performance (i.e. more deformation capacity) of pile-deck structures compared to retaining walls. In line with this trend it is found that PBD methodology is developed to significant lesser extent for retaining walls (especially anchored sheet pile walls) than for pile-deck structures. Therefore the present study focuses on performance-based seismic design of anchored sheet pile quay walls.

In the seismic design methodology there are generally three levels of seismic analysis available, i.e. simplified analysis (pseudo-static), simplified dynamic analysis and dynamic analysis. Simplified analysis of anchored sheet pile quay walls is associated with conventional design methodology. Simplified dynamic analysis can be used to obtain a first estimate of permanent-displacement of a structure after exceeding limit equilibrium, based on an assumed failure mode. This type of analysis has to be made more suitable for anchored sheet pile quay walls. In dynamic analysis the seismic behaviour of a structure can be simulated by means of finite element software.

Experience has shown that it is desirable to consider sheet pile quay walls in a less conservative way in (preliminary) seismic design for which pseudo-static methodology is commonly applied. Therefore the general objective of the present study is to propose improvements on (simplified) seismic design methodologies for anchored sheet pile quay walls by considering deformation behaviour. For this purpose a research methodology is developed in which pseudo-static, permanent-displacement and FE analysis are employed, calibrated with an experimental reference case that considers a typical anchored sheet pile quay wall.

The reference case is taken from a conference paper. It reports on a shake table test under centrifugal gravity which is performed on a scale model of an existing sheet pile quay wall with a batter pile anchor. The quay is situated in homogeneous soil that consists of coarse densified sand. Due to the soil condition liquefaction effects are prevented. Sequential seismic loading of increasing severity is applied during the shake table testing. Measurement results that are reported in the reference case paper comprise bending moments in the sheet pile wall, normal forces in the anchor rod and horizontal displacements of the sheet pile wall.

For simplified analysis a calibrated D-SHEET PILING model of the reference case anchored sheet pile quay wall is created. Through an iterative pseudo-static calculation procedure in which D-SHEET PILING and reference case dynamic bending moment results are fitted, it is attempted to find a deformation-based seismic load reduction for structural forces in the sheet pile wall that can be applied in pseudo-static design methodology.

For simplified dynamic analysis an analytical limit equilibrium model is developed, based on the failure behaviour of the reference case. The goal of this model is that it can compute the critical acceleration of the anchored quay structure and estimate the sheet pile forces at this critical state. These abilities are validated with PLAXIS 2D and checked with the reference case measurements respectively. Six accelerograms in the reference case soil column, obtained with equivalent linear site-response analysis (with SHAKE2000), are combined with the computed critical acceleration for permanent-displacement (sliding-block) analysis.

For dynamic analysis a calibrated PLAXIS 2D model of the reference case anchored sheet pile quay wall is created. Dynamic performance of the PLAXIS 2D model is validated with SHAKE2000 by comparing site-response analysis results of both models. Pseudo-static and pseudo-dynamic calculations are applied to obtain the critical acceleration. Dynamic calculations with six bedrock motions are carried out to simulate the reference case experiment. PLAXIS 2D calculation results are used to validate simplified and simplified dynamic analysis results and to gain insight in the seismic failure behaviour of the anchored sheet pile quay wall.

Approaches for (simplified) performance-based seismic analysis of a typical anchored sheet pile quay wall are proposed as a result of the research. For pseudo-static methodology a deformation-based seismic load reduction for structural forces in the sheet pile wall is proposed. For the present reference case it is concluded that a reduction in the range of 45% to 50% is allowable. For simplified dynamic analysis a limit equilibrium model is proposed to compute the critical acceleration of the present quay structure and to estimate sheet pile forces at this critical state. It is concluded that the ability of the limit equilibrium model is satisfactory. Although subjected to uncertainty, permanent-displacement analysis results indicate that the sliding-block analysis, originally developed for embankments, is possibly not suitable for anchored sheet pile quay walls. For dynamic analysis it is concluded that PLAXIS 2D is able to compute the reference case failure behaviour reasonably well, despite some computational setbacks. Complementary is the conclusion that PLAXIS 2D pseudo-static approach proves to be suitable to determine the critical acceleration of an anchored sheet pile structure in contrast to pseudo-dynamic approach which appears less suitable for that matter. In addition the performance-based design principle is linked to the present study so that an idea about the seismic performance limits of anchored sheet pile quay walls in quantitative terms can be provided.

As a result of the present study findings it is recommended to perform more extensive research on the ability of permanent-displacement analysis to evaluate the amount of sliding displacement of an anchored sheet pile quay wall. In line with this recommendation it is found that further research on site-response analysis is desirable in the application of simplified dynamic and dynamic analysis. In general it is recommended to create more seismic test cases with different setups for a broader validity of the present results, to develop a seismic test case for the Groningen earthquake situation, to add measurement instrumentation to new and existing structures for verification of research results and to make such (raw) measurement data available to the public.

Nomenclature

Abbreviations

ASCE	American Society of Civil Engineers
CLE	Contingency Level Earthquake
DA	Dynamic Analysis
DL	Reference sea level
DSHA	Deterministic Seismic Hazard Analysis
EERI	Earthquake Engineering Research Institute
EPRI	Electric Power Research Institute
FDM	Finite Difference Method
FEM	Finite Element Method
FFT	Fast Fourier Transformation
HTVB	Hiap Teck Venture Berhad
JFESP	JFE Steel Corporation
JMA	Japanese Meteorological Agency
K-NET	Kyoshin Network
KIK-NET	Kiban Kyoshin Network
KNMI	Koninklijk Nederlands Meteorologisch Instituut
MDE	Maximum Design Earthquake
MLIT	Japanese Ministry of Land, Infrastructure, Transport and Tourism
M-O	Mononobe-Okabe
MSK	Medvedev-Spoonheuer-Karnik
MMI	Modified Mercalli Intensity
NIED	National Research Institute for Earth Science and Disaster Prevention
NCHRP	National Cooperative Highway Research Program
NGA	New Generation Attenuation database
NSSMC	Nippon Steel & Sumitomo Metal Corporation
OCDI	Overseas Coastal Area Development Institute of Japan
OLE	Operating Level Earthquake
PA	Pushover Analysis
PARI	Port and Airport Research Institute, Japan
PBD	Performance-Based Design
PEER	Pacific Earthquake Engineering Research Center
PIANC	International Navigation Association
POLB	Port Of Long Beach
PSHA	Probabilistic Seismic Hazard Analysis
RHDHV	Royal HaskoningDHV
SA	Simplified Analysis
SDA	Simplified Dynamic (or Displacement-based) Analysis
SDOF	Single Degree Of Freedom
SSI	Soil-Structure Interaction
TNO	Nederlandse Organisatie voor Toegepast-Natuurwetenschappelijk Onderzoek
USACE	United States Army Corps of Engineers
USGS	United States Geological Survey

Symbols

A	cross-sectional area of structural element [m^2]
a_c	critical (or yield) acceleration [m/s^2]
$a_{\text{h or v}}$	(design) ground acceleration in horizontal or vertical direction [m/s^2]
a_{max}	maximum acceleration [m/s^2]
B_m	width of reference case field (or scale) model [m] (or [mm])
b	acting width of the beam (sheet pile) in D-SHEET PILING [m]
C	damping matrix of the soil-structure system
$C_{1, 2}$	relaxation coefficients in PLAXIS 2D viscous boundary formulations [-]
c	cohesion of the soil material [kN/m^2]
D_{50}	soil material mid-particle diameter [mm]
D_n	Newmark permanent displacement [m]
D_{wall}	embedment depth of sheet pile quay wall [m]
d_{eq}	equivalent thickness of plate element in PLAXIS 2D [m]
E	Young's modulus of the soil or structure material [kN/m^2]
E_{50}^{ref}	secant soil stiffness in standard drained triaxial test [kN/m^2]
$E_{\text{oed}}^{\text{ref}}$	tangent soil stiffness for primary oedometer loading [kN/m^2]
$E_{\text{ur}}^{\text{ref}}$	unloading-reloading soil stiffness [kN/m^2]
E_D	dissipated energy in the soil during one hysteretic load cycle [$\text{kg}\cdot\text{m}^2/\text{s}^2$]
E_s	stored energy at maximum shear strain in the soil [$\text{kg}\cdot\text{m}^2/\text{s}^2$]
EA	axial stiffness of the structural element [kN/m]
EI	bending stiffness of the structural element [kNm^2/m]
F	force vector of the soil-structure system
F_{anchor}	force in the anchor tie rod [kN]
$F_{\text{h or v}}$	pseudo-static seismic force in horizontal or vertical direction [kN]
$F_{\text{max,comp}}$	Maximum compressive force in an anchor tie rod [kN]
$F_{\text{max,tens}}$	Maximum tensile normal force in an anchor tie rod [kN]
F_m	dynamic moment factor [-]
F_p	dynamic thrust factor [-]
G	shear modulus of the soil material [kN/m^2]
G_0	initial or very small-strain shear modulus of the soil material [kN/m^2]
G_{max}	maximum shear modulus of the soil material [kN/m^2]
G_s	secant shear modulus of the soil material [kN/m^2]
f	frequency [Hz]
f_0	natural frequency [Hz]
f_1	Rayleigh damping target frequency 1 [Hz]
f_2	Rayleigh damping target frequency 2 [Hz]
f_p	total pressure on the beam (sheet pile) per running meter, including the reaction of the soil springs in D-SHEET PILING [kN/m]
g	gravitational acceleration [m/s^2]
H	out plane force in structural element [kN]
H_m	height of reference case field (or scale) model [m] (or [mm])
H_{soil}	height of soil deposit [m]
H_{tot}	total height of sheet pile quay wall [m]
H_{wall}	retaining height of sheet pile quay wall [m]
h	height of sheet pile profile [mm]
h_a	height schematized anchor pile in limit-equilibrium model [m]
$h_{a,w}$	height of the water table with respect to toe of anchor pile in limit-equilibrium model [m]
h_T	height of the vertical failure plane of the limit-equilibrium model [m]

h_w	water depth in front of the sheet pile wall [m]
h_1	vertical height of the failure plane beneath the sliding mass of the limit-equilibrium model [m]
I	moment of inertia of the structural element [m^4]
I_a	Arias Intensity [m/s]
K	stiffness matrix of the soil-structure system
$K_{A(E)}$	(dynamic) active soil pressure coefficient [-]
$K_{P(E)}$	(dynamic) passive soil pressure coefficient [-]
K_0	neutral soil pressure coefficient [-]
k	soil material permeability [m/s]
$k_{1, 2, 3}$	moduli of subgrade reaction [kN/m^3]
k_{cr}	critical (or yield) seismic coefficient [-]
k_h	horizontal seismic coefficient [-]
k_v	vertical seismic coefficient [-]
k_s	shear correction factor in PLAXIS 2D structural calculations [-]
L_a	length of anchor tie rod [m]
L_m	length of reference case field (or scale) model [m] (or [mm])
L_{plate}	length of plate element in PLAXIS 2D [m]
λ	anchor spacing [m]
M	mass matrix of the soil-structure system
$M_{(max)}$	(maximum) bending moment in the sheet pile quay wall [kNm]
M_p	maximum plastic bending moment of a structural element [kNm]
m	power for defining the amount of stress-level dependency of the soil stiffness moduli [-]
m_b	body wave magnitude [-]
M_L	Richter local magnitude [-]
M_S	surface wave magnitude [-]
M_w	moment magnitude [-]
N	normal force in structural element or normal force in the failure plane beneath the sliding mass of the limit-equilibrium model [kN]
N'	effective component of the normal force in the failure plane beneath the sliding mass of the limit-equilibrium model [kN]
N_p	maximum plastic normal force of a structural element [kN]
N_{sf}	scale factor in reference case [-]
$P_{r;max;point}$	maximum point resistance [MPa]
p_a	active soil pressure on the retaining wall [kN/m^2]
p_p	passive soil pressure on the retaining wall [kN/m^2]
p_{ref}	reference soil stress [kPa]
$P_{A(E)}$	(dynamic) active soil thrust on the retaining wall [kN]
$P_{P(E)}$	(dynamic) passive soil thrust on the retaining wall [kN]
p_w	water pressure [kN/m^2]
P_w	water thrust on the wall [kN]
PGA	peak ground acceleration [m/s^2]
PGV	peak ground velocity [m/s^2]
PGD	peak ground displacement [m]
q	ductility factor [-]
q_c	cone resistance [MPa]
Q	shear force in the structural element [kN]
R_f	failure ratio in PLAXIS 2D HSsmall model [-]
RD	relative density [%]
r	reduction factor on pseudo-static seismic load (deformation-based) [-]
r_u	pore pressure ratio [-]

S	shear force along the failure plane beneath the sliding mass of the soil-structure system [kN]
S_a	spectral acceleration [m/s^2]
T	force in anchor tie rod [kN]
T_0	smoothed predominant spectral period [s]
T_{avg}	average spectral period [s]
T_m	mean period [s]
T_p	predominant spectral period [s]
T_s	site period [s]
t	time [s]
U_1	hydrostatic force in failure plane beneath the sliding mass of the limit-equilibrium model [kN]
U_2	hydrostatic force in front of sheet pile quay wall in the limit-equilibrium model [kN]
$U_{2,w}$	Westergaard hydrodynamic force over the water depth in front of sheet pile quay wall [kN]
U_3	hydrostatic force behind the vertical failure plane of the limit-equilibrium model [kN]
$\ddot{\mathbf{u}}$	acceleration vector of the soil-structure system
$\dot{\mathbf{u}}$	velocity vector of the soil-structure system
\dot{u}_x	seismic wave velocity in x-direction [m/s]
\dot{u}_y	seismic wave velocity in y-direction [m/s]
\mathbf{u}	displacement vector of the soil-structure system
u	horizontal soil displacement [m]
u_{anchor}	horizontal displacement of the sheet pile quay wall at anchor level [mm]
u_{seabed}	horizontal displacement of the sheet pile quay wall at seabed level [mm]
W	mass of the soil-structure system (including added mass) [kg]
w	horizontal displacement of the beam (sheet pile) in D-SHEET PILING [m]
V_p	compression wave velocity of the soil material [m/s]
V_s	shear wave velocity of the soil material [m/s]
X_i	factor in D-SHEET PILING depending on number of CPT's and anchors in the model
x	coordinate along the axis of the beam (sheet pile) in D-SHEET PILING [m]
z	depth in soil column [m]
α_{AE}	angle of the planar failure surface behind the retaining wall with respect to the horizontal [°]
α_N, β_N	Newmark numerical integration coefficients [-]
α_R	Rayleigh damping coefficient associated with mass [-]
β_R	Rayleigh damping coefficient associated with stiffness [-]
β	inclination angle of the backfill with respect to the horizontal [°]
γ_{av}	average unit weight of soil [kN/m ³]
γ_b	buoyant unit weight of soil [kN/m ³]
γ_{dry}	dry unit weight of the soil [kN/m ³]
γ_{eq}	equivalent unit weight of soil [kN/m ³]
γ_{sat}	saturated unit weight of the soil [kN/m ³]
γ_{unsat}	unsaturated unit weight of the soil [kN/m ³]
γ_w	unit weight water [kN/m ³]
γ	shear strain [-]
γ^*	modified shear strain in PLAXIS 2D calculations for better numerical results [-]
$\gamma_{0.7}$	shear strain level at which G_s is reduced to 72.2% of G_0 [-]
γ_c	maximum shear strain [-]
Δu	excess pore pressure [kN/m ²]
Δx	elongation [m]
δ	soil wall friction angle [°]
ε_N	normal strain [-]

ε_2	out of plane strain [-]
η	dynamic viscosity of the (soil) material [kg/m·s]
θ	inclination angle of the retaining wall interface with respect to the vertical [°]
θ_{fp}	angle of the failure plane beneath the sliding mass of the limit-equilibrium model, with respect to the horizontal [°]
κ	curvature of a structural element [1/m]
λ	ratio between saturated height and total height of the retaining wall [-]
ν	Poisson's ratio [-]
ξ	(hysteretic) damping ratio [%]
ρ	volumetric mass density of (soil) material [kg/m ³]
σ	total soil stress [kN/m ²]
σ'	effective soil stress [kN/m ²]
σ_N	normal stress [kN/m ²]
σ_2	out of plane stress [kN/m ²]
τ	shear stress [kN/m ²]
φ	internal friction angle of the soil [°]
φ_{crit}	internal friction angle of the soil corresponding to shearing observed in a simple shear test on soil loose enough to be in a critical state, with zero dilatation [°]
φ_{max}	internal friction angle of the soil corresponding to maximum soil strength [°]
ϕ	diameter anchor tie rod [mm]
ψ	inclination angle of the seismic coefficient k with the vertical [°]
ψ_{max}	dilation angle of the soil material [°]
$\omega_{1,2}$	Rayleigh damping angular frequencies [rad/s]

Contents

Preface	i
Abstract	ii
Nomenclature	iv
1. Introduction.....	1
1.1. Topic description	1
1.2. Contents	1
2. General theoretical background.....	2
2.1. Earthquakes.....	2
2.1.1. Earthquake sources.....	2
2.1.2. Earthquake size.....	4
2.1.3. Seismic waves	4
2.2. Seismic hazards and port structures.....	5
2.2.1. Ground shaking hazard	6
2.2.2. Soil liquefaction hazard.....	8
2.2.3. Tsunami hazard.....	8
2.2.4. Quay wall structures and typical seismic failure modes	9
2.3. Seismic design methodology	11
2.3.1. Conventional seismic design	11
2.3.2. Performance-based seismic design.....	12
2.4. Site response analysis.....	16
2.4.1. Local site effects	16
2.4.2. Equivalent linear site-response analysis	17
2.4.3. Nonlinear site-response analysis	17
2.5. Seismic structural analysis.....	18
2.5.1. Simplified analysis.....	18
2.5.2. Simplified displacement-based analysis	21
2.5.3. Dynamic analysis.....	23
2.6. Trends in seismic design of quay structures.....	25
3. Research description	26
3.1. Problem definition	26
3.2. Research question	27
3.3. Outline of the research methodology	27
3.3.1. Step 1: Reference case selection	28
3.3.2. Step 2: Simplified analysis.....	28
3.3.3. Step 3: Simplified dynamic analysis	29

3.3.4.	Step 4: Dynamic analysis.....	30
3.3.5.	Step 5: Evaluation of analysis results.....	30
4.	Reference case	31
4.1.	Reference case selection	31
4.2.	Reference case definition	31
4.2.1.	Model setup: geometry and parameters.....	31
4.2.2.	Testing procedure.....	33
4.2.3.	Test results.....	35
5.	Seismic analysis of the reference case	37
5.1.	Simplified analysis: pseudo-static.....	37
5.1.1.	Introduction	37
5.1.2.	D-SHEET PILING model.....	38
5.1.3.	Static calibration of the D-Sheet Piling model with the reference case	40
5.1.4.	Pseudo-static calculations.....	43
5.1.5.	Results.....	44
5.2.	Simplified dynamic analysis: permanent-displacement	49
5.2.1.	Introduction	49
5.2.2.	Limit-equilibrium model: critical acceleration	49
5.2.3.	Limit equilibrium model: structural forces in the sheet pile wall	52
5.2.4.	SHAKE2000 model: site-response analysis	53
5.2.5.	SLAMMER model: permanent-displacement analysis	57
5.2.6.	Results.....	60
5.3.	Dynamic analysis: finite element method	62
5.3.1.	Introduction	62
5.3.2.	PLAXIS 2D model.....	62
5.3.3.	Static calibration of the PLAXIS 2D model with the reference case.....	65
5.3.4.	Pseudo-static and pseudo-dynamic computation of the critical acceleration	66
5.3.5.	Dynamic calibration of the PLAXIS 2D model: site-response analysis	69
5.3.6.	Calibrated dynamic calculations with the PLAXIS 2D model.....	74
6.	Evaluation.....	82
6.1.	Reference case.....	82
6.2.	Simplified analysis	83
6.3.	Simplified dynamic analysis	85
6.4.	Dynamic analysis	86
6.5.	Accuracy in the present study	89
6.6.	The performance-based design principle in the present study.....	90
6.7.	Reflection on PGA as the predominant seismic design parameter	92

7.	Conclusions and recommendations	93
7.1.	Conclusions.....	93
7.2.	Recommendations.....	94
8.	References.....	96
	Appendix A: Soil pressure theories	102
	Appendix B: Software.....	110
	Appendix C: D-SHEET PILING reports	122
	Appendix D: Earthquake recorders at Port of Sendai	123
	Appendix E: Expressions in the limit-equilibrium model	124
	Appendix F: SHAKE2000 input files	126
	Appendix G: SHAKE2000 site-response analysis results (SLAMMER input)	130
	Appendix H: PLAXIS 2D input motions at bedrock level.....	133
	Appendix I: Lists of figures and tables.....	136

1. Introduction

1.1. Topic description

The continuously growing world population and associated urban activity combined with the amount of significant earthquakes occurring every year makes seismic risk a persisting actual topic on a global scale. The probability of a major earthquake occurring near an area with a dense population and significant industrial activity may be considered relatively small but the societal and economic impact on the other hand can be devastating, as examples in the past have shown (PIANC, 2001). Also regions which experience lower seismic activity can be expected to suffer from considerable damage. An actual example of this is the increased seismic risk in the flood prone province of Groningen in the Netherlands due to natural gas extraction (Deltares, 2014b). In either way it is of great importance that seismic risk is mitigated by e.g. increasing seismic resistance of civil works.

Ports are civil works which have a major societal and economic importance. Ports are considered “lifeline systems that function as embarkation, terminus, storage and maintenance facilities for the transport of cargoes and people via water (...) which serve nations throughout the world as key centres for commerce and financial growth” (ASCE, 1998). The loss of these port functions due to earthquake induced damage and the corresponding devastating impact on national and even international scale justifies the effort to design port infrastructure with sufficient seismic resistance. Quay structures are infrastructural elements of primary importance for the functioning of the port lifeline system.

Conventional seismic design is force-based i.e. that structures are designed to have sufficient capacity to withstand a pseudo-static seismic design force. The two main setbacks of this limit force-balance approach are that 1) no insight is provided about the performance of the structure when exceeding the limit equilibrium state and 2) in general it results in uneconomic designs when demanding that the structure can completely resist a very high seismic design force corresponding to rare seismic activity. These setbacks in combination with new insights obtained in the 1990's about seismic behaviour of structures cleared the way for the alternative Performance-Based Design (PBD) methodology. After experiencing a number of devastating seismic events it was observed that key design parameters for the performance of structures under seismic loading are stress states and deformations of soil and structure rather than just a seismic design force. Furthermore it was recognized that to some extent permanent deformations are allowable. The PBD methodology is based on these key design parameters and considers multiple (probabilistic) levels of earthquake motion combined with different degrees of allowable damage. (PIANC 2001, ASCE 1998)

This graduation thesis is embedded in the general topic of performance-based seismic design of quay structures. Typical quay types are gravity-based quay walls, sheet pile quay walls and pile-deck structures. The observed trend in seismic quay design is that gravity and sheet pile type structures (i.e. retaining walls) are associated with areas with zero to low seismicity while pile-deck structures are generally the preferred solution in areas with higher seismicity. This can be explained by the more favourable seismic performance of pile-deck structures compared to retaining walls. In line with this trend it is noticed that PBD methodology is developed to a significantly lesser extent for retaining walls (especially anchored sheet pile walls) than for pile-deck structures. Therefore the scope of this thesis comprises seismic performance of anchored sheet pile quay walls.

1.2. Contents

Prior to elaboration on the scope of this graduation thesis a general theoretical overview and observed trends in seismic quay design are provided in chapter 2. The deduced problem description can be found in chapter 3, leading to the scope and general research question of this graduation thesis, followed by a description of the research methodology. Chapter 4 presents the case study which will serve as a physical reference for the research (i.e. seismic analysis). In chapter 5 the seismic analysis is documented and chapter 6 evaluates the results of the analysis. Chapter 7 presents conclusions and recommendations. In chapter 8 the consulted references can be found. Appendices provide relevant background on different aspects of the present study.

2. General theoretical background

General theoretical background relevant for seismic quay design is presented in this chapter. Section 2.1 provides a general introduction to earthquakes. Section 2.2 contains information about seismic hazards affecting port structures. Section 2.3 zooms in on seismic design methodology (conventional and performance-based), while sections 2.4 and 2.5 elaborate on seismic analysis approaches (soil and structure) that are available for seismic design. Closing off section 2.6 discusses the current trends in seismic design which provide a starting point for the research of the present study.

2.1. Earthquakes

A brief but complete introduction to earthquakes can be found in (Kramer, 1996). It is noted that this publication is the one that is referred to in multiple other relevant documents (e.g. ASCE 1998, PIANC 2001, NCHRP 2008, Visone 2008, Besseling 2012) when introducing fundamentals of earthquake engineering. For this reason (Kramer, 1996) is used as the main reference in this section.

2.1.1. Earthquake sources

There are different sources of earthquake motion. The main source is tectonic activity. Other sources of earthquakes that can be distinguished are volcanic activity, underground detonation of chemical or nuclear devices, reservoir filling behind dams (Kramer, 1996) and mining / natural gas extraction (Province of Groningen, the Netherlands (Deltares, 2014b)). In this paragraph the focus is on tectonic activity (main source) and the extraction of natural gas in Groningen (actual topic of national interest).

2.1.1.1. Tectonic activity

Tectonic activity is associated with the relative movement of plates of the broken earth's surficial crust. The movement is driven by gravitational forces in combination with shear stresses acting on the bottom surface of the crust plates. These shear stresses are caused by lateral movement of the convective mantle beneath the crust. This convective movement is due to a temperature gradient which is the result of temperature increasing from surficial crust towards mantle, outer core and inner core of the earth. (Kramer, 1996)

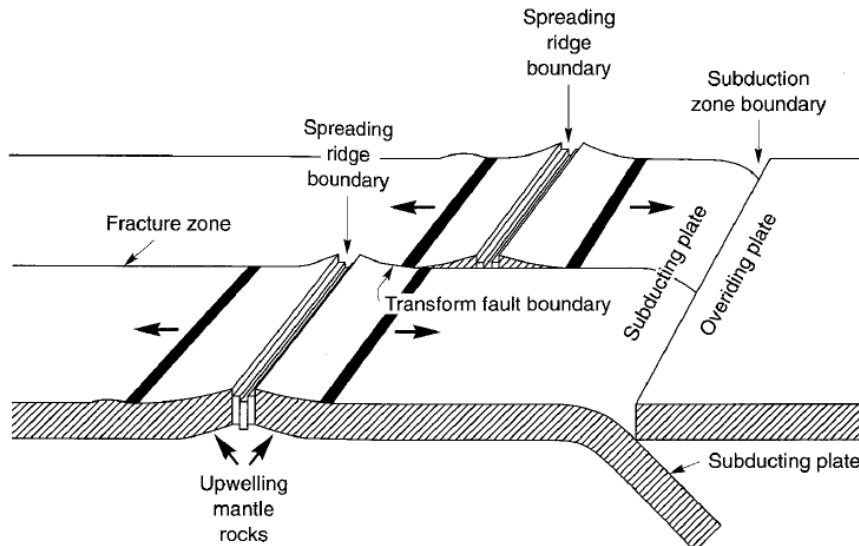


Figure 2.1: Types of plate boundaries (Kramer, 1996)

As adjacent crust plates experience movement relative to each other strain stresses at their boundaries build up and strain energy is accumulated. At a certain moment this strain energy is released either in a smooth continuous way or in a sudden manner. Earthquakes are associated with the sudden release of strain energy. The amount of strain energy that can be accumulated (and thus released) between adjacent plates depends on the type of boundary (subduction zone, transform fault and spreading ridge, see Figure 2.1). On a more local

scale the discontinuities between two portions of crust are referred to as faults (with lengths in the order of several meters to hundreds of kilometres). Faults exist between adjacent plates but also within plates. Faults can be characterized by their planar orientation and direction of movement (strike-slip, reverse and normal, see Figure 2.2). (Kramer 1996, ASCE 1998)

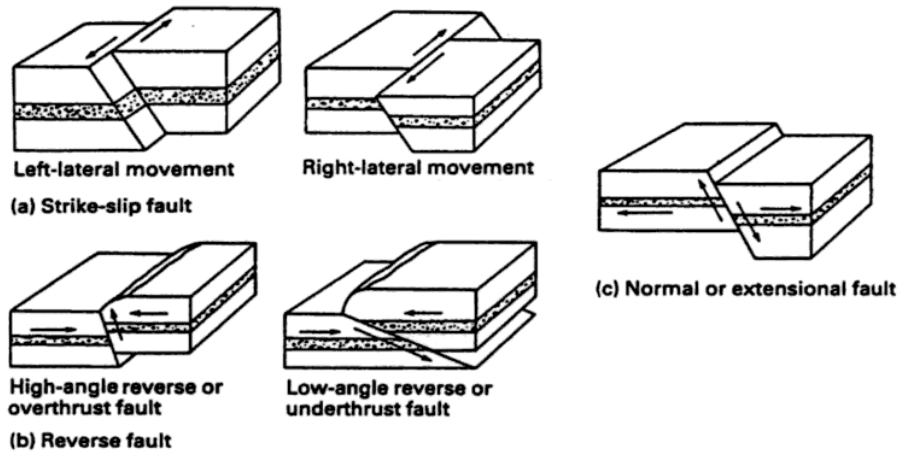


Figure 2.2: Fault types, adapted from (ASCE, 1998)

Fault movement generates seismic waves which travel from source to top of bedrock at a certain location of interest and from there via local soil deposits towards the ground surface where they hit structures. Along their path towards ground surface the seismic waves are altered in amplitude, duration and frequency content (Kramer 1996, ASCE 1998, USACE 1999, PIANC 2001). More information on seismic wave attenuation in general and on how to determine altered ground surface motion from a bedrock motion signal is provided in paragraph 2.1.3 and paragraph 2.2.1 / section 2.4 respectively.

2.1.1.2. Seismic activity due to natural gas extraction

It is believed that in the Province of Groningen in the Netherlands seismic activity has emerged due to natural gas extraction. This natural gas extraction has resulted in compaction of the subsoil in the order of 10 to 30 centimetres. The possible mechanism that induces seismic activity is differential compaction along existing faults (see Figure 2.3). Seismic waves are generated at a depth of circa 2.5 kilometres beneath the ground surface and while travelling upwards damped by amongst others a thick salt layer and magnified again by the upper soft local soil conditions. (TNO 2009, lectures by Deltares and KNMI 2014)

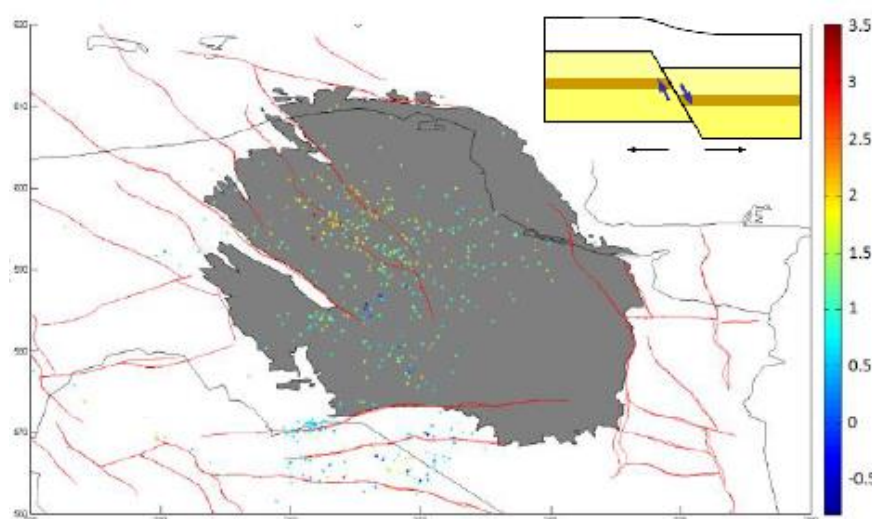


Figure 2.3: Orientation earthquake magnitudes and faults (red lines) experiencing differential compaction at the location of the Groningen gas field (grey marking), adapted from (TNO, 2009)

2.1.2. Earthquake size

An important parameter in earthquake engineering is the size of earthquakes. It is common practice to describe this size in a qualitative (earthquake intensity) and a quantitative (earthquake magnitude) way. (Kramer, 1996)

2.1.2.1. Earthquake intensity

This oldest measure for determining earthquake size qualitatively describes effects of earthquakes at a certain location. The intensity measure is based on observed damage and (preferably rational and unemotional) human feedback. A widely used scale in English-speaking countries is the Modified Mercalli Intensity (MMI) scale which consists of twelve descriptive levels of earthquake intensity (II-XII). Other intensity scales are the Japanese Meteorological Agency (JMA) scale and the Medvedev-Spoonheuer-Karnik (MSK) scale applied in Central and Eastern Europe. (Kramer, 1996)

2.1.2.2. Earthquake magnitude

A more objective measure for earthquake size is the quantitative earthquake magnitude. Magnitude scales are predominantly based on ground motion measurements. The best known magnitude scale is the Richter Local Magnitude (M_L) scale, ranging from 0 to 10 [-]. Because this scale does not consider different types of seismic waves (see paragraph 2.1.3.) other scales have been proposed. These are e.g. the Surface Wave Magnitude (M_S) scale and the Body Wave Magnitude (m_b) scale. Another magnitude scale is the Moment Magnitude (M_w) scale which is not based on ground motion characteristics but on a direct measure of fault rupture factors: the seismic moment. This is a desirable scale for describing larger earthquake sizes at which measured ground motion characteristics become less dependent of earthquake size (saturation phenomenon). (Kramer, 1996)

2.1.3. Seismic waves

Fault movement generates seismic waves. In subparagraph 2.1.2.2 it was noticed that there are two main types of seismic waves that can be distinguished: body waves and surface waves.

2.1.3.1. Body waves

Body waves are the seismic waves that travel from source to site via the interior of the earth. Body waves are divided in so called primary (p)-waves and secondary (s)-waves. A graphical representation of these waves is given in Figure 2.4.

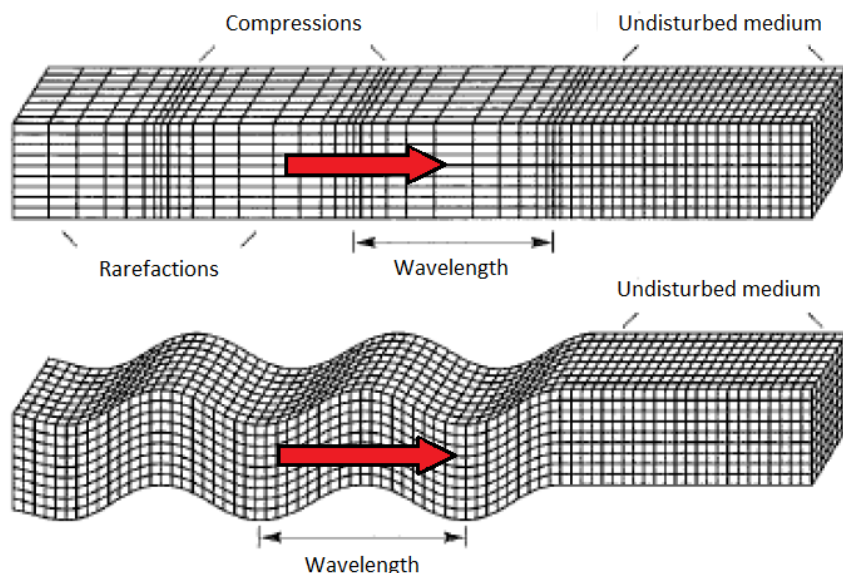


Figure 2.4: Body waves: p-waves (top) and s-waves (bottom), adapted from (Kramer, 1996)

P-waves are compressional or longitudinal waves (analogous to sound waves) able to travel through fluids and solids. P-wave propagation through the earth's interior is characterized by successive compression and

rarefaction of the interior. The motion of the material particles is parallel to the wave propagation direction. S-waves are shear or transverse waves able to travel through solids only (shear stiffness required) in which they cause shearing deformations. A subdivision of s-waves can be made based on the direction of the perpendicular material particle movement: sh-waves (horizontal plane movement) and sv-waves (vertical plane movement). Larger stiffness of the medium through which a wave travels means higher wave celerity. Compression stiffness of geological material is larger than shear stiffness. Therefore p-waves travel faster than s-waves and will thus arrive earlier at a certain site. (Kramer, 1996)

2.1.3.2. Surface waves

Surface waves can be subdivided in two types which are of importance for engineering purposes, i.e. Rayleigh waves and Love waves. A graphical representation of these waves is given in Figure 2.5.

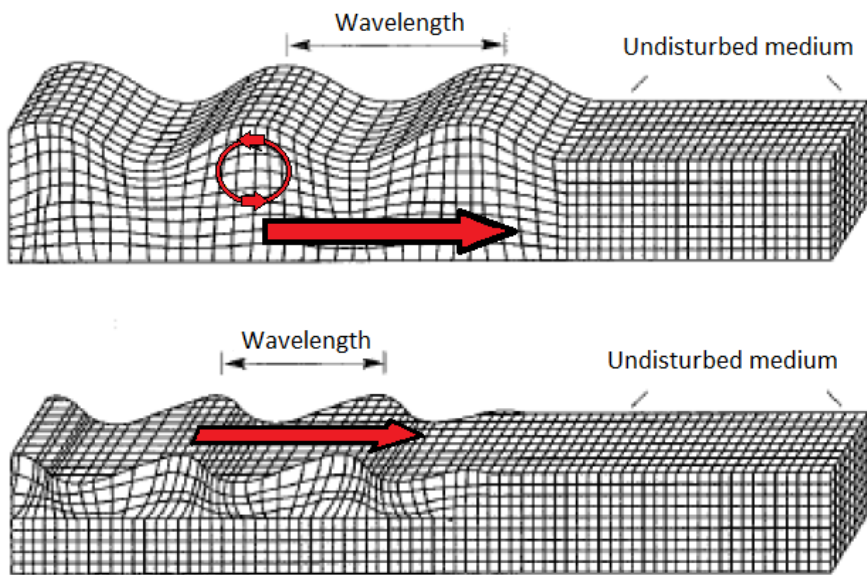


Figure 2.5: Surface waves: Rayleigh waves (top) and Love waves (bottom), adapted from (Kramer, 1996)

Rayleigh waves, analogous to water waves, are the product of interaction between p-waves, sv-waves and the ground surface (resulting in both vertical and horizontal particle motion). Love-waves are the product of interaction between sh-waves and a soft surficial layer (resulting in only horizontal particle motion). While body waves are more dominant near the source of the earthquake, surface waves will be more dominant further away from the source in producing ground motions. This is due to the interaction processes which are required to create surface waves. (Kramer, 1996)

2.2. Seismic hazards and port structures

In subparagraph 2.1.1.1 it was mentioned that fault movement generates seismic waves which travel from source to top of bedrock at a certain location of interest and from there via local soil deposits towards the ground surface where they hit structures. Port structures are affected by the ground shaking associated with seismic wave propagation. Other seismic hazards that affect port structures are liquefaction of loosely packed sand in the soil-structure system due to critical ground shaking and possible tsunami loading which can develop after vertical tectonic displacement of a deep water seabed. A graphical overview of seismic hazards affecting port structures is presented in Figure 2.6. (PIANC, 2001)

In line with (PIANC, 2001) these seismic hazards are treated in paragraphs 2.2.1, 2.2.2, and 2.2.3 respectively. Furthermore a short overview of different types of quay wall structures is given in paragraph 2.2.4 in combination with their typical (seismic) failure modes.

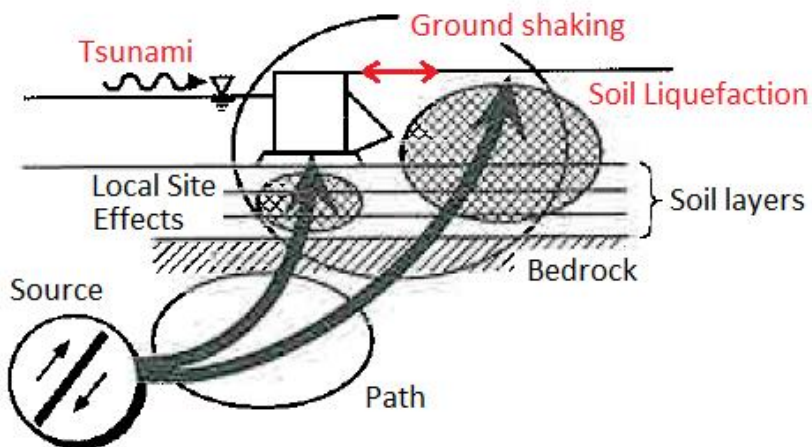


Figure 2.6: Overview seismic hazards affecting port structures, adapted from (PIANC, 2001)

2.2.1. Ground shaking hazard

2.2.1.1. Seismic hazard analysis

The characteristics of the bedrock motion at a specific site are determined by performing Seismic Hazard Analysis which can be Deterministic (DSHA) or Probabilistic (PSHA). In DSHA some specific earthquake scenario is considered and the corresponding bedrock motion is estimated from regional geologic setting, historic seismicity of the area and the geologic configuration along the path from source to site of which the latter affects seismic wave attenuation. In PSHA the bedrock motion is defined probabilistically by also taking into account uncertainties in earthquake locations and frequencies of occurrence around the site of interest and additionally uncertainties in the source-to-site attenuation. (ASCE 1998, USACE 1999, PIANC 2001)

2.2.1.2. Characterization of ground motion

The most important characteristics of ground motion are amplitude, duration and frequency content. A typical (bedrock) ground motion recording associated with tectonic activity is shown in Figure 2.7. It is a measurement of acceleration of the ground in the time domain, known as an accelerogram. The highest peak in the accelerogram is the Peak Ground Acceleration (PGA). In earthquake engineering this PGA is the key parameter for defining the amplitude of strong ground motion. Derived measures from it are the Peak Ground Velocity (PGV) or Peak Ground Displacement (PGD). PGA can be used by itself or applied to scale relevant response spectra or time histories (see section 2.5). (Kramer 1996, ASCE 1998, PIANC 2001)

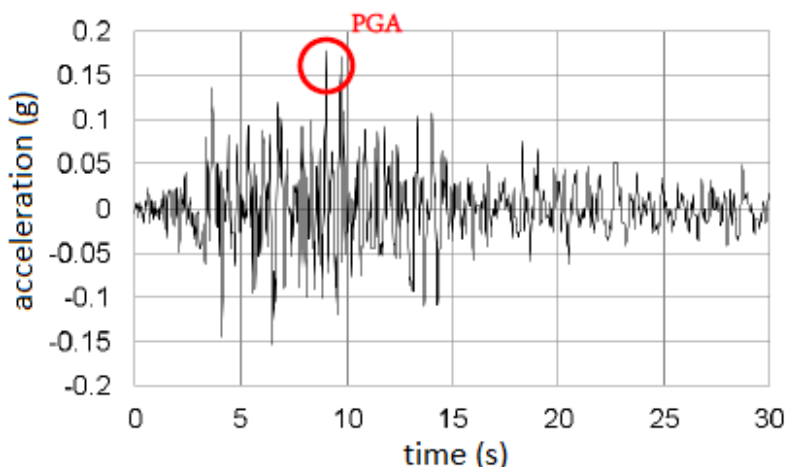


Figure 2.7: Accelerogram associated with tectonic activity and corresponding PGA (from lecture at DUT by Deltares, 2014)

Concerning the duration of a ground motion the total duration of a recording can be considered but in earthquake engineering the time between the first and last exceedance of some critical threshold acceleration (absolute value) is more commonly used. (Kramer, 1996)

The frequency content of ground motions is captured in spectra. By applying Fast Fourier Transformation (FFT) ground motion recordings can be translated into Fourier Amplitude Spectra which show the distribution of the amplitude of motion with respect to frequency (or period). Analogous with ocean wave spectra it holds that an almost sinusoidal wave recording would give a very narrow spectrum and a very irregular wave recording a broad spectrum due to the larger variety in the frequency content. The most common used spectra in earthquake engineering are Response Spectra. Response spectra are obtained by applying an input ground motion to a number of Single Degree Of Freedom (SDOF) oscillators which all have the same damping ratio (ξ)ⁱ and a different natural frequency / period. The maximum response of each oscillator to the input motion is plotted against its natural frequency or period. (Kramer 1996, ASCE 1998, Holthuijsen 2007)

ⁱ The damping ratio is defined as $\xi = 1$ for critical damping, i.e. exactly the amount of damping needed to let a SDOF system that is released from an initial excitation u_0 , smoothly stop as fast as possible without rebouncing. A system is underdamped when $\xi < 1$ (oscillatory decay with amplitude decreasing to zero) and overdamped when $\xi > 1$ (exponential decay to equilibrium without oscillation).

2.2.1.3. Site-response analysis

When seismic waves are travelling from top of bedrock towards ground level via the local soil deposits amplitude, duration and frequency content are altered, which means that accelerograms and spectra are altered. The analysis of this altering is called site-response analysis, which is schematically shown in Figure 2.8. Elaboration on site-response analysis is provided in section 2.4.

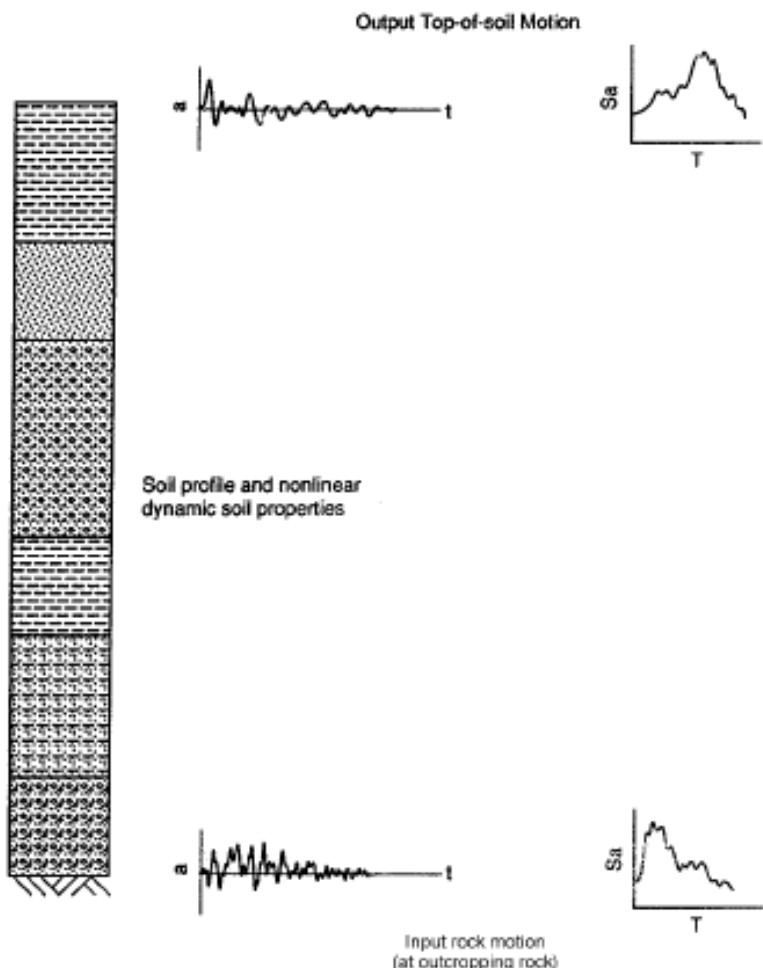


Figure 2.8: Schematic of (one dimensional) site-response analysis, adapted from (USACE, 1999)

2.2.1.4. Structural response

The frequency content of the ground shaking at ground level is important for the assessment of the response of structures. Application of the earlier described response spectra for structural response analysis is a common, relatively simple method. Site specific response spectra are used to assess structural response by entering the spectrum at the natural period of each significant mode of vibration of the structure in order to obtain the amplitude of response of that mode. The obtained response amplitudes of the significant modes are (together with the mode shapes and the modal participation factors) used to compute the maximum response at any location in the structure for all significant modes. (ASCE, 1998)

The description of analysing structural response using response spectrum methodology finalises the general overview of how ground shaking affects port structures. The commonly used response spectrum method is used as a first example in this subparagraph. Other methods available for assessing structural seismic response are e.g. pseudo-static method (more simple) and time history methods (more advanced). A more complete and elaborate introduction to the different methods for analysis of structural response can be found in section 2.5.

2.2.2. Soil liquefaction hazard

The transformation of a substance into a liquid is referred to as 'liquefaction'. Cohesionless, saturated, loosely packed soils are prone to liquefaction. The strength of these soils is due to friction and interlocking between soil particles. Forces due to self-weight and any additional loading are partly carried by the interlocking soil particles (effective stress) and partly by the pore water (pore water pressure). The total soil stress is the sum of effective stress and pore water pressure. When a shear deformation is applied to the cohesionless soil, for instance due to earthquake ground shaking, the loosely packed soil particles try to densify. The pore water has to flow away to make this possible but it can't immediately within the time frame of earthquake shaking. The result is an increase in pore pressure and a corresponding decrease in effective stress which can reach the point that effective stresses are zero. At that point the soil has transformed from a solid to a liquefied state. Soil strength is lost and large deformations occur until the pore water has drained sufficiently. The drainage of the water (sometimes together with soil particles) results in a denser packing of the soil and thus permanent settlement. (Kramer 1996, ASCE 1998, PIANC 2001)

Because port structures, and quay wall structures especially, derive their strength and stability from the soil the vulnerability of these structures in case of liquefaction is clear. Loosely packed sandy soil packages in earthquake prone port areas should be avoided. Soil improvement (artificial densification) can offer a solution.

2.2.3. Tsunami hazard

A vertical tectonic displacement of a deep water seabed (or possibly submarine landslides / submarine volcanic activity) and corresponding displacement of the water column can result in a tsunami wave which is characterized by a long period and thus a large wave length (several hundred kilometres) but a low amplitude (less than 1 meter) when propagating over deep water. These waves which are difficult to detect can travel for thousands of kilometres before entering shallow coastal zones. Due to shoaling in the shallow coastal water the wave length decreases and the amplitude increases dramatically. The direct wave impact (with heights up to tens of meters) and the large onshore wave run-up are known to have had a devastating effect on coastal ports.

The current solutions for mitigating the amount of devastation caused by an incoming tsunami are implementation of early warning systems (facilitating timely evacuation) and construction of structures acting as barriers at bay mouths and coastlines. (ASCE 1998, PIANC 2001, Holthuijsen 2007)

2.2.4. Quay wall structures and typical seismic failure modes

2.2.4.1. General

Although a lot of hybrid types of quay wall structures are applied the following general types can be distinguished (ASCE 1998, PIANC 2001, de Gijt 2004):

- Gravity types (e.g. massive wall, block wall, caisson wall, L-wall, cellular sheet pile wall)
- Sheet pile types (e.g. cantilever sheet pile bulkhead, anchored sheet pile bulkhead, relieving platform with sheet pile wall)
- Pile-deck types (e.g. piers, wharves, jetties)
- Other (e.g. diaphragm walls, structures on special foundations)

An overview of this classification of quay wall structures is presented in Figure 2.9.

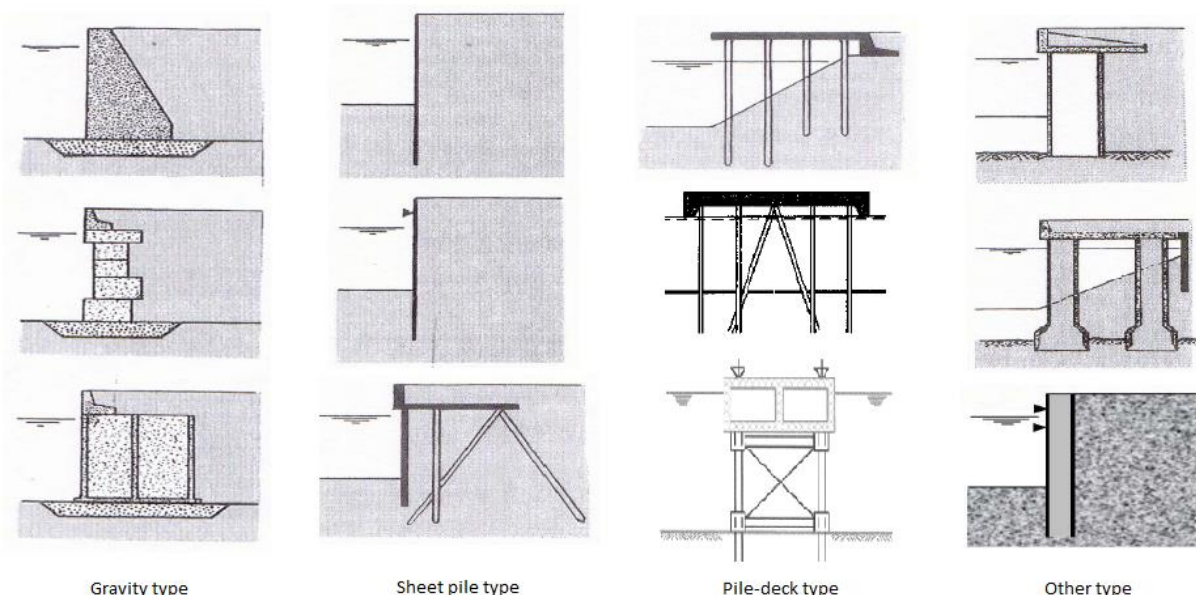


Figure 2.9: Typical quay wall structures, adapted from (PIANC, 2001) and (de Gijt, 2004)

Both (PIANC, 2001) and (de Gijt, 2004) (extensively) provide real life examples of typical port structure failures associated with earthquakes. Typical failure modes for gravity, sheet pile and pile-deck structures are extracted from this and presented in the following subparagraphs. It should be noted that apart from the typical failure modes treated below also loss of overall macro-stability of the soil-structure system can be a failure mode for all quay structures.

2.2.4.2. Failure modes of gravity-based structures

Typical failure modes of gravity-based structures which can be induced by seismic loading are seaward horizontal sliding (loss of horizontal stability), overturning (loss of rotational stability) and vertical (differential) settlement (failure of the subsoil due to liquefaction). See Figure 2.10 for an overview.

2.2.4.3. Failure modes of sheet pile structures

Typical failure modes of sheet pile structures which can be induced by seismic loading are anchor failure (displacement, pull-out, cracking), sheet pile wall failure (displacement, local buckling, cracking), tie rod failure (displacement, cracking) and embedment failure (passive soil wedge failure). See Figure 2.11 for an overview.

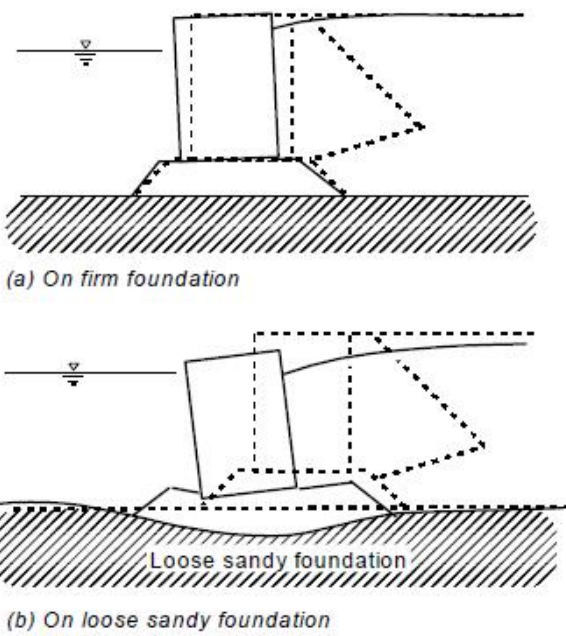


Figure 2.10: Typical failure modes of gravity-based quay walls, adapted from (ASCE, 1998) and (PIANC, 2001)

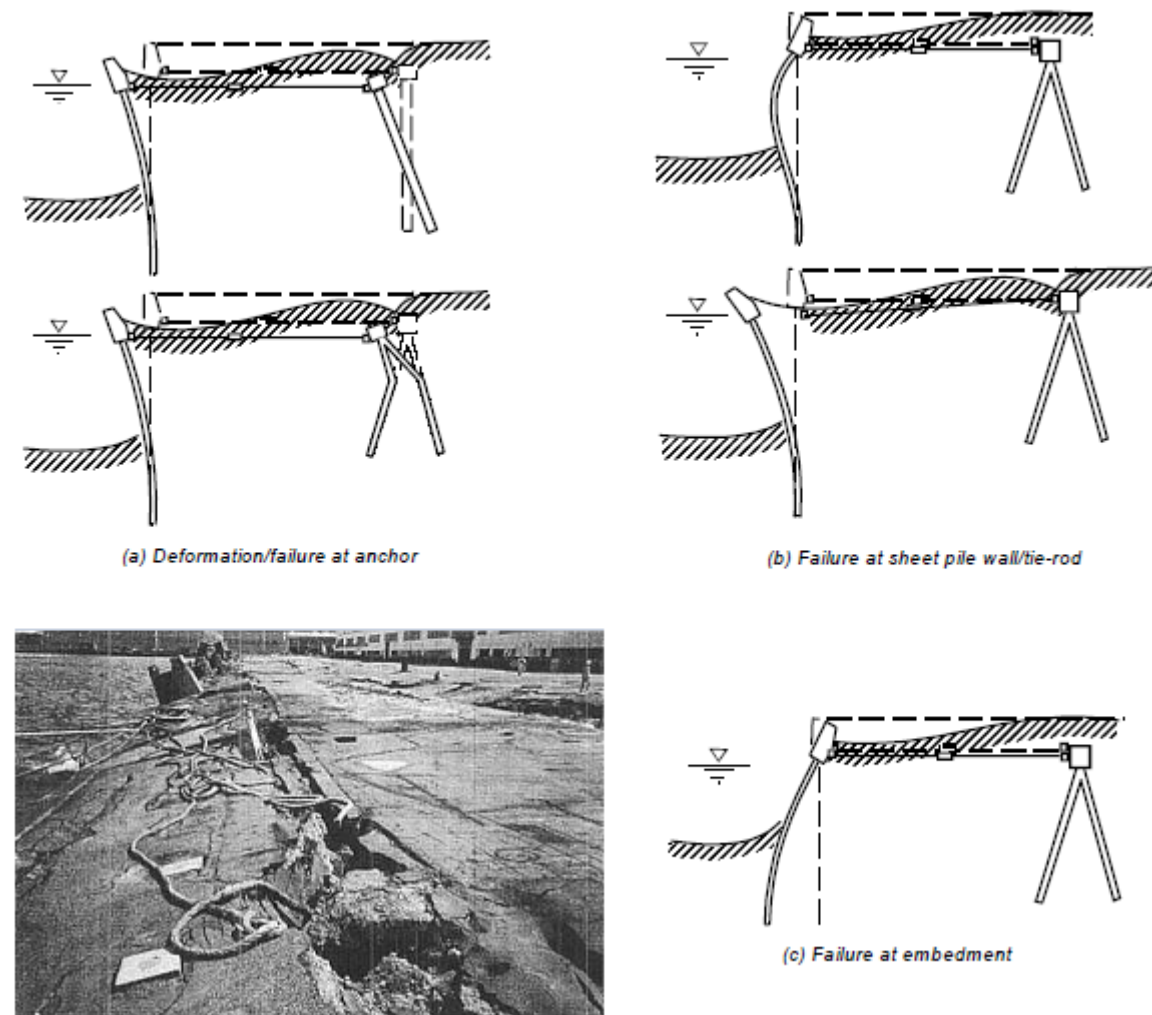


Figure 2.11: Typical failure modes of sheet pile quay walls, adapted from (EERI, 1993) and (PIANC, 2001)

2.2.4.4. Failure modes of pile-deck structures

Typical failure modes of pile-deck structures which can be induced by seismic loading are deformations of the deck and plastic hinging of the piles (near the deck and beneath ground level) due to inertial loading at the deck, a horizontal loading from a possible retaining structure behind the deck and/or lateral displacement of the subsoil. See Figure 2.12 for an overview.

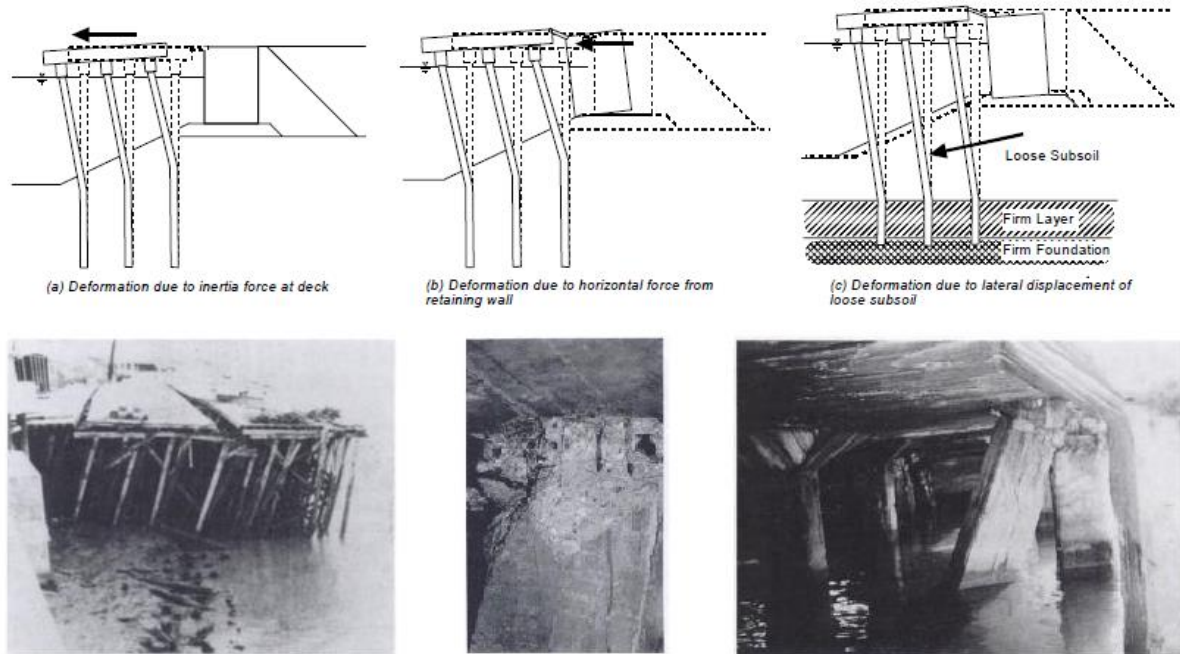


Figure 2.12: Typical failure modes of pile-deck structures, adapted from (ASCE, 1998) and (PIANC, 2001)

2.3. Seismic design methodology

2.3.1. Conventional seismic design

Conventional seismic design is force-based i.e. that structures are designed to have sufficient capacity to withstand a seismic design force. The seismic force is obtained by multiplying the self-weight and added mass of the system with a design value of the PGA divided by the gravitational acceleration and this force is taken into account in the (elastic) limit force equilibrium. As such the structure is designed in a pseudo-static way (see paragraph 2.5.1 for further elaboration and formulations).

Advantages of the conventional approach are that it is simple and quick, it is common practice and thus understood by a larger amount of people and it is integrated in standard design software. The two main setbacks of this force-balance approach are that:

1. No insight is provided in the performance of the structure when exceeding elastic limit equilibrium;
2. It generally results in uneconomic designs when demanding that the structure can completely resist a very high seismic design force corresponding to rare seismic activity.

These setbacks became more pronounced after a number of devastating seismic events in the 1990's after which it was observed that key design parameters for the performance of structures under seismic loading are stress states and deformations of soil and structure rather than seismic forces. Furthermore it was recognized that to some extent permanent deformations are allowable. This cleared the way for an alternative seismic design methodology known as Performance-Based Design. (ASCE 1998, PIANC 2001)

2.3.2. Performance-based seismic design

The basic concept of Performance-Based Design (PBD) methodology is that it considers multiple probabilistic levels of earthquake motion combined with different degrees of required performance. The higher the consequences of failure, the higher the required performance is, and equivalently the higher the demand on the degree of sophistication of the seismic analysis methods that are applied. The results of the seismic analysis are compared to the damage criteria (allowable damage) per performance level. These damage criteria are expressed as allowable stress states, strains and deformations (the key parameters for seismic performance). A clear example of a flowchart for PBD methodology is provided in (PIANC, 2001) and shown in Figure 2.13. (ASCE 1998, PIANC 2001, USACE 2007, POLB 2009, ASCE 2013)

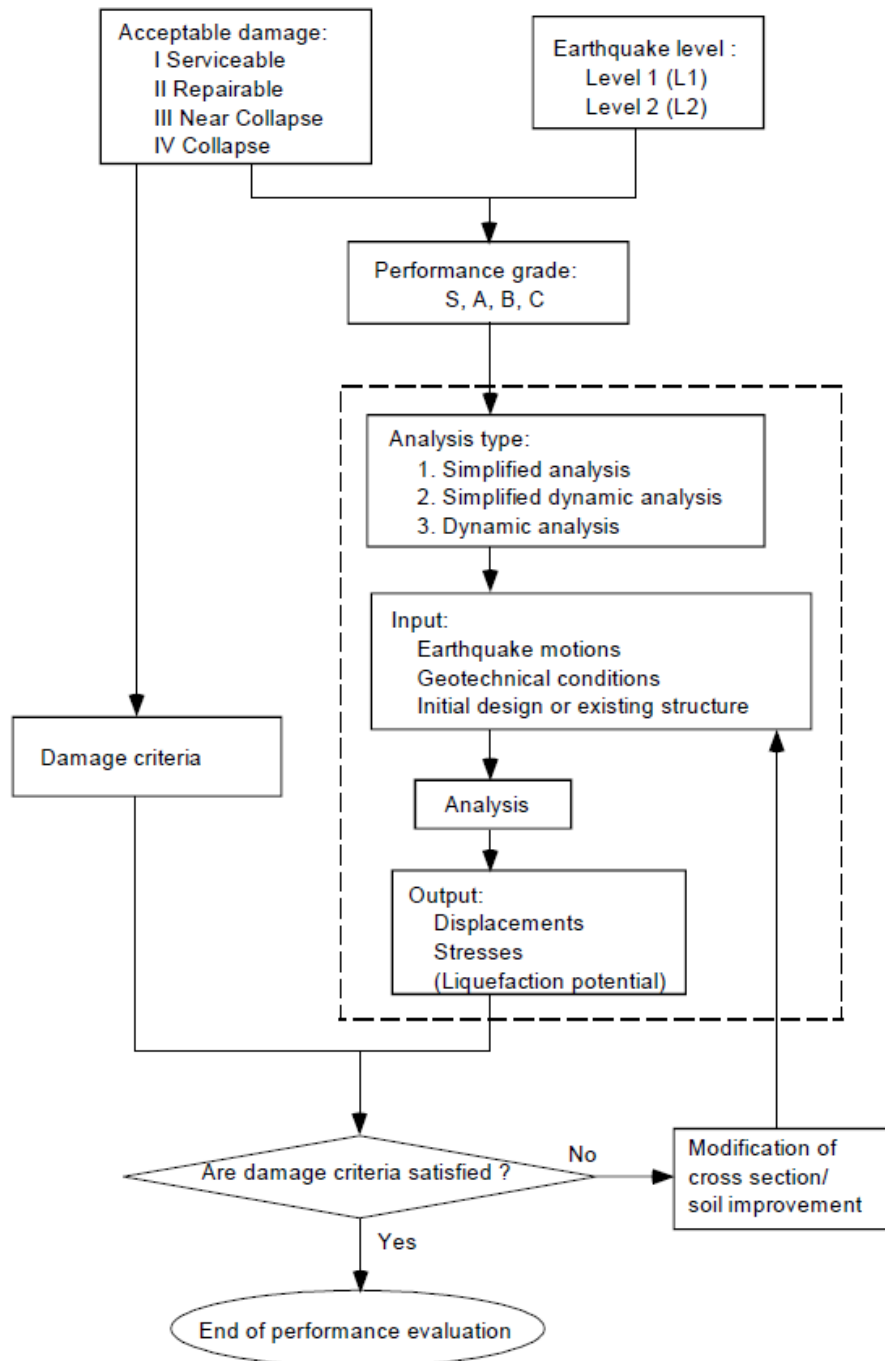


Figure 2.13: Example flowchart Performance-Based Design Methodology, adapted from (PIANC, 2001)

2.3.2.1. Design requirements in PBD methodology

Establishing design requirements in PBD methodology is typically done by combining multiple levels of seismic performance with multiple probabilistic levels of earthquake motion and different degrees of structural importance. These aspects and the combination of it are treated in this subparagraph.

Structural importance

The consequences of failure of a certain structure are accounted for in PBD. This is done by defining the importance of a structure by using importance grades. The different available guidelines use different grading systems but the basis for all is consideration of the following characteristics:

- Whether the structure is open to the public (human fatality risk)
- Whether the structure is important for post-earthquake event recovery of the region
- Whether the structure is important for the economy of the region (economic risk)
- Whether at the structure hazardous goods are handled (environmental risk)

All mentioned importance factors are associated with quay wall structures. Therefore higher importance classes for quay walls are common. In Figure 2.13 structural importance is covered by the ‘performance grades’, i.e. S (critical structure), A (primary structure), B (ordinary structure), C (small, easily restorable structure). (ASCE 1998, PIANC 2001, NEN-EN1998-1, Besseling 2012, ASCE 2013)

Levels of seismic performance

Due to the high societal and economic significance of ports it is desirable to design quay wall structures (which are of primary importance for the functioning of the port) for multiple (typically three) levels of seismic performance:

- Serviceability: continued operation, minor or negligible damage
- Damage control: interrupted operation due to a certain amount of allowed damage, although controllable and repairable within reasonable time (e.g. 6 months)
- Collapse control: complete loss of serviceability, unrepairable damage allowed, although no collapse in order that life safety is protected

In Figure 2.13 levels of seismic performance are covered by the ‘acceptable damage’ degrees. It is noted that (PIANC, 2001) additionally recognizes a fourth level (‘Collapse’) which is employed for small easily restorable structures. (ASCE 1998, PIANC 2001, NEN-EN1998-1, USACE 2007, ASCE 2013)

Levels of earthquake motion

In line with defining levels of seismic performance also levels of earthquake motion are considered in PBD. A two-level design approach is used commonly but also the extension to three can be found. An overview of typically used (probabilistic) earthquake motion levels for port structures:

- Level 1 - Operating Level Earthquake (OLE):
 - Associated with the serviceability performance level
 - 50% probability of exceedance during lifespan, typically 50 years, which results in a return period of 72 years
- Level 2 – Contingency Level Earthquake (CLE):
 - Associated with the damage control performance level
 - 10% probability of exceedance during lifespan, typically 50 years, which results in a return period of 475 years
- Level 3 – Maximum Design Earthquake (MDE):
 - Associated with the collapse control performance level
 - No specific return period

It can be seen in Figure 2.13 that (PIANC, 2001) uses a two-level approach in which levels L1 and L2 comply with level 1 and level 2 defined above. (ASCE 1998, PIANC 2001, NEN-EN1998-1, USACE 2007, POLB 2009, ASCE 2013)

Establishing design requirements

By combining the above mentioned aspects design requirements can be established. This is illustrated by Figure 2.14 in which a table from (ASCE, 2013) is shown. The table is developed for the seismic design of pile-supported piers and wharves. It is noted that 'Design Classification' refers to structural importance.

Design Classification	Seismic Hazard Level and Performance Level					
	Operating Level Earthquake (OLE)		Contingency Level Earthquake (CLE)		Design Earthquake (DE)	
	Ground Motion Probability of Exceedance	Performance Level	Ground Motion Probability of Exceedance	Performance Level	Seismic Hazard Level	Performance Level
High	50% in 50 years (72-year return period)	Minimal Damage	10% in 50 years (475-year return period)	Controlled and Repairable Damage	Design Earthquake per ASCE 7 [2.1]	Life-Safety Protection
Moderate	n/a	n/a	20% in 50 years (224-year return period)	Controlled and Repairable Damage	Design Earthquake per ASCE 7 [2.1]	Life-Safety Protection
Low	n/a	n/a	n/a	n/a	Design Earthquake per ASCE 7 [2.1]	Life-Safety Protection

Figure 2.14: Example design requirements for pile-supported piers and wharves (ASCE 2013)

2.3.2.2. Damage criteria

In line with the established design requirements allowable damage per performance level has to be specified in engineering terms such as displacements, rotations, stress states (elastic - plastic) and limit strains (ductility). These so-called damage criteria are treated in general in this subparagraph per quay wall structure as considered in paragraph 2.2.4.

Gravity-based structures

Referring to Figure 2.10 (typical failure modes of gravity-based quay walls) the following damage criteria parameters can be distinguished for both gravity structure and apron:

- Amount of permanent horizontal displacement per performance level
- Amount of permanent differential settlement per performance level
- Amount of permanent tilting per performance level

Displacements and settlements are measured in a length unit or in percentage when normalized. Tilting is measured in degrees / radians. (PIANC 2001, USACE 2007)

Sheet pile structures

Referring to Figure 2.11 (typical failure modes of sheet pile quay walls) the following damage criteria parameters can be distinguished:

- Displacements (sheet pile wall and apron including anchor):
 - Amount of permanent horizontal displacement per performance level
 - Amount of permanent differential settlement per performance level
 - Amount of permanent tilting per performance level

- Stress states and limit strains:
 - Stress and strain states in sheet pile wall above and below harbour bottom per performance level (elastic – plastic (hinging))
 - Stress and strain states in tie rod per performance level (elastic – plastic)
 - Stress and strain states in anchor per performance level (elastic – plastic (hinging))

Stress states and strains per performance level are defined in terms of elasticity and amount of plasticity. The limited amount of plastic strain or ductility limit can be defined by the ductility factor. In case of bending the limit strain [-] can be translated into a limit curvature [1/length] and this limit curvature via the plastic hinge length into the plastic rotation capacity [-].

Because PBD methodology considers the performance of the separate structural elements a preferred sequence of structural elements reaching their limit state with increasing seismic loading can be specified. In this way damage becomes controllable and thus repairable to a certain extent. The preferred sequence for an anchored sheet pile wall is shown in Figure 2.15. (PIANC 2001, POLB 2009, ASCE 2013)

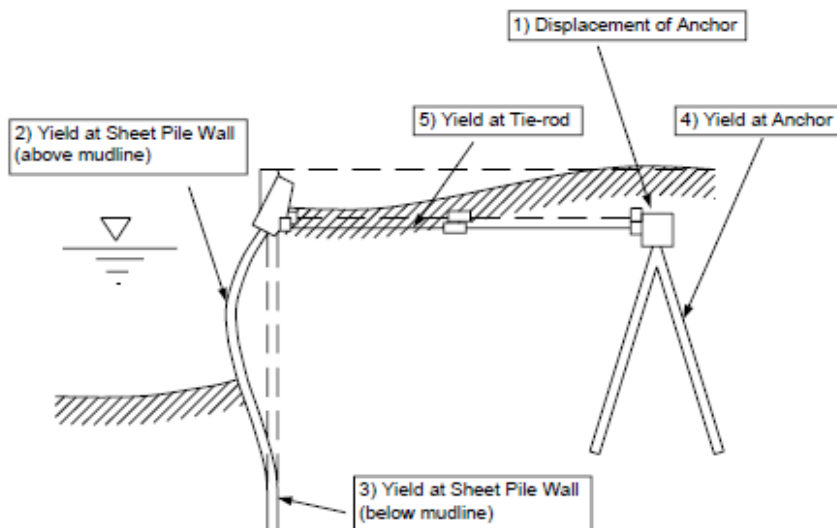


Figure 2.15: Preferred yield sequence of an anchored sheet pile wall (PIANC 2001, Visone 2008)

Pile-deck structures

Referring to Figure 2.12 (typical failure modes of pile-deck structures) the following damage criteria parameters can be distinguished:

- Displacements (pile-deck system):
 - Amount of permanent horizontal displacement per performance level
 - Amount of permanent differential settlement per performance level
 - Amount of permanent tilting per performance level
- Stress states and limit strains:
 - Stress and strain states in deck per performance level (elastic – plastic)
 - Stress and strain states in pile cap per performance level (elastic – plastic (hinging))
 - Stress and strain states in pile top per performance level (elastic – plastic (hinging))
 - Stress and strain states in embedded part of pile per performance level (elastic – plastic (hinging))

In the same way as for the sheet pile structure a desired yielding sequence for a pile-deck structure can be specified as well. It is shown in Figure 2.16. (PIANC 2001, POLB 2009, ASCE 2013)

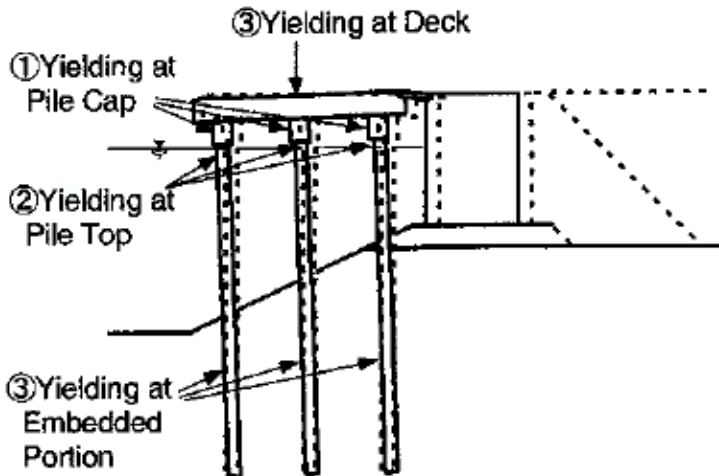


Figure 2.16: Preferred yield sequence of a pile-deck structure (PIANC, 2001)

2.3.2.3. Seismic Analysis

Figure 2.13 shows that after setting the design requirements a suitable type of seismic analysis has to be chosen. This choice depends on the design phase (preliminary or more final) and on the required performance of the structure. Input for the analysis consists of a model for the existing or newly designed structure, the geotechnical conditions and the earthquake motions. The latter two are of importance for site response analysis (section 2.4) and the combination of the three for the seismic behaviour of the soil-structure system (section 2.5). The results of seismic analysis are interpreted and compared with the damage criteria. If the damage criteria are not satisfied the soil-structure design should be altered or possibly a more advanced (and generally less conservative) analysis method should be applied. In the end this iterative process should lead to a safe and economic design.

2.4. Site response analysis

2.4.1. Local site effects

In subparagraph 2.2.1.3 it was mentioned that when seismic waves are travelling from top of bedrock towards ground level via the local soil deposits amplitude, duration and frequency content of the seismic signal are altered. This altering by the local soil deposits is referred to as 'local site effects'. It is due to the dynamic response of the soil which is governed by its strength and stiffness and cyclic nonlinear characteristics. When subjected to cyclic (earthquake) loading soils show nonlinear, inelastic, stress-strain behaviour: at small deformation of the soil (low strain levels) the soil stiffness is high and the damping is low and at larger deformation of the soil (high strain levels) the soil stiffness is low and the damping is higher.

Besides the stiffness and damping of a soil package being dependent on the amount of (cyclic) loading, the stiffness and strength of the soil package decreases towards ground level. In general reduced strength and stiffness amplify ground shaking motion so a seismic signal tends to be amplified when travelling upwards through the local soil deposits. Especially local soft soil layers (which are typical for a marine environment and the Netherlands) can significantly amplify typical frequencies of ground motion. Furthermore it is known that stiff soil conditions transfer energy to the higher frequency range while softer soil conditions transfer energy to the lower frequency range.

Different methods with increasing degree of sophistication for analysing local site response are available. In engineering practice prescribed site amplification factors (based on statistical analysis of existing data) are applied or site-specific response analysis is used. Site amplification factors are often specified in codes and are

used to simply scale bedrock PGA or bedrock response spectra to ground level PGA or ground level response spectra respectively. Site-specific response analysis (which includes layering of the soil) is generally performed by (1D) equivalent linear analysis or nonlinear analysis. The following paragraphs consider these two methods. Because it is common in earthquake engineering practice to consider vertically propagating shear waves only and neglect surface waves this will generally also be the input for site-response analysis. (Kramer 1996, ASCE 1998, PIANC 2001, Besseling 2012)

2.4.2. Equivalent linear site-response analysis

For the sake of computational efficiency an often used approach is *one-dimensional equivalent linear site-response analysis*. In this approach it is assumed that the soil layering is purely horizontal and the soil layers extend infinitely in all lateral directions. Although this is not strictly realistic it is sufficiently satisfactory for engineering purposes at many sites.

Equivalent linearity is used to capture the nonlinear soil behaviour in a simplified but reasonable way. Equivalent linear analysis attempts to find equivalent linear values for nonlinear soil parameters (stiffness and damping) which are compatible with the level of strain induced per soil layer. An example: the equivalent linear shear modulus G (representing shear stiffness) is generally taken as a secant shear modulus.

The behaviour of this soil schematization matches the behaviour of an equivalent linear Kelvin-Voigt solid (mass - parallel-spring-dashpot system). For this solid the 1D shear wave equation becomes:

$$\rho \frac{\partial^2 u}{\partial t^2} = G \frac{\partial^2 u}{\partial z^2} + \eta \frac{\partial^3 u}{\partial z^2 \partial t} \quad (1)$$

In which:

- u = horizontal displacement [m]
- z = depth in (soil) material column [m]
- t = time [s]
- ρ = volumetric mass density of the (soil) material [kg/m^3]
- G = shear modulus of the (soil) material [kN/m^2]
- η = dynamic viscosity of the (soil) material [$\text{kg}/\text{m}\cdot\text{s}$]

The solution of this equation corresponding to a local soil package depends on the thickness, stiffness and damping characteristics of each soil layer. This solution is referred to as the transfer function of the local soil package. It translates bedrock motion characteristics into ground level motion characteristics. (Kramer 1996, Ordóñez 2012)

2.4.3. Nonlinear site-response analysis

Nonlinear site-response analysis actually considers nonlinear, inelastic stress-strain behaviour of the soil package. The equations of motion are numerically integrated in small time steps. At the beginning of each time step there is a feed-back to the stress-strain relationship so that appropriate soil properties for that time step can be found. In this way the site-specific nonlinear inelastic stress-strain relationship is followed by small incrementally linear steps. The finite element programs which can be employed for this can also include the option to calculate site response in the 2D and 3D space. The advantage is that the attenuation of all the different kind of seismic waves can be calculated and that irregularities in the soil space can be accounted for, which should give a more accurate result. The main disadvantage is the higher complexity and longer calculation time. (Kramer 1996, Besseling 2012)

2.5. Seismic structural analysis

At the beginning of this section it was mentioned that a higher performance demand generally requires a structural seismic analysis method with a higher capability. Different ways of categorizing the available analysis methods can be found in literature (e.g. ASCE 1998, USACE 1999, PIANC 2001, USACE 2007, OCDI 2009, POLB 2009, ASCE 2013). In the present study the categorization of (PIANC 2001) will be used because this guideline is the result of an international workgroup while the other guidelines are produced on a national level. According to (PIANC, 2001) the structural seismic analysis methods can be categorized based on level of sophistication and capability as follows:

- Simplified Analysis
“Appropriate for evaluating approximate threshold limit for displacements and/or elastic response limit and an order-of-magnitude estimate for permanent displacements due to seismic loading”
- Simplified Displacement-based Analysisⁱⁱ
“Possible to evaluate extent of displacement/stress/ductility/strain based on assumed failure modes”
- Dynamic Analysis
“Possible to evaluate both failure modes and the extent of the displacement/stress/ductility/strain”

ⁱⁱ It is noted that in (PIANC, 2001) this level of seismic structural analysis is referred to as ‘Simplified Dynamic Analysis’. The author prefers ‘Simplified Displacement-based Analysis’, because while one of the two general methods associated with this level of analysis is indeed simplified dynamic, the other is nonlinear static (see paragraph 2.5.2).

The following paragraphs will give an introduction to these levels of seismic structural analysis.

2.5.1. Simplified analysis

Simplified Analysis (SA) is generally performed for preliminary design and in case of small easily restorable structures also for final design. Depending on the type of structure the two methods in SA approach are pseudo-static method and response spectrum method (PIANC, 2001). The latter was already to some extent treated in paragraph 2.2.1.

2.5.1.1. Pseudo-static method

The general principle of pseudo-static method (or conventional force-balance approach) is that a static force equivalent to the seismic loading is inserted in the force balance calculation of the structure. This equivalent static (inertia) force is basically calculated by multiplying a seismic coefficient with the structural mass (including added mass of soil and water when relevant). This seismic coefficient is equal to a certain design ground acceleration divided by the acceleration of gravity. In formula for both vertical and horizontal earthquake shaking (Kramer 1996, PIANC 2001, NEN-EN1998-5, USACE 2007, NCHRP 2008, Visone 2008, OCDI 2009):

$$F_h = \left(\frac{a_h}{g}\right) W = k_h W \quad (2)$$

$$F_v = \left(\frac{a_v}{g}\right) W = k_v W \quad (3)$$

In which:

- $F_{h\text{ or }v}$ = pseudo-static seismic force in horizontal or vertical direction [kN]
- $a_{h\text{ or }v}$ = design ground acceleration in horizontal or vertical direction [m/s^2]
- g = gravitational acceleration [m/s^2]
- W = mass of the structural system (including added mass) [kg]

The pseudo-static approach is primarily focused on force equilibrium and thus on the sliding or rotational stability of a structure which is treated as a rigid body. The structural analysis is therefore elastic and provides an approximate threshold limit for displacements and/or an elastic response limit. As earlier mentioned no

insight is given in the structural performance (stress and strain states / ductility) after exceeding force equilibrium. Only a crude approximation concerning permanent deformations can be obtained by combining pseudo-static approach with statistical analysis of case history data. Furthermore the method neither accounts for the dynamics of the interacting soil-structure system nor for the characteristics of the ground motion. (PIANC 2001, USACE 2007)

The types of quay wall structures on which pseudo-static approach is generally applied when performing SA are gravity-based structures and sheet-pile structures, i.e. retaining walls. An important aspect in pseudo-static analysis of retaining walls is the calculation of the dynamic earth pressures on the retaining wall which depends on the ability of the wall to yield / move relative to the soil, i.e. whether an active soil state can develop. If not, elastic analysis is applied, i.e. multiplying the seismic coefficient with the soil unit weight times the retaining height squared. If so, the Mononobe-Okabe method, developed by Okabe (1926) and Mononobe & Matsuo (1929), can be used. In this method pseudo-static accelerations are applied on an active (or passive) wedge as defined in static Coulomb (1776) theory. The pseudo-static soil thrust is subsequently obtained from force equilibrium of the wedge. For more background on this topic and corresponding formulas one is referred to Appendix A. Besides the soil thrust (static + dynamic) on the retaining structure also static and hydrodynamic water forces should be taken into account. (Kramer 1996, PIANC 2001, NEN-EN1998-5)

An interesting aspect concerning pseudo-static analysis of retaining walls is the possibility offered by NEN-EN1998-5 to allow a reduction on the seismic loading. This reduction is captured in a factor r through which is seismic coefficient is divided, as can be seen in equation (4):

$$F_h = (k_h/r) \cdot W \quad (4)$$

The reduction factor accounts "for the amount of permanent displacement which is both acceptable and actually permitted by the adopted structural solution. (...) Conceptually, the factor r is defined as the ratio between the acceleration value producing the maximum permanent displacement compatible with the existing constraints, and the value corresponding to the state of limit equilibrium (onset of displacements). Hence, r is greater for walls that can tolerate larger displacements." Thus application of this reduction factor r actually is to some extent application of displacement-based design, i.e. PBD approach. The values for factor r which can be used according to NEN-EN1998-5 are shown in Figure 2.17.

Type of retaining structure	r
Free gravity walls that can accept a displacement up to $d_r = 300 \alpha \cdot S$ (mm)	2
Free gravity walls that can accept a displacement up to $d_r = 200 \alpha \cdot S$ (mm)	1,5
Flexural reinforced concrete walls, anchored or braced walls, reinforced concrete walls founded on vertical piles, restrained basement walls and bridge abutments	1

Figure 2.17: Displacement reduction factors according to NEN-EN1998-5^{iii, iv, v}

ⁱⁱⁱ The product αS is the seismic coefficient in which $\alpha = a_g/g$ and S a soil dependent factor

^{iv} In case of liquefaction susceptibility $r = 1$ should be applied

^v For retaining walls higher than 10 m, 1D site response analysis and an average value for a_g along the height of the wall is recommended.

The contradiction between the $r = 1$ demand for flexural anchored retaining walls and the allowed permanent displacement when applying PBD for these walls according to Figure 2.15 (PIANC, 2001) is noted.

2.5.1.2. Response spectrum method

In paragraph 2.2.1 it was described that (elastic) response spectra are obtained by applying an input ground motion to a number of Single Degree Of Freedom (SDOF) oscillators which all have the same damping ratio (typically $\xi = 0.05$, which stands for 5% critical damping) and a different natural frequency / period. The maximum response of each oscillator to the input motion is plotted against its natural frequency or period. An impression of this process is provided in Figure 2.18.

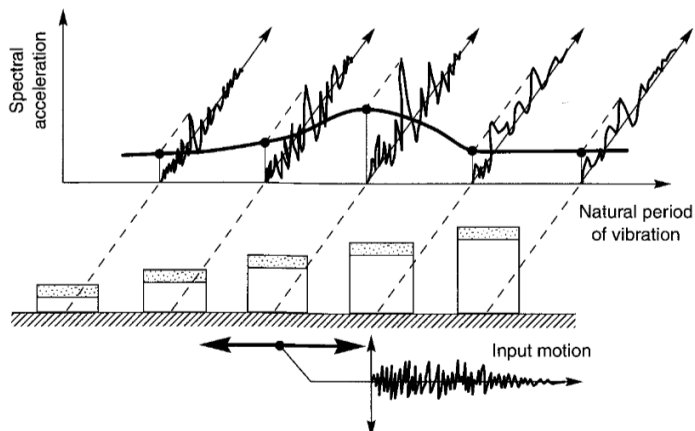


Figure 2.18: The elastic response spectrum obtained by plotting the spectral accelerations against the periods of vibrations of the SDOF system (Kramer, 1996)

Application of these response spectra for structural response analysis is a common method in earthquake engineering associated with buildings, i.e. constructions which are generally on top of the ground. Equivalently in SA for port structures the response spectrum method is generally applied for pile-deck structures and cranes on quay walls. (ASCE 1998, PIANC 2001, NEN-EN1998-1, NEN-EN1998-5)

Many codes and standards provide different design elastic response spectra for different soil classifications where the response per soil classification generally is based on the soil characteristics of the upper 30 meters of the soil profile and 5% critical damping. Some codes provide guidance for a higher %-critical damping through which the design response spectrum can beneficially be lowered. Another interesting possibility offered by e.g. NEN-EN1998-1 is the lowering of response spectra by accounting for ductile behaviour via the factor q (which has, as one would expect, a low value for e.g. a masonry structure and a high value for e.g. a steel structure). Response spectra per soil classification as given by NEN-EN1998-1 are shown in Figure 2.19.

The response spectra are used to assess structural response by entering the spectrum at the natural period of each significant mode of vibration of the structure in order to obtain the amplitude of response of that mode. The obtained response amplitudes of the significant modes are (together with the mode shapes and the modal participation factors) used to compute the maximum response at any location in the structure for all significant modes. Approaches for evaluating and combining the maximum responses are available to account for the occurrence of the maximum responses of each mode at different times. (ASCE 1998)

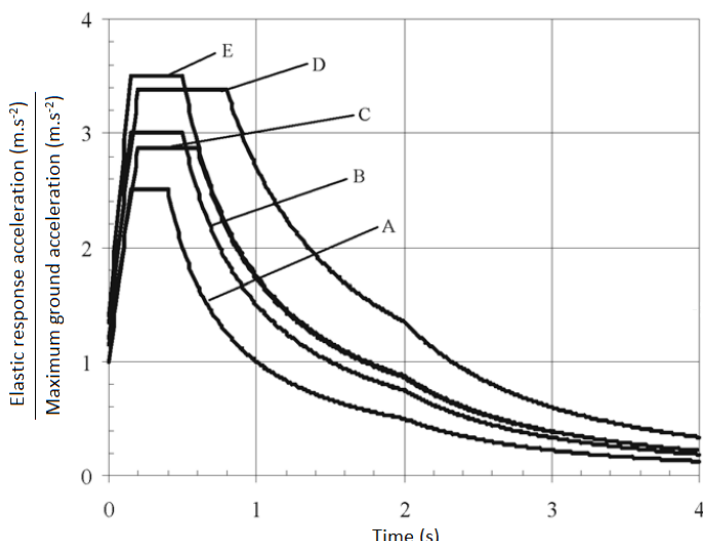


Figure 2.19: Elastic response spectra for different soil classifications according to NEN-EN1998-1

2.5.2. Simplified displacement-based analysis

According to (PIANC, 2001) Simplified Displacement-based Analysis (SDA) is appropriate for preliminary design in case of structures with critical or primary importance and for final design in case of more ordinary structures. SDA is considered to be too sophisticated for small easily restorable structures. Depending on the type of structure the two main methods in SDA approach are Newmark sliding block analysis (or more generally referred to as permanent-displacement analysis) and Pushover analysis combined with response spectrum method. (PIANC 2001)

2.5.2.1. Newmark sliding block analysis

The types of quay wall structures on which permanent-displacement analysis is generally applied when performing SDA are gravity-based structures and sheet-pile structures, i.e. retaining walls. The method assumes a failure mode (sliding) and can be employed to evaluate the amount of displacement. It is a tool for displacement-based design. (PIANC, 2001)

In traditional Newmark (1965) analysis a structure or soil body under seismic loading is modelled as a rigid block which starts to move (accelerate) along its base when the critical (yield) acceleration is exceeded. It is analogous to the well-known model of a block on a slope which starts to slide when the angle of the slope increases to such an extent that the gravity force parallel to the slope exceeds the resisting friction force. (Elms 2000, PIANC 2001, Jibson 2011)

The earthquake ground motion input for permanent-displacement analysis is typically represented by time-histories (accelerograms) at ground level. These are obtained by performing e.g. equivalent linear site-response analysis on recorded (or artificially generated) accelerograms at bedrock level. The critical (yield) or threshold acceleration is determined from limit-equilibrium of the soil-structure system. By plotting the threshold acceleration in the time-history at ground level and integrating the excess acceleration twice, the permanent displacement due to sliding is obtained. This procedure is presented in Figure 2.20. It is noted that this commonly applied procedure is one-dimensional (longitudinal excitation) while research has indicated that lateral excitation can produce significant additional displacement. (Elms 2000, PIANC 2001, Jibson 2011)

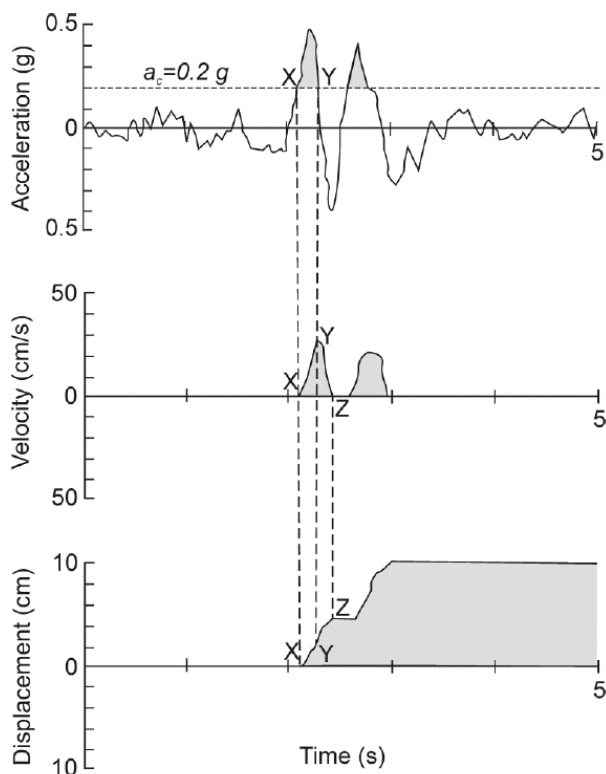


Figure 2.20: Newmark analysis procedure, adapted from (Jibson, 2011)

A key assumption of the traditional Newmark method is that the sliding object is treated as a rigid-plastic body, i.e. that the body does not deform internally, does not displace permanently at seismic loads below the critical acceleration level and that it, in case of displacement, deforms plastically at constant stress along a discrete basal shear surface. Other simplifying assumptions are that similar values are taken for the static and dynamic shearing resistance of the soil; that the critical acceleration remains constant during the analysis (by assuming strain independency); and that 'upslope' displacement is prohibited. Thanks to continuous research efforts during the last 50 years these latter three simplifications can be discarded in more recent applications of Newmark analysis. But another simplifying assumption, which cannot be discarded in permanent-displacement analysis, is that the effects of dynamic pore pressure are neglected. This assumption is considered generally valid for overconsolidated clay and very dense or dry sands though. (Jibson, 2011)

Another result of research efforts for the improvement of traditional Newmark analysis is that next to rigid-block analysis also decoupled and coupled Newmark analysis have become available for systems containing a soil body. In decoupled analysis a dynamic-response analysis of the soil body is performed without assuming a failure plane and the resulting time-history is successively used as input for a rigid-block analysis by which the permanent displacement is computed. In this way the effect of the dynamic response on the permanent sliding is estimated. It does not account for the effects of sliding displacement on the ground motion though. In coupled Newmark analysis one can account for the effect of plastic sliding displacement on the ground motions because the dynamic response of the sliding mass and the permanent displacement are modelled together in this case. For decoupled analysis the method of Makdisi & Seed (1978) is currently most-widely applied and for coupled analysis Bray & Travasarou (2007) have developed an empirical relation. (Jibson, 2011)

2.5.2.2. Pushover analysis

In Pushover Analysis (PA) the ductile behaviour of a structure is modelled by applying an incrementally increasing load, corresponding to the primary mode shape, up to failure of the structure or exceedance of limiting plastic strains. During the analysis plastic hinges are introduced to account for non-linear behaviour. This nonlinear static analysis provides insight in post-elastic behaviour of a structure on a local level. Permanent displacement capacity of a structure is obtained and it is a particular useful tool for evaluating preferred yielding sequences of structures (see Figure 2.15 and Figure 2.16). An example of a pushover curve and plastic hinge sequence resulting from PA are shown in Figure 2.21. (USACE 2007, POLB 2009, ASCE 2013, RHDHV 2014)

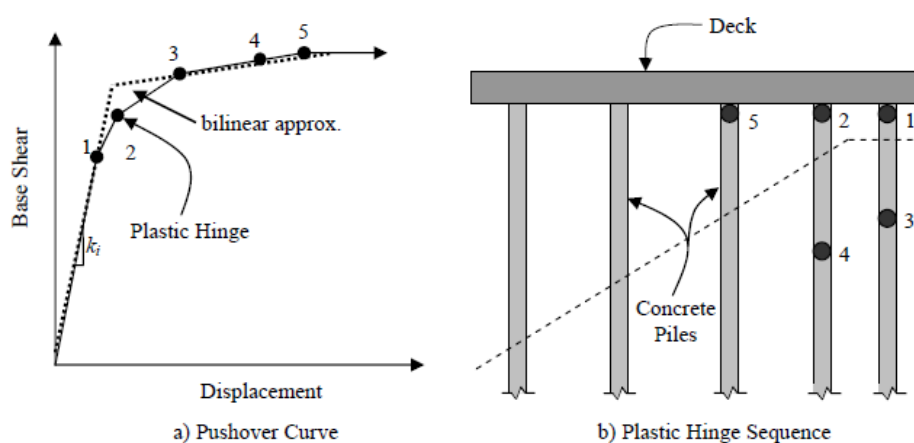


Figure 2.21: Pushover curve and plastic hinge sequence of a pile-deck structure (POLB, 2009)

The actual displacement of e.g. a deck, when subjected to a certain seismic motion, is obtained by plotting a response spectrum and capacity spectrum together in an acceleration-displacement format. The acceleration-displacement response spectrum is a translation of the familiar acceleration-period response spectrum and the capacity spectrum is a translation of the pushover curve. The spectra cross each other at the performance point or actual displacement. This point has to be found iteratively by shifting the elastic response spectrum.

This shifting is required to account for ductile (i.e. plastic) material behaviour in the structure. An example of such a procedure is presented in Figure 2.22. (Pscharis, RHDHV 2014)

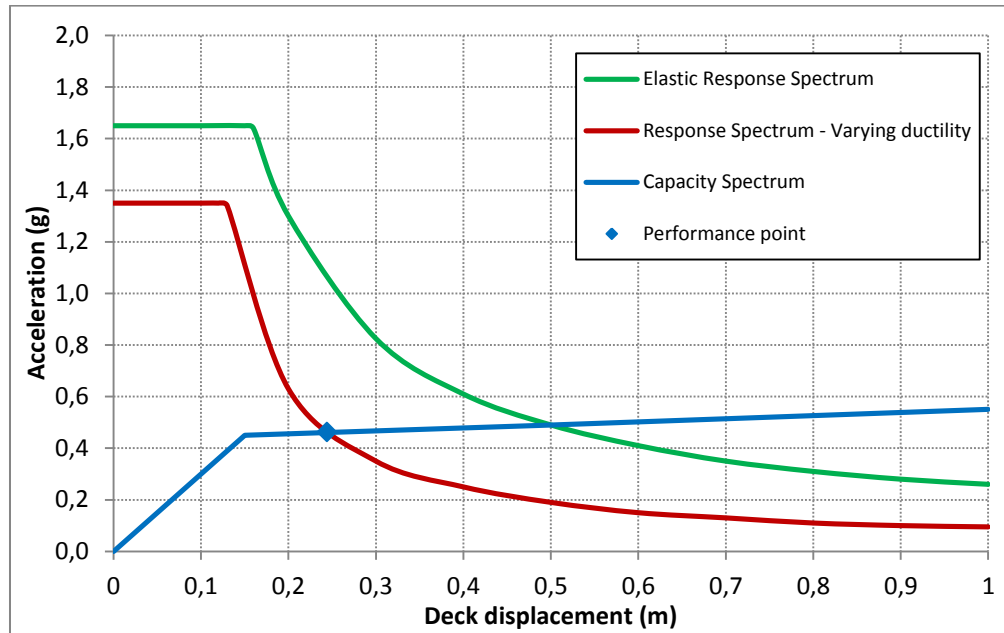


Figure 2.22: Bilinear capacity spectrum and response spectra plot for determining structural performance, adapted from (RHDHV, 2014)

According to (PIANC, 2001) PA is appropriate for pile-deck structures and cranes on quay walls. Furthermore it is a commonly used method in seismic analysis of buildings. However the performance based approach recommended for anchored sheet-pile quay walls in (PIANC, 2001) (see paragraph 2.3.2) suggests that PA can also be a useful tool for displacement-based design of retaining wall structures. In (Visone, 2008) PA is actually employed for seismic analysis of retaining walls.

2.5.3. Dynamic analysis

According to (PIANC, 2001) Dynamic Analysis (DA) is only appropriate for final design of structures of critical or primary importance. It can therefore be a relevant tool for final design of quay wall structures. In DA Finite Element (FE) and Finite Difference (FD) methods are generally employed. These numerical methods offer the following modelling possibilities (PIANC, 2001):

- Geotechnical modelling: (equivalent) linear, nonlinear, 2D, 3D
- Structural modelling: linear, bilinear, nonlinear, 2D, 3D

A significant aspect in the dynamics of a soil-structure system like a retaining wall or a deck on piles is the interaction of the structure with the surrounding and underlying soil, particularly at locations with predominantly soft soil materials. This effect, Soil Structure Interaction (SSI) can be included in FEM and FDM calculations. The two ways of including SSI is through a separate (uncoupled) or integrated (coupled) approach. Coupled DA considers soil and structure dynamics simultaneously using one model. Uncoupled DA uses different models for soil and structure dynamics separately and iteratively reruns each model based on the results of the other until the responses of soil and structure match each other. This uncoupled DA procedure is schematized in Figure 2.23. The complete seismic response of the interacting soil-structure system is obtained by adding the free field seismic motion acting on the foundation (kinematic loading) and the structural seismic motion acting on the soil (inertial loading). The seismic motion input for DA consists of time-histories applied at the base (bedrock) of the analysis domain chosen for the soil-structure system. (ASCE 1998, PIANC 2001, USACE 2007)

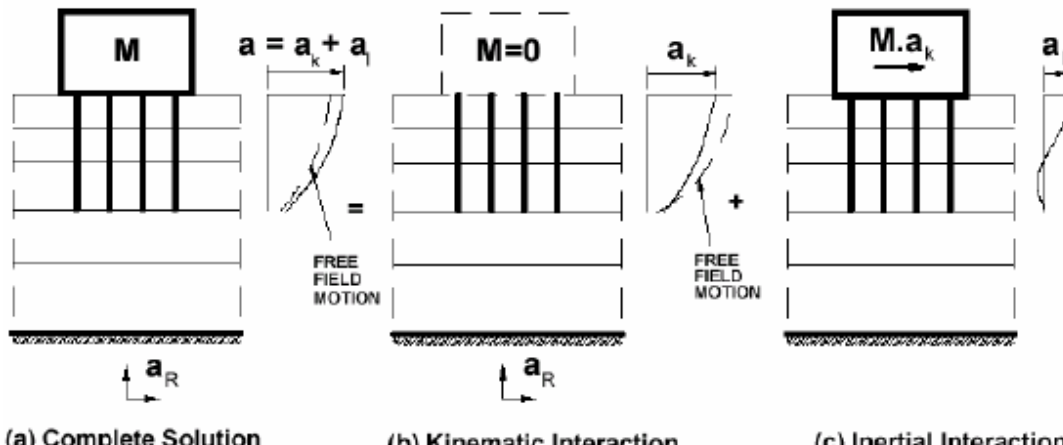


Figure 2.23: The principle of uncoupled DA accounting for SSI (USACE, 2007)

The sensitivity of the response of the soil-structure system to the seismic input motions is recognized to be high. This is why many codes prescribe that a number of different time-histories should be used as input. Furthermore it is of importance that prior to performing any kind of (dynamic) analysis on a soil-structure system the seismic response of the used numerical model should be tested. A comparison between the model results and available field measurement results or theoretical solutions of the (dynamic) problems should be made in order to validate the modelling techniques and corresponding model parameters. Such validation studies on the response of FE models are e.g. performed for PLAXIS. (Brinkgreve 2010, Besseling 2012, Dey *et al.* 2013)

In section 2.4 (site-response analysis) already some remarks were made on numerical time integration of a nonlinear soil system. For numerical integration many different techniques are available. A fundamental classification is the explicit or implicit character of a numerical integration technique. In DA of soil-structure systems implicit schemes are generally preferred because of better stability properties. A commonly applied family of implicit numerical integration schemes is the Newmark (1959) family developed for both blast and seismic loading. It has been widely applied for dynamic analysis and has been modified and improved by different researchers. The standard equations of the numerical integration scheme (USACE 2003, Visone 2008, PLAXIS 2014-4):

$$\mathbf{u}^t = \mathbf{u}^{t-dt} + dt\dot{\mathbf{u}}^{t-dt} + \left(\left(\frac{1}{2} - \alpha_N \right) \ddot{\mathbf{u}}^{t-dt} + \alpha_N \ddot{\mathbf{u}}^t \right) dt^2 \quad (5)$$

$$\dot{\mathbf{u}}^t = \dot{\mathbf{u}}^{t-dt} + \left((1 - \beta_N) \ddot{\mathbf{u}}^{t-dt} + \beta_N \ddot{\mathbf{u}}^t \right) dt \quad (6)$$

The Newmark coefficients, α_N and β_N , determine the accuracy and stability of the numerical integration process. By following this scheme and satisfying the dynamic equilibrium equation at the end of every time step the acceleration ($\ddot{\mathbf{u}}$), velocity ($\dot{\mathbf{u}}$) and displacement (\mathbf{u}) at every time step are determined from the acceleration ($\ddot{\mathbf{u}}^{t-dt}$), velocity ($\dot{\mathbf{u}}^{t-dt}$) and displacement (\mathbf{u}^{t-dt}) at the end of the previous time step. The dynamic equilibrium equation satisfied at each time step (USACE 2003, Visone 2008, PLAXIS 2014-4):

$$\mathbf{M}\ddot{\mathbf{u}}^t + \mathbf{C}\dot{\mathbf{u}}^t + \mathbf{K}\mathbf{u}^t = \mathbf{F} \quad (7)$$

The mass (**M**) and stiffness (**K**) matrices of the soil-structure system in this equation of motion are relatively easy to estimate. Determining the damping (**C**) matrix of the soil-structure system is more problematic. This is due to the different sources of damping with different physical backgrounds which can be relevant for seismic analysis (USACE 2003, Spijkers *et al.* 2006, Besseling 2012):

- Structural material damping
- Structural friction damping
- Soil material damping in saturated permeable soils
- Soil material damping in dry and impermeable soils
- Soil radiation damping
- Hydrodynamic damping
- Local damping due to strong nonlinear soil behaviour near the structure

Without further elaboration on the different types of damping at this point the summation provides an idea of the complexity of the dynamics of a soil-structure system. Mainly due to computational limitations and a gap in physical understanding an equivalent critical viscous damping percentage for the system (see also 2.4.2.1) is often defined in practice in which the different damping effects are covered by approximation. Setbacks concerning nonlinearity and frequency (in)dependency of damping types are associated with this practical solution. (Spijkers *et al.* 2006, Besseling 2012)

2.6. Trends in seismic design of quay structures

In this section some trends in seismic design of quay structures on global scale are discussed as indicated by the availability of specific literature and as observed by employees of RHDHV who are involved in seismic analysis and design of port structures.

In general it is observed that the pile-deck structure is the type of quay structure which is most commonly applied in areas characterized by high seismicity (e.g. the Pacific Coast of the Americas and South-East Asia). This is due to the favourable seismic behaviour of the structure. By designing the pile-deck construction is such a way that the deck is much stiffer than the (vertically placed) piles a structural system is developed that efficiently dissipates seismic energy through elastic and controllable plastic deformation of the piles. In retaining wall systems generally no structural elements are included that can dissipate seismic energy to the same extent by deformation. Therefore the dimensions of these constructions and associated costs increase rapidly with increasing seismic loading. In Japan, a country associated with high seismicity, very heavy sheet pile type quay structures are applied but this can be explained by the nearby presence of their heavy industry and corresponding experience. Apart from the Japan example the pile-deck structure is generally the only quay type applied in new design in areas with high seismicity, as is also indicated by new American seismic port structure codes (POLB 2009, ASCE 2013) focusing only on PBD of pile-deck structures.

Retaining wall structures are found on a larger scale in areas which experience lower seismicity or traditionally were not associated with earthquakes at all (e.g. Province of Groningen). Sheet pile quay walls are commonly applied in such reasons. A constraint for gravity-based structures is often the strength of upper soil deposits and the availability of construction material (e.g. solid rock). In the Middle East region these constraints are for instance positively fulfilled which is the reason why gravity-based quay structures are applied to a larger extent there.

3. Research description

General theoretical background and observed trends serve as a base for defining a research focus. In section 3.1 a problem definition is presented from which the general research question is deduced in section 3.2. An outline of the research methodology for answering the research question is described in section 3.3.

3.1. Problem definition

The observed trend in seismic quay design is that gravity and sheet pile type structures are associated with areas with zero to low seismicity while pile-deck structures are generally the preferred solution in areas with higher seismicity. This can be explained by the more favourable seismic performance of pile-deck structures compared to retaining walls. A more quantitative view of this trend is presented in Figure 3.1.

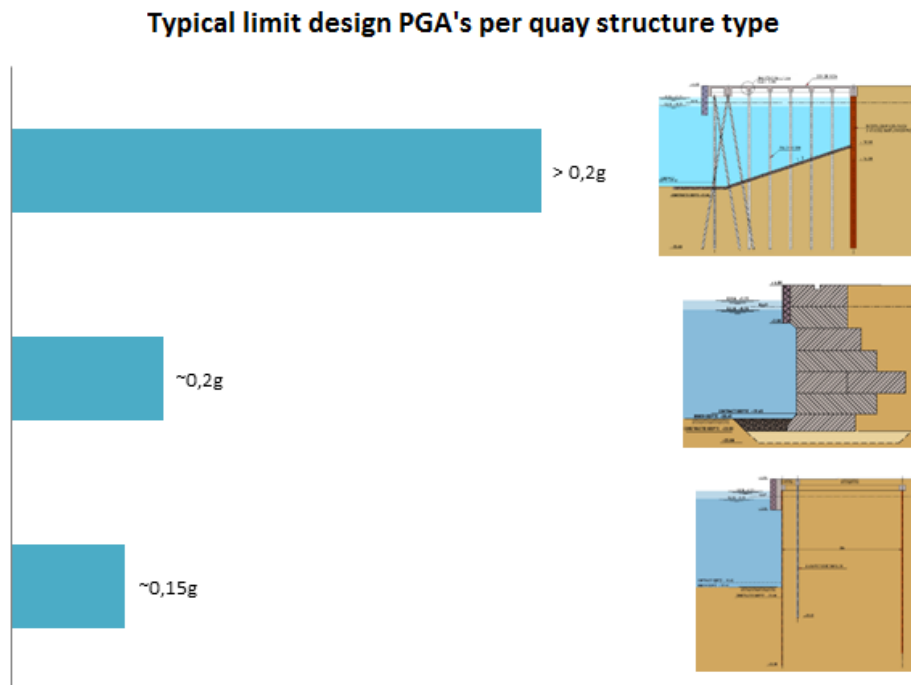


Figure 3.1: Typical limit design PGA's corresponding to different quay structure types (derived from conversations with D.J. Peters and A. Wiggers of RHDHV)

The limit design PGA's in the figure are estimated values from practice. In case of new design, sheet pile walls are applied up to a seismic demand of approximately 0.15g m/s^2 and gravity-based walls up to a somewhat higher value. Seismic demands higher than these values (i.e. design PGA's $> 0.2\text{g m/s}^2$) generally result in application of pile-deck structures.

As a result of the above it is experienced that already during the preliminary phase of seismic quay design, retaining wall structures are excluded when seismic demand becomes more significant. This is certainly not always desirable because retaining walls generally require less space than pile-deck structures, while space can be an important design requirement. Therefore the question arises whether this exclusion is always necessary and correct, or in other words, to what extent retaining walls can withstand seismic loading outside the typical 0.15g range.

The trend presented in Figure 3.1 is in line with the observation in literature that PBD methodology is developed to a significantly larger extent for pile-deck structures than for retaining walls, especially anchored sheet-pile walls. Guidelines for design of sheet pile quay walls are currently predominantly based on pseudo-static design. The limitations and corresponding conservativeness of this design methodology were already mentioned but an illustrative example of this can be obtained by comparing literature.

According to NEN-EN1998-5 no reduction on seismic load accounting for permanent displacement capability should be applied in pseudo-static design of flexural anchored retaining walls ($r = 1$). In contrast (PIANC, 2001) allows for a certain amount of permanent horizontal displacement at the top of the sheet pile wall corresponding to the serviceability performance level. An upper horizontal displacement value of 1.5% of the sheet pile retaining height is proposed (i.e. 150 mm in case of a retaining height of 10 m). Furthermore, based on 110 case histories, (Kitajima & Uwabe, 1979) provide permanent displacement values corresponding to different degrees of damage of anchored sheet pile walls and an upper bound envelope for horizontal seismic coefficients allowing a seismic load reduction in case that $a_{max} > 0.2g$. On average this comes down to a reduction factor on the seismic load of $r = 1.67$. (Ebeling & Morrison 1992, ASCE 1998, Nozu et al. 2004).

From the observed trends in seismic quay design and the notion of limited available practical guidance for applying PBD methodology in case of anchored sheet pile quay walls a focus on this type of quay wall is deduced. Different references suggest that for anchored sheet pile quay walls a certain level of permanent deformation is allowable and therefore less conservative simplified design. By doing so it may result in a better evaluation of the quay types in preliminary design phase. In addition it can possibly prevent unnecessary negative advice on the performance of existing sheet pile quay walls on which seismic analysis is performed.

3.2. Research question

Practice shows that it is desirable to consider sheet pile quay walls in a less conservative way in (preliminary) seismic analysis and design (and it is noted that literature provides starting points for this). It results in the following general research question:

“Can (simplified) seismic design methodologies for anchored sheet pile quay walls be improved by considering deformation behaviour?”

The general research question yields a number of sub-questions which are associated with topics that are treated during research:

- Which research papers on seismic behaviour of flexural retaining walls are available?
- Which software can effectively be applied for the different levels of seismic analysis?
- Which soil models can be applied in the different levels of seismic analysis?
- To which extent is a reduction factor on the seismic load in pseudo-static analysis allowable?
- What are possible seismic deformation and failure mechanisms of an anchored sheet pile wall?
- How do anchor characteristics influence the deformation mechanisms?
- For simplified dynamic analysis, how can the critical acceleration of an anchored sheet pile wall be determined?
- How can traditional permanent-displacement analysis be applied on an anchored sheet pile wall?
- What is the influence of wall height, i.e. the effect of seismic wave amplification along the wall in case of e.g. $H_{wall} > 10$ m?
- What are characteristic values for upper limits of allowed residual deformation and corresponding (structural) damage?

3.3. Outline of the research methodology

In order to find answers to the general research question and sub questions a research methodology is deduced. The outline of the methodology, consisting of five steps, is given in this section. An overview of the complete research process is provided by the flowchart in Figure 3.2. The general objective of the research is to obtain more insight in the seismic behaviour of anchored sheet pile quay walls and the performance of seismic analysis methods in order to give recommendations on the application of simplified seismic analysis methodology for this type of quay wall.

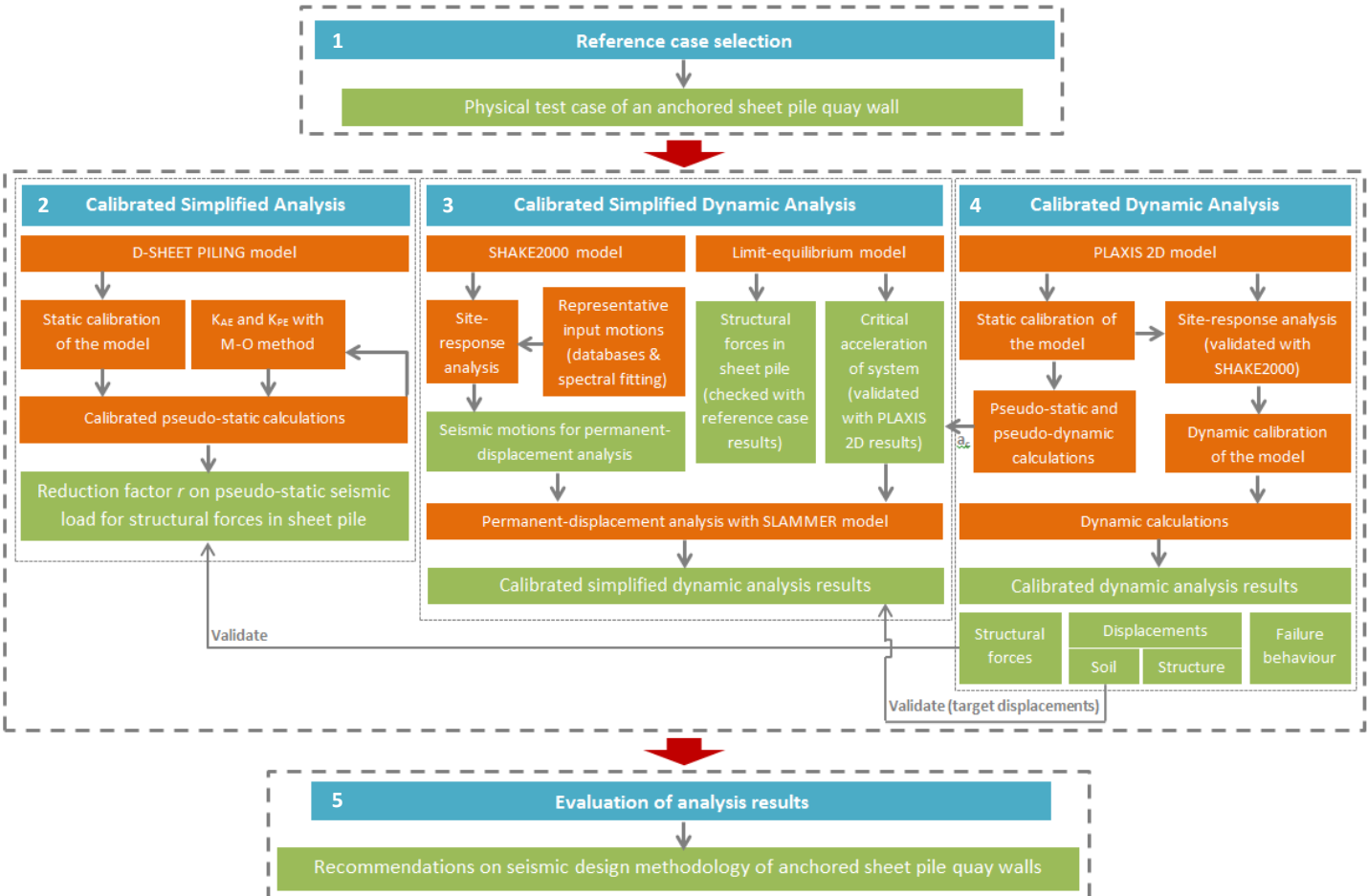


Figure 3.2: Flowchart of the research methodology

In the following the research steps are shortly explained. More extensive elaboration on and execution of the research steps can be found in chapters 4 (reference case), 5 (seismic analysis) and 6 (evaluation).

3.3.1. Step 1: Reference case selection

The selection of a representative case study with sufficient qualitative data from physical testing is an essential base for gaining insight in seismic behaviour of an anchored sheet pile quay wall. In this way more meaningful model calculation results can be obtained because a connection with reality is maintained. Model results are compared with physical results; ‘checking models with models only’ is prevented. A suitable reference case is selected from a large number of papers. A suitable paper considers a basic anchored sheet pile quay wall from a field case and/or performs centrifuge / shaking table testing and provides sufficient information on test setup, input signal, parameters and qualitative and quantitative test results. As a result the conference paper “Evaluation of the Seismic Performance of Dual Anchored Sheet Pile Wall” by Higuchi et al. (2012) is selected.

3.3.2. Step 2: Simplified analysis

After the selection of a suitable reference case the next step is performing calibrated simplified analysis (SA). The general approach in this research step is:

- Setting up a calibrated D-SHEET PILING model
- Calculating pseudo-static input parameters for the model
- Performing pseudo-static calculations with the model
- Comparison of calculation results with reference case measurement results
- Iteratively obtaining a reduction factor on the seismic load that creates a match between calculation and reference case results

Traditional iterative pseudo-static hand calculation procedure is described in e.g. (Ebeling & Morrison, 1992). It is a process of determining internal forces and dimensions of the anchored sheet-pile structure corresponding to static and seismic loading and which outputs an anchored sheet pile design which does not experience displacement under the pseudo-static seismic design load. More suitable for a calibrated comparison with the reference case is the application of D-SHEET PILING software (Deltares Systems). This is due to the positive characteristic that it gives bending moments, shear forces and displacements of the anchored sheet pile structure as output and an insight in the amount and distribution of actively and passively mobilised soil. Therefore it is a deliberate choice to apply the widely used D-SHEET PILING software for this step of the research methodology. For background information on D-SHEET PILING one is referred to Appendix B, section B.1.

3.3.3. Step 3: Simplified dynamic analysis

Calibrated simplified dynamic analysis (SDA) starts where the calibrated pseudo-static analysis stops. It gives the possibility to evaluate the extent of permanent displacement after exceeding limit force equilibrium, based on an assumed failure mode. The general approach in this research step is:

- Computing the critical acceleration with a (validated) analytical limit-equilibrium model developed for the reference case setup
- Checking the ability of the limit-equilibrium model to compute structural forces in the sheet pile wall
- Performing calibrated site-response analysis with dedicated software SHAKE2000
- Performing permanent-displacement (i.e. Newmark) analysis with dedicated software SLAMMER, using the critical acceleration obtained with the limit-equilibrium model and accelerograms obtained from the site-response analysis
- Comparison of SLAMMER calculation results with the reference case target displacements

In agreement with (PIANC, 2001) that Newmark-analysis needs to be applied for retaining wall structures, the general approach found in papers for investigating the failure behaviour of retaining walls under seismic loading, is application of time-history analysis. Examples are (Towhata & Islam, 1987), (Neelakantan *et al.*, 1992), (Richards & Elms, 1992), (Zeng & Steedman, 1993) and (Conti *et al.*, 2012). (Conti *et al.*, 2012) reason that it is evident that the traditional Newmark rigid-sliding-block schematisation is not suitable for embedded retaining walls and suggest two agreeing papers that propose failure mechanisms suitable for anchored sheet pile walls, i.e. (Neelakantan *et al.*, 1992) - rigid rotation of the wall around anchor point in case of a sufficiently long anchor and (Towhata & Islam, 1987) - translation mechanism of wall and retained soil wedge. For cantilever walls (Conti *et al.*, 2012) propose the use of Blum method.

The goal of the approach presented in this paragraph is to derive a for SDA useable limit-equilibrium model of an anchored sheet-pile quay wall corresponding to a realistic failure mechanism. From the limit-equilibrium the critical acceleration is computed. Furthermore it is attempted to develop the model to such an extent that also structural forces in the sheet pile during the limit-equilibrium state can be estimated with it.

The calculated critical acceleration, in combination with representative accelerograms, will be used in permanent-displacement analysis. Site-response analysis is needed to translate input (bedrock) motions into representative accelerograms, located in the centre of gravity of the system's failure wedge. According to (Kavazanjian, 2013) the strong motions used in permanent-displacement analysis of embankments have to be considered at this particular location.

SHAKE2000 (GeoMotions, LCC) is dedicated software for performing amongst others equivalent linear 1D site response analysis and four variants of permanent-displacement analysis. SLAMMER (USGS) is software especially developed for carrying out the different available variants of permanent-displacement analyses for landslides (both rigorous and empirical). For background information on SHAKE2000 and SLAMMER one is referred to Appendix B, section B.2.

3.3.4. Step 4: Dynamic analysis

The final analysis step employs the most sophisticated level of modelling, dynamic analysis (DA). This type of analysis is not restricted to previously assumed failure mechanisms. It will be used to check SA and SDA results and to model the overall seismic failure behaviour of the anchored sheet pile wall. The general approach in this research step:

- Setting up a calibrated PLAXIS 2D model
- Performing static calculations with the model
- Determining the reference case critical acceleration with the model
- Performing dynamic calculations with the model
- Comparison with results from SA and SDA
- Comparison with results from reference case conditions

Calibrated dynamic analysis is necessary to check the SA and SDA results, validate the developed limit-equilibrium model from step 3 and to create insight in the seismic failure behaviour of the anchored sheet pile quay wall under consideration. The combination of the obtained results must lead to a better understanding of the performance of the soil-structure system and the ability to propose improvements for simplified seismic design methodologies.

Finite element software must be applied for dynamic analysis. Examples of such software are PLAXIS code (developed in The Netherlands), FLAC code (developed in the U.S.) and FLIP code (developed in Japan). Applying PLAXIS code for FE soil system modelling is common practice in The Netherlands, but also in e.g. Italy. Direct knowledge and experience with PLAXIS is available nearby. Furthermore different PLAXIS validation studies are carried out on seismic response of PLAXIS code and dynamic calculation results of the code are considered to be reasonably good, (Brinkgreve *et al.* 2007, Visone 2008, Besseling 2012, Dey *et al.* 2013). Therefore PLAXIS code will be used for the present study. More specifically, in order to prevent extensive modelling difficulties, PLAXIS 2D (instead of 3D) will be adapted. The expectation is that PLAXIS 2D will generate output which adds sufficient value within the scope of the present study. For background information on PLAXIS 2D one is referred to Appendix B, section B.3.

3.3.5. Step 5: Evaluation of analysis results

The research methodology is concluded with the evaluation of the analysis results by means of a discussion. From this evaluation the conclusions and recommendations are deduced and their validity discussed. In this way answers to the research question provided.

4. Reference case

In this chapter the first step of the research methodology is discussed. It concerns the selection and definition of a suitable reference case. Figure 4.1 shows the location of the current step within the research process.

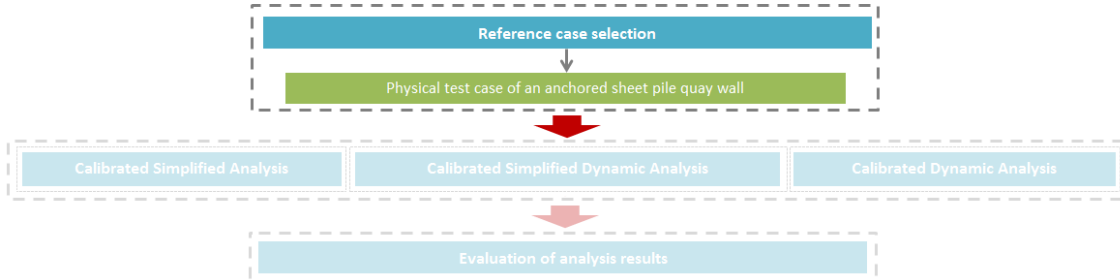


Figure 4.1: Step 1 of the research methodology: selecting a reference case

4.1. Reference case selection

The selection of a representative case study with sufficient qualitative data from physical testing is an essential base for gaining insight in seismic behaviour of an anchored sheet pile quay wall. A suitable reference case is found after consulting a large number of papers available on Scopus, Web of Science, Google Scholar, Springer, etc. It is the conference paper "*Evaluation of the Seismic Performance of Dual Anchored Sheet Pile Wall*" by Higuchi et al. (2012). It is suitable because it considers a basic anchored sheet pile quay wall, performs centrifuge / shaking table testing and provides relevant information on test setup, input signal, parameters and qualitative and quantitative test results.

The paper was presented on the 15th World Conference on Earthquake Engineering (2012) and published by Higuchi S., Miki K. & Nakamura Y. (OBAYASHI Co., Japan), Morikawa Y. & Sugano T. (Port and Airport Research Institute, Japan), Kikuchi Y. (Tokyo University of Science, Japan), Hoshino M. (Japan Port Consultants, Ltd., Japan) and Higashiyama K. (Tohoku Regional Development Bureau, Ministry of Land, Infrastructure, Transport and Tourism, Japan). In the paper the seismic behaviour of a sheet pile quay wall is investigated in case it has one anchor and in case it is dual anchored. Introducing an additional anchor at a lower level of the sheet pile wall has the goal to reduce bending moments in the sheet pile wall and tension forces in the original anchor. Such a solution can e.g. be applied when seismic resistance of an existing quay wall must be improved.

The authors firstly conduct centrifuge experiments with a scale model (derived from an existing quay wall) to investigate and compare the seismic behaviour of the single and the dual anchored sheet pile quay wall. Furthermore 2D effective stress analyses are conducted with the finite element model FLIP to investigate its performance compared to the experiment. Closing off the positive performance of a dual anchored sheet pile quay wall is demonstrated with a field example, i.e. a dual anchored quay wall which survived the 2011 Great East Japan Earthquake.

4.2. Reference case definition

Relevant for the present research methodology is the behaviour of the centrifuge model of the single anchored sheet pile quay wall (the dual anchored model will not be considered). This section elaborates on the reference case single-anchor model setup, testing procedure and centrifuge test results.

4.2.1. Model setup: geometry and parameters

A conceptual overview of the anchored sheet pile quay wall model is shown in Figure 4.2. The dimensions of both the real field and scaled centrifuge model are provided in the figure. The scale is 1:30. The overall dimensions of the field model are $L_m = 57$ m (scaled to 1900 mm), $B_m = 12$ m (400 mm) and $H_m = 21$ m (700 mm). The water depth is 9.5 m (317 mm). The total height of the sheet pile wall is 15 m (500 mm) consisting of retaining height $H_{wall} = 12.5$ m (417 mm) and embedment depth $D_{wall} = 2.5$ m (83 mm). The anchoring consists

of a horizontal tie rod, located 1.5 m (50 mm) beneath the top of the wall, and batter piles, located 12 m (400 mm) behind the wall. Figure 4.2 furthermore provides an overview of the measurement devices used in the tests and their locations in the model. (Higuchi *et al.*, 2012)

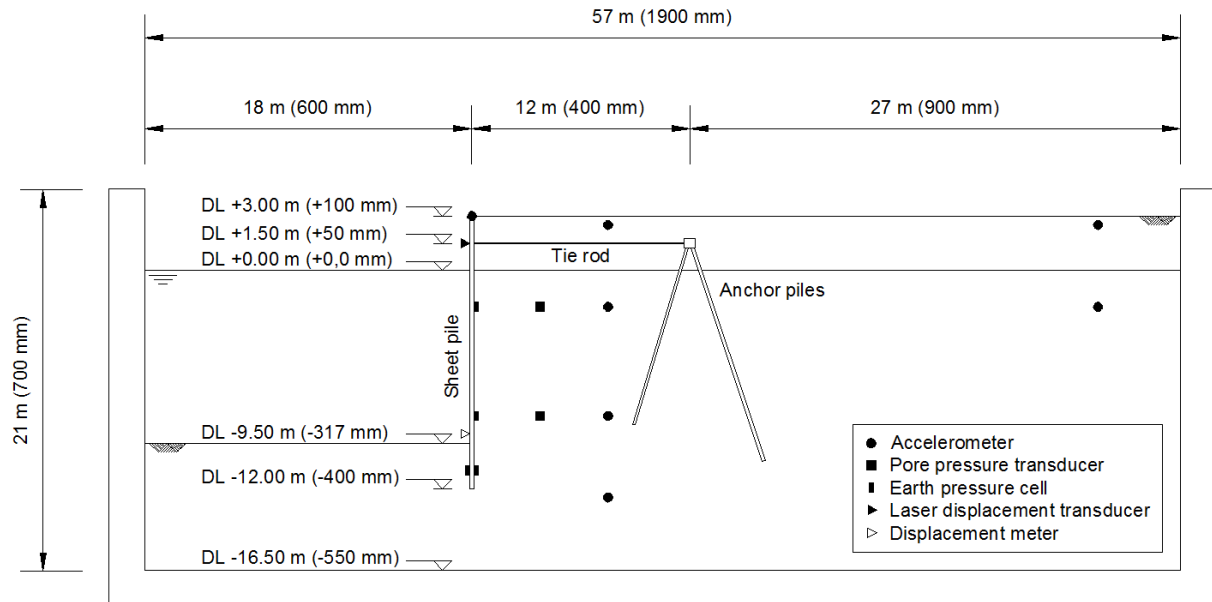


Figure 4.2: Conceptual overview of the single anchored sheet pile quay wall model, showing both field and centrifuge (scale) model geometry, adapted from (Higuchi *et al.*, 2012)

The characteristics of the structural elements (for both the field model and the scale model) are summarized in Table 4.1. The scaled dimensions of the structural elements were determined according to the similitude shown in Table 4.2.

Table 4.1: Summary of modelling structural elements, adapted from (Higuchi *et al.*, 2012)

Structural element	Field model (existing structure)	Centrifuge scale model
Sheet pile	Sheet pile VL h = 200 mm	Thin steel sheet (wave form) h = 67 mm
Anchor pile	Steel H-beam 388 mm x 402 mm x 15 mm x 15 mm	Steel bar front: 8x10 mm ² ; back: 13x13 mm ²
Anchor rod	Tie rod φ42 mm	Steel rod φ3 mm
Anchor spacing	1.5 m	50 mm

Table 4.2: Similitude of the centrifuge (30g), adapted from (Higuchi *et al.*, 2012)

Items	Symbol	Similarity ($N_{sf} \cdot g$)	Scaling under 30g centrifugal gravity
Length	l	$1/N_{sf}$	1/30
Density	ρ	1	1
Strain	ϵ	1	1
Acceleration	a	N_{sf}	30
Velocity	v	1	1
Displacement	u	$1/N_{sf}$	1/30
Stress	σ	1	1
Time	t	$1/N_{sf}$	1/30
Frequency	f	N_{sf}	30
Bending stiffness	EI	$1/N_{sf}^4$	$1/30^4$
Axial stiffness	EA	$1/N_{sf}^2$	$1/30^2$

The following is noted about the scaling of the structural elements:

- Sheet pile: equivalent in bending stiffness
- Batter anchor pile: equivalent in the circumference (axial stiffness of the soil-pile system)
- Tie rod: equivalent in the axial stiffness (area)

Shake table tests on the scale model are conducted while simultaneously undergoing 30g centrifugal gravity, in order to simulate soil stress conditions corresponding to field dimensions. The field soil condition is assumed stiff by the authors so in the scale model coarse silica sand ($D_{50} = 1.2$ mm) is used and compacted to a relative density $RD = 80\%$ ($\rho_s = 2\text{ g/cm}^3$). A photo of the model during preparation is shown in Figure 4.3.

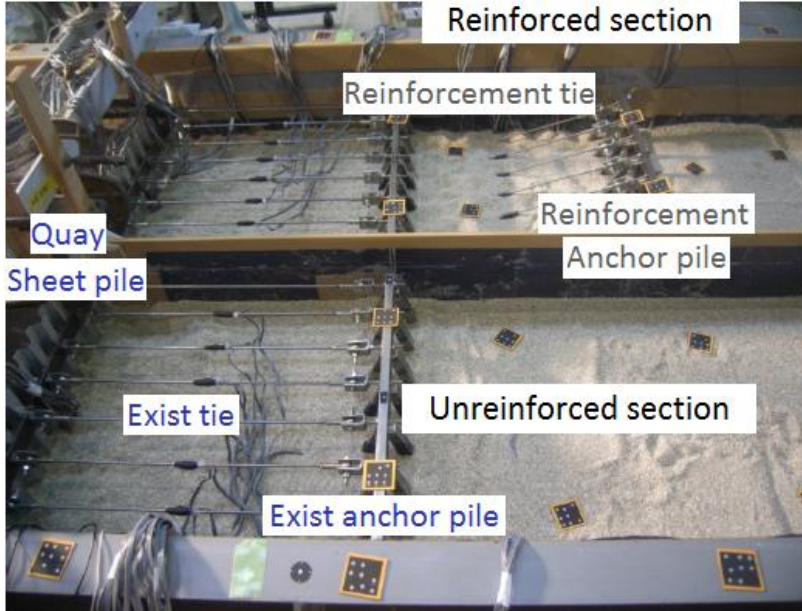


Figure 4.3: Photo of the centrifuge model during preparation, adapted from (Higuchi et al., 2012)

As mentioned, only the ‘unreinforced section’ is considered in the present study. In total there are 8 tie rods which are spaced 50 mm in the scale model and 1.5 m in the field model.

4.2.2. Testing procedure

The outline of the testing procedure is shown in Figure 4.4. It can be seen that prior to the real seismic testing (CASE-100 to CASE-600) an initial process (CASE-000) was carried out.

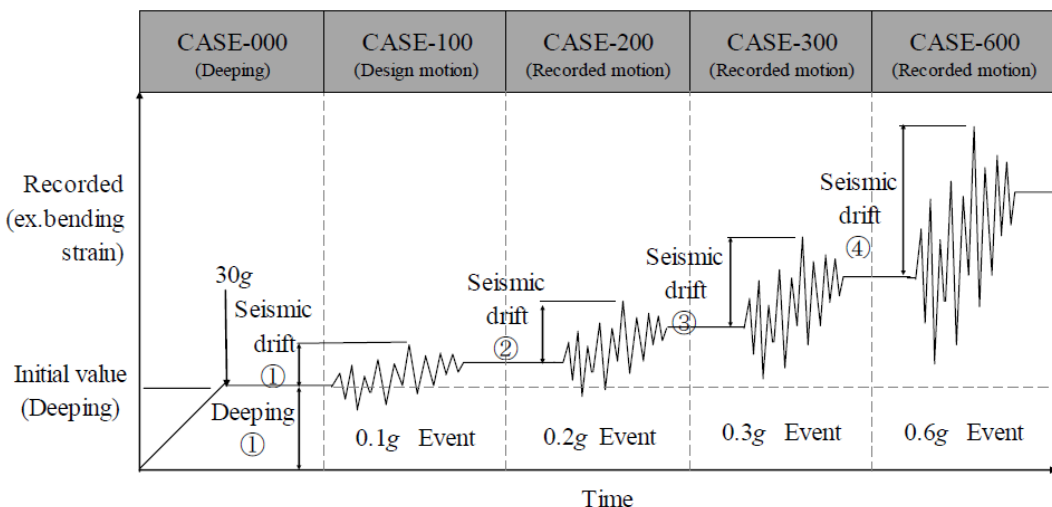


Figure 4.4: Outline centrifuge testing procedure (Higuchi et al., 2012)

The static CASE-000 consists of two steps. During the first step a centrifugal gravity of 25g was applied to the scale model to simulate the initial stress condition of the situation before deepening of the harbour bottom (water depth equals DL -7.5 m). Soil and structure experience deformation due to the centrifugal force and initial stresses are generated in the tie rods. Subsequently centrifugal gravity is released and the bottom in front of the sheet pile deepened. Then a centrifugal gravity of 30g is applied to the model in order to simulate the initial stress condition of the deepened situation (water depth equals DL -9.5 m).

The seismic (shake-table) testing consists of successively introducing four seismic events to the scale model (CASE-100, CASE-200, CASE-300 and CASE-600), under a centrifugal gravity of 30g. The input signals corresponding to the seismic events have maximum acceleration amplitudes of 0.1g, 0.2g, 0.3g and 0.6g respectively (field values). On scale level this means that input motions with maximum acceleration amplitudes of 3g, 6g, 9g and 18g are applied. As can be seen from Figure 4.4 for CASE-100 an artificially created design motion is used and for CASE-200, -300 and -600 a motion recorded during a real earthquake. The artificial motion is typically applied for the design of port facilities with high seismic resistance. The recorded motion was obtained at Port of Sendai, Takamatsu wharf, during the 2008 Iwate-Miyagi inland earthquake. Figure 4.5 shows the two input motions (top: artificial, bottom: recorded).

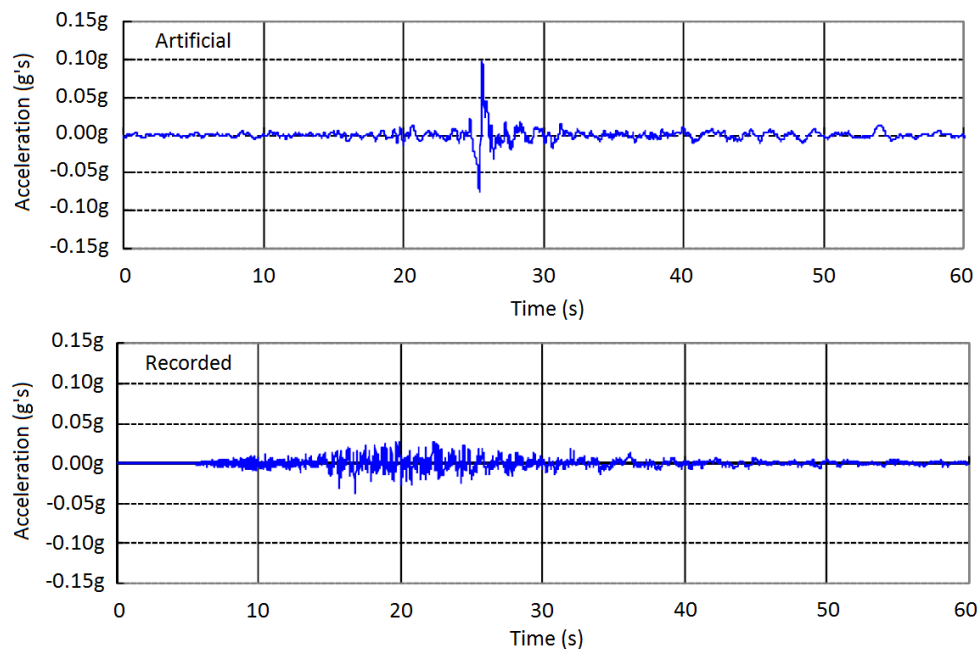


Figure 4.5: Input motions: artificial accelerogram (top) and 2008 Iwate-Miyagi inland earthquake record (bottom), adapted from (Higuchi *et al.*, 2012)

It is desirable to obtain the data files of the time-histories applied in the shake-table experiments so that they can be applied in step 3 (Newmark-analysis) and step 4 (FE analysis) of the present research methodology. After some investigation it is found that at Port of Sendai three earthquake recorders are present. The recorder at Takamatsu wharf, which is nowadays not in use anymore, was operated by the Tohoku Regional Development Bureau from the Ministry of Land, Infrastructure, Transport and Tourism (MLIT). Nearby are recorders from the Japanese Port and Airport Research Institute (PARI) and the Japanese National Research Institute for Earth Science and Disaster Prevention (NIED). See Appendix D for a geographical overview.

In the NIED online strong motion database time-histories recorded from 1996 till present can be obtained. The extensive database is the result of a dense seismographic network (K-NET and KIK-NET). A number of records are available of the ground motions during the 2008 Iwate-Miyagi inland earthquake in Sendai. In the PARI database earthquake motions in Japanese ports, recorded since 1962, are collected. A recorded time-history of the 2008 Iwate-Miyagi inland earthquake at Port of Sendai, which seems to have significant similarities with the recorded motion applied in (Higuchi *et al.*, 2012), is found in this database (record ID: F2660 N-S component).

Unfortunately Takamatsu wharf recordings are not found after numerous searches. Furthermore it is evident that the artificial motion cannot be obtained from any of the databases. Authors of the article were contacted for this matter but without success. To overcome this difficulty in a reasonable manner, the following approach will be adopted for the SDA and DA research steps:

- The F2660 record, obtained at ground level, will be translated to a motion at bedrock level via (reverse) site-response analysis in SHAKE2000. This is possible as the soil column beneath the PARI Sendai-G recorder is provided at the PARI database website.
- The obtained bedrock motion, which can be scaled to desired PGA values, will be the input motion for the reference case soil column at bedrock level and the corresponding site-response analysis. The distance between the PARI and MLIT recorder sites is less than 2 kilometers.
- For the F2660 record, similar records will be collected by comparing frequency spectra. In this way it is attempted to gather multiple representative records for SDA and DA.
- A replica of artificial time-history will be constructed out of a record with similar characteristics. This is in this case considered as a reasonable approach as the 0.1g peak is assumed to be the only important characteristic of the artificial time-history. This assumption will be checked in chapter 5 (seismic analysis of the reference case).

4.2.3. Test results

The test results provided in (Higuchi *et al.*, 2012) comprise bending moments of the quay wall, axial forces in the ties and maximum displacements of the quay wall, measured after each shake event. The paper presents the test results in graphical form and in tables using characteristic maximum values. A summary of the test results relevant for the present study is given in Table 4.3. Figure 4.6 shows the measured bending moment lines in the sheet pile per load case. All the presented values are field model values.

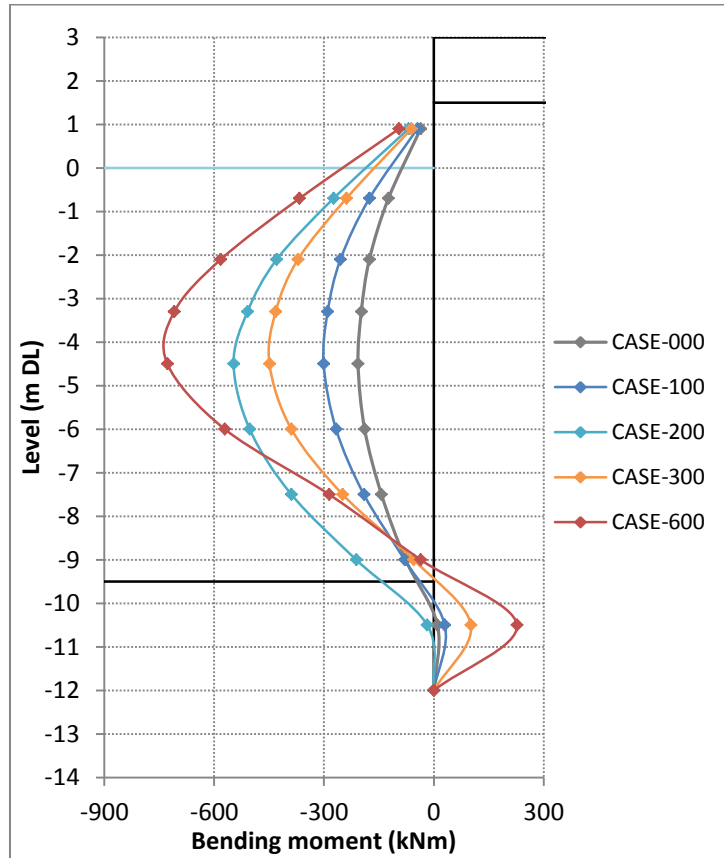


Figure 4.6: Measured bending moments in the sheet pile per load case (field model values), from (Higuchi *et al.*, 2012)

Table 4.3: Reference case test results (field model values), from (Higuchi *et al.*, 2012)

Case	M _{MAX} [kNm]	F _{ANCHOR} [kN]	u _{ANCHOR} [mm]	u _{SEABED} [mm]
000	207	108	14	6
100	301	182	20	9
200	547	261	66	41
300	449	262	93	64
600	728	308	232	195

It is noted that after CASE-300 the bending moments in the sheet pile structure have decreased and the displacements significantly increased with respect to CASE-200. This suggests passive soil failure in front of the quay wall after which the wall has moved. In the bending moment lines of CASE-300 and CASE-600 it can be seen that the point of contra-flexure (located at the seabed) has moved up approximately one meter, which again suggest passive wedge failure during CASE-300 at which the soil is pushed upwards. Considering the relatively small penetration depth of the sheet pile it is also likely that the failure mechanism with push-up of the passive soil wedge will occur. During CASE-600 passive soil resistance apparently redevelops and bending moments increase. An impression of the pushed up passive soil wedge is provided in Figure 4.7.

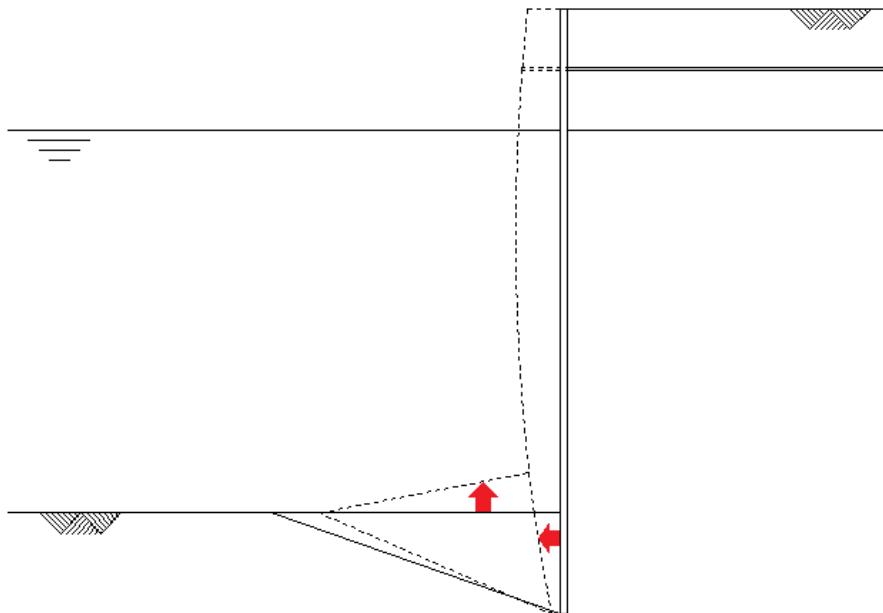


Figure 4.7: Push-up of soil wedge due to wall displacement after passive failure (applying conservation of soil mass)

A final note must be made concerning liquefaction. It is not considered to be of importance in the reference case. Looking at the measurement setup (see Figure 4.2) it can be concluded that pore pressure development is monitored during testing. (Higuchi *et al.*, 2012) do not consider liquefaction in their paper though which suggests that is not of importance. And referring to the soil condition in the test setup (coarse and very dense sand) it is reasonable to expect that the liquefaction potential is indeed negligible.

5. Seismic analysis of the reference case

In this chapter the execution of the seismic analysis part (steps 2, 3 and 4) of the research methodology is described. It consists of three levels of (calibrated) seismic analysis, i.e. simplified analysis (pseudo-static), simplified dynamic analysis (permanent-displacement) and dynamic analysis (finite element). Per seismic analysis step elaboration on the applied approach is provided. Corresponding theoretical background and setup properties can be found in the appendices. This chapter is a prerequisite for chapter 6 in which the results of the analysis will be evaluated.

5.1. Simplified analysis: pseudo-static

5.1.1. Introduction

In this section the second step of the research methodology is discussed. It concerns calibrated simplified analysis. Figure 5.1 shows the location of the current step within the research process.

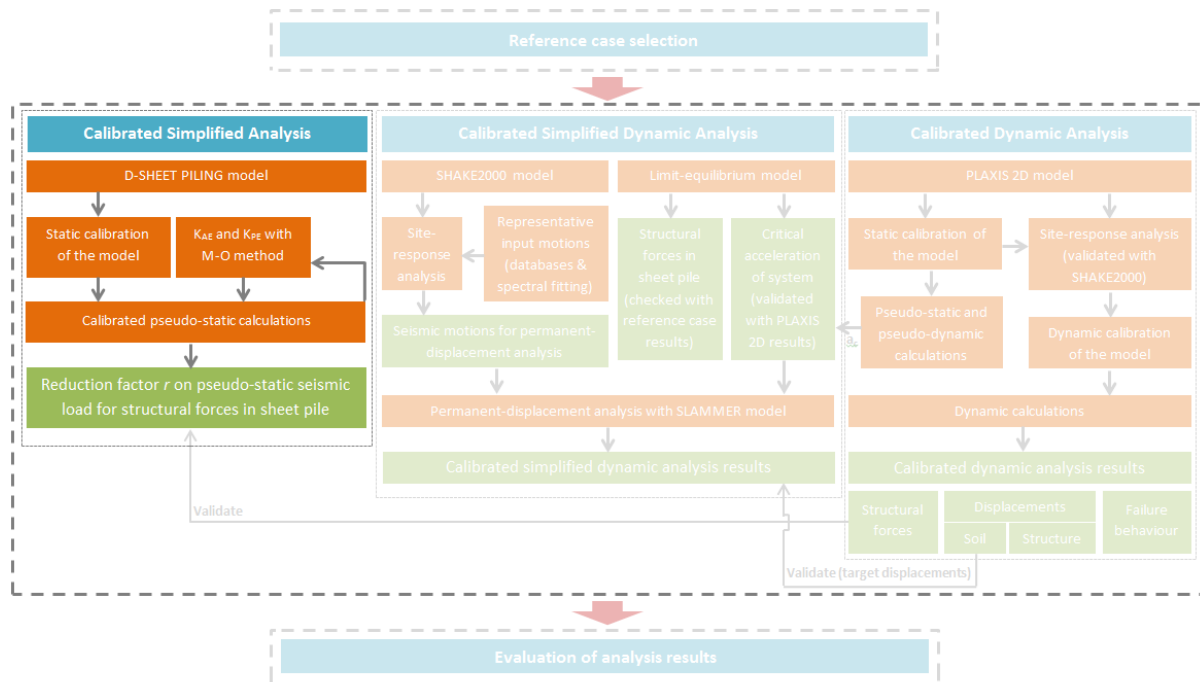


Figure 5.1: Step 2 of the research methodology: calibrated simplified analysis

The flowchart shows that a D-SHEET PILING model of the reference case is created by using the case properties as input parameters. The model is calibrated with the reference case by fitting static D-SHEET calculation results with the reference case static measurement results (CASE-000).

Subsequently pseudo-static seismic load input parameters for the model are calculated as described in (Ebeling & Morrison, 1992). These are dynamic soil pressure coefficients computed with Mononobe-Okabe method (see paragraph A.2.1) and outward hydrodynamic pressure calculated with Westergaard solution (see paragraph A.2.3). For this purpose an Excel-sheet is written. In the formulations of the pseudo-static input parameters the seismic load is accounted for by the horizontal seismic coefficient k_h , i.e. the PGA value in terms of g. So in the present study the calculated pseudo-static input parameters contain the (field) PGA values of the accelerograms that are applied in the reference case, i.e. 0.1g (CASE-100), 0.2g (CASE-200), 0.3g (CASE-300) and 0.6g (CASE-600). After entering the dynamic soil pressure coefficients and hydrodynamic pressures in D-SHEET PILING, the computations can be made.

The D-SHEET computation results for the forces in the sheet pile are compared with the reference case measurements. After comparison the original PGA values (and by that the pseudo-static input parameters) are iteratively adapted to reduce differences between reference case and D-SHEET results until a fit is found. In this way a deformation-based seismic load reduction factor (on the PGA) for structural forces in the sheet pile is proposed for application in pseudo-static methodology.

5.1.2. D-SHEET PILING model

In this paragraph the setup of the D-SHEET PILING model is discussed. The reference case properties which are inputted in the model are the field model properties. The field model geometry input for the D-SHEET Piling model is deduced from Figure 4.2.

5.1.2.1. Sheet piling properties

As is shown by Table 4.1 the sheet piling is of the type VL with $h = 200$ mm. This is a standard Japanese U-type sheet pile. The relevant properties of this sheet pile are shown in Table 5.1 (JFE Steel Corporation, Nippon Steel & Sumitomo Metal, Hiap Teck Venture Berhad, Anshan The Third Steel Rolling Co., Ltd.):

Table 5.1: VL Sheet piling properties relevant for D-SHEET PILING input

Sheet pile parameters	Value per m
Bending stiffness [kNm^2/m']	1.3230E+05
Maximum elastic moment [kNm/m']	1118.25 ^{vi}
Section area [cm^2/m']	268.00
Profile height [mm]	200.00

^{vi} Value corresponding to steel grade S355

For a vertical balance check D-SHEET PILING demands some additional sheet pile parameters, i.e. the maximum point resistance $P_{r,\max;\text{point}}$ and a factor X_i depending on the number of CPT's and the number of anchors. The latter is kept default ($X_i = 0.72$) corresponding to one CPT and one anchor. The maximum point resistance, or the representative cone resistance at the bottom of the sheet piling, is determined with the help of CUR166 and NEN-9997-1. A value of 15.50 MPa is found. Although the input for these two parameters must be such that vertical balance is found by the model, the calculation results relevant for the research conducted in the present study do not appear to be sensitive to these parameters.

5.1.2.2. Soil material properties

The soil parameter model applied in the D-SHEET PILING calculations is the K_A , K_θ , K_p basic model. In this model the option is provided to define the soil pressure coefficients manually. This is a required feature for fitting calculation and reference case results based on a reduction of the seismic load. It is noted that in this model the soil pressure coefficient values are constant per soil layer. More background on the available soil parameter models in D-SHEET PILING can be found in section B.1.

Besides the manual definition of the soil pressure coefficients a number of other soil material parameters have to be defined. In paragraph 4.2.1 it was described that the field soil condition is assumed stiff by (Higuchi *et al.*, 2012) so in the scale model coarse silica sand ($D_{50} = 1.2$ mm) is used and compacted to a relative density RD = 80% ($\rho_s = 2\text{g/cm}^3$). With this information and the content of the publications (Bolton, 1986), NEN-9997-1 and (CROW, 2004) the relevant soil parameter values are estimated.

In (CROW, 2004) a number of correlations are provided with respect to the relative density (RD). For RD = 80% it holds that the sand is classified as being (very) dense / compact (p.80) and that the corresponding angle of internal friction (ϕ) typically has a value around 40° (p.335, p.371). When consulting (Bolton, 1986) such a friction angle probably only corresponds to maximum soil strength in case of dense silica (quartz) sand. Maximum soil strength in terms of a friction angle (ϕ_{\max}) consists of the critical friction angle (ϕ_{crit}) plus (0.8 times) the dilation angle (ψ_{\max}). ϕ_{crit} is defined as “the angle of shearing observed in a simple shear test on soil loose enough to be in critical state, with zero dilatation”. Through ψ_{\max} the extra component of strength due to

dilatancy in a dense soil is taken into account. According to (Bolton, 1986) it typically holds for quartz sand that $\varphi_{crit} = 33^\circ$. Subsequently empirical relations in the paper give a range $\varphi_{max} = 40^\circ - 45^\circ$ in case that RD=80%. (Bolton, 1986) comments however that “there is not a one-to-one correspondence between φ_{max} and relative density, even at a given stress level, since the dilatancy-related component of strength is $\varphi_{max} - \varphi_{crit}$, and φ_{crit} is a function of mineralogy”. Although literature provides an indication, uncertainty remains to exist. As a starting point $\varphi = 40^\circ$ is chosen.

In (CROW, 2004) a typical value for the cone resistance (q_c) that corresponds to dense sand conditions is 20 MPa at least (p.223, p.367). NEN-9997-1 classifies this as being stiff clean sand with $\gamma_{dry} = 20 \text{ kN/m}^3$ and $\gamma_{sat} = 22 \text{ kN/m}^3$. For this specific soil condition CUR166 (table 3.3) gives low and high characteristic values for the moduli of subgrade reaction (k_1, k_2, k_3) corresponding to the tri-linear soil spring curve applied by D-SHEET PILING (see Figure B.1). Middle values in between the low and high characteristic values will be used. For this matter it is noted that the sensitivity of D-SHEET PILING calculation results to the k_1 -, k_2 - and k_3 -values is low. According to (CROW, 2004) a typical range for the permeability (k) is $1.10^{-3} - 1.10^{-4}$ in case it holds that $D_{50} = 1.2 \text{ mm}$ (p.339). An overview of the relevant soil parameters and their indicative values determined from literature is provided in Table 5.2.

Table 5.2: Soil material properties relevant for D-SHEET PILING input

Soil parameter	Value
Dry unit weight $\gamma_{dry} [\text{kN/m}^3]$	20
Saturated unit weight $\gamma_{sat} [\text{kN/m}^3]$	22
Cohesion $c [\text{kN/m}^2]$	0
Friction angle $\varphi [^\circ]$	40
Wall friction angle $\delta [^\circ]$	Between 0 and 1 φ
Modulus of subgrade reaction $k_1 [\text{kN/m}^3]$	65.000
Modulus of subgrade reaction $k_2 [\text{kN/m}^3]$	32.500
Modulus of subgrade reaction $k_3 [\text{kN/m}^3]$	16.250
Relative density RD [%]	80
Permeability $k [\text{m/s}]$	5.10^{-4}

For a sheet pile wall retaining sand (Ebeling & Morrison, 1992) recommend a wall-friction angle of $\varphi/2$ while CUR166 recommends $2\varphi/3$. Disagreement exists and moreover the wall-friction angle has a significant effect on the value of the passive soil pressure coefficient (K_p), see paragraph B.1.3. Therefore the wall-friction angle will be determined along the way during this research step.

The active and passive soil pressure coefficients (K_a and K_p respectively) are determined with the Mononobe-Okabe equations which in the static case reduce to the Coulomb equations (see paragraphs B.1.2 and B.2.1). Although it is noted that according to (Kramer, 1996) the Coulomb equations heavily over-predict K_p values in case that $\delta > \varphi/2$, the M-O and Coulomb equations are the starting point for the SA research step. If necessary an alternative for the static case can be found in the Log-spiral method and corresponding tables of Caquot & Kerisel (1948) (see paragraph B.1.3). The neutral soil pressure coefficient (K_0) is determined with the Jáky formula (see paragraph B.1.2) in which the soil friction angle is the only variable. Therefore K_0 remains constant, depending on the soil friction angle.

5.1.2.3. Loads

In the static case the loading on the wall is due to static soil and hydrostatic pressure. Seismic loading is translated into dynamic soil and hydrodynamic pressure on the wall. As discussed in the previous part the static and dynamic soil pressures will be computed with Coulomb and M-O equations respectively. The restrained water in the backfill is taken into account in these soil pressure equations (see paragraph B.2.3). The outward hydrodynamic pressure is calculated with the Westergaard (1931) solution (see paragraph B.2.3). In D-SHEET PILING this outward hydrodynamic pressure can only be taken into account by implementing a maximum of 10 horizontal line loads on the sheet pile wall which in total must resemble the Westergaard pressure distribution.

5.1.2.4. Anchor properties

The horizontal steel anchor rods of the reference case prototype have a length of 12 m, a diameter of 42 mm and are spaced 1.5 m. This results in the D-SHEET PILING anchor input parameters as shown in Table 5.3.

Table 5.3: Anchor properties relevant for D-SHEET PILING input

Anchor parameters	Value
Level [m DL]	1.50
E-Modulus [kN/m ²]	2.100E+08
Section area [m ² /m']	9.236E-04
Anchor length [m]	12.00
Angle [°]	0.00
Yield force [kN/m']	328.00 ^{vii}

^{vii} Value corresponding to steel grade S355

In the anchor properties menu of D-SHEET PILING also an anchor wall height can be put in to check stability of the anchor according to Kranz (1953). The inputted height of the anchor wall does not have any influence on the present calculation results. D-SHEET PILING just models the anchor as being fixed at its end and no distinction between types of anchorage can be made. Displacement of the anchorage can be accounted for by decreasing axial stiffness (and thus increasing strain).

5.1.2.5. Layout of the model

The resulting layout of the D-SHEET PILING model, which matches with the input parameter values as determined in this paragraph, is shown in Figure 5.2.

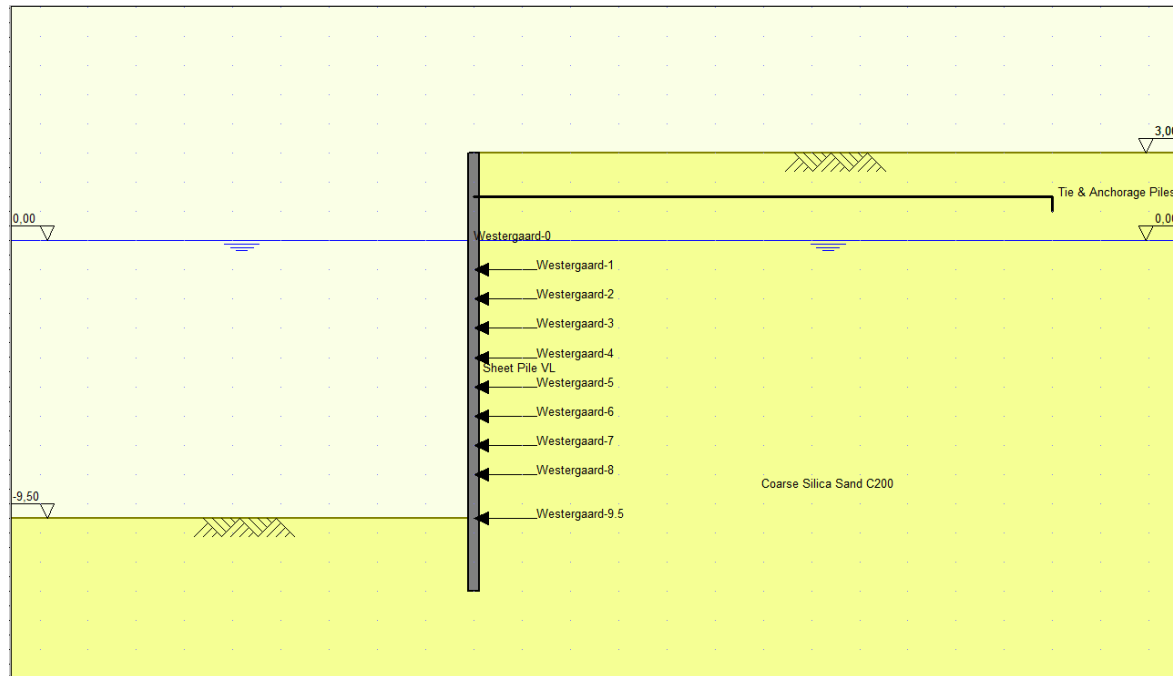


Figure 5.2: Layout of the D-SHEET PILING model

5.1.3. Static calibration of the D-Sheet Piling model with the reference case

In this part the calibration of the D-SHEET PILING model with the static reference case condition (CASE-000) is discussed. The corresponding D-SHEET PILING CASE-000 report with model setup and calculation results can be found in Appendix C, section C.1. In the following the results and findings of the calibration process are listed and discussed.

Static calibration results:

- The bending moment line calculated by D-SHEET PILING fits the bending moment line of the reference case
- The anchor force calculated by D-SHEET PILING is a factor 0.5 too low
- The displacement at the anchor calculated by D-SHEET PILING is a factor 0.2 too low
- The displacement at the seabed calculated by D-SHEET PILING is a factor 2.0 too high

Static calibration findings:

- The Coulomb (or static Mononobe-Okabe) active and passive soil pressure coefficients that are originally calculated from the soil material parameters in Table 5.2, have to be lowered to the values $K_A = 0.15$ and $K_p = 10.32$. This lowering is only possible and physically explainable by including an arching effect above the anchor system (neglecting the soil above the anchors in the D-SHEET PILING model) and setting the value of the friction angle to $\varphi = 45^\circ$. Concerning the K_p -value a wall-friction angle of $\varphi/4$ is to be selected.
- The actual displacement mechanism is not correctly resembled by the D-SHEET PILING model. This also results in an incorrect calculation result of the force in the anchor rod. In the current static calibration the axial stiffness of the anchor rod is not reduced.
- A bending moment line fit can be found by calibrating the D-SHEET PILING model. It can therefore be used to investigate a deformation-based seismic load reduction factor for structural forces in the sheet pile wall.

Explanation of static calibration findings:

- The assumed arching effect is explained by the fact that the anchor rods have a relatively small spacing with respect to each other (1.5 m) and are connected to the continuous batter pile beam. This anchor system can possibly start working as a relieving floor due to arching of the very stiff soil above the anchor system, thus resulting in a decrease of active soil pressure.
- Although the value of the friction angle is considered to be very high, explanations can be given for this. First of all it is reasoned from (Higuchi *et al.*, 2012) that due to the continuously applied 30g centrifugal gravity on the scale model, the already very stiff soil condition (RD=80%) is probably densified even further. This would result in initial stress conditions that are unrealistically high. (Higuchi *et al.*, 2012) indeed mention overestimated soil stiffness after the simulation of the initial stress conditions. Furthermore it can be noted that the applied friction angle is within the empirical maximum friction angle (φ_{max}) range discussed in (Bolton, 1986).

The graphical results of the calibration process can be seen in Figure 5.3. It shows the static fits of the bending moment line and the corresponding shear force line and resulting soil stress distribution. The reference case shear force and soil stress data have been obtained by computing the first and second derivative of the bending moment data respectively. Due to the limited amount of bending moment measurement data the derivatives are not very precise and therefore deviate at the locations where the shear force and soil stress curves rapidly change direction. This can be seen at anchor level in the shear force line and at toe level in the soil pressure distribution. A satisfactory fit with the D-SHEET PILING calculation results is found though.

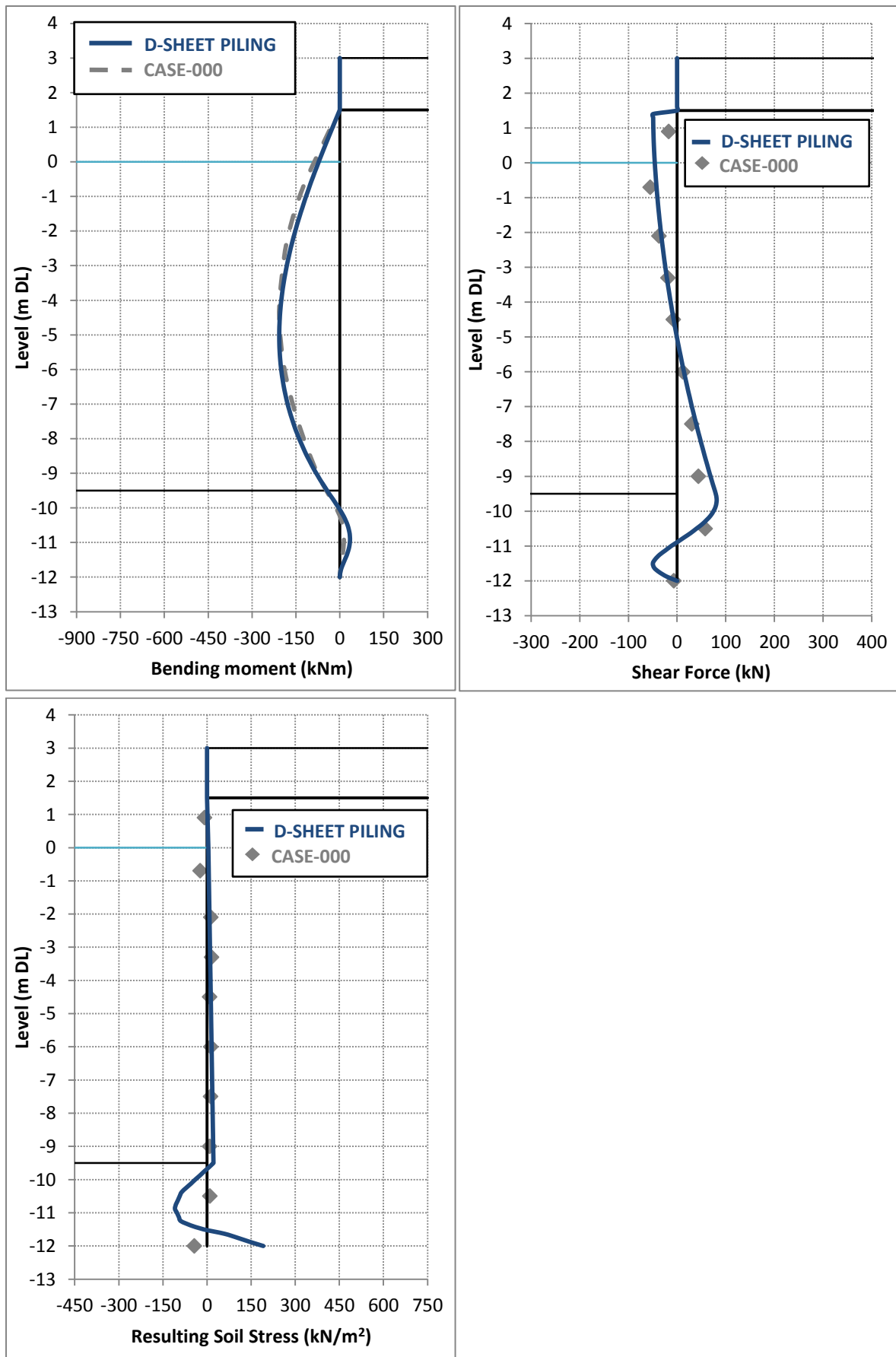


Figure 5.3: Fit of calculated structural forces with CASE-000 measurements after static calibration of the D-SHEET PILING model

5.1.4. Pseudo-static calculations

As was mentioned the pseudo-static input, i.e. dynamic soil pressures and hydrodynamic pressures, will be calculated according to M-O method and Westergaard solution respectively. Seismic input for the calculations are the field model PGA values corresponding to the seismic shake events (0.1g, 0.2g, 0.3g and 0.6g). For every seismic load case these PGA values, and therefore the pseudo-static pressure input in D-SHEET PILING, will be iteratively adapted until a fit is obtained between the reference case bending moment measurements and the bending moments calculated by D-SHEET PILING. For the sake of clarity this procedure is more specifically described in the following scheme.

1. Calculation of the inclination angle of the seismic coefficient with the vertical (ψ)

The angle ψ [°] is the parameter in the M-O equations by which the pseudo-static seismic load (seismic coefficient) is accounted for, as can be seen from equation (8).

$$\psi = \tan^{-1} \left(\frac{k_{he}}{1-k_v} \right) \quad (8)$$

In the calculations of ψ the vertical seismic coefficient k_v is set to zero, as is customary for sheet pile walls. The horizontal seismic coefficient k_h is translated into an equivalent horizontal seismic coefficient k_{he} [-] to account for saturation of the soil in front and behind the quay wall (see A.2.3.2).

2. Calculation of dynamic soil pressure coefficients (K_{AE}) and (K_{PE}) and hydrodynamic pressure (p_w)

The calculated seismic inclination angles are implemented in the M-O equations (9) and (10) for active K_{AE} [-] and passive K_{PE} [-] dynamic soil pressure respectively.

$$K_{AE} = \frac{\cos^2(\varphi-\theta-\psi)}{\cos\psi\cos^2\theta\cos(\delta+\theta+\psi)\left[1 + \sqrt{\frac{\sin(\delta+\varphi)\sin(\varphi-\beta-\psi)}{\cos(\delta+\theta+\psi)\cos(\beta-\theta)}}\right]^2} \quad (9)$$

$$K_{PE} = \frac{\cos^2(\varphi+\theta-\psi)}{\cos\psi\cos^2\theta\cos(\delta-\theta+\psi)\left[1 - \sqrt{\frac{\sin(\delta+\varphi)\sin(\varphi+\beta-\psi)}{\cos(\delta-\theta+\psi)\cos(\beta-\theta)}}\right]^2} \quad (10)$$

Due to geometry of the anchored sheet pile wall under consideration the angles θ [°] and β [°] are equal to zero (no inclination of wall and backfill). The calculated K_{AE} - and K_{PE} -values are manually entered in D-SHEET PILING.

In the Westergaard solution for outward hydrodynamic water pressure p_w [kN/m²] the horizontal seismic coefficient is directly applied, as can be seen in equation (11).

$$p_w = \frac{7}{8} k_h \gamma_w \sqrt{z_w H_{wall}} \quad (11)$$

The p_w -values at locations z_w [m] along the water depth h_w [m] are manually entered in D-SHEET PILING.

3. Deducing a deformation-based reduction on the pseudo-static seismic load

The D-SHEET computation results for the forces in the sheet pile are compared with the reference case measurements. After comparison the original k_h -values of the shake events (and by that the K_{AE} -, K_{PE} - and p_w -values) are iteratively reduced by means of a factor r , i.e. $\left(\frac{k_h}{r}\right)$, until a fit is found between reference case and D-SHEET results. In this way a deformation-based reduction factor on the pseudo-static load for structural forces in the sheet pile is deduced.

For more extensive background on the applied equations one is referred to Appendix A.

The calibrated D-SHEET PILING setup, as determined in the previous paragraph, is the starting point for the pseudo-static fitting. So for the angles of internal friction and wall friction (also parameters of the M-O equations) it holds that $\varphi = 45^\circ$ and δ is determined per case, as it is the expectation that this parameter will vary with every deformed configuration of the soil-structure system. The axial stiffness of the anchor rod is not reduced in any case. The values from Table 5.1, Table 5.2 and Table 5.3 apply (except for φ , as is discussed). In accordance with the reference case test results (see paragraph 4.2.3 and Figure 4.7) the seabed level is heightened with a meter in the D-SHEET PILING model for CASE-300 and CASE-600.

Concerning the neglecting of the dry soil above the anchor system because of arching it can be expected that this arching effect will be destroyed when shaking increases. Therefore the neglecting of the top soil is a starting point for finding pseudo-static fits but it will be abandoned when a proper fit can be found without the arching effect.

An additional point of consideration is the possible reduction of active soil pressure due to the expected confinement of the soil between the sheet piling and the closely spaced batter piles. This idea is extracted from (Nishimura *et al.*, 2012) in which “the dynamic and non-dynamic interactions between a gravity-type quay wall and a backfill ground are investigated by centrifuge model testing, considering cases in which a rigidly cement-stabilised ground existed at varying distances from the quay wall. (...) At non-dynamic active states, when the friction along the quay wall back was fully mobilised, the earth pressure was smaller from a narrowly confined fill than from a fully extending one. The perfect plasticity theory, considering wall frictions, explained the results well. (...) During shaking, the existence of stabilised soil in the proximity of the quay wall resulted in reduced active pressure in both the dry sand and the underwater cases. In the dry cases, the reduction in active earth pressure seemed to derive mainly from the friction arching effect. In the underwater cases, a more dominant role in reducing the active pressure was played by the variation in pore water pressure due to both the water’s dynamic motion and the interactions with the soil skeleton.”

The findings of (Nishimura *et al.*, 2012) are translated to the D-SHEET PILING case by defining a minimum value for the angle of the active failure plane with respect to the horizontal which corresponds to the failure plane reaching from the heel of the sheet pile towards, and no further than, the anchorage beam above the batter piles. This failure plane angle can be computed with equation (A13). The minimum angle has a value of $\alpha_{AE} = \tan^{-1}(13.5 \text{ m}/12 \text{ m}) = 48.4^\circ$, as can be calculated from the geometry of the reference case shown by Figure 4.2.

5.1.5. Results

In Table 5.4 the pseudo-static input parameters that result from the fitting procedure are summarized per shake event.

Table 5.4: Calibrated pseudo-static input parameters

Parameter	CASE-100	CASE-200	CASE-300	CASE-600
Active M-O soil pressure coefficient K_{AE} [-]	0.18	0.21	0.24	0.32
Passive M-O soil pressure coefficient K_{PE} [-]	12.38	10.48	11.73	24.56
Wall friction angle δ [°]	$\approx\varphi/3$	$\approx\varphi/3$	$\approx 0.4\varphi$	$2\varphi/3$
Westergaard resultant force ^{viii} [kN]	39.48	86.87	118.45	252.70

^{viii} Although the resultant Westergaard force is given in Table 5.4 the hydrodynamic pressure input in D-SHEET PILING consists of horizontal line loads on the sheet pile wall, resembling the Westergaard pressure distribution.

The M-O active soil pressure coefficients increase with increasing seismic coefficient, as does the Westergaard hydrodynamic pressure. The values of the M-O passive soil pressure coefficients are influenced by the value of the seismic coefficient, the push-up of the passive soil wedge (allowing for the expected redevelopment of passive soil pressure after passive failure), and the altering of the wall-friction angle.

In CASE-100 the soil above the anchor system was neglected in order to obtain a proper fit which is physically explainable. From CASE-200 onward the soil above the anchor system no longer had to be neglected so this indicates that the arching effect was destroyed during the shaking heavier than 0.1g. Only in CASE-600 the failure plane angle had to be limited to the pre-determined minimum value so that the failure plane did not reach behind the anchorage beam (see Figure 5.4). It is noted that only in CASE-600 the calculated anchor force (279 kN) approaches the measured anchor force (308 kN).

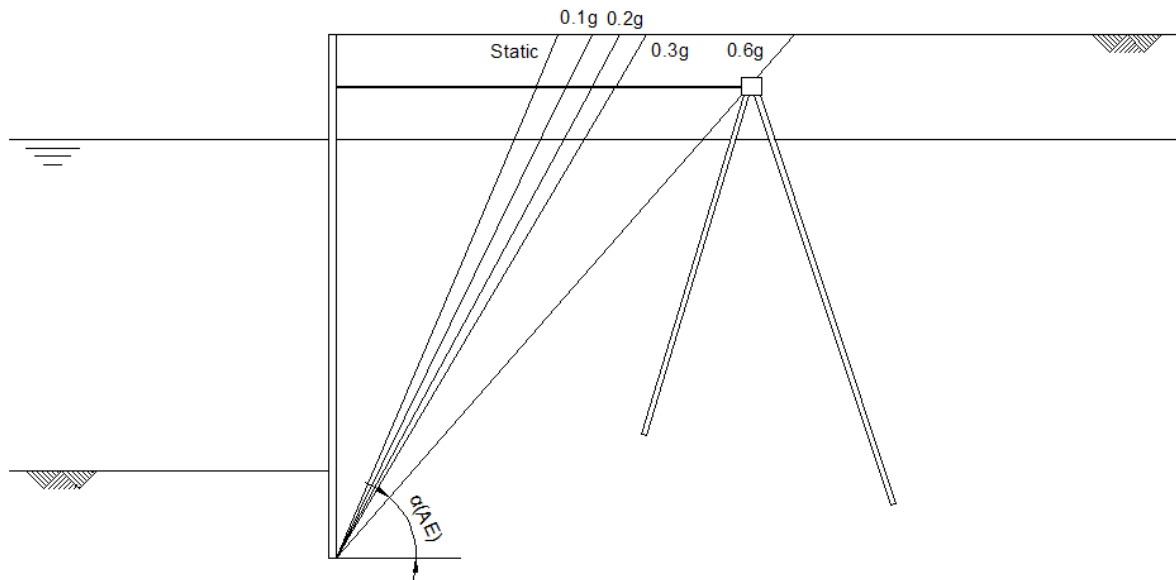


Figure 5.4: Computed active failure plane angles (α_{AE}) and corresponding Coulomb and M-O failure planes

The obtained reductions on the seismic loads corresponding to the calibrated pseudo-static input parameters of Table 5.4 are listed in Table 5.5. The reductions are specified by the reduction factor r . As explained in paragraph 5.1.4 the horizontal seismic coefficients of the reference case shake events are divided by this factor after which the reduced seismic coefficients are applied in the Mononobe-Okabe and Westergaard solutions that compute the pseudo-static input parameters for the D-SHEET model.

Table 5.5: Obtained reduction factors on seismic loading resulting from calibrated pseudo-static calculations

Parameter	CASE-100	CASE-200	CASE-300	CASE-600
Seismic coefficient k_h [-]	0.10	0.20	0.30	0.60
Reduced seismic coefficient k_h [-]	0.05	0.11	0.15	0.32
Reduction factor r [-]	2.00	1.82	2.00	1.86

The bending moment line fits for the different seismic load cases are shown in Figure 5.5. In Figure 5.6 and Figure 5.7 the corresponding shear force and resulting soil stress fits are provided. In these figures the reference case shear force and soil stress data have been obtained by computing the first and second derivative of the bending moment data respectively. Again, due to the limited amount of bending moment measurement data the derivatives are not very precise and therefore deviate at the locations where the shear force and soil stress curves rapidly change direction. This can be seen at anchor level in the shear force line and at toe level in the soil pressure distribution. Satisfactory fits with the D-SHEET PILING calculation results are found though. In sections C.2 to C.5 the corresponding D-SHEET PILING reports can be found.

The results obtained after performing calibrated simplified analysis indicate that in pseudo-static methodology a deformation-based seismic load reduction for structural forces in the sheet pile is allowable. The obtained reductions for the present reference case are in the range of 45% to 50% ($r = 1.82$ to $r = 2.00$).

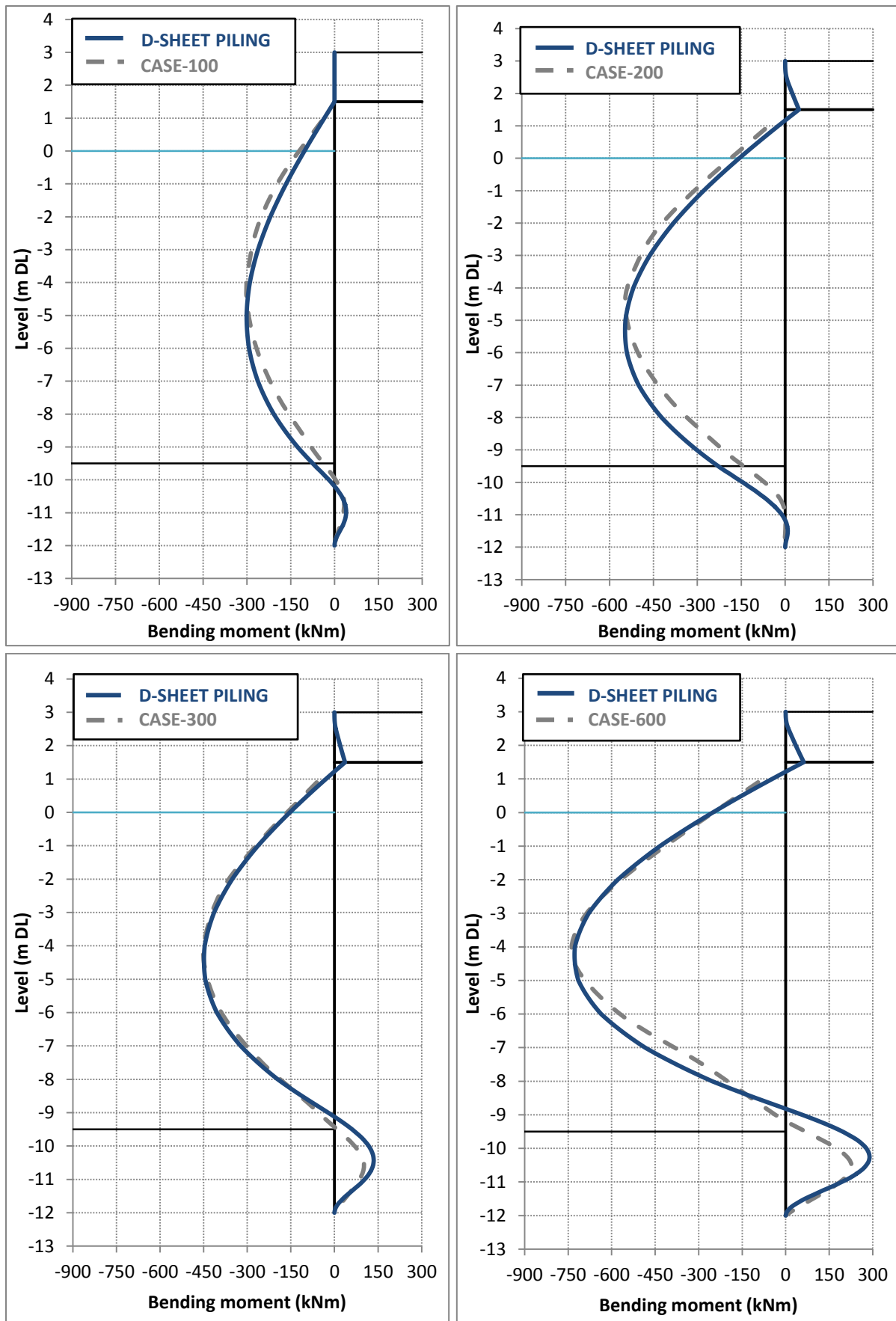


Figure 5.5: Bending moment line fits between D-SHEET PILING pseudo-static results and reference seismic load cases

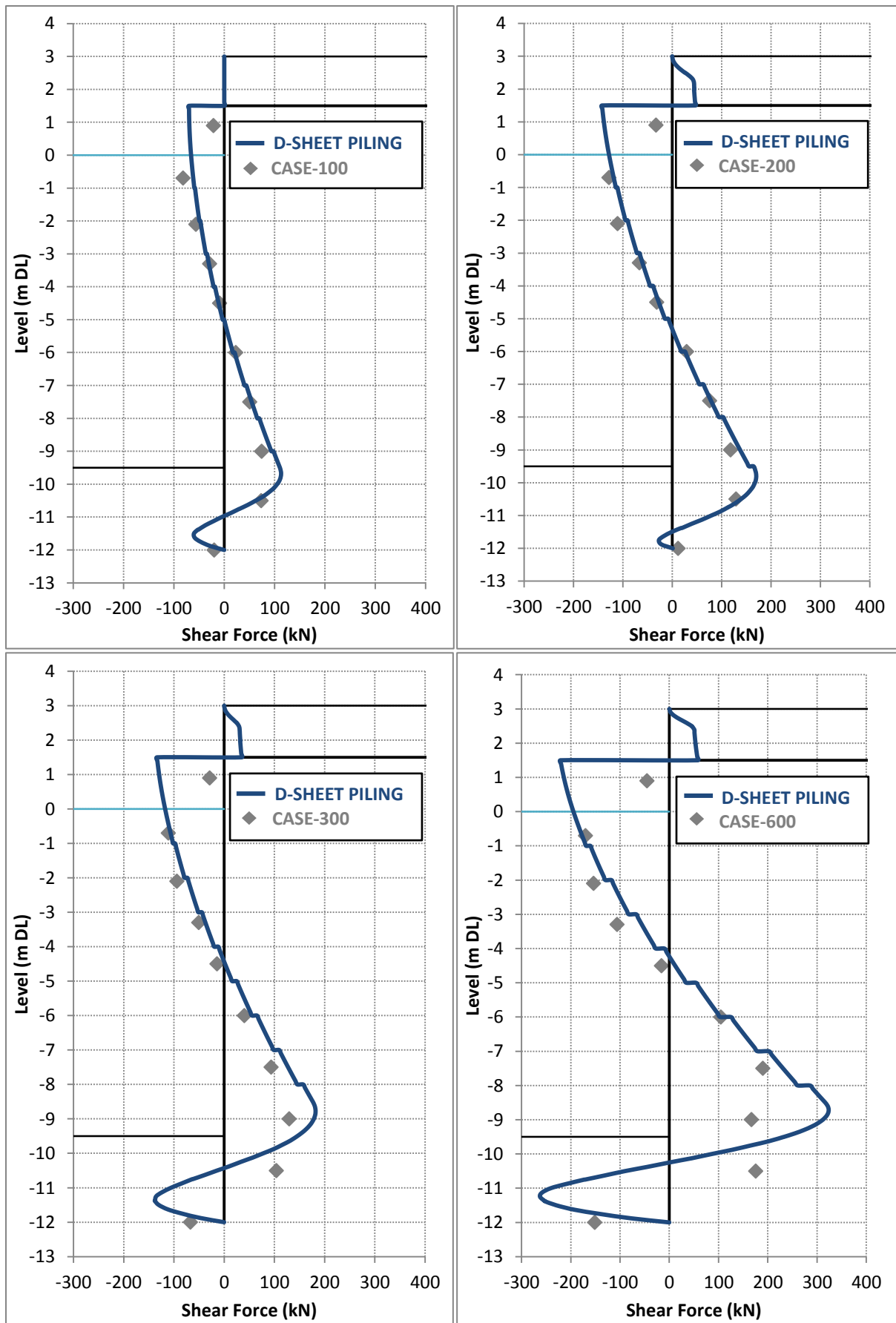


Figure 5.6: Shear force line fits between D-SHEET PILING pseudo-static results and reference seismic load cases

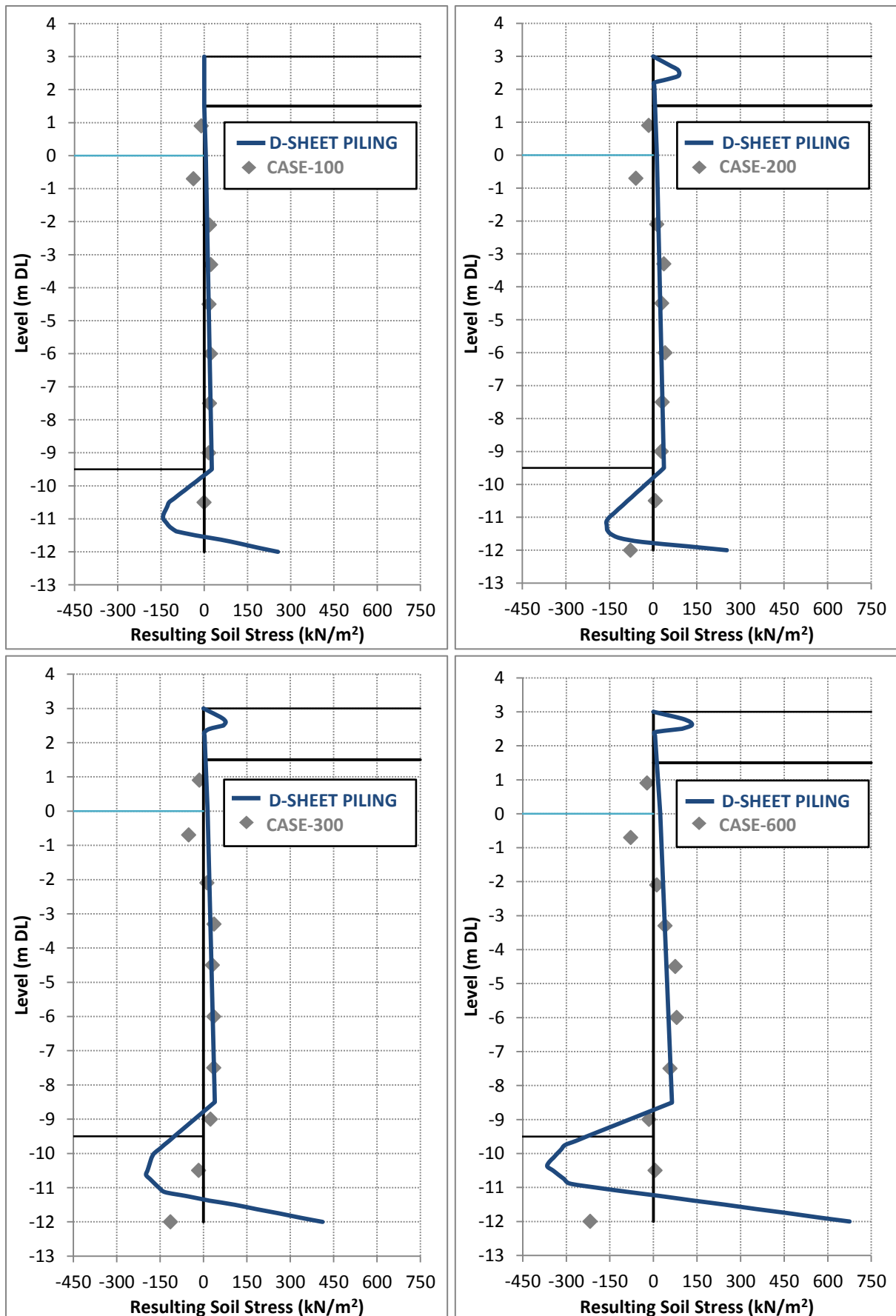


Figure 5.7: Resulting soil stress fits between D-SHEET PILING pseudo-static results and reference seismic load cases

5.2. Simplified dynamic analysis: permanent-displacement

5.2.1. Introduction

In this section the third step of the research methodology is discussed. It concerns calibrated simplified dynamic analysis. Figure 5.8 shows the location of the current step within the research process.

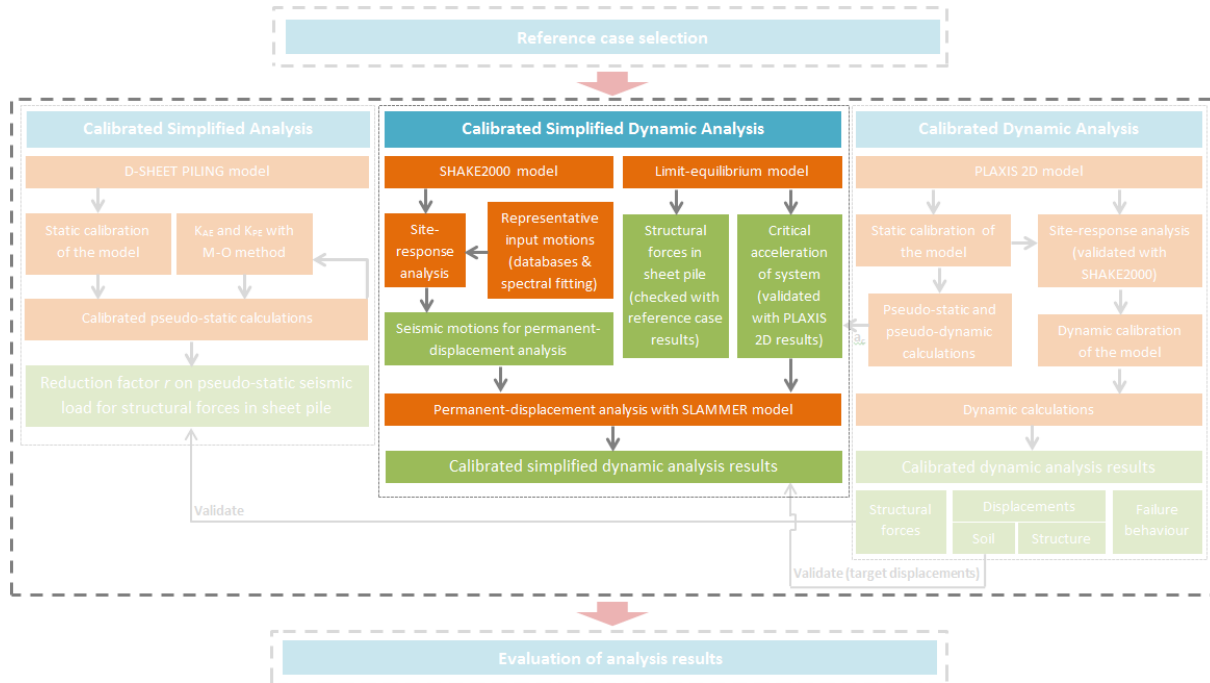


Figure 5.8: Step 3 of the research methodology: calibrated simplified dynamic analysis

It was stated in paragraph 3.3.3 that the cited papers in (Conti *et al.*, 2012) provide a starting point for the SDA step of the research methodology. A failure mechanism that fits the reference case behaviour is derived and from this an analytical limit equilibrium model deduced. The limit equilibrium model is used to compute the critical acceleration of the anchored sheet pile quay wall and furthermore it is investigated whether the model is able to compute structural forces in the sheet pile wall. The computed critical acceleration (validated with PLAXIS 2D results), in combination with input time histories representative for the case study, is applied to perform permanent-displacement analysis. The dedicated software SHAKE2000 (site-response analysis) and SLAMMER (permanent-displacement analysis) will be applied for this. The SLAMMER calculation results will be compared with the reference case results.

5.2.2. Limit-equilibrium model: critical acceleration

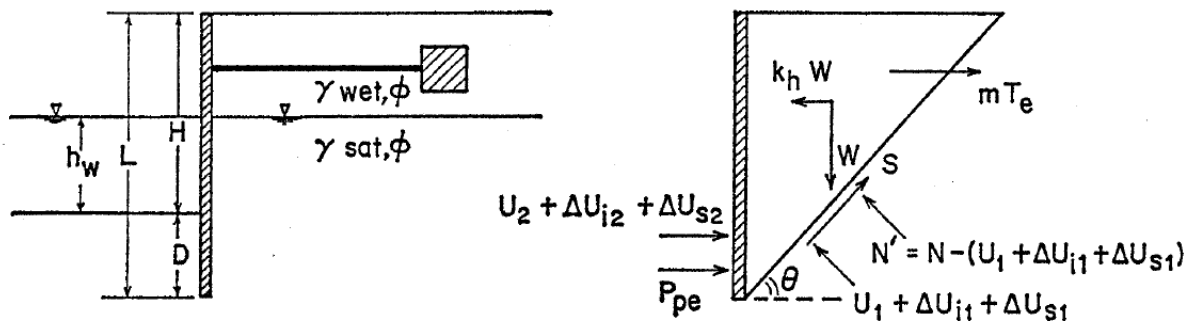
An important input parameter for every simplified displacement analysis is the critical acceleration of the structure within a soil-structure system. This is the earthquake acceleration at which the structure starts to displace permanently, or in other words, beyond which the pseudo-static equilibrium is exceeded. This critical acceleration can analytically be computed from a pseudo-static limit equilibrium state corresponding to an assumed failure mechanism. A more sophisticated possibility is to determine it from FE calculations in which no failure mechanism is assumed.

Looking at the reference case displacement measurements it is concluded that a translation failure mechanism is most suitable to consider in the present SDA. The earlier cited paper by Towhata & Islam (1987) proposes a translation mechanism for a sheet pile quay wall with a block anchor in which the sheet pile and active wedge behind it act as one rigid body (considered reasonable because of no cracks occurring between bulkhead and soil). The upper part of Figure 5.9 illustrates the limit equilibrium model of this failure mechanism. The term mT_e accounts for the contribution of the anchor force in the equilibrium which is zero ($m=0$) in case of

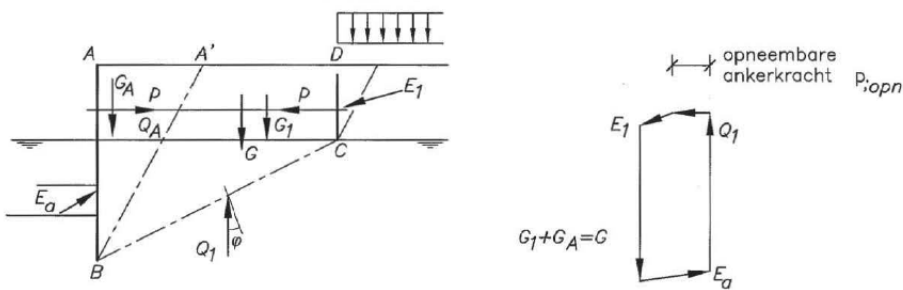
liquefaction around the anchorage or when the anchorage is situated within the active failure wedge. The resistance of the passive failure wedge in front of the sheet pile wall is represented by the dynamic passive soil thrust (P_{PE}).

The failure mechanism proposed by Towhata & Islam (1987) is a good starting point for deriving a reasonable failure mechanism for the present reference case in which a batter pile anchor is considered and liquefaction is neglected. By schematizing the batter pile anchor by an average vertical anchor pile, applying the concept of Kranz (1953) limit-equilibrium anchor stability ($T = 0$), and combining this with the Towhata & Islam (1987) model, a seismic translation failure mechanism is derived in which the sheet pile, the Kranz confined soil wedge and anchor act as a rigid sliding block. The concept of Kranz (1953) stability is illustrated by the lower part of Figure 5.9 and the newly derived limit equilibrium model and corresponding seismic failure mechanism for the reference case is presented in Figure 5.10. From this new model the (horizontal) critical seismic coefficient (also referred to as yield coefficient) can be computed from horizontal and vertical equilibrium of forces. It is noted that vertical acceleration is neglected because all sliding-block analyses only use horizontal motions.

Some remarks are made on beforehand about the derived failure mechanism of Figure 5.10. The schematization of the average anchor pile which moves along with the confined soil wedge and the sheet pile incorporates simplifications. It is expected that in real life the batter piles do not purely translate along horizontally but bend, rotate and translate towards the sheet pile wall. Furthermore failure planes are expected to be curved to a certain extent. Another point of simplification is that the rigid body schematization of Towhata & Islam (1987), applied in the present failure mechanism, incorporates that the friction between wall and soil is not considered (i.e. $\delta = 0$). Because the sheet pile in reality will not only translate but also bend (and possibly also rotate somewhat) the question arises whether this simplification is reasonable. Comparing the critical acceleration obtained by the derived failure mechanism with reference case and FE calculation results should give more insight in this matter.



Towhata & Islam (1987): Anchored sheet pile quay wall and equivalent limit equilibrium model



Kranz (1953): Limit equilibrium model for total stability of an anchored sheet pile wall

Figure 5.9: Towhata & Islam (1987) and Kranz (1953) limit equilibrium models corresponding to sliding along assumed failure planes, adapted from (Towhata & Islam 1987) and (CUR 166) respectively

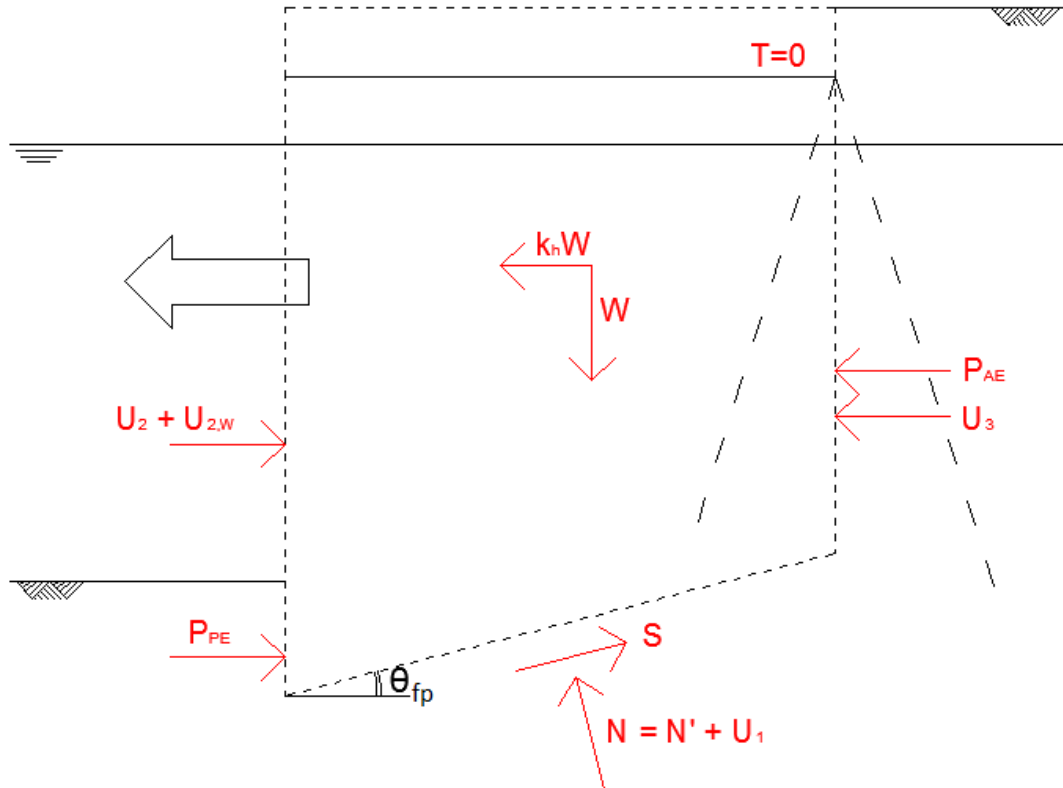


Figure 5.10: Seismic translation failure mechanism of anchored sheet pile quay wall with batter pile anchor - based on Kranz (1953) and Towhata & Islam (1987) limit equilibrium models

The forces acting on the translating body, depicted in Figure 5.10, are listed in the following. For the corresponding expressions one is referred to Appendix E. It is noted that the forces are acting per meter width.

- k_h = horizontal seismic coefficient [-]
- N = normal force in the failure plane beneath the sliding mass, whose effective component is denoted by N' [kN]
- P_{AE} = dynamic active soil thrust behind the vertical failure plane [kN]
- P_{PE} = dynamic passive soil thrust in front of the sheet pile [kN]
- S = shear force along the failure plane beneath the sliding mass [kN]
- T = force in anchor tie ($=0$) [kN]
- U_1 = Hydrostatic force 1, in the failure plane beneath the sliding mass [kN]
- U_2 = Hydrostatic force 2, in front of the sheet pile [kN]
- $U_{2,w}$ = Westergaard hydrodynamic force over the water depth in front of the sheet pile [kN]
- U_3 = Hydrostatic force 3, behind the vertical failure plane [kN]
- W = weight of sliding soil body [kN]
- θ_{fp} = angle of the failure plane beneath the sliding mass, with respect to the horizontal [$^\circ$]

From horizontal and vertical equilibrium of the forces in Figure 5.10 the critical or yield seismic coefficient can iteratively be computed. With Excel the critical accelerations consistent with the earlier determined soil material properties (see Table 5.2), i.e. $\varphi = 40^\circ - 45^\circ$, $\gamma_{dry} = 20 \text{ kN/m}^3$ and $\gamma_{sat} = 22 \text{ kN/m}^3$ are computed. The results are summarized in Table 5.6.

Table 5.6: Critical seismic coefficients computed with the limit equilibrium model, derived for the reference case

Friction angle φ [$^\circ$]	Unit weights $\gamma_{dry} / \gamma_{sat}$ [kN/m^3]	Yield coefficient k_{cr} [-]
40	20 / 22	0.206
45	20 / 22	0.288

By comparing the computed yield coefficient range in Table 5.6 with the reference case test results discussed in paragraph 4.2.3 (during the experiment ‘sliding’ of the sheet pile quay wall initiates when the seismic load is increased from 0.2g to 0.3g), it can be seen that the proposed limit-equilibrium model appears to give satisfactory results. A comparison between the limit-equilibrium model and the calibrated PLAXIS 2D model in paragraph 5.3.4 will indicate again that the limit-equilibrium model indeed performs well.

5.2.3. Limit equilibrium model: structural forces in the sheet pile wall

In this paragraph it is investigated whether the newly derived limit-equilibrium model can also be used to estimate structural forces in the sheet pile wall that occur when the soil-structure system is subjected to the critical acceleration. It is attempted to compute the shear forces (and from that the bending moments) in the sheet pile wall by dividing the sliding mass of the limit-equilibrium model into slices. For each of these slices a sub-equilibrium of forces (equivalent to the forces in the original limit-equilibrium model) is derived. From these force-equilibria the resulting horizontal (shear) forces in the sheet pile wall are computed. The above is clarified in Figure 5.11.

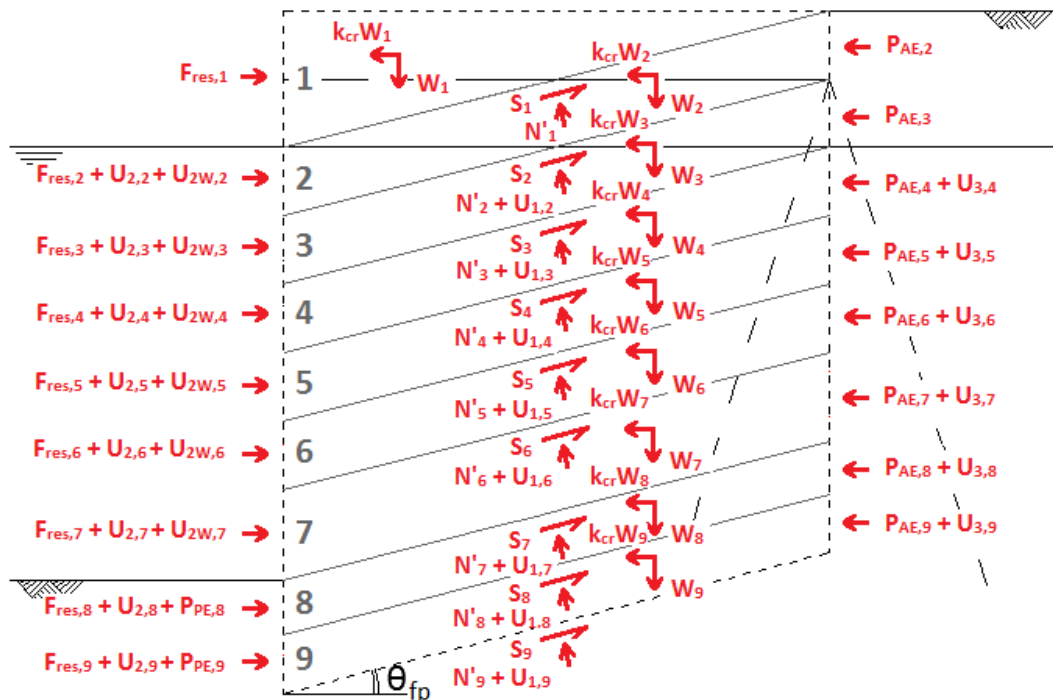


Figure 5.11: Sub-equilibria of forces in the limit-equilibrium model in order to compute shear forces in sheet pile wall

An Excel sheet is used for computing the force-equilibria and the resulting shear forces in the sheet pile wall. In this spreadsheet it is also checked that the total of the i sub-forces in the i slices add up to the force values that are computed in the original limit-equilibrium model (e.g. $P_{AE} = \sum P_{AE,i}$). The computed shear force line, corresponding to the soil setup and limit-equilibrium critical acceleration ($k_{cr} = 0.287$) that follow from the PLAXIS 2D calibration (see paragraphs 5.3.2 to 5.3.4), is shown in the left graph of Figure 5.12. For comparison the shear forces corresponding to the bending moment measurements of CASE-300 ($k_h = 0.300$) are plotted in this graph.

In the right graph of Figure 5.12 the bending moment line obtained from integrating the shear force line of the limit-equilibrium model is plotted. It is noted that this bending moment line is integrated from a simplified version of the shear force line (mitigating the lowest negative part of the shear force line, as the dashed green line in the left graph indicates) for a better integration result with the few available shear force data points. Again for comparison the bending moment measurements of CASE-300 ($k_h = 0.300$) are plotted in the same graph.

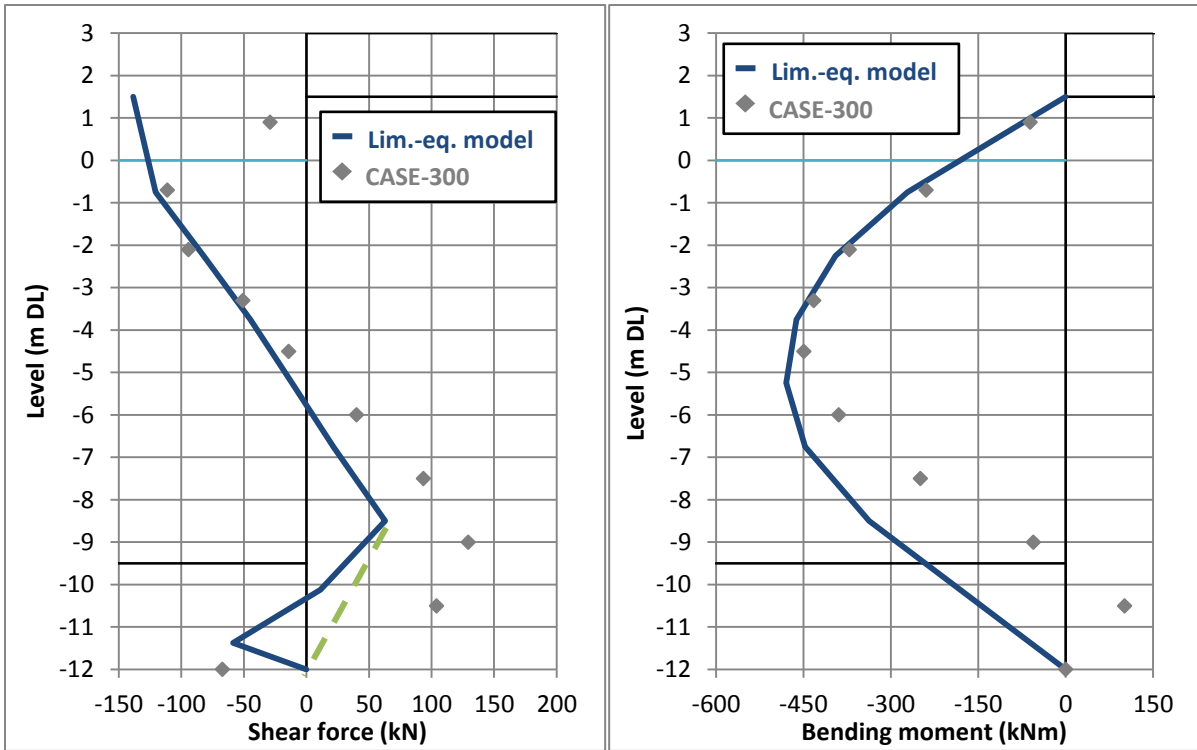


Figure 5.12: Shear force line (left) and bending moment line (right) computed with the limit-equilibrium model and compared with CASE-300 measurements

By comparing the shear force and bending moment lines of the limit-equilibrium model with the measurements of the reference case corresponding to a somewhat higher seismic coefficient ($k_h = 0.287$ versus $k_h = 0.300$) it can be seen that the limit-equilibrium model performs quite well. The maximum values computed with the limit-equilibrium model approach the maximum values measured in the reference case. That the maximum bending moment value of the limit-equilibrium model exceeds the maximum bending moment value of the reference case (while it corresponds to a lower seismic coefficient) is explained by an erroneous assumption that is embedded in the way of computing the force-equilibria as shown by Figure 5.11. It is assumed in this schematization that the slices of the sliding mass are rigid bodies which transfer the forces one-to-one onto the sheet pile wall, while in reality these soil bodies deform internally through which transferred forces onto the wall are reduced. The deviating bending moment shape beneath sea bed level is explained by the fact that for the critical acceleration the passive soil condition is fully plastic and thus no passive soil resistance exists. In contrast it is for the CASE-300 measurements expected from the reference case behaviour that passive soil resistance has redeveloped again after passive soil failure.

5.2.4. SHAKE2000 model: site-response analysis

The software tool SHAKE2000 will be applied to obtain strong ground motions in the soil column of the reference case, representative for the recorded motion used in the reference case. In this paragraph the corresponding approach and the relevant model input and output settings will be discussed. For the complete SHAKE2000 input files one is referred to Appendix F.

5.2.4.1. Approach

As was stated in paragraph 4.2.2 the North-South component of the PARI F2660 record, obtained at ground level, will be translated to a motion at bedrock level via (reverse) site-response analysis in SHAKE2000. This is possible as the soil column beneath the PARI Sendai-G recorder is provided at the PARI database website, and thus can be inputted in SHAKE2000. Subsequently the obtained bedrock motion, which can be scaled to desired PGA values, will be the input motion for the reference case soil column at bedrock level and the corresponding site-response analysis. For the PARI F2660 record, similar records will be collected by comparing frequency spectra. Comparable records will be collected from the imported SLAMMER database (consisting mainly of

(horizontal) strong motion records downloaded from the New Generation Attenuation (NGA) database, which is maintained by the Pacific Earthquake Engineering Research Center (PEER) at the University of California, Berkeley). The site-response analysis procedure outlined above will be applied for the comparable records as well. In this way it is attempted to gather multiple representative records for SDA and DA. An overview of the procedure is provided in Figure 5.13. It is noted that 1-D equivalent linear site-response analysis will be applied.

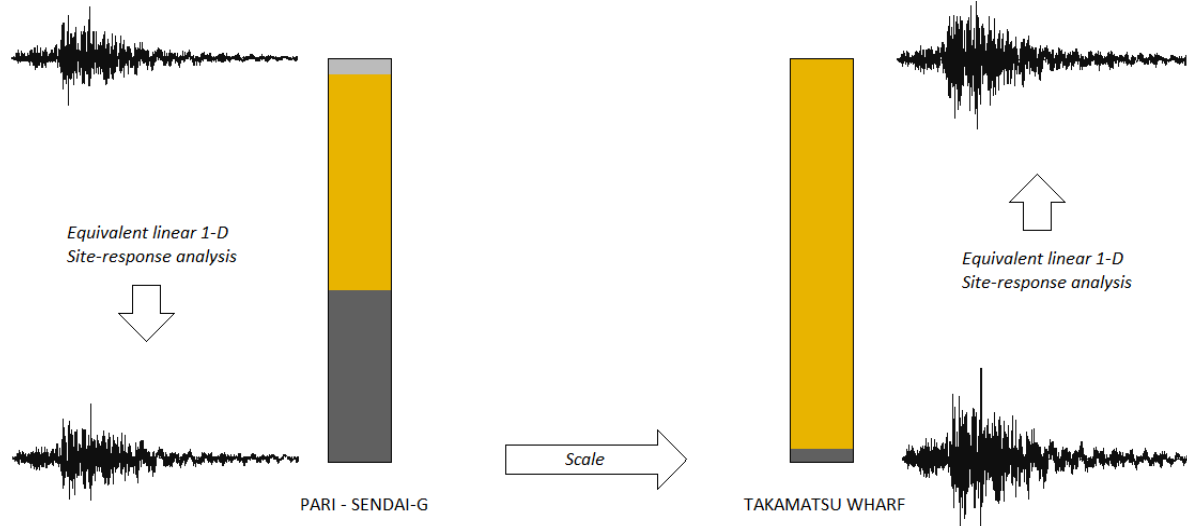


Figure 5.13: SHAKE2000 site-response analysis procedure

At this point it must be noted that during the reverse site-response analysis only the altering of the vertical shear wave by local site effects is accounted for. It for instance does not account for the interaction processes that can occur during an actual earthquake when different types of seismic waves attenuate from different directions through the subsoil and affect each other. Earthquake shaking recorded at ground level includes the effects of these interactions. So from the horizontal earthquake shaking that is measured at ground level (and taken as the vertical shear wave in seismic analysis) the actual bedrock waves that occurred during the earthquake can never be obtained by site-response analysis. For engineering practice such analysis is considered to be sufficient though.

5.2.4.2. Dynamic soil properties

The dynamic properties of the soil material in the columns are defined by shear modulus (G/G_{\max}) and damping curves which respectively describe the reduction of the shear modulus and the increase of damping in a soil layer with increasing strain. A number of such curves are implemented in SHAKE2000. For the sand material the Seed & Idriss (1970) average sand curves are applied. For the rock material the EPRI (1993) rock curves are used. In Figure 5.14 these curves are shown.

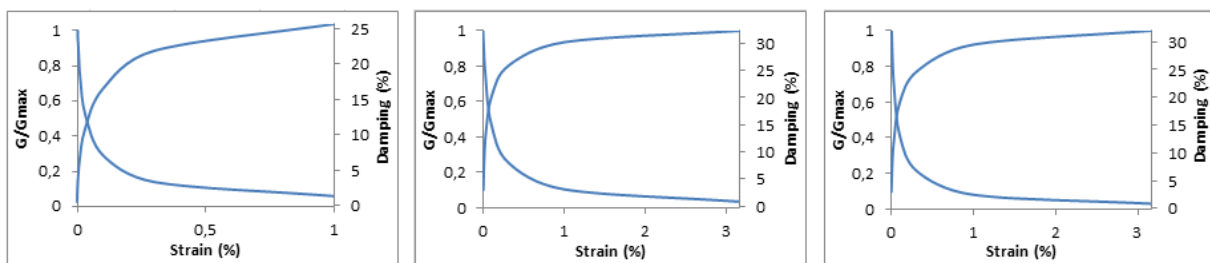


Figure 5.14: Dynamic soil properties: G/G_{\max} and Damping curves for average sand (Seed & Idriss, 1970), 20-50ft rock (EPRI, 1993) and 51-120ft rock (EPRI, 1993) respectively

5.2.4.3. Soil columns

The soil profiles of the PARI Sendai-G recorder and the reference case with their corresponding input parameters are given in Table 5.7 and Table 5.8 respectively. Sufficient calculation accuracy is obtained by dividing the sand layers in SHAKE2000 in sublayers of 1 to 2.5 meters.

Table 5.7: Soil column beneath PARI Sendai-G recorder

Soil column beneath PARI recorder				
Depth w.r.t. ground level	Soil type	Unit weight [kN/m ³]	Damping ratio [-]	Maximum shear wave velocity [m/s]
0.0 to -7.5 m	Sand	17.5 / 18.5	0.05	130 / 180
From -7.5 m	Rock	24.0	0.02	820

Table 5.8: Soil column at reference case

Soil column at reference case				
Depth w.r.t. DL	Soil type	Unit weight [kN/m ³]	Damping ratio [-]	Maximum shear wave velocity [m/s]
+3.0 to -16.5 m	Sand	20.0 / 22.0	0.05	250
From -16.5 m	Rock	24.0	0.02	820

5.2.4.4. Input motions

The North-South component of the PARI F2660 motion, recorded in Port of Sendai during the 2008 Iwate-Miyagi inland earthquake, is taken as the basic motion. The accelerogram is shown in Figure 5.15.

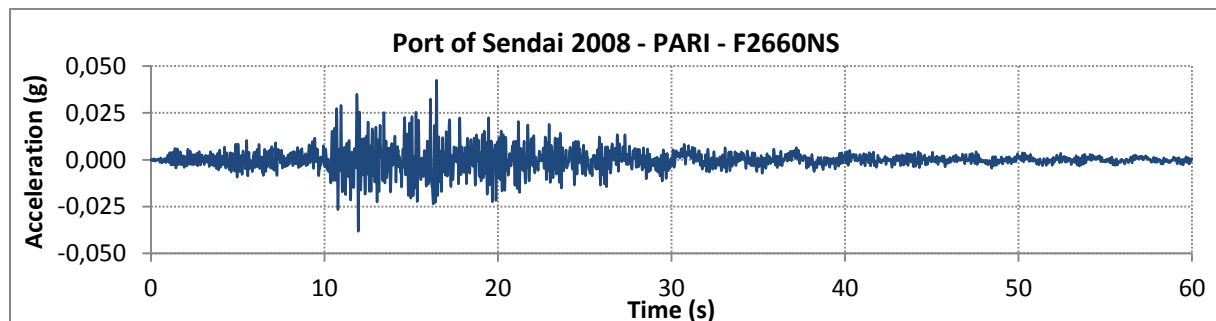


Figure 5.15: Accelerogram N-S component of the PARI F2660 motion, recorded at Port of Sendai in 2008

Comparable records are collected from the SLAMMER database by matching acceleration spectra. Five ‘fitting’ records out of a total of twenty-five hundred records were chosen. The result, computed with SHAKE2000, is shown in Figure 5.16. The five strong motions were recorded during the following earthquakes respectively: Northridge 1994; Niigata 2001; Whittier Narrows 1987.

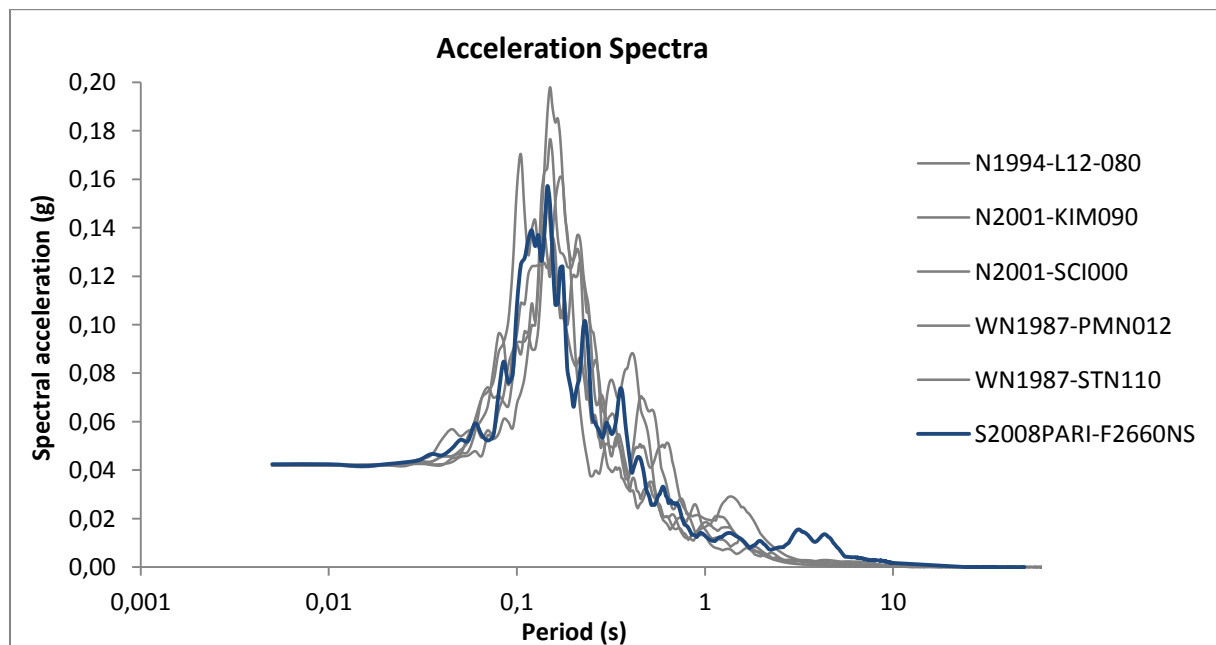


Figure 5.16: Acceleration spectra of earthquake motions at ground level, compared to the PARI-F2660NS ground motion

The total of six records represented in Figure 5.16 will be used in the site-response analysis procedure, to be executed with SHAKE2000. The six motions at ground level are translated to PARI Sendai-G site bedrock motions by means of downward site-response analysis. The bedrock motions are successively scaled to 0.2g, 0.3g and 0.6g motions which are introduced at the bottom (bedrock level) of the reference case soil column for upward site-response analysis.

5.2.4.5. Output settings

For the PARI Sendai-G and reference case soil columns the following is computed:

- Acceleration time histories at any layer
- Shear stress and strain time histories at intermediate layers
- Response spectra (spectral displacement as a function of period) at the surface and intermediate layer for different damping ratios
- Fourier amplitude spectra (acceleration amplitude as a function of frequency) at the surface, intermediate layers and bedrock
- Amplification spectra (amplification ratio as function of frequency) between bedrock, intermediate and surface layer
- Strain-compatible damping, shear moduli, maximum shear strain, maximum shear stress, shear wave velocity, peak acceleration and cyclic stress ratio over the depth of the soil column

For permanent-displacement analysis with SLAMMER the acceleration time histories obtained in the layer of the reference case soil column which contains the centre of gravity of the failure wedge will be used. Figure 5.17 shows this centre of gravity. It was mentioned earlier that according to (Kavazanjian, 2013) the strong motions used in permanent-displacement analysis of embankments have to be considered at this particular location.

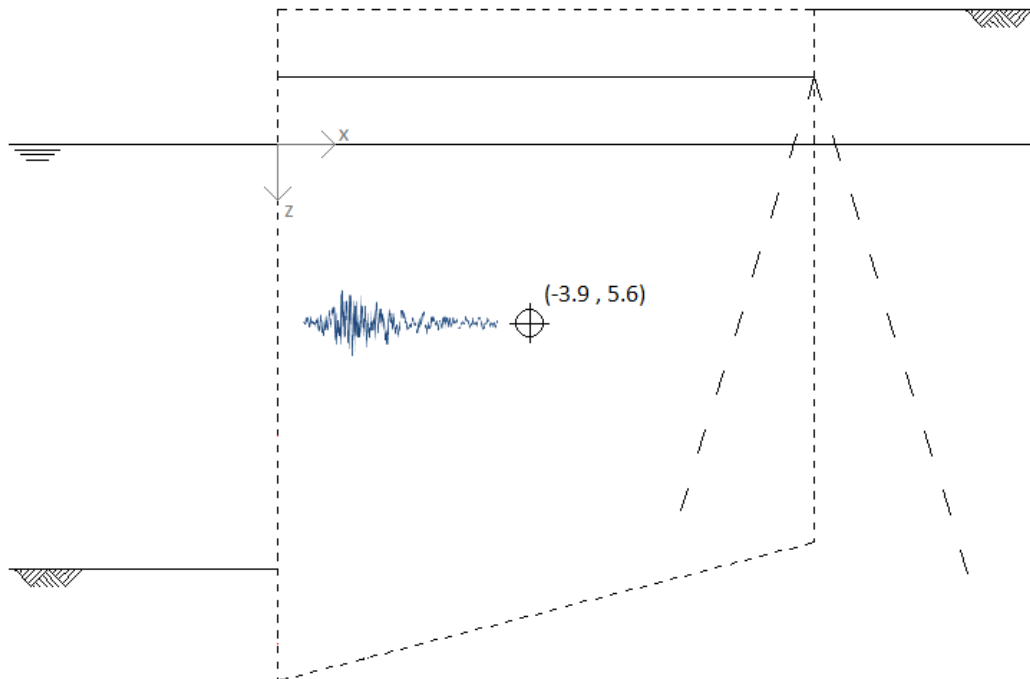


Figure 5.17: Centre of gravity of the schematized failure wedge (sliding mass) of the anchored sheet pile quay wall

A point of interest concerning the obtained peak accelerations in the soil column is that for the CASE-200 and CASE-300 records the peak accelerations are eventually magnified when travelling towards ground level. For the CASE-600 records though, the peak accelerations are eventually reduced when travelling towards ground level. This possibly indicates that there is some kind of maximum peak acceleration equilibrium for the present soil column. An example of this observation is presented in Figure 5.18.

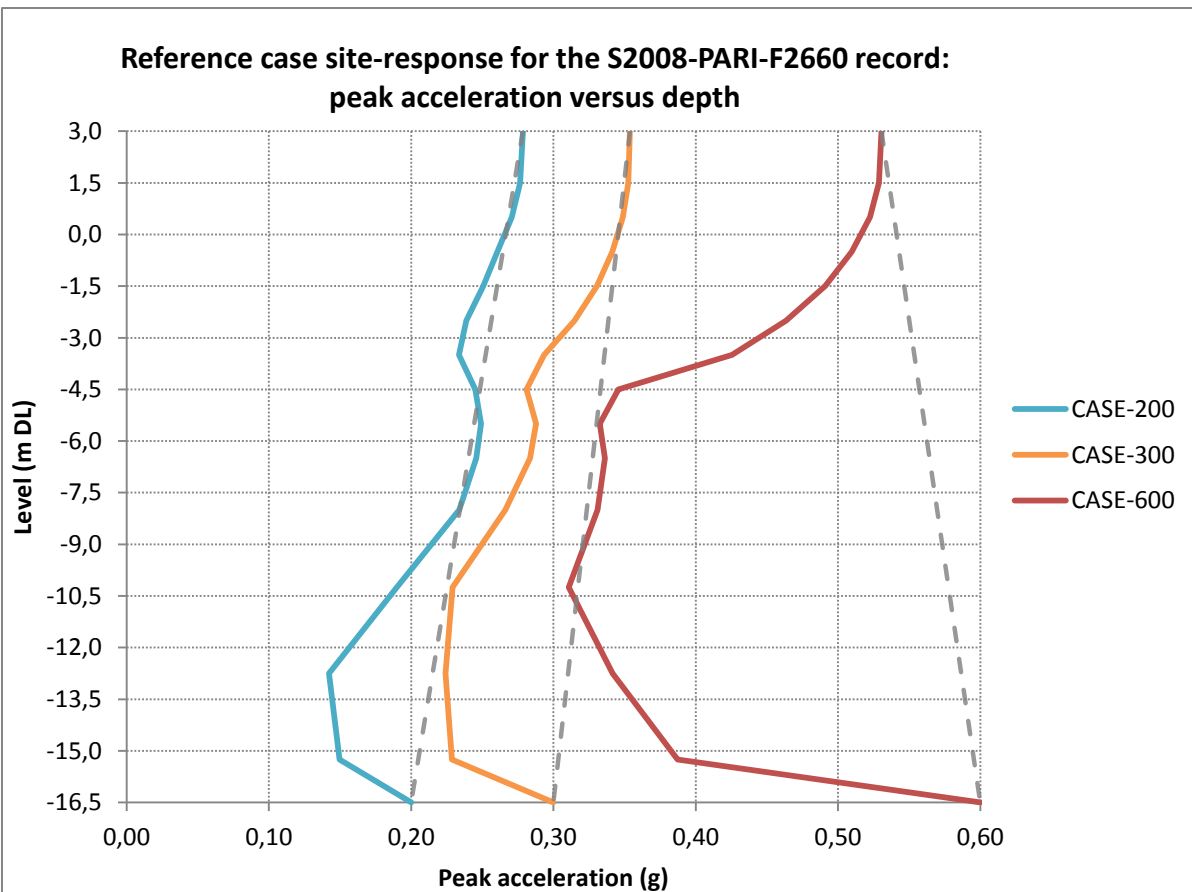


Figure 5.18: Site-response (peak acceleration vs depth) for the S2008-PARI-F2660 record, computed with SHAKE2000

5.2.5. SLAMMER model: permanent-displacement analysis

5.2.5.1. Approach

With SLAMMER permanent-displacement analysis for shake events CASE-300 (0.3g) and CASE-600 (0.6g) is performed. CASE-100 (0.1g) and CASE-200 (0.2g) are not considered in this research phase as it is deduced from the reference case that permanent sliding displacement initiates when the seismic load is increased from 0.2g to 0.3g. Two types of permanent-displacement analysis will be carried out: rigorous and empirical. The critical acceleration needed for the analyses is computed with the limit-equilibrium model of paragraph 5.2.2 and validated with the PLAXIS 2D model (paragraph 5.3.4). The accelerograms needed for the rigorous analyses are obtained with SHAKE2000 (paragraph 5.2.4). The parameters needed for the empirical analyses are automatically calculated by SLAMMER from the SHAKE2000 accelerograms.

5.2.5.2. Rigorous and empirical analysis

The two types of permanent-displacement analysis that SLAMMER offers are applied: rigorous and simplified (i.e. empirical). The rigorous analysis calculates the displacement of the sliding mass by integrating the peaks of the time histories over the threshold acceleration twice. This critical acceleration is the important input parameter which in this case will be defined as being constant. In case of rigid-block analysis a choice can be made between displacements in downslope only or both down- and upslope direction. For decoupled and coupled analyses some additional input parameters are necessary, i.e. the height of the soil mass, the shear wave velocities above and below the slip surface, the damping ratio and the soil model (linear elastic or equivalent linear). The simplified variants of permanent-displacement analysis in SLAMMER are based on empirical regression relationships which predict ground displacement based on ground motion parameters such as PGA and PGV. Different empirical relationships for rigid-sliding-block analysis are used. For an overview and background on these relationships one is referred to Appendix B, section B.2.

5.2.5.3. Model settings

The CASE-300 and CASE-600 acceleration time histories in the centre of gravity of the sliding mass will be used for rigorous permanent-displacement analysis with SLAMMER. All these input motions, obtained with SHAKE2000, are plotted in Appendix G. For the rigorous rigid-sliding-block analysis the displacement will only be calculated in ‘downslope’ direction. Referring to the geometry of the soil-structure system it can be expected that only significant displacement towards the sea can occur. For the decoupled and coupled permanent-displacement analysis the input options as summarized by Table 5.9 are selected.

Table 5.9: Rigorous decoupled / coupled permanent-displacement analysis parameters

Parameter	Value	Comment
Height [m]	15	Total length sheet pile wall
Shear wave velocity (material above slip surface) [m/s]	250	In correspondence with SHAKE2000 setup
Shear wave velocity (material above slip surface) [m/s]	250	In correspondence with SHAKE2000 setup
Damping ratio [%]	5	In correspondence with SHAKE2000 setup
Reference strain [%]	0.05	Default value
Soil model [-]	Linear / Equivalent linear	Checking performance of both soil models

The critical acceleration for the permanent-displacement analysis is calculated both with the limit-equilibrium model and the calibrated PLAXIS 2D model (see paragraph 5.3.4). The calibrated critical acceleration value computed with PLAXIS 2D will be applied in the SLAMMER analysis as it follows from a more refined calculation. From Table 5.19 it can be seen that the PLAXIS 2D critical acceleration result (which is closely approached by the limit-equilibrium model result!) has a value of $a_c = 0.27g$.

This critical acceleration is not only applied in rigorous but also in empirical SLAMMER analysis. The empirical relationships for Newmark calculations that are considered (see paragraph B.2.2. for background information):

- Saygili and Rathje (2008)
 - a. Displacement as a function of critical acceleration and peak acceleration
 - b. Displacement as a function of critical acceleration, peak acceleration and peak velocity
 - c. Displacement as a function of critical acceleration, peak acceleration, peak velocity and Arias intensity
- Jibson (2007)
 - a. Displacement as a function of critical acceleration and peak acceleration
 - b. Displacement as a function of critical acceleration and Arias intensity
 - c. Displacement as a function of critical acceleration, peak acceleration and Arias intensity
- Jibson et al. (1998, 2000)
 - o. Displacement as a function of critical acceleration and Arias intensity
- Jibson (1993)
 - o. Displacement as a function of critical acceleration and Arias intensity
- Ambraseys and Menu (1988)
 - o. Displacement as a function of critical acceleration and peak acceleration

The empirical relationships for rigid-sliding-block analysis that also require an input value for the moment magnitude M_w are not taken into account. The reason is that the applied earthquake records are scaled to different peak accelerations, which has the consequence that the consistency of the records with the originally determined M_w values is lost. This is also the reason that only empirical Newmark relationships are considered and not the available empirical coupled relationships, as these also require the input of M_w . In Table 5.10 the empirical input parameters (apart from the critical acceleration) of the different CASE-300 and CASE-600 earthquake signals are presented.

Table 5.10: Input parameters of the different CASE-300 and CASE-600 earthquake signals for the empirical Newmark rigid-sliding-block analyses

Motion	Peak acceleration [m/s ²]	Peak velocity [m/s]	Arias intensity (I_a) [m/s] ^{ix}
CASE-300			
S2008PARI-F2660NS	0.273	39.1	2.634
N1994-L12-180	0.247	27.9	1.642
N2001-KIM090	0.301	33.0	1.743
N2001-SCI000	0.302	29.8	1.963
WN1987-PMN012	0.289	35.7	1.559
WN1987-STN110	0.341	33.2	2.824
CASE-600			
S2008PARI-F2660NS	0.379	73.6	6.723
N1994-L12-180	0.372	58.0	2.719
N2001-KIM090	0.376	63.9	4.884
N2001-SCI000	0.454	56.7	4.274
WN1987-PMN012	0.392	53.8	3.780
WN1987-STN110	0.441	64.8	5.646

^{ix} The Arias intensity is a parameter that reflects both acceleration amplitude and frequency content of the strong ground motion under consideration. It is obtained by integration of the accelerogram over its entire duration: $I_a = \frac{\pi}{2g} \int_0^{\infty} [a(t)]^2 dt$. (Kramer, 1996)

5.2.5.4. Target displacements

The permanent-displacement results that SLAMMER computes have to be checked with certain target displacements, i.e. the horizontal drift displacements of the soil-structure system due to sliding. ‘Drift displacement’ in this case refers to the increase of sliding displacement associated with a subsequent shake event. The target displacements are, just as the applied accelerograms, located at the centre of gravity of the sliding mass (see Figure 5.17). To determine the target displacements calibrated dynamic calculations with PLAXIS 2D are to be performed, which output dynamic displacement contours from which the target displacements can be determined. Paragraph 5.3.6 treats this process and presents the results in Table 5.26.

In Table 5.11 the target displacements computed with the calibrated PLAXIS 2D model, as shown in Table 5.26, are provided. The permanent-displacement results that are computed with SLAMMER will be compared with these target displacements (in the next paragraph - 5.2.6). Because permanent-displacement results strongly depend on the specific accelerogram properties, an acceptance range around the computed target displacements is set. A range of +/-50% is chosen as this is a commonly applied range for permanent-displacement analysis. The acceptance range values corresponding to the target displacements are also shown in Table 5.11.

Table 5.11: Target displacements and corresponding acceptance ranges

Motion	Target (drift) displacement [mm]	Acceptance range values [mm]
CASE-200 >> CASE-300		
S2008PARI-F2660NS	17	8 – 26
N1994-L12-180	13	6 – 20
N2001-KIM090	23	11 – 35
N2001-SCI000	29	14 – 44
WN1987-PMN012	29	14 – 44
WN1987-STN110	31	15 – 47
CASE-300 >> CASE-600		
S2008PARI-F2660NS	147	73 – 221
N1994-L12-180	149	74 – 224
N2001-KIM090	148	74 – 222
N2001-SCI000	138	69 – 207
WN1987-PMN012	145	72 – 218
WN1987-STN110	132	66 – 198

5.2.6. Results

Rigorous and empirical permanent-displacement analyses are performed. The displacements computed with SLAMMER are compared with the target displacements of the reference case. The results are summarized in this paragraph.

5.2.6.1. Rigorous analysis results

The SLAMMER rigorous analysis results for the two soil model options (linear elastic and equivalent linear) combined with the three permanent-displacement analysis options (rigid, decoupled and coupled) are presented in Table 5.12. SLAMMER displacement results are marked green when situated within the target displacement acceptance range and are marked red when situated outside the acceptance range.

Table 5.12: SLAMMER rigorous permanent-displacement analysis results

Motion	Computed displacements [mm]					
	Linear elastic soil			Equivalent linear soil		
	Rigid	Decoupled	Coupled	Rigid	Decoupled	Coupled
CASE-200 >> CASE-300						
S2008PARI-F2660NS	0	5	5	0	8	11
N1994-L12-180	0	1	1	0	8	11
N2001-KIM090	0	3	3	0	7	8
N2001-SCI000	0	9	8	0	6	7
WN1987-PMN012	0	5	5	0	15	16
WN1987-STN110	1	7	8	1	11	14
CASE-300 >> CASE-600						
S2008PARI-F2660NS	11	40	36	11	69	72
N1994-L12-180	5	25	23	5	33	36
N2001-KIM090	12	39	38	12	68	70
N2001-SCI000	13	25	24	13	20	22
WN1987-PMN012	18	40	37	18	38	42
WN1987-STN110	63	87	85	63	73	91

5.2.6.2. Empirical analysis results

The SLAMMER empirical analysis results for the nine empirical relationships (Saygili & Rathje 2008 (a, b, c), Jibson 2007 (a, b, c), Jibson et al. 1998, Jibson 1993 and Ambraseys & Menu 1988) are presented in Table 5.13. SLAMMER displacement results are marked green when situated within the target displacement acceptance range and are marked red when situated outside the acceptance range.

Table 5.13: SLAMMER empirical permanent-displacement analysis results

Motion	Computed displacements [mm]								
	Empirical relationship								
	S&R, 2008a	S&R, 2008b	S&R, 2008c	J, 2007a	J, 2007b	J, 2007c	J et al., 1998	J, 1993	A&M, 1988
CASE-200 >> CASE-300									
S2008-F2660NS	0	0	0	0	6	1	17	23	0
N1994-L12-180	0	0	0	0	2	0	8	12	0
N2001-KIM090	0	0	0	0	2	1	9	13	0
N2001-SCI000	0	0	0	0	3	1	11	15	0
WN1987-PMN012	0	0	0	0	2	1	8	11	0
WN1987-STN110	2	1	2	1	7	1	19	26	2
CASE-300 >> CASE-600									
S2008-F2660NS	5	12	20	1	55	4	70	91	5
N1994-L12-180	4	7	8	1	6	2	18	24	4
N2001-KIM090	5	9	14	1	25	3	43	57	5
N2001-SCI000	16	20	25	4	18	6	35	47	14
WN1987-PMN012	7	9	12	2	14	3	29	39	6
WN1987-STN110	14	22	32	4	36	6	54	71	12

5.2.6.3. Discussion of results

Rigorous and empirical permanent-displacement analyses have been performed for the calibrated critical acceleration $a_c = 0.27g$. From the results presented in Table 5.12 and Table 5.13 it can be seen that both rigorous and empirical analysis do not output the target displacements of the reference case. The permanent-displacement results are mostly outside the 50%-range and when inside the 50%-range the results are on the low boundary.

Based on the above results no hard conclusions can be drawn on the performance of the different rigorous and empirical analysis options but a few things are mentioned. It is noted that for the rigorous analysis it is found that the results within the target displacement range all correspond to decoupled and coupled calculations, mostly combined with the equivalent linear soil option. This is to be expected as these more advanced analysis options probably apply better to the complex anchored sheet pile situation than the rigid and linear elastic options. In the empirical analysis only the relationships by (Jibson *et al.*, 1998) and (Jibson, 1993) output a few 'green results'.

In general the question arises whether rigorous and empirical permanent-displacement analyses, which are traditionally developed for embankments / landslides, are suitable for anchored sheet pile quay walls. On the other hand it is noted that the applied earthquake signals have a big influence on the permanent-displacement results and that these earthquake signals include an uncertainty as they are all an approximation of the reference case earthquake record. This matter will be discussed in more detail in section 6.3.

5.3. Dynamic analysis: finite element method

5.3.1. Introduction

In this section the fourth step of the research methodology is discussed. It concerns calibrated dynamic analysis. Figure 5.19 shows the location of the current step within the research process.

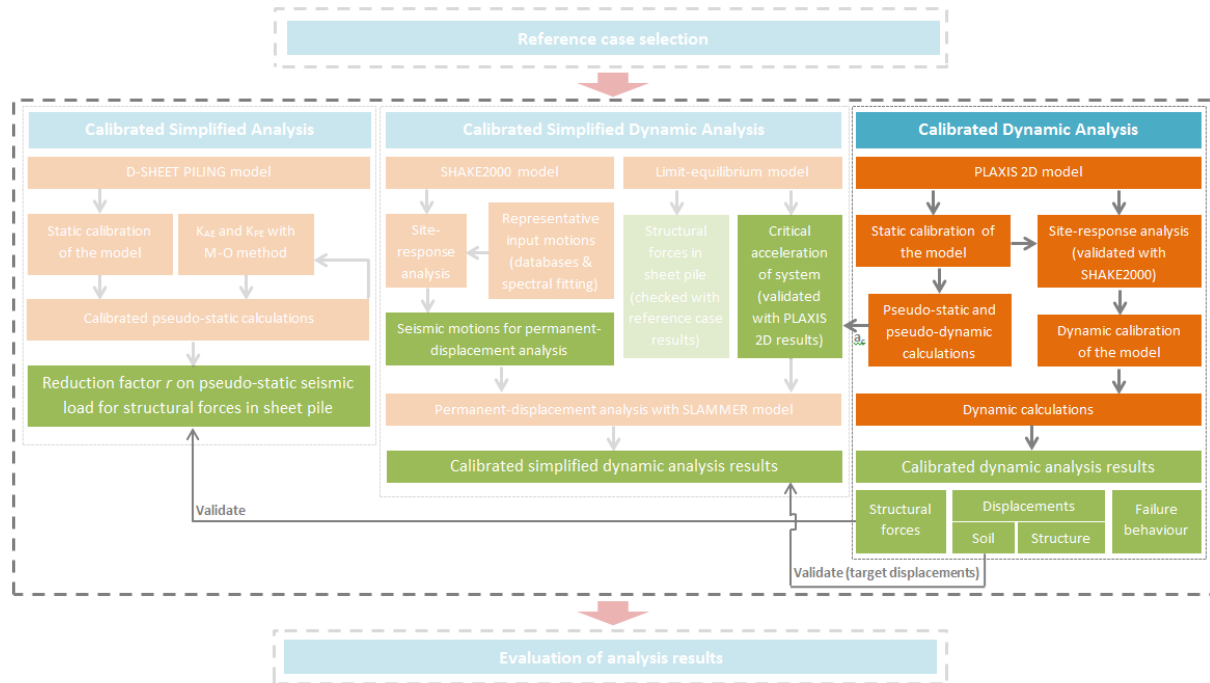


Figure 5.19: Step 4 of the research methodology: calibrated dynamic analysis

The general approach in this step of the research methodology is to set up a calibrated PLAXIS 2D model of the reference case which is statically and dynamically calibrated. Dynamic performance of the PLAXIS 2D model is validated with SHAKE2000 by comparing site-response analysis results of both models. Pseudo-static and pseudo-dynamic calculations are carried out with the statically calibrated model to obtain the critical acceleration of the anchored sheet pile quay wall. Dynamic calculations are carried out with the dynamically calibrated model for the six representative bedrock motions. PLAXIS 2D calculation results (i.e. structural forces, structure and soil displacements, failure planes) will be compared with SA and SDA results and are used to validate the developed limit-equilibrium model and to create insight in the seismic failure behaviour of the anchored sheet pile quay wall under consideration. The combination of the obtained results must lead to a better understanding of the performance of the soil-structure system and the ability to propose improvements for simplified seismic design methodologies.

5.3.2. PLAXIS 2D model

An impression of the layout of the PLAXIS 2D model built for the dynamic analysis step is provided in Figure 5.20. In the following the setup of the different aspects of the model will be discussed.

5.3.2.1. Geometry

The geometry applied in the PLAXIS 2D model is the same as the reference case model, as can be deduced from Figure 5.20. This geometry is extended though if it would appear necessary for computational reasons. See e.g. paragraph 5.3.4 where the critical acceleration is computed. The layout of the geometry requires application of the plane strain model.

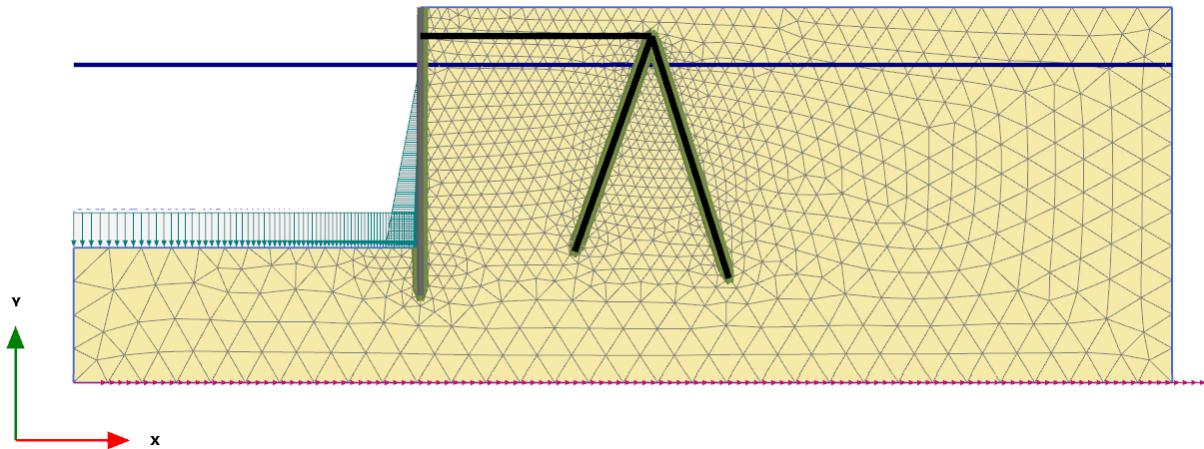


Figure 5.20: Layout PLAXIS 2D model

5.3.2.2. Soil material

The soil material model that will be used in the PLAXIS 2D setup is the Hardening Soil with small strain-stiffness (HSsmall) model. The choice for this model is due to the fact that it is applicable to the reference case soil condition and that it introduces hysteretic material damping in dynamic calculations. All the relevant specifics and parameters of the HSsmall model plus underlying other models are discussed in paragraph B.3.1. A first estimation of the HSsmall parameters for quartz sand based on the relative density (RD) is given in (Brinkgreve *et al.*, 2010). As the relative density is one of the few soil parameters provided in (Higuchi *et al.*, 2012), the paper of (Brinkgreve *et al.*, 2010) will be used to determine the HSsmall parameters on first hand. From the set of empirical relationships (all a function of RD) proposed in the paper, the parameter values shown in Table 5.14 are computed. For the empirical expressions one is referred to (Brinkgreve *et al.*, 2010). HSsmall parameters other than the ones mentioned in the table are set to their default values.

Considering higher relative density values than the reference case value (RD = 80) in Table 5.14 is because of the simulated initial stress conditions in the reference case. It was already mentioned in the static calibration of the D-SHEET PILING model (paragraph 5.1.2) that due to the applied centrifuge process, simulated initial stress conditions are likely overestimated (very high stiffness of the soil package, lowering e.g. the initial bending moments in the sheet pile quay wall). These initial conditions are thought to be the result of further densification of the soil material due to the 30g centrifugation under which the shake table test procedure is performed.

Table 5.14: HSsmall model input parameters based on RD, derived from (Brinkgreve *et al.*, 2010)

RD [%]	$\gamma_{\text{unsat}} / \gamma_{\text{sat}}$ [kN/m ³]	E_{50}^{ref} [kN/m ²]	$E_{\text{oed}}^{\text{ref}}$ [kN/m ²]	$E_{\text{ur}}^{\text{ref}}$ [kN/m ²]	G_0^{ref} [kN/m ²]
80	18.2 / 20.3	48.000	48.000	144.000	114.000
90	18.6 / 20.4	54.000	54.000	162.000	121.200
100	19.0 / 20.6	60.000	60.000	180.000	128.000
RD [%]	m [-]	$\gamma_{0.7}$ [-]	ϕ [°]	Ψ_{\max} [°]	R _f [-]
80	0.450	$1.2 \cdot 10^{-4}$	38.0	8.0	0.900
90	0.419	$1.1 \cdot 10^{-4}$	39.3	9.3	0.888
100	0.388	$1.0 \cdot 10^{-4}$	40.5	10.5	0.875

5.3.2.3. Structural elements

The structural elements that need to be modelled are the sheet pile wall, the anchor rod and the anchor batter piles. The tie rod is modelled with the node-to-node anchor. Both the sheet pile wall and the batter piles are modelled with the 2D plate element (surrounded by interfaces to account for soil-structure interaction). For the modelling of the batter piles one could suggest that the 2D embedded pile row would also suffice. But as

was reasoned in B.3.2.3, it is not advisable to use these elements in a situation where an anchored sheet pile wall is loaded up to failure, as is the case in the present study. The structural input parameters of the sheet pile wall, batter pile and anchor rod elements are presented in Table 5.15, Table 5.16 and Table 5.17 respectively. For background on the element models and corresponding parameters one is referred to paragraph B.3.2.

Table 5.15: 2D Plate (sheet pile) input parameters

Sheet pile parameters	Value
Material model	Elastic ^x
Isotropic material	Yes
End bearing	Yes
Axial stiffness EA ₁ = EA ₂ [kN/m]	5.620·10 ⁶
Bending stiffness EI [kNm ² /m]	1.323·10 ⁵
Weight [kN/m/m]	2.1
Poisson's ratio v [-]	0.0 ^{xi}

^xThe elastic model is applicable as the loads on the structural elements stay within the elastic range of the steel material

^{xi}In case of sheet pile walls (relatively flexible in the out of plane direction) it is advised to set v to zero.

Table 5.16: 2D Plate (batter H-pile) input parameters

Batter pile parameters	Value
Material model	Elastic
Isotropic material	Yes
End bearing	Yes
Axial stiffness EA ₁ = EA ₂ [kN/m]	2.509·10 ⁶
Bending stiffness EI [kNm ² /m]	68.60·10 ³
Weight [kN/m/m]	0.94
Poisson's ratio v [-]	0.0

Table 5.17: Node-to-node anchor (tie rod) input parameters

Anchor rod parameters	Value
Material model	Elastic
Axial stiffness EA [kN/m]	290.9·10 ³
Anchor spacing [m]	1.5

5.3.2.4. Other

Other relevant aspects of the PLAXIS 2D model setup concern the applied mesh size, (dynamic) boundary conditions, additional Rayleigh damping in dynamic calculations, (earthquake) accelerograms and phasing. To obtain results with the highest possible accuracy a 15-noded very fine mesh is used. Because of the relatively simple layout of the model, computation time remains acceptable despite this mesh size.

For the static calculations default model boundary conditions can be used (standard fixities). For the dynamic calculations other model boundary conditions are required. For dynamics viscous boundary conditions with relaxation coefficients C₁ = 1 and C₂ = 0.25 are chosen (see B.3.1.6 for background information).

Another aspect in dynamic calculations is the addition of some frequency-dependent Rayleigh damping (in the soil material and if necessary in the structural elements) to supplement the frequency-independent hysteretic damping in the soil material introduced by the HSsmall model. The amount of Rayleigh damping will be determined during dynamic calibration of the model. Background theory on hysteretic and Rayleigh damping in the HSsmall model can be found in B.3.1.5.

For determining the critical acceleration of the model (as a validation of the limit-equilibrium model results in Table 5.6) a linearly increasing acceleration signal is introduced at the x_{min}, x_{max} and y_{min} boundaries of the PLAXIS 2D model via a prescribed horizontal displacement along these boundaries. As a comparison to these pseudo-dynamic calculations, also the pseudo-static calculation option in the PLAXIS 2D model is used for determining the critical acceleration.

In the dynamic calculations the seismic input motions will be introduced at the y_{min} boundary of the PLAXIS 2D model via a prescribed horizontal displacement along this boundary. For the CASE-100 event a replica of the reference case artificial motion is introduced in the model, while for the CASE-200, CASE-300 and CASE-600 events the representative bedrock accelerograms obtained with SHAKE2000 are applied. In order to validate the dynamic performance of the PLAXIS 2D model a separate site-response analysis for the PLAXIS soil column will be executed and compared with the site-response analysis results obtained with SHAKE2000.

Concerning the phasing of the calculations, the procedure proposed in (Higuchi *et al.*, 2012) will be held on to. The chronologic phasing in the PLAXIS 2D model: initial phase, static phase (seabed at DL -7.5 m), static phase (seabed at DL -9.5 m), CASE-100, CASE-200, CASE-300 and CASE-600. Computations concerning the critical acceleration and the site-response analysis are carried out in separate models.

5.3.3. Static calibration of the PLAXIS 2D model with the reference case

During the static calibration of the PLAXIS 2D model the same findings concerning the soil material parameters emerge, as was the case during the static calibration of the D-SHEET PILING model. Higher values for soil parameters are needed than the values derived from a relative density of 80%. So again this is in line with the thoughts about the overvalued initial stress conditions of the test case. Static calibration is achieved by applying soil material parameters corresponding to a relative density of 100% (see Table 5.14) and taking into account arching of soil above the anchors by again mitigating the soil package above the anchors.

The static calibration of the PLAXIS 2D model involves a bending moment line (and shear force line) match with the reference case. The reference case anchor force cannot be matched exactly but PLAXIS 2D does approach it. Furthermore the PLAXIS 2D sheet pile wall displacements are in the same range as the reference case displacements. For the latter it is noted that PLAXIS 2D calculates higher displacements near the seabed than near the anchor, while it is the other way around in the reference case. The static results are summarized in Table 5.18. The bending moment and shear force line fits are shown in Figure 5.21.

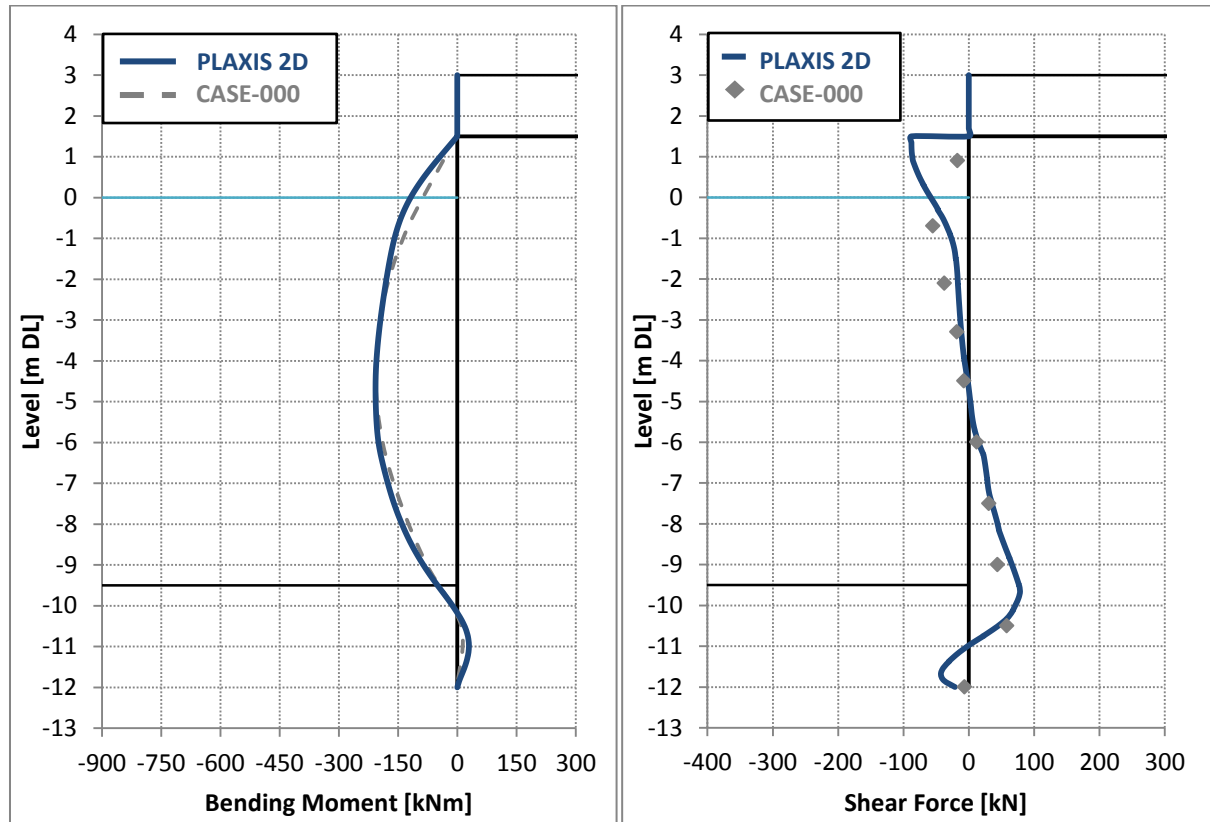


Figure 5.21: Bending moment and shear force line fits between PLAXIS 2D and reference case results

Table 5.18: PLAXIS 2D static calibration results

CASE-000	M _{MAX} [kNm]	F _{ANCHOR} [kN]	u _{ANCHOR} [mm]	u _{SEABED} [mm]
Reference case	207	108	14	6
PLAXIS 2D	207	132	6	12
Ratio (P2D / Ref. case)	1.00	1.22	0.43	2.00

It must be mentioned at this point that in (Higuchi *et al.*, 2012) comparative FE calculations with FLIP code are performed and that these FE results also differ from the test measurements. In other words, FLIP code, although within an acceptable range, also computes higher structural forces and deviating displacements.

5.3.4. Pseudo-static and pseudo-dynamic computation of the critical acceleration

PLAXIS 2D computations are carried out in order to validate the ability of the limit-equilibrium model, derived from Kranz (1953) and Towhata & Islam (1987), to calculate the critical acceleration of the present anchored sheet pile quay wall. For a more extensive validation both the model setups of RD = 80% and RD = 100% are considered. Furthermore PLAXIS 2D results are required to determine the critical acceleration as accurately as possible for SDA in section 5.2.

In PLAXIS two options for determining the critical acceleration can be employed. The first is the pseudo-static option in which a global acceleration (in terms of g) is introduced to model dynamic forces in a pseudo-static way. For this the ‘plastic’ calculation type followed by a safety analysis is used in order to check if the factor of safety has reduced to 1.00. The second option is to uniformly apply a linearly increasing acceleration signal onto the model along its x_{\min} , x_{\max} and y_{\min} boundaries by means of a prescribed displacement. For this the ‘dynamic’ calculation type is used. In case of both options the geometry of the model is extended for computational reasons.

5.3.4.1. Pseudo-static calculation

The pseudo-static calculation results for both the RD80% and RD100% setup are illustrated by Figure 5.22 and Figure 5.23 respectively. The figures show the failure plane corresponding to the point at which the structure starts to displace permanently. More specifically the plots show the incremental deviatoric strain after the last load step. For both figures it holds that the safety factor has reached the value 1.00.^{xii} For the RD80% setup a critical acceleration $a_c = 0.211g$ is calculated and for the RD100% setup $a_c = 0.268g$.

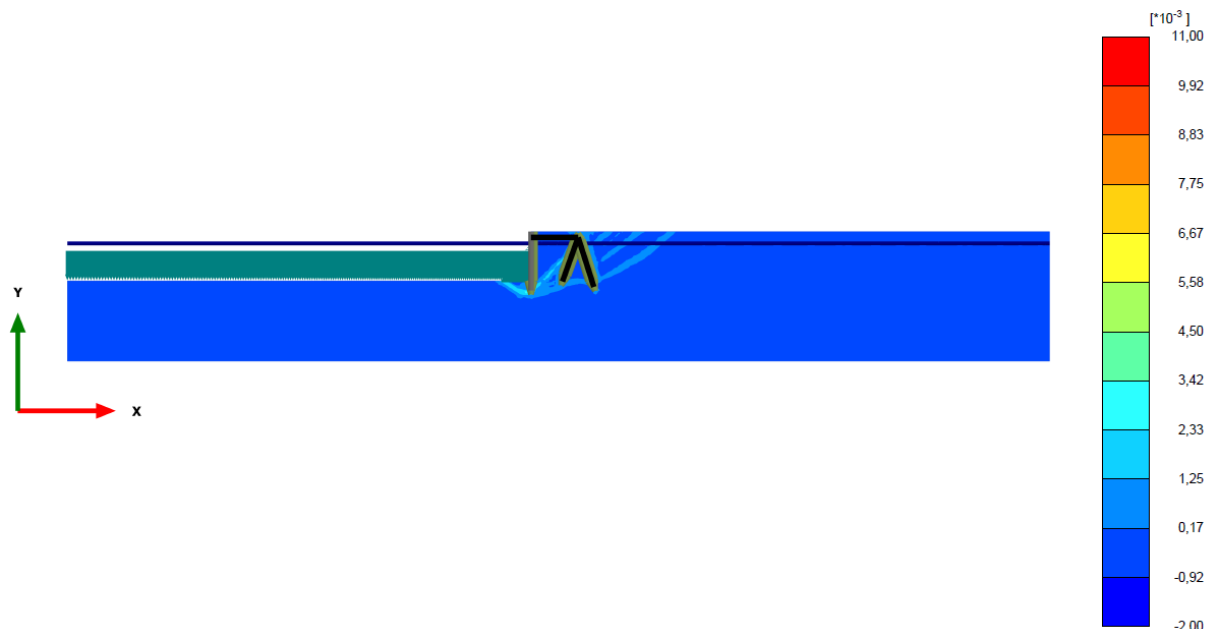


Figure 5.22: Failure plane (incremental deviatoric strain $\Delta\gamma_s$) corresponding to the pseudo-static critical acceleration and the soil parameter setup for a relative density of 80%

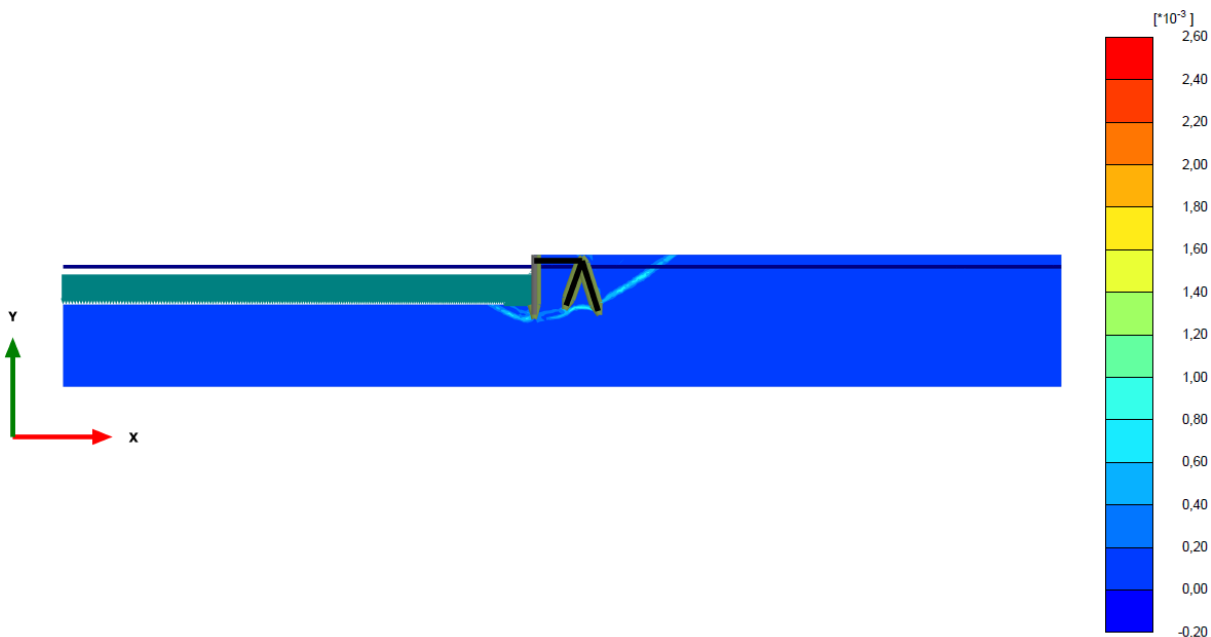


Figure 5.23: Failure plane (incremental deviatoric strain Δy_s) corresponding to the pseudo-static critical acceleration and the soil parameter setup for a relative density of 100%

^{xii} With the mesh set to 'very fine' the model unrealistically calculates very high peak values locally in front of the sheet pile wall, resulting in numerical instability when approaching a safety factor of 1.00. Therefore $\tan(\phi)$, which controls the failure criterion (see paragraph B.3.1), has been increased with 10% and a safety factor of 1.10 is computed. So the plots actually correspond to a safety factor of 1.10, which in this case is equivalent to a safety factor of 1.00.

5.3.4.2. Pseudo-dynamic calculation

In Figure 5.24 the linearly increasing acceleration signals that are uniformly applied along the boundaries of the RD80% and RD100% model are depicted. The specific durations and acceleration contents of the signals are arbitrarily chosen in such a way that PLAXIS 2D computes pseudo-dynamic output with the best possible graphical quality.

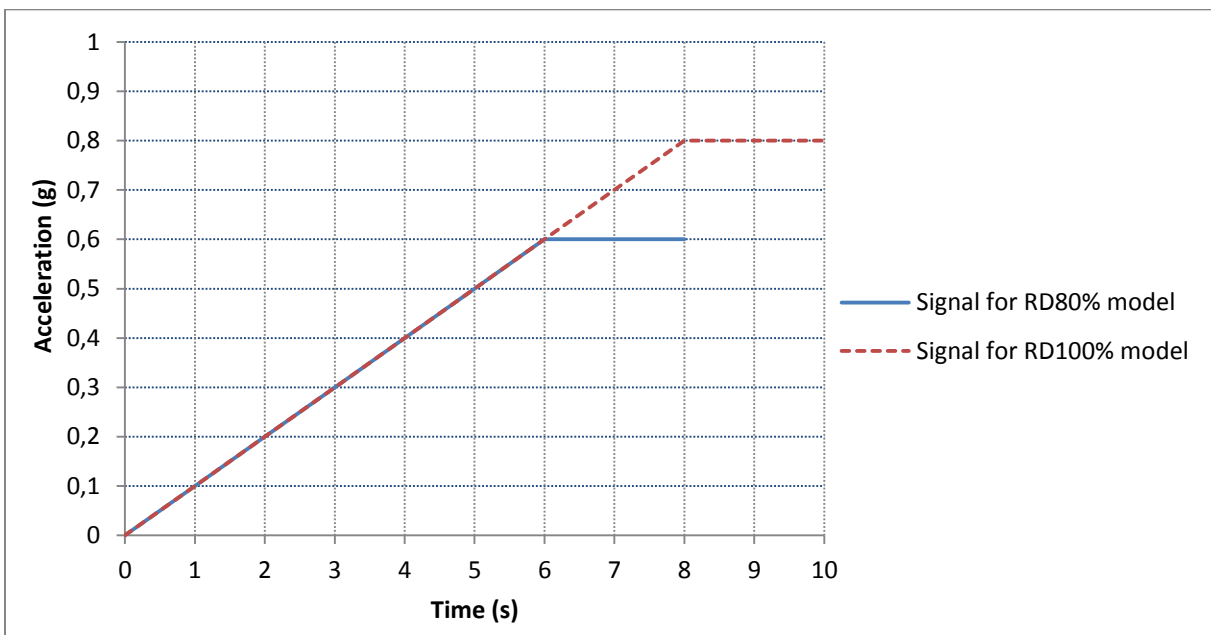


Figure 5.24: Linearly increasing acceleration signals applied in pseudo-dynamic analysis

The pseudo-dynamic calculation results for both the RD80% and RD100% setup are illustrated by Figure 5.25 and Figure 5.26 respectively. The figures show the horizontal acceleration output (in g's) in which the critical failure plane of the anchored sheet pile wall can be recognized. In both plots the critical failure plane lies within the yellow range. This complies with $a_c = 0.21g$ for the RD80% setup and $a_c = 0.27$ for the RD100% setup.

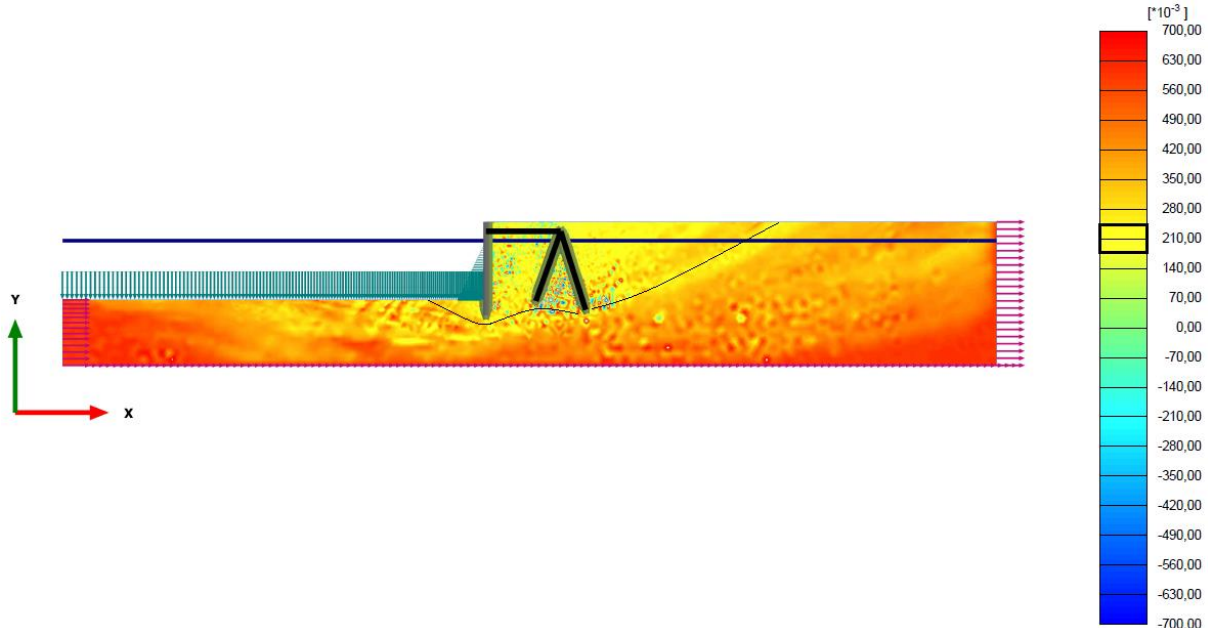


Figure 5.25: Failure plane (horizontal accelerations in g's) corresponding to the pseudo-dynamic critical acceleration and the soil parameter setup for a relative density of 80%

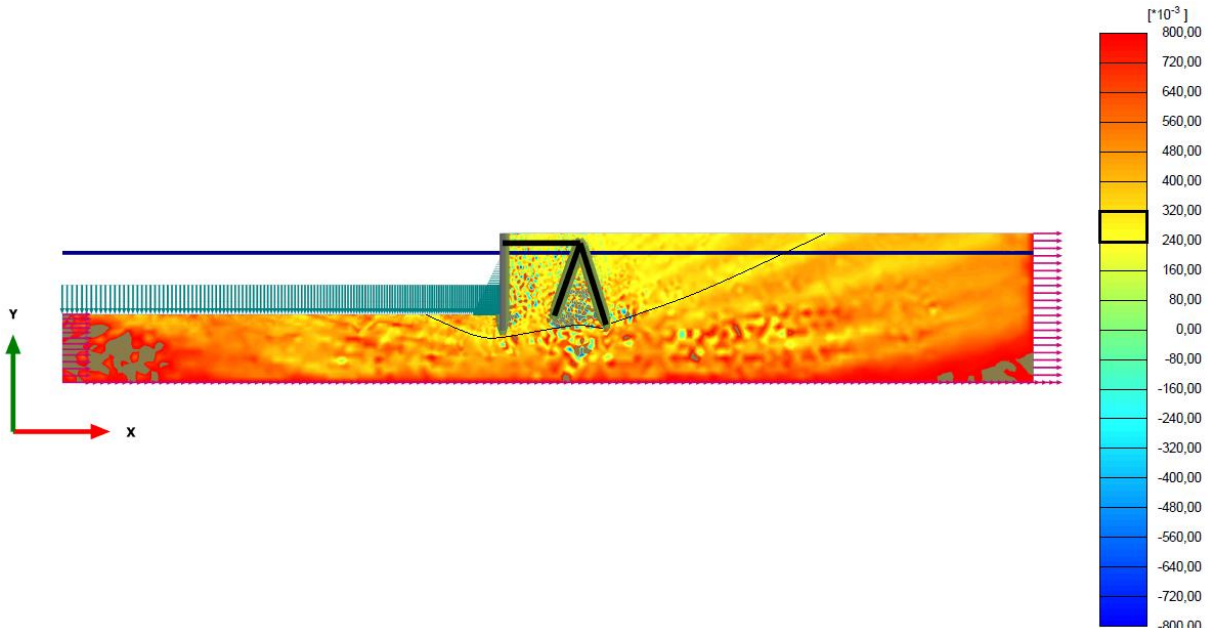


Figure 5.26: Failure plane (horizontal accelerations in g's) corresponding to the pseudo-dynamic critical acceleration and the soil parameter setup for a relative density of 100%

It must be noted that the acceleration output obtained with the pseudo-dynamic option is to a certain extent ambiguous. As can be seen in the figures, unrealistic peak acceleration patterns are found near boundaries and interfaces. After consulting the PLAXIS support service an explanation was found for these patterns. By applying the acceleration signals on the model boundaries not all mass is directly accelerating along with it. Because of this inertia effect large internal stresses are introduced in the soil which causes a large amount of plasticity. Due to this plasticity the model is not fully converging anymore (i.e. global error below the tolerated

error) within the default maximum number of iterations, causing the global error to increase in time. As a result the strange effects in the acceleration plots may occur. Although it has been attempted to obtain less ambiguous plots by increasing the number of iterations, better results were not acquired. At this point it is therefore concluded that the pseudo-dynamic approach for determining the critical acceleration is not that suitable for an anchored sheet pile structure (while it is for embankments).

5.3.4.3. Comparison with limit-equilibrium model

Table 5.19 shows the comparison between the critical accelerations computed with the limit-equilibrium model and with the PLAXIS 2D model for the separate soil material setups. The performance of the analytical limit-equilibrium model is indeed satisfactory, as it calculates almost the same critical accelerations as the FE model. Furthermore it is mentioned that the computed critical accelerations match the reference case behaviour where 'sliding' of the sheet pile quay wall initiates when the seismic load is increased from 0.2g to 0.3g.

Table 5.19: Critical accelerations obtained with the limit-equilibrium and the PLAXIS 2D model

Critical acceleration			
Soil material setup	Limit-equilibrium model ^{xiii}	PLAXIS 2D model	Ratio (LE / P2D)
RD80%	0.22g	0.21g	1.05
RD100%	0.29g	0.27g	1.07

^{xiii} In the limit-equilibrium calculations the friction angle is calculated as $\varphi = [(\varphi) + (\varphi+\psi_{\max})]/2$ to account to an average extent for the angle of dilatancy in this model.

5.3.5. Dynamic calibration of the PLAXIS 2D model: site-response analysis

The final part of the fourth research step comprises calibrated dynamic calculations with the PLAXIS 2D model. Firstly the dynamic performance of the PLAXIS 2D model has to be calibrated with the reference case. This is achieved by performing site-response analysis on a 1D soil column of the statically calibrated PLAXIS 2D model which is supplemented with the required amount of Rayleigh damping. During dynamic calibration the PLAXIS 2D site-response analysis results will be checked with SHAKE2000 site-response analysis results.

5.3.5.1. Site-response analysis model setup

From the layout of the PLAXIS 2D model (Figure 5.20) and the statically calibrated HSSmall soil material setup an equivalent 1D soil column is derived, which is applied in the site-response analysis. Figure 5.27 shows the layout of the soil column, projected on the layout of the anchored sheet pile quay wall model.

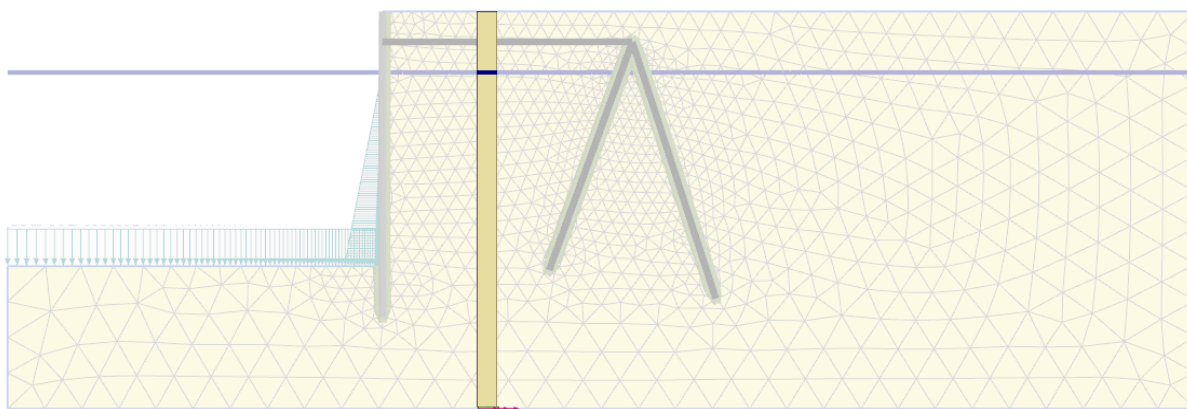


Figure 5.27: 1D soil column model in PLAXIS 2D for site-response analysis

It can be seen from the figure that the soil column has the same height as the anchored sheet pile quay wall model and that the seismic input motions are introduced to the model by a prescribed horizontal displacement at the y_{min} boundary (bedrock level). The seismic input motions for the PLAXIS 2D site-response analysis are the scaled PARI F2660NS bedrock motions (obtained with the reverse site-response analysis in SHAKE2000). These motions are shown in Appendix H, section H.1.

In the site-response analysis model the following dynamic boundary conditions are applied (one is referred to B.3.1.6 for background information on these boundary conditions):

- x_{\min} - and x_{\max} - boundaries: tied degrees of freedom
- y_{\min} -boundary: compliant base^{xiv}
- y_{\max} -boundary: none (standard fixities)

^{xiv} From testing with the current soil column it appears that the compliant base condition at the y_{\min} -boundary gives the same site-response analysis results as the none (standard fixities) condition.

From the site-response analysis it is to be determined how much Rayleigh damping has to be added to the soil so that the hysteretic material damping (automatically present in the HSsmall model) in combination with the Rayleigh damping results in proper dynamic behaviour of the PLAXIS 2D model, representative for the reference case. The Rayleigh damping target frequencies f_1 and f_2 are derived from the natural frequency of the soil column and the predominant spectral period of the applied earthquake signals respectively. The natural frequency of the soil deposit is calculated by:

$$f_0 = \frac{V_s}{4H_{\text{soil}}} \quad , \text{with: } V_s = \sqrt{\frac{G}{\gamma_{\text{unsat}}/g}} \quad (12)$$

In which:

- f_0 = natural frequency of the soil deposit [Hz]
- V_s = maximum shear wave velocity of the soil material [m/s]
- H_{soil} = height of the soil deposit (from bedrock level to ground level) [m]
- G = shear modulus of the soil material [kN/m^2]
- γ_{unsat} = unsaturated unit weight of the soil material [kN/m^3]
- g = gravitational acceleration [m/s^2]

From the calibrated PLAXIS 2D soil parameters (RD100% setup) it is computed that $V_s = 257 \text{ m/s}$. This matches with the estimated value of the shear wave velocity of the sand in the SHAKE2000 setup ($V_{s, \text{SHAKE2000}} = 250 \text{ m/s}$). Subsequently it can be computed that $f_0 = 3.29 \text{ Hz}$. Therefore a value of $f_1 = 3 \text{ Hz}$ is chosen for the first Rayleigh damping target frequency. The second Rayleigh damping target frequency is derived from the predominant spectral period T_p of the applied earthquake signals. From Figure 5.16 it can be seen that the value of T_p has a value of approximately 0.1 seconds. So for the second target frequency a value of $f_2 = 10 \text{ Hz}$ is chosen.

After defining the target frequencies a number of site response analyses are performed in PLAXIS 2D with damping ratio's in the range of 2% - 5%. Successively the PLAXIS 2D results are compared with the SHAKE2000 site-response analysis results. The damping ratio which gives the most satisfactory results is $\xi = 5\%$. It is noted that this is quite a high value for a Rayleigh damping ratio applied in an HSsmall model (which already introduces hysteretic damping) but this can possibly be explained by the very stiff and dense characteristics of the soil. The resulting Rayleigh damping setup is summarized in Table 5.20. The corresponding site-response analysis results are treated in the next part of this paragraph.

Table 5.20: Rayleigh damping properties

Rayleigh damping parameter	Value
damping ratio ξ	5%
target frequency f_1	3 Hz
target frequency f_2	10 Hz
Rayleigh coefficient α_R	1.450
Rayleigh coefficient β_R	$1.224 \cdot 10^{-3}$

5.3.5.2. Site-response analysis results

In Figure 5.28, Figure 5.29 and Figure 5.30 the PLAXIS 2D site-response analysis results are presented for CASE-200, CASE-300 and CASE-600 respectively. The motions at the centre of gravity of the soil-structure system obtained with both PLAXIS 2D and SHAKE2000 are plotted. It can be seen from the figures that the PLAXIS 2D motions are overall in good agreement with the SHAKE2000 motions. Differences exist in the acceleration amplitude peaks. PLAXIS 2D outputs more severe peaks than SHAKE2000. This effect increases with increasing shake event. Fourier analysis of the signals confirms this observation.

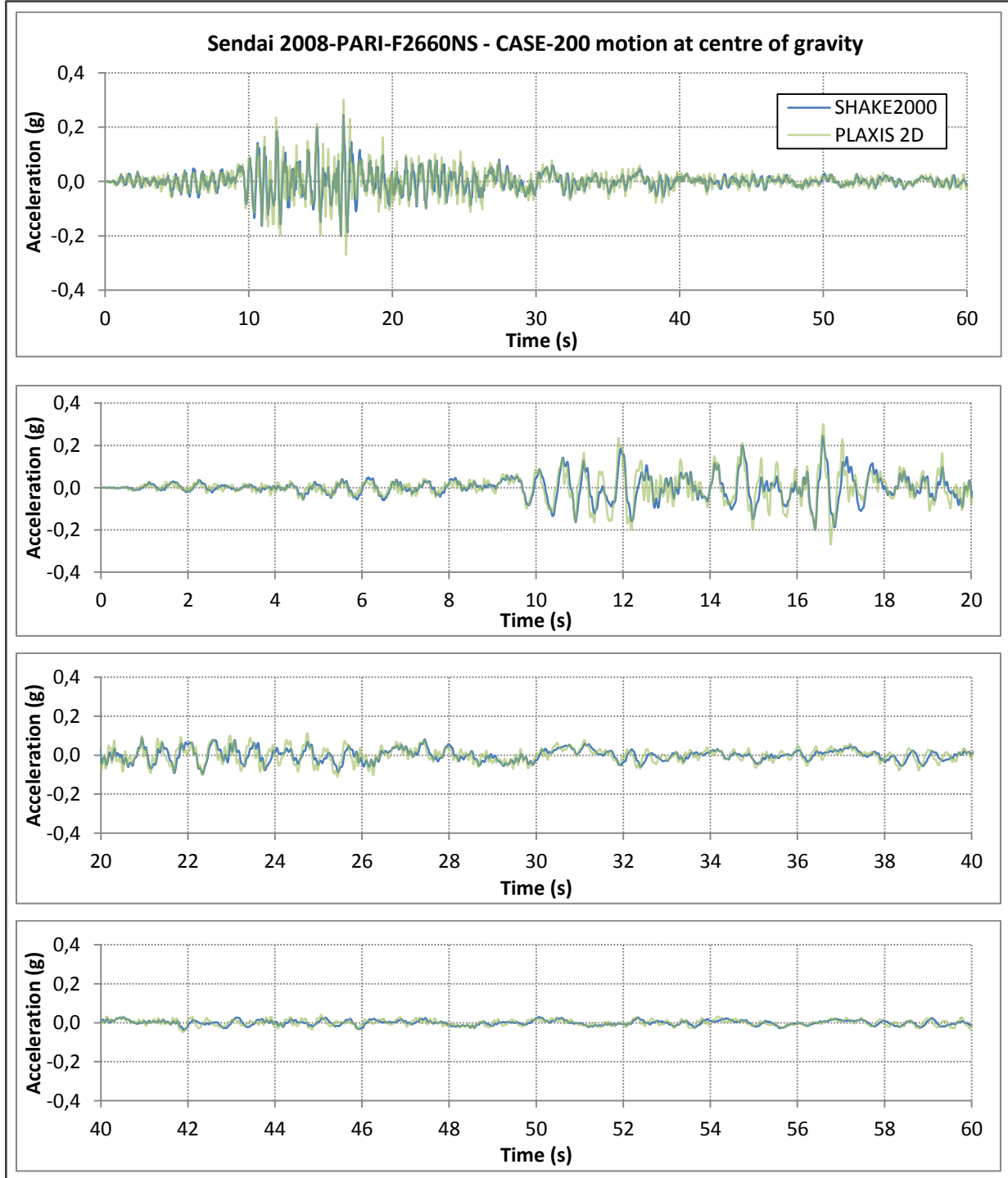


Figure 5.28: PLAXIS 2D site-response analysis result for the CASE-200 event, compared with SHAKE2000 result

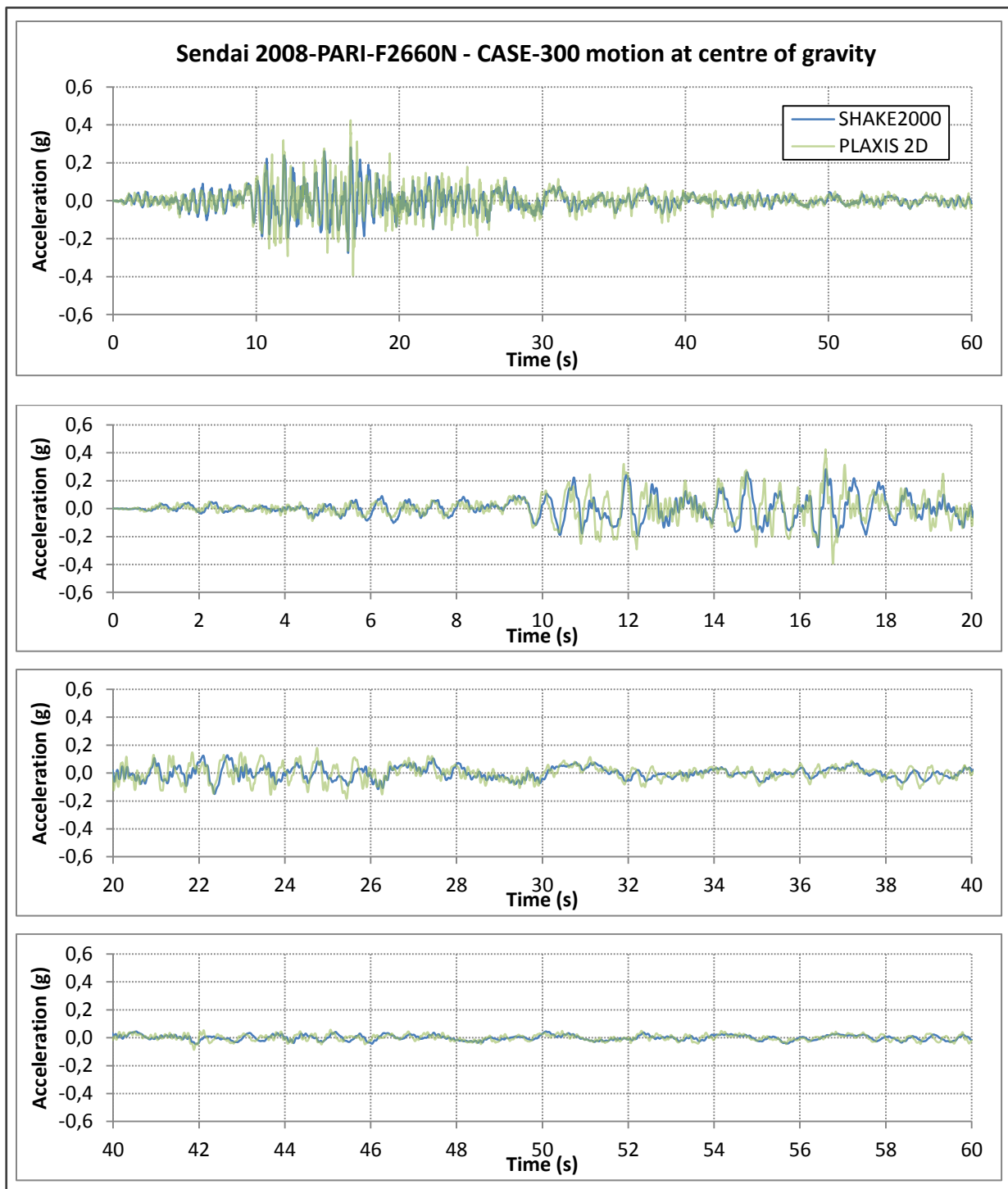


Figure 5.29: PLAXIS 2D site-response analysis result for the CASE-300 event, compared with SHAKE2000 result

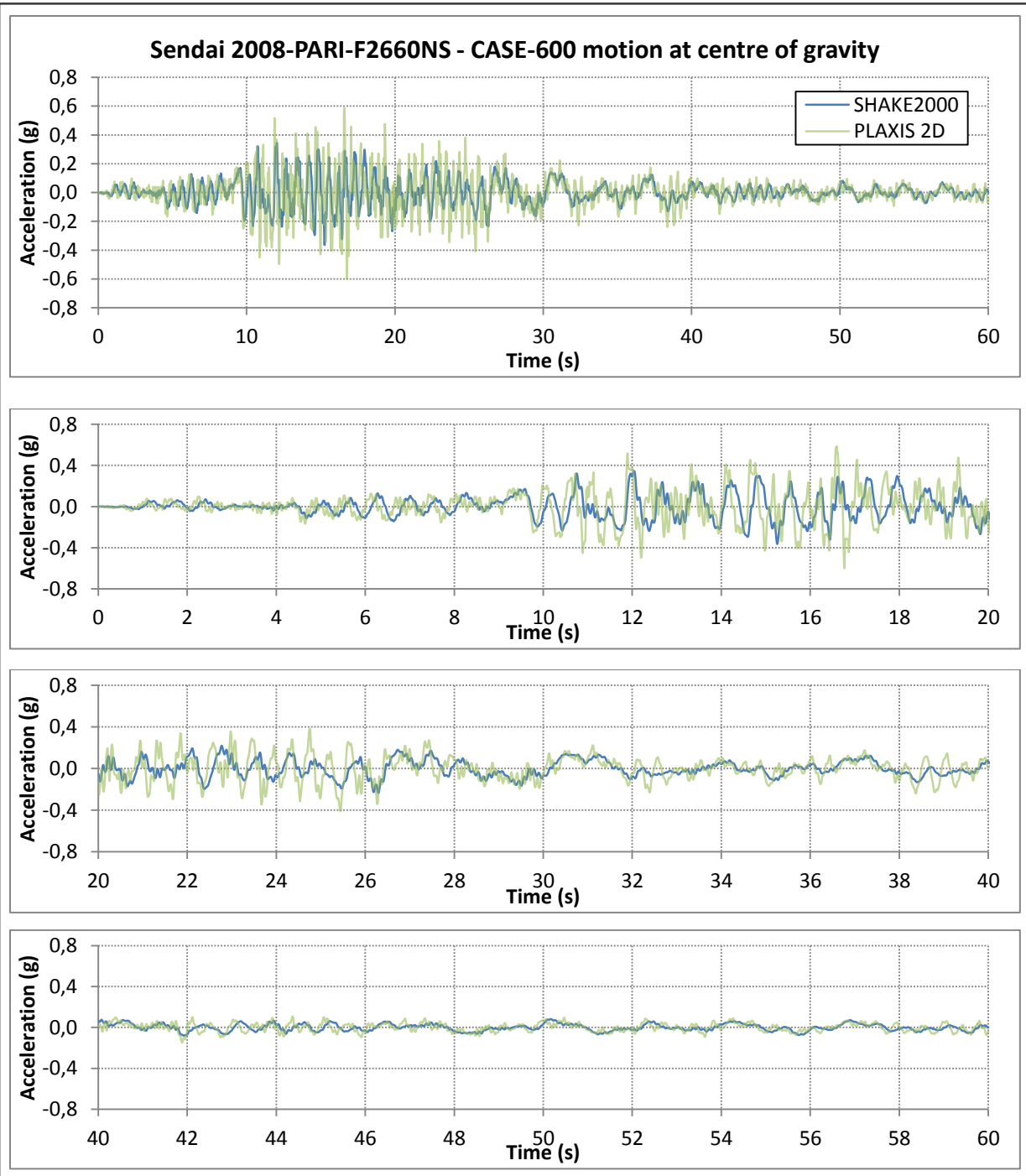


Figure 5.30: PLAXIS 2D site-response analysis result for the CASE-600 event, compared with SHAKE2000 result

Despite the higher acceleration amplitudes that PLAXIS 2D computes in the site-response analysis in comparison to SHAKE2000, the dynamic setup of the PLAXIS 2D model is considered to be satisfactory. The overall agreement of the signals is good, the PLAXIS 2D positive and negative amplitude peaks are equally large (symmetrical) and the added amount of Rayleigh damping in the PLAXIS 2D model is already significant (although not unrealistic). Furthermore the overestimation of amplitude peaks by PLAXIS 2D is thought to be embedded in the functioning of the HSsmall model, as will be discussed in chapter 6.

The dynamic setup of the PLAXIS 2D model as presented in the above will be applied for CASE-200, CASE-300 and CASE-600 dynamic calculations. For CASE-100 it is investigated separately which Rayleigh damping target frequencies give the best fit with the reference case results as in CASE-100 a completely different accelerogram is applied. For consistency the Rayleigh damping ratio is kept at a value of $\xi = 5\%$ though.

5.3.6. Calibrated dynamic calculations with the PLAXIS 2D model

In this paragraph the PLAXIS 2D dynamic calculations and its results are discussed, which are used for the validation of the several findings obtained during simplified and simplified dynamic analysis. First the setup of the PLAXIS 2D model is summarized shortly and successively the dynamic results are presented.

5.3.6.1. Model setup for dynamic calculations

The soil material setup for the dynamic calculations is the statically calibrated setup discussed in paragraphs 5.3.2 and 5.3.3 (Table 5.14 - RD100%), supplemented with the amount of Rayleigh damping discussed in paragraph 5.3.5 (Table 5.20). As said the Rayleigh damping target frequencies presented in Table 5.20 apply to the CASE-200, CASE-300 and CASE-600 shake events. For the CASE-100 shake event a deviating target frequency range is selected because an accelerogram with different frequency content is used in this case.

The setup of the structural elements for the dynamic calculations is as presented in Table 5.15, Table 5.16 and Table 5.17. No Rayleigh damping is added to the structural elements. From a test run with PLAXIS 2D it appeared that Rayleigh damping added to the sheet pile wall did not have significant effect on the dynamic calculation results. This agrees with the expectation that the frequencies of the predominant modes of the sheet pile wall are outside the predominant frequency range of the seismic load. Furthermore soil characteristics have a much stronger influence on the structural forces in the anchored sheet pile wall than the characteristics of the structural elements itself.

In order to resemble the experiment of the reference case closely the overall geometry of the PLAXIS 2D model is kept equal to the test model (field) dimensions (see Figure 5.20). To mitigate boundary effects in this relatively small geometry viscous boundary conditions are introduced to the x_{\min} - and x_{\max} -boundaries of the PLAXIS 2D model. As mentioned in paragraph 5.3.2 the relaxation coefficient values are set to $C_1 = 1.00$ and $C_2 = 0.25$. In Appendix B (B.3.1.6) it is explained that experience until now has learned that this setting results in a reasonable absorption of shear waves to such an extent that it is considered sufficient for practical applications. Indeed it is seen from a test run with the current PLAXIS 2D model that the viscous boundaries perform well when compared to the same PLAXIS 2D model with extended geometry (100 meters in both horizontal directions). At the y_{\min} -boundary a compliant-base boundary condition is introduced. It was concluded in the site-response analysis in paragraph 5.3.5 that this boundary condition performs well. The mesh-size is kept at 'very fine with local refinements' for the most accurate calculation results.

In paragraph 5.3.2 it was stated that the subsequent (seismic) load events in the PLAXIS 2D model follow the same phasing as in the reference case experiment, i.e. initial phase, static phase (seabed at DL -7.5 m), static phase (seabed at DL -9.5 m), CASE-100, CASE-200, CASE-300 and CASE-600. The accelerograms of the shake events that are applied at bedrock level in the PLAXIS 2D model are presented in Appendix H, section H.2. A summary of these records is given in Table 5.21.

Table 5.21: Accelerograms applied in PLAXIS 2D dynamic calculations

Accelerogram	Shake event
Artificial	CASE-100
Port of Sendai 2008 – PARI – F2660NS	
Northridge 1994 – L12-180	
Nisqually 2001 – KIM090	CASE-200, CASE-300, CASE-600
Nisqually 2001 – SCI000	
Whittier Narrows 1987 – PMN012	
Whittier Narrows 1987 – STN110	

The accelerograms applied for the CASE-200, CASE-300 and CASE-600 events are the same as those selected for the permanent-displacement analysis in paragraph 5.2.4 (see Figure 5.16). By using multiple records more calculation results are obtained and furthermore the dynamic displacement contours computed for every accelerogram in PLAXIS 2D are required to validate permanent-displacement results of SLAMMER.

5.3.6.2. Dynamic calculation results

In this part the PLAXIS 2D dynamic calculation results are discussed. The overall results and structural force results per shake event are presented in tables and graphs respectively. Furthermore sheet pile and soil displacement results are considered separately. It is noted that all PLAXIS 2D results correspond to the situation after each shake event (as is the case for the experiment measurements). For all the PLAXIS 2D bending moment computations it is checked that the maximum value during shaking is on average only 3% higher than the value after shaking.

CASE-100

The CASE-100 shake event follows after the static CASE-000. For the CASE-100 event the artificial motion is applied (see Appendix H, paragraph H.2.1) and similar to the calibrated D-SHEET PILING calculation the soil above the anchors is neglected as the CASE-100 shaking is not considered to be severe enough to destroy the arching effect. Furthermore it was said that the Rayleigh damping target frequencies presented in Table 5.20 only apply to the CASE-200, CASE-300 and CASE-600 shake events. For the CASE-100 shake event a deviating target frequency range is selected because an accelerogram with different frequency content is used in this case. The CASE-100 target frequency range of the Rayleigh damping in the soil is set to $f_1 = 0.01$ Hz and $f_2 = 10$ Hz (with $\xi = 5\%$). With this setup the PLAXIS 2D model outputs the results as presented in Table 5.22 and Figure 5.31.

Table 5.22: PLAXIS 2D dynamic calculation results for CASE-100 (artificial motion), compared to reference case results

CASE-100	M_{MAX} [kNm]	F_{ANCHOR} [kN]	u_{ANCHOR} [mm]	u_{SEABED} [mm]
Reference case	301	182	20	9
PLAXIS 2D	302	160	22	26
Ratio (P2D / Ref. case)	1.00	0.88	1.10	2.89

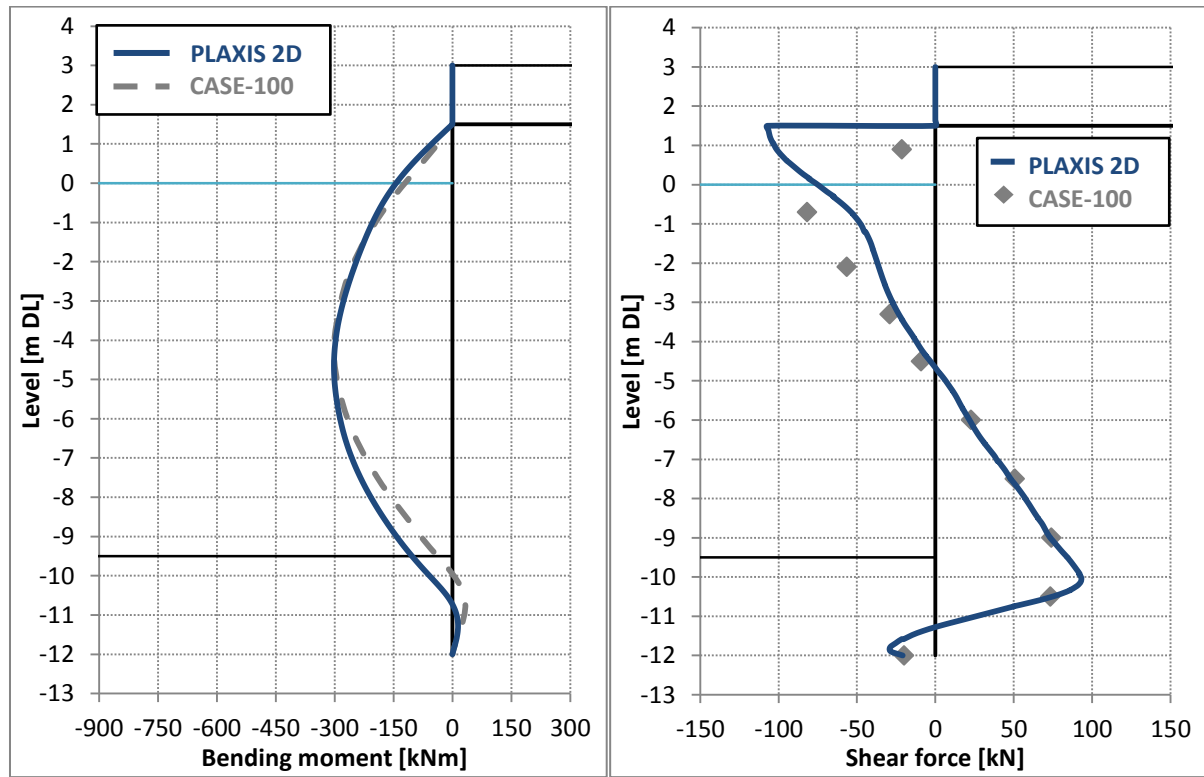


Figure 5.31: PLAXIS 2D bending moment and shear force line results for CASE-100, compared to reference case results

It can be seen that a good fit is found between PLAXIS 2D and reference case structural force results. The same holds for the displacement at anchor level, while PLAXIS 2D overestimates the displacement at seabed level for the CASE-100 shake event.

CASE-200

The CASE-200 shake event follows after the CASE-100 event. For CASE-200 the six earthquake records as presented in Table 5.21 (scaled to 0.2g) are applied (see also Appendix H, paragraph H.2.2 to paragraph H.2.7). Similar to the calibrated D-SHEET PILING calculation the soil above the anchors is no longer neglected as from CASE-200 onwards shaking is considered to be severe enough to destroy the arching effect. Furthermore the Rayleigh damping target frequencies as presented in Table 5.20 apply from CASE-200 onwards. For the CASE-200 shake events the PLAXIS 2D model outputs the results as presented in Table 5.23 and Figure 5.32. Both the results per input motion (blue contour lines) and the average of these results (solid blue line) are shown.

Table 5.23: PLAXIS 2D dynamic calculation results for CASE-200 (multiple motions), compared to reference case results

CASE-200		M _{MAX} [kNm]	F _{ANCHOR} [kN]	u _{ANCHOR} [mm]	u _{SEABED} [mm]
Reference case		547	261	66	41
PLAXIS 2D	S2008-PARI-F2660NS	463	303	66	58
	N1994-L12-180	455	280	57	50
	N2001-KIM090	454	296	64	53
	N2001-SCI000	490	296	74	60
	WN1987-PMN012	472	291	66	56
	WN1987-STN110	502	314	78	60
Average		473	297	68	56
Ratio (P2D / Ref. case)	S2008-PARI-F2660NS	0.85	1.16	1.00	1.41
	N1994-L12-180	0.83	1.07	0.86	1.22
	N2001-KIM090	0.83	1.13	0.97	1.29
	N2001-SCI000	0.90	1.13	1.12	1.46
	WN1987-PMN012	0.86	1.11	1.00	1.37
	WN1987-STN110	0.92	1.20	1.18	1.46
Average		0.86	1.14	1.03	1.37

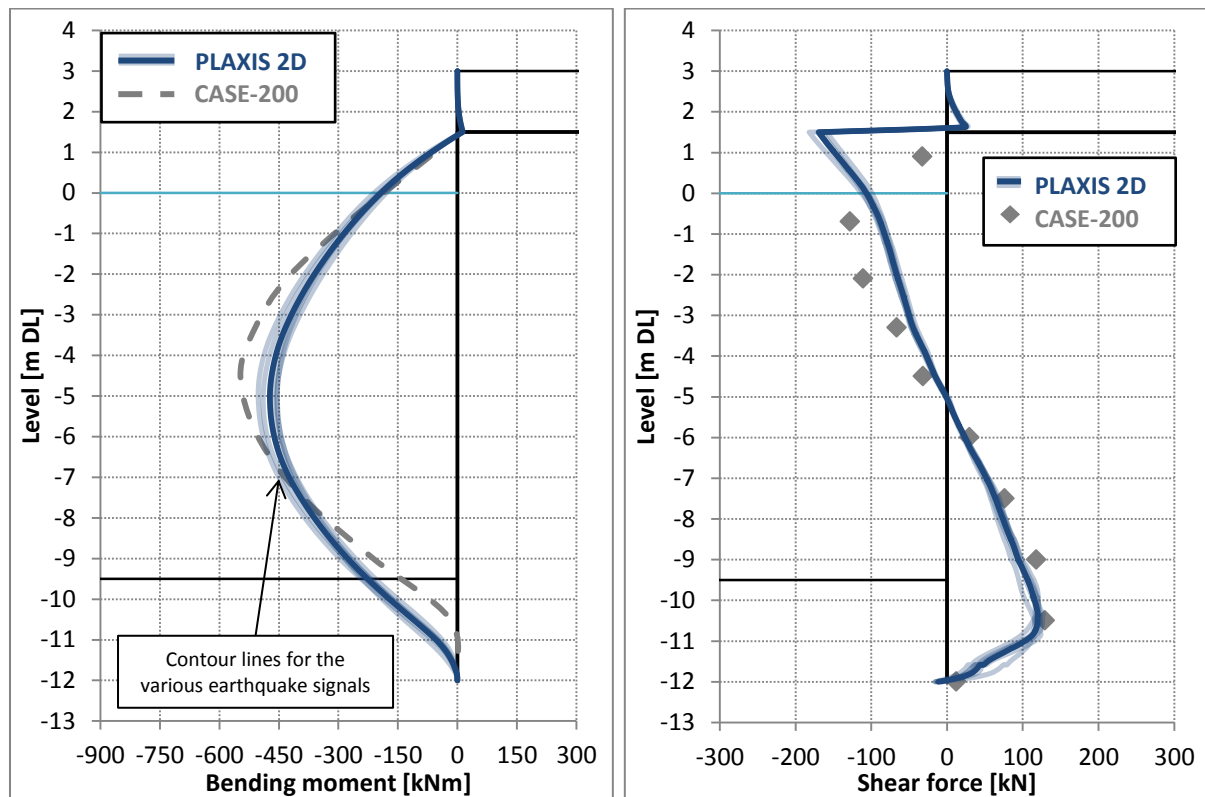


Figure 5.32: PLAXIS 2D bending moment and shear force line results for CASE-200, compared to reference case results

It can be seen that the reference case bending moment results are on average underestimated by PLAXIS 2D by 14% while the anchor force is overestimated by 14%. There is a good fit between the reference case

measurement and the average PLAXIS 2D result for the displacement at anchor level. PLAXIS 2D overestimates the displacement at seabed level on average by 37%. The PLAXIS 2D displacement behaviour of the sheet pile wall does agree with the reference case though, i.e. the displacement at anchor level is larger than the displacement at seabed level.

CASE-300

Subsequently to the CASE-200 shake event the CASE-300 event is introduced to the PLAXIS 2D model. Again the six earthquake records as presented in Table 5.21 (scaled to 0.3g) are applied to the model. The PLAXIS 2D model outputs the results as presented in Table 5.24 and Figure 5.33. The results per input motion and the average of these results are shown.

Table 5.24: PLAXIS 2D dynamic calculation results for CASE-300 (multiple motions), compared to reference case results

CASE-300		M _{MAX} [kNm]	F _{ANCHOR} [kN]	u _{ANCHOR} [mm]	u _{SEABED} [mm]
Reference case		449	262	93	64
PLAXIS 2D	S2008-PARI-F2660NS	573	336	109	91
	N1994-L12-180	562	319	95	76
	N2001-KIM090	570	335	108	82
	N2001-SCI000	620	366	141	105
	WN1987-PMN012	586	333	120	91
	WN1987-STN110	651	355	146	102
Average		594	341	120	91
Ratio (P2D / Ref. case)	S2008-PARI-F2660NS	1.28	1.28	1.17	1.42
	N1994-L12-180	1.25	1.22	1.02	1.19
	N2001-KIM090	1.27	1.28	1.16	1.28
	N2001-SCI000	1.38	1.40	1.52	1.64
	WN1987-PMN012	1.31	1.27	1.29	1.42
	WN1987-STN110	1.45	1.35	1.57	1.59
Average		1.32	1.30	1.29	1.42

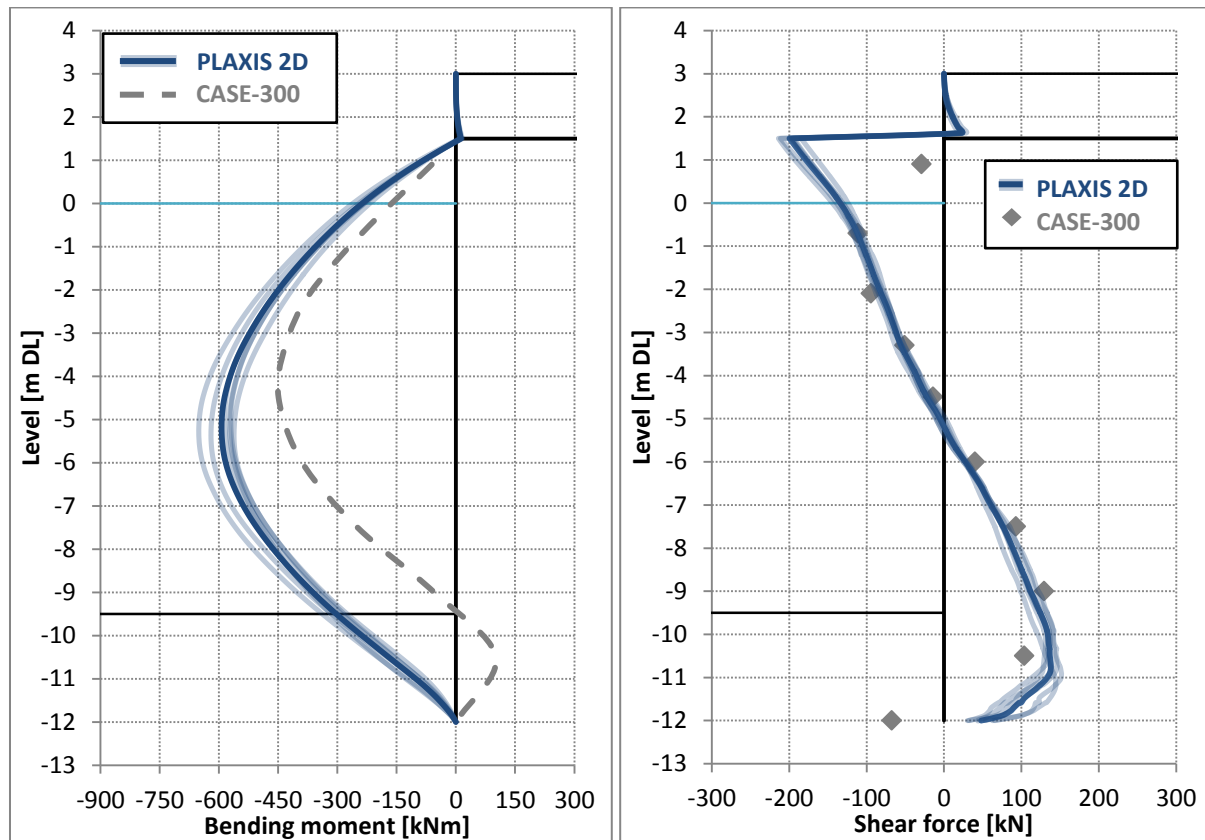


Figure 5.33: PLAXIS 2D bending moment and shear force line results for CASE-300, compared to reference case results

It can be seen that the reference case bending moment results are on average overestimated by PLAXIS 2D by 32% and that the bending moment line shape deviates at the embedment level. The calculated shear force line agrees rather well with the reference case results though. PLAXIS 2D on average overestimates the anchor force by 30%. Also the displacements of the sheet pile wall are overestimated: at anchor level on average by 29% and at seabed level on average by 42%. Agreeing with the reference case is that the displacement at anchor level is larger than the displacement at seabed level.

CASE-600

Subsequently to the CASE-300 shake event the CASE-600 event is introduced to the PLAXIS 2D model. Again the six earthquake records as presented in Table 5.21 (scaled to 0.6g) are applied to the model. The PLAXIS 2D model outputs the results as presented in Table 5.25 and Figure 5.34.

Table 5.25: PLAXIS 2D dynamic calculation results for CASE-600 (multiple motions), compared to reference case results

CASE-600		M _{MAX} [kNm]	F _{ANCHOR} [kN]	u _{ANCHOR} [mm]	u _{SEABED} [mm]
Reference case		728	308	232	195
PLAXIS 2D	S2008-PARI-F2660NS	735	355	511	422
	N1994-L12-180	726	408	245	188
	N2001-KIM090	768	409	274	210
	N2001-SCI000	772	463	387	310
	WN1987-PMN012	794	395	301	228
	WN1987-STN110	795	433	397	301
Average		765	411	353	277
Ratio (P2D / Ref. case)	S2008-PARI-F2660NS	1.01	1.15	2.20	2.16
	N1994-L12-180	1.00	1.32	1.06	0.96
	N2001-KIM090	1.05	1.33	1.18	1.08
	N2001-SCI000	1.06	1.51	1.67	1.59
	WN1987-PMN012	1.09	1.29	1.30	1.17
	WN1987-STN110	1.09	1.41	1.71	1.54
Average		1.05	1.33	1.52	1.42

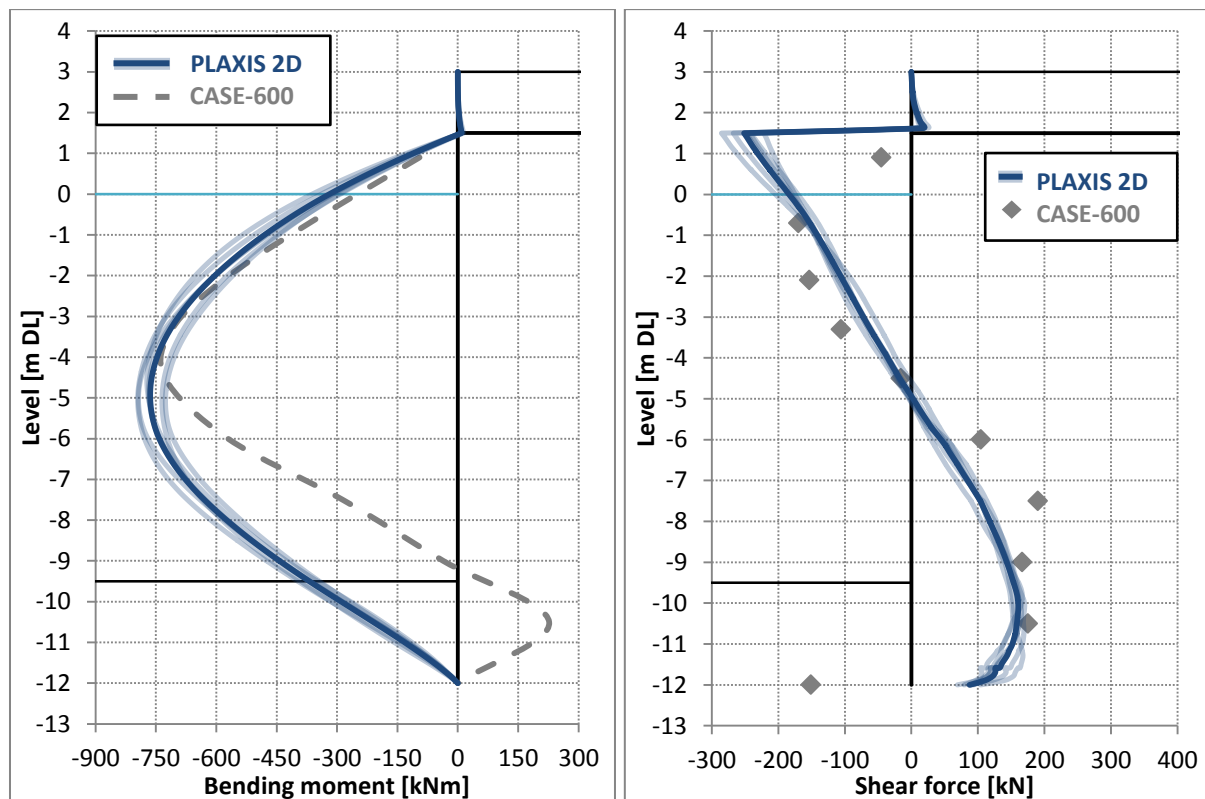


Figure 5.34: PLAXIS 2D bending moment and shear force line results for CASE-600, compared to reference case results

It can be seen that the reference case bending moment results are on average well estimated by PLAXIS 2D with an accuracy of 5% but that the bending moment line shape again deviates at the embedment level. PLAXIS 2D overestimates the anchor force by 33% on average and also the sheet pile wall displacements are overestimated: at anchor level on average by 52% and at seabed level on average by 42%. Agreeing with the reference case is that the displacement at anchor level is again larger than the displacement at seabed level.

Taking the bending moment and displacement results of CASE-200, CASE-300 and CASE-600 into account it appears that PLAXIS 2D does not simulate the exact failure behaviour of the reference case. Passive soil resistance is not sufficiently redeveloped in the PLAXIS 2D model after sliding commences, while in the reference case this is expected to happen. This can especially be seen from the difference between PLAXIS 2D and reference case in bending moment line shapes and the larger displacements calculated by PLAXIS 2D. Possible explanations for this are discussed in section 6.4.

An additional comment is made about the shear force lines. It can be seen for e.g. the CASE-600 shear force line that PLAXIS 2D does not compute zero shear force at toe level. One explanation is the presence of a friction force beneath the toe of the sheet pile wall. It can be present in reality and in PLAXIS 2D this force may be situated in the interface-element between sheet pile and soil (beneath the lowest node of the sheet pile). Another explanation is that the shear force line is possibly affected by the drift that the entire PLAXIS 2D model experienced during computations.

Displacements of the sheet pile wall

The (average) displacements of the sheet pile wall for the subsequent shake events as computed by PLAXIS 2D, and compared to the reference case measurements, are plotted in Figure 5.35. It again shows that the amount of sliding displacement is overestimated by PLAXIS 2D (as was discussed above) but that the type of failure behaviour (i.e. sliding with a larger displacement at anchor level than at seabed level) matches with the reference case.

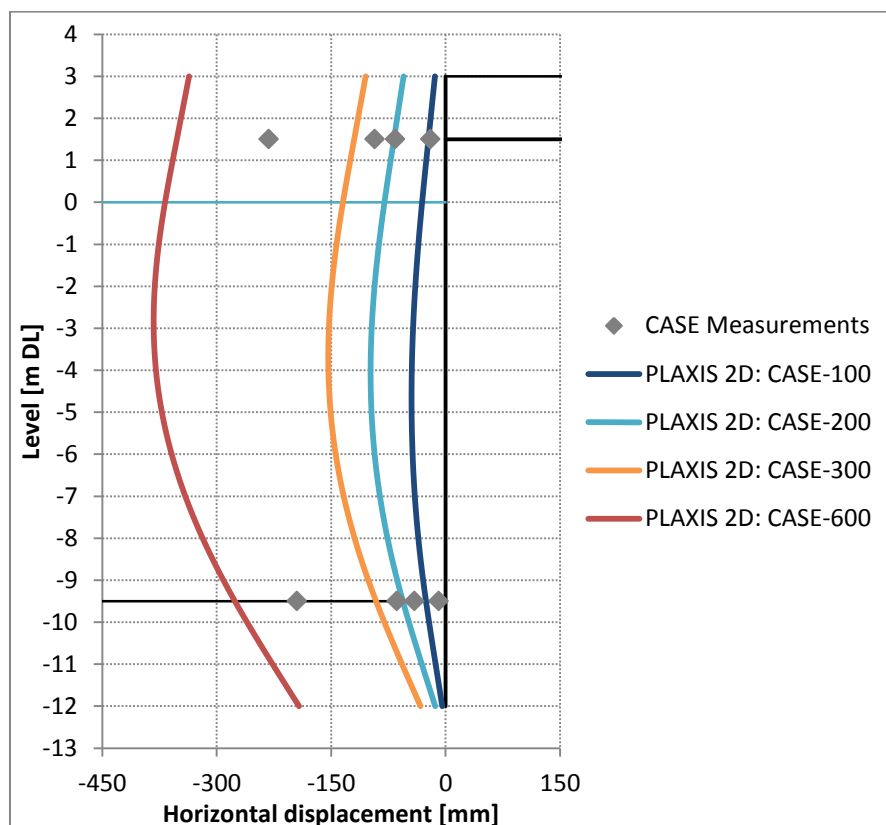


Figure 5.35: PLAXIS 2D dynamic displacement results, compared to reference case results

Soil displacements

In Figure 5.36 an example is shown of the horizontal soil displacements that PLAXIS 2D computes for the S2008-PARI-F2660NS motion scaled to the CASE-300 event. The amount of horizontal displacement per location is indicated by the coloured contours in the plot. The legend next to the plot translates the colours into quantitative horizontal displacement values^{xv}.

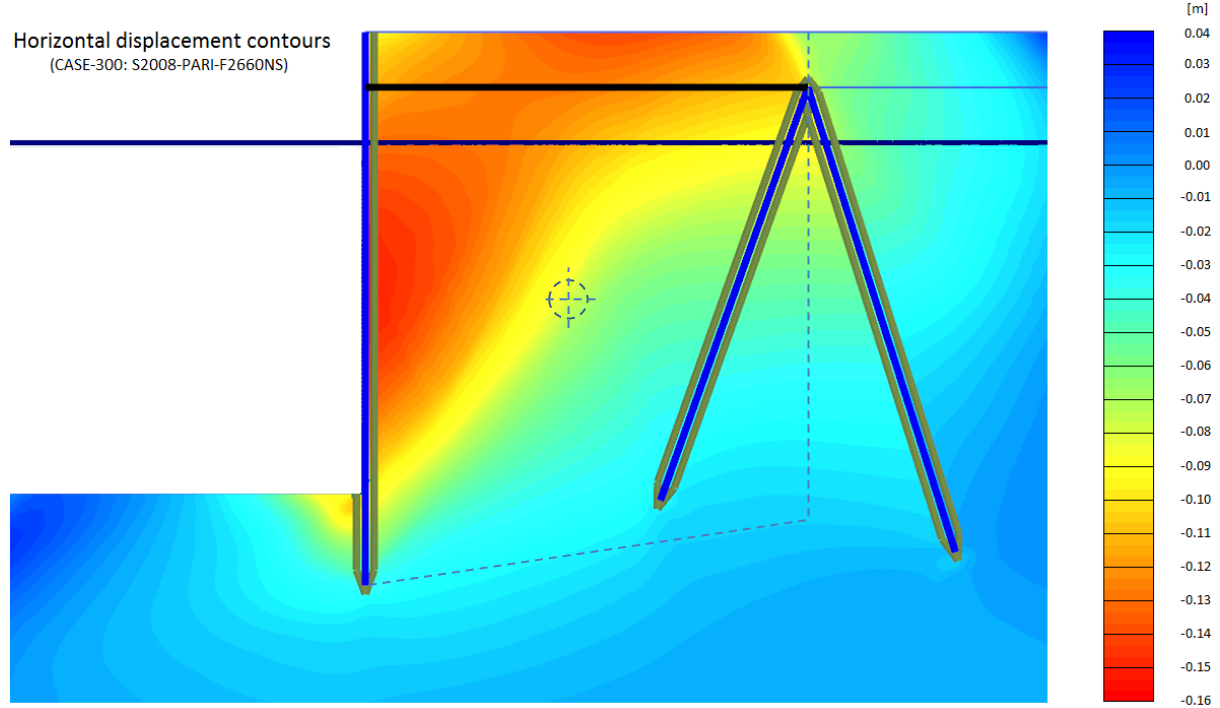


Figure 5.36: PLAXIS 2D dynamic displacement results: Example of horizontal displacement contours for the CASE-300 S2008-PARI-F2660NS motion

^{xv} It is noted that these values are corrected for the drift displacement of the entire model. Although the drift correction option has been turned on in the calculations, the entire model is shifted during dynamic calculations.

The schematized failure wedge that was assumed in the limit-equilibrium model of the simplified dynamic analysis is indicated in Figure 5.36 by the dashed lines. The corresponding centre of gravity of the schematized failure wedge is also shown in the figure. The horizontal displacements in this centre of gravity, computed with PLAXIS 2D are used to validate the permanent-displacement results of SLAMMER. The results of this validation were presented in paragraph 5.2.6. The procedure of defining the target displacements for the validation of the SLAMMER results is illustrated by the following example that applies to Figure 5.36:

From the horizontal displacement data corresponding to the plot in Figure 5.36 it can be determined that the displacement at the schematized centre of gravity is 75 mm and that the sheet pile displacement at seabed level is 91 mm. So in this case the ratio between the displacement at the centre of gravity and the sheet pile displacement at seabed level is $75/91 = 0.82$. This ratio is successively applied to translate the displacement at seabed level measured in the reference case to an equivalent reference case displacement at the schematized centre of gravity, i.e. $u_{c.g.} = 0.82 \cdot u_{seabed} = 0.82 \cdot 64 = 53$ mm. A setback of this procedure is that it assumes that the PLAXIS 2D ratio also holds for the reference case. The advantage is that the overestimation of the displacements by PLAXIS 2D (see e.g. Figure 5.35) does not bias the validation of the permanent-displacement results.

By following the same procedure as illustrated by the example above for all six input motions used in CASE-200, CASE-300 and CASE-600, the results as presented in Table 5.26 are obtained.

Table 5.26: PLAXIS 2D dynamic calculation results: displacements at the centre of gravity of the schematized failure wedge (sliding mass) of the anchored sheet pile quay wall

Motion	Shake event	Displacement at centre of gravity of schematized failure wedge due to sliding [mm]	Drift displacement between subsequent shake events [mm]	
S2008-PARI-F2660NS	CASE-200	36	CASE-200 >> CASE-300 CASE-300 >> CASE-600	17
	CASE-300	53		147
	CASE-600	200		
N1994-L12-180	CASE-200	35	CASE-200 >> CASE-300 CASE-300 >> CASE-600	13
	CASE-300	48		149
	CASE-600	197		
N2001-KIM090	CASE-200	36	CASE-200 >> CASE-300 CASE-300 >> CASE-600	23
	CASE-300	59		148
	CASE-600	207		
N2001-SCI000	CASE-200	34	CASE-200 >> CASE-300 CASE-300 >> CASE-600	29
	CASE-300	63		138
	CASE-600	201		
WN1987-PMN012	CASE-200	34	CASE-200 >> CASE-300 CASE-300 >> CASE-600	29
	CASE-300	63		145
	CASE-600	208		
WN1987-STN110	CASE-200	36	CASE-200 >> CASE-300 CASE-300 >> CASE-600	31
	CASE-300	67		132
	CASE-600	199		

6. Evaluation

In this chapter the fifth step of the research methodology is treated. It concerns the evaluation the research results. Figure 6.1 shows the location of the current step within the research process.

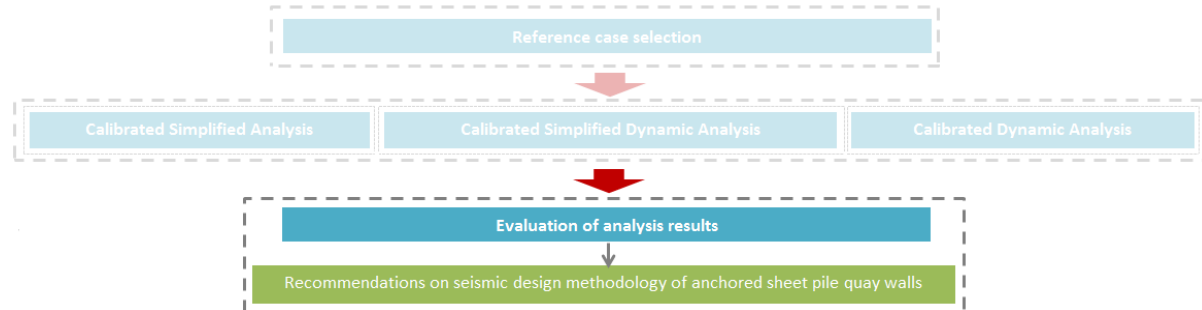


Figure 6.1: Step 5 of the research methodology: evaluation of the analysis results

The findings corresponding to each research step are evaluated separately and linked to each other where this applies. Furthermore the research results are linked to the performance-based design principle and an additional reflection on the PGA as the predominant parameter in current seismic design practice is included. Evaluation of the research findings is required to obtain proper conclusions and recommendations and by that answers to the research question.

6.1. Reference case

The selected reference case, used for calibration of the seismic analysis models, is discussed before evaluating the results of the three levels of seismic analysis. Aspects in the reference case that are sources of uncertainty for the calibrated seismic analysis process are addressed in this section.

Centrifuge process in the shake-table testing procedure

An important aspect in the reference case is the testing procedure in which a 30g centrifugal gravity is continuously applied on the quay wall scale model during static and dynamic tests in order to simulate initial stress conditions corresponding to field model dimensions. From both information in the paper by (Higuchi *et al.*, 2012), in which the reference case is presented, and the D-SHEET PILING and PLAXIS 2D model calibration results it is reasoned that unrealistically large initial stress conditions are introduced in the test scale model. This is most likely caused by the 30g centrifugal gravity which is expected to densify the already stiff soil condition (RD=80%) even further. And with the resulting further increase of the high soil stiffness the structural forces in the sheet pile and anchor tie simultaneously decrease.

(Higuchi *et al.*, 2012) indeed mention that soil stiffness is overestimated after simulation of initial stress conditions. Furthermore (Higuchi *et al.*, 2012) perform comparative FE calculations with FLIP code and conclude that their FE results differ from the test measurements due to the issues with the simulation of the initial stress conditions. The calibration results of the present study agree with these observations.

Test model setup data

From a large amount of papers that have been considered, the conference paper by (Higuchi *et al.*, 2012) provides the most suitable reference case for the present study. Nonetheless uncertainty is introduced due to limited availability of test model setup data.

It is explained in paragraph 4.2.2 that the data files of both the artificial and the recorded accelerogram of the reference case experiment could not be obtained, while it is desirable to have these data files for calibrated

simplified dynamic analysis (SDA) and calibrated dynamic analysis (DA). (For calibrated simplified analysis (SA) only PGA values are of importance.) In short the following is done to overcome this difficulty in a reasonable manner:

- A replica of the artificial motion is constructed out of a record with similar characteristics (the 0.1g peak is assumed to be the only important characteristic of the artificial record).
- For the recorded motion an accelerogram with the best possible comparable features, recorded nearby the test site during the same earthquake, is selected (S2008-PARI-F2660NS). For this F2660 record, similar records are collected from another database by fitting frequency spectra and subsequently these records are subjected to a (reverse) site-response analysis procedure. In this way it is attempted to gather multiple representative records for SDA and DA.

Although reasonable the above approach introduces uncertainty into the SDA and DA results with regard to the test model results. A main (non-quantifiable) uncertainty is introduced by the selection of the F2660 record as it remains an approximation of the recorded motion of the reference case experiment. The multiple records similar to the F2660 record and the site-response analysis procedure are applied to increase the amount of SDA and DA results and the quality of these results respectively. In this way it is attempted to decrease uncertainty and to provide a stronger base for conclusions and recommendations. The effect of this attempt is evaluated in sections 6.3 and 6.4.

Another source of uncertainty is the limited information provided in the conference paper on the soil properties of the test model. Nonetheless sufficient starting points in literature are found, which are used to calibrate the soil setups of the applied models with the reference case. Through this calibration the uncertainties in the model outputs associated with the soil parameters are mitigated. The information provided in the conference paper on the structural properties of the test model is sufficient and therefore uncertainty is considered to be negligible for that matter.

Availability of seismic test cases

In general something must be noted about the availability of seismic test cases for anchored sheet pile quay walls. First of all it appears, from considering a large amount of papers, that the amount of physical testing on seismic behaviour of anchored sheet pile quay walls is limited. Furthermore it is found that the public availability of the corresponding experiment / measurement data is limited as well. Therefore it is concluded for the sake of research that it is desirable to create more seismic test cases of anchored sheet pile quay walls and to increase the public availability of the test data.

6.2. Simplified analysis

Calibrated simplified analysis is performed in section 5.1 in order to find an improvement for traditional pseudo-static design methodology of anchored sheet pile quay walls.

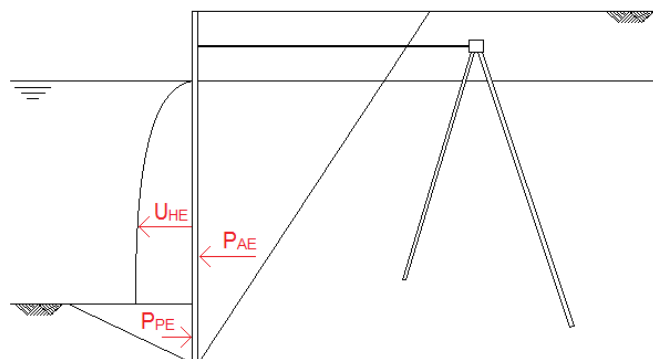


Figure 6.2: Pseudo-static model

Calibration

In section 6.1 it is discussed that the reference case measurements are influenced by the overvalued soil stiffness due to the centrifuge process in the reference case experiment. This is reflected in the calibration of the D-SHEET PILING model by exceptionally high values for a number of soil parameters and the assumption of arching of the very stiff soil above the anchor tie rods during the static situation and the 0.1g shake event. When comparing the D-SHEET PILING and the PLAXIS 2D calibration it is found that the same calibration results are found for the PLAXIS 2D model: again the assumption of arching during the static situation and 0.1g shake event and very high soil parameter values are required. Although somewhat unusual, these calibration results are physically explainable by means of the reference case centrifuge procedure.

Reduction factor

After determining the calibrated model settings, the iterative pseudo-static calculations are performed in which D-SHEET PILING force results are fitted with the reference case measurements. From these fits a deformation-based seismic load reduction for structural forces in the sheet pile wall is determined. The reduction is specified by the reduction factor r . As explained in paragraph 5.1.4 the horizontal seismic coefficients of the reference case shake events are divided by this factor after which the reduced seismic coefficients are applied in the Mononobe-Okabe and Westergaard solutions that compute the pseudo-static input parameters for the D-SHEET model. The obtained reductions in the calibrated simplified analysis, for the 0.1g, 0.2g, 0.3g and 0.6g shake events, are in the range of 45% to 50% (i.e. $r = 1.82$ to $r = 2.00$).

Validation

Calibrated dynamic PLAXIS 2D calculations are performed in order to validate structural force results of the D-SHEET PILING model. An important difference for this validation is that the D-SHEET PILING calculations had to be made separately per seismic load case while in the PLAXIS 2D model it is attempted to simulate the experiment in an exact manner by applying the subsequent shake events in one model calculation. So this means that in D-SHEET PILING the push-up of the seabed level due the passive soil wedge failure is manually introduced while it is expected from the PLAXIS 2D model that it simulates this failure behaviour during calculations. The latter could not be realised entirely due to computational limitations, as will be discussed in section 6.4.

As a result the calibrated PLAXIS 2D model was not able to simulate the measured structural forces in the sheet pile wall as good as the calibrated D-SHEET PILING model for the larger shake events. The PLAXIS 2D results are in a reasonable range though (especially when realising that the authors of the reference case article faced similar problems when simulating the experiment with their FE-model), see also 5.3.6.2:

- CASE-100 event: PLAXIS 2D sheet pile force results match reference case / D-SHEET PILING results
- CASE-200 and CASE-300 events: PLAXIS 2D sheet pile force results deviate (CASE-200: 14% and CASE-300: around 30%) from reference case / D-SHEET PILING results due to computational limitations in simulating reference case failure behaviour^{xvi}
- CASE-600 event: PLAXIS 2D, D-SHEET PILING and reference case show approximately same result for maximum bending moment

^{xvi} Regarding the deviating PLAXIS 2D results an additional remark must be made. After a test run with PLAXIS 2D for a separate CASE-300 event with the push-up of the seabed level manually introduced, it appeared that PLAXIS 2D was able to match reference case / D-SHEET PILING results.

Concerning deformation behaviour it appears that the PLAXIS 2D model simulates the (sliding) displacement behaviour of the sheet pile quay wall rather well while the D-SHEET PILING model is not able to compute such displacement behaviour due to its limitations. And correspondingly D-SHEET PILING is not able to compute the forces in the anchor tie rod properly while PLAXIS 2D is better able to do so.

Conclusion

So it is observed that D-SHEET PILING and PLAXIS 2D show the same, physical explainable, calibration behaviour with respect to the reference case. And although PLAXIS 2D experiences some computational setbacks in simulating the exact failure behaviour of the reference case, it is reasonably well able to compute structural forces and displacements. It is therefore concluded that the results obtained from calibrated simplified analysis show that in pseudo-static methodology a deformation-based seismic load reduction for the present reference case for structural forces in the sheet pile is allowable. These reductions are in the range of 45% to 50% (factor $r = 1.82$ to $r = 2.00$). These results follow from a sound calibration with the reference case and a reasonable validation with PLAXIS 2D.

6.3. Simplified dynamic analysis

New limit-equilibrium model

In order to make traditional Newmark-sliding-block / permanent-displacement analysis more suitable for an anchored sheet pile quay wall a limit-equilibrium model for the reference case is developed. The goal of this model is to estimate the critical acceleration of the anchored sheet pile quay wall in a simple and analytical manner and to compute corresponding forces in the sheet pile at the critical state. The ability of the limit-equilibrium model to estimate the critical acceleration is checked with the reference case behaviour and validated for two soil setups with a calibrated PLAXIS 2D model. The outcome for the critical acceleration calculations is positive. The difference between limit-equilibrium and PLAXIS 2D results is 5% and 7% for the two considered soil setups. Furthermore the critical acceleration computed with both models matches with the failure behaviour observed in the reference case experiment.

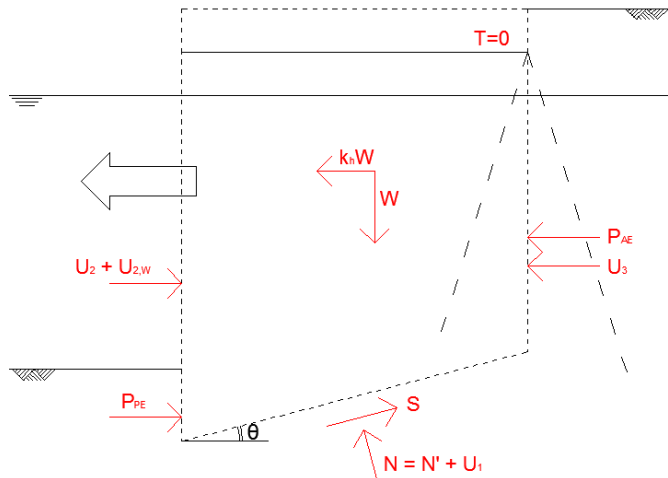


Figure 6.3: Limit-equilibrium model

The ability of the limit-equilibrium model to compute structural forces in the sheet pile at the critical state is checked with the reference case measurements and is considered to be positive as well. By comparing the structural forces that the limit-equilibrium model computes for the critical acceleration of 0.29g with the CASE-300 (0.3g) measurements, a difference of only 7% is found for the maximum bending moment value.

Site-response analysis with SHAKE2000

A (reverse) site-response analysis procedure with SHAKE2000 is performed for different earthquake records in order to obtain multiple representative records for the permanent-displacement analysis with SLAMMER and additionally for dynamic analysis with PLAXIS 2D (as will be discussed in section 6.4).

In paragraph 5.2.4 (Figure 5.18) an outcome of the SHAKE2000 site-response analysis is presented, i.e. the development of peak acceleration of the scaled S2008-PARI-F2660NS records when travelling from bedrock to ground level. For the CASE-200 and CASE-300 record the peak accelerations are eventually magnified when

travelling towards ground level. For the CASE-600 record though, the peak acceleration is eventually reduced when travelling towards ground level. Similar behaviour is found for the other five earthquake records. This observation possibly reveals that there is some kind of maximum peak acceleration equilibrium for the present soil column (one layer, dense coarse silica sand, height 20m). More SHAKE2000 runs with a larger amount of earthquake records (with differing frequency content) and a larger variety of soil column setups (with differing soil materials and heights) are definitely needed to obtain a generally valid conclusion on this topic though.

Concerning the site-response analysis procedure it was discussed in section 6.1 that similar earthquake records are fitted with the F2660 record based on frequency content but that a non-quantifiable uncertainty exists as the F2660 record remains an approximation of the recorded motion of the reference case. This uncertainty is reflected in the SLAMMER permanent-displacement analysis results.

Permanent-displacement analysis with SLAMMER

In paragraph 5.2.6 (Table 5.12 and Table 5.13) the permanent-displacement results of SLAMMER are presented. It is observed that both rigorous and empirical analysis do not output the target displacements of the reference case. Most of the results are more than 50% too low. One explanation is that both the rigorous and empirical permanent-displacement analyses, which are originally developed for embankments / landslides, are not that suitable for anchored sheet pile quay walls. The validity of this explanation is questionable though, as the exact properties of the applied earthquake signals have a big influence on the permanent-displacement results. And as mentioned the properties of the earthquake signals applied in SLAMMER remain an uncertain approximation of the earthquake signal applied in the reference case. Another uncertainty on this matter is the performance of SHAKE2000. It represents the analytical solution, which is considered to perform better than PLAXIS 2D (which outputs signals with acceleration peaks that are thought to be too high, see section 6.4), but the exact performance with respect to the reference case remains unknown. So again, more research effort on the signal processing is desirable.

6.4. Dynamic analysis

Calibration

In section 6.2 it was already discussed that PLAXIS 2D and D-SHEET PILING show the same, physically explainable, calibration behaviour with respect to the reference case. Calibration is reached in PLAXIS 2D by an HSsmall model soil setup corresponding to a relative density of 100% (instead of 80%). Furthermore arching of the soil above the anchors during the static situation and CASE-100 is assumed.

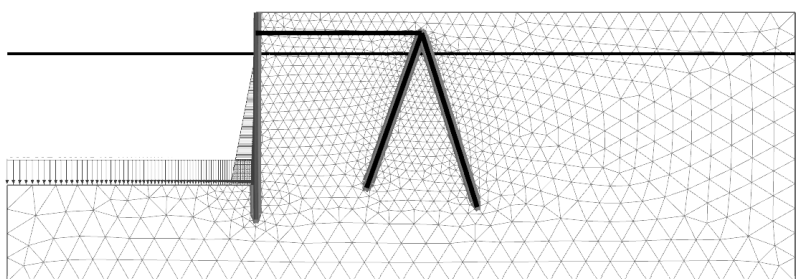


Figure 6.4: Finite element model

Concerning the dynamic setup a site-response analysis on a 1D soil column of the PLAXIS 2D model is performed and subsequently the dynamic performance of the PLAXIS 2D model is validated with the output of the SHAKE2000 site-response analysis. It is explained in subparagraph 5.3.5.2 that the dynamic setup of the PLAXIS 2D model is considered to be satisfactory, despite the higher acceleration amplitudes which PLAXIS 2D computes in comparison to SHAKE2000. The overall agreement between the signals is good, the PLAXIS 2D positive and negative amplitude peaks are equally large (symmetrical) and the added amount of Rayleigh damping in the PLAXIS 2D model is already significant (although not unrealistic).

From a conversation with an expert it is concluded that PLAXIS 2D may well overestimate the amplitude peaks due to the functioning of the hysteretic damping in the HSsmall model. In B.3.1.5 it is explained how frequency-independent hysteretic material damping is included in the HSsmall model (see Figure B.5). An assumption in the model is that upon load reversal the small-strain shear stiffness in the hysteresis loop is reset. This assumption neglects e.g. inertia effects of the material which results in an underestimation of the amount of hysteretic damping. This is an aspect that can explain the overestimated acceleration amplitude peaks in the processed earthquake signal.

Pseudo-static and pseudo-dynamic analysis

In paragraph 5.3.4 calibrated pseudo-static and pseudo-dynamic analyses with PLAXIS 2D are carried out in order to validate the ability of the limit-equilibrium model to estimate critical accelerations, as is discussed in section 6.3. A relevant observation was that the pseudo-static approach appears to be suitable to determine the critical acceleration of an anchored sheet pile structure. The pseudo-dynamic approach is not very suitable for that matter, while it is for embankments. The presence of the structural elements in the accelerated soil embankment is thought to give computational problems in the pseudo-dynamic approach.

Dynamic analysis – main discussion

Calibrated dynamic calculations with PLAXIS 2D are carried out to validate force and displacement results of simplified and simplified dynamic analyses and to simulate failure behaviour. During these calculations it is attempted to simulate the reference case experiment in an exact manner by applying the subsequent shake events in one model calculation. So this means that it is expected from the PLAXIS 2D model that it simulates the reference case failure behaviour. This is not realised entirely, as can be seen from the results in paragraph 5.3.6. Compared to the reference case measurements PLAXIS 2D computes a deviating bending moment line for the heavier shake events and larger sliding displacements of the sheet pile wall. This difference is probably due to the redevelopment of passive soil resistance in the reference case after sliding commences, which is not simulated by the PLAXIS 2D model. Two main explanations are presented.

A first explanation is that the failure behaviour of the reference case is partly influenced by the experiment setup, i.e. the steel container around the test model. The container wall at the seabed side is situated relatively nearby the sheet pile. Therefore it might be possible that the seabed is pushed up to a larger extent due to the presence of the wall. This idea is illustrated by Figure 6.5 by means of the concept of ‘lower-bound failure theorem’ and ‘upper-bound failure theorem’ from the structural mechanics field - see (Vrouwenvelder & Witteveen, 2003) for full definitions.

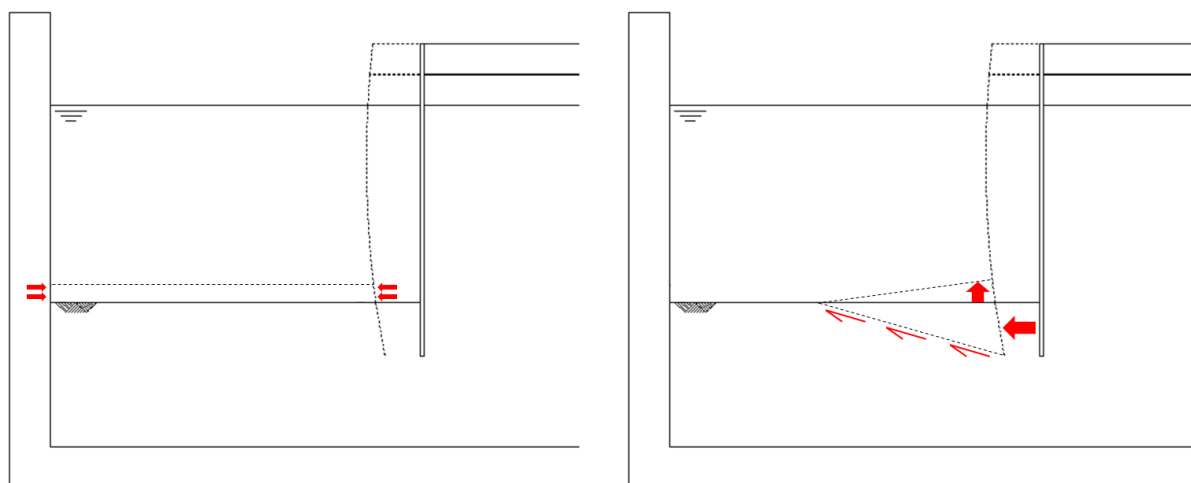


Figure 6.5: Larger push-up of seabed at sliding of sheet pile due to presence of steel container – a combination of a lower bound failure mechanism (strut - left side) and upper bound failure mechanism (plastic failure plane - right side)

The upper-bound for failure is in this case interpreted as the passive soil failure in which full plasticity is mobilised at the failure plane of the soil wedge (right side of Figure 6.5). The lower bound for failure is interpreted as the development of a strut-mechanism between the container wall and the sheet pile wall without plastic flow (left side of Figure 6.5). True failure is expected to be a combination of the lower and upper failure mechanism (and therefore situated between the lower and upper boundary). The resulting larger push-up of the seabed is thought to cause redevelopment of passive soil resistance beneath sea bed level. With viscous boundary conditions in PLAXIS 2D this behaviour could not be simulated as the soil is not pushed up at these boundaries and with rigid boundary conditions the model becomes numerically instable.

The second explanation is purely computational. First of all it is possible that the overestimation of acceleration amplitude peaks of the processed earthquake signals influences the dynamic calculation results. Moreover, dynamic calculation phases in PLAXIS 2D always apply the pore pressures calculated in the previous calculation phase. So when performing multiple subsequent dynamic calculations phases, as is presently the case, the pore pressures are never brought back to hydrostatic conditions. In the reference case experiment on the other hand, it might have been the case that subsequent shake events were applied with sufficient intermediate time to restore hydrostatic conditions. Neglecting the restoring of hydrostatic conditions in the PLAXIS 2D simulation between subsequent shake events may contribute to the disability to simulate the redevelopment of the passive soil resistance.

Restoring hydrostatic conditions between two subsequent dynamic events can be taken into account in PLAXIS 2D by introducing a so-called plastic nil-step though. This is a plastic calculation phase in which no additional loading is applied and which can be used to solve large out-of-balance forces and to restore equilibrium after large loadings (e.g. seismic loadings). However, if a stress field is created that is far from equilibrium (as is the case in the present simulation due to generation of large displacements) the plastic nil-step may fail to converge. Indeed this is observed because the renewed stress conditions of the plastic nil-step are difficult to match with the large displacements. So therefore the hydrostatic pore pressure conditions cannot be restored in the present PLAXIS 2D simulation.

As a result of the above the calibrated PLAXIS 2D model is not able to simulate the measured structural forces in the sheet pile wall exactly for the larger shake events. The PLAXIS 2D results are in a reasonable range though, as was discussed in section 6.2. Furthermore PLAXIS 2D overestimates the anchor force and the amount of sliding displacement, especially for the heavier shake events, but the type of failure behaviour (i.e. sliding with a larger displacement at anchor level than at seabed level) matches with the reference case. For the validation of the permanent-displacement results of SLAMMER a procedure was proposed in subparagraph 5.3.6.2 to prevent biasing of the validation by overestimated soil displacements.

Dynamic analysis – other observations

To conclude this section two other observations concerning the dynamic analysis are discussed. Significant drift of the entire model during dynamic calculations is observed (despite using the drift correction option in PLAXIS 2D) but the displacement results are corrected for this model drift. It is not unthinkable though that the model drift has some influence on the calculation results.

The PLAXIS 2D calculation results for the six different earthquake records show that the fitting of these records on frequency content (acceleration spectra) has worked properly. It can be seen in paragraph 5.3.6 that the bending moment and shear force lines corresponding to the different earthquake records match each other well. In addition the good fit between CASE-100 measurements and PLAXIS 2D calculation results shows that the artificial record is reconstructed properly.

6.5. Accuracy in the present study

It is difficult for the present study to give a quantification of the accuracy of the research results. The research is based on the outputs of several seismic analysis models which are calibrated with one physical reference case. Nonetheless some qualitative comments will be given on the accuracy. In order to do so the definition of accuracy according to ISO 5725-1:1994, i.e. accuracy as a combination of ‘trueness’ and ‘precision’, will be held on to. This concept of accuracy is explained by Figure 6.6.

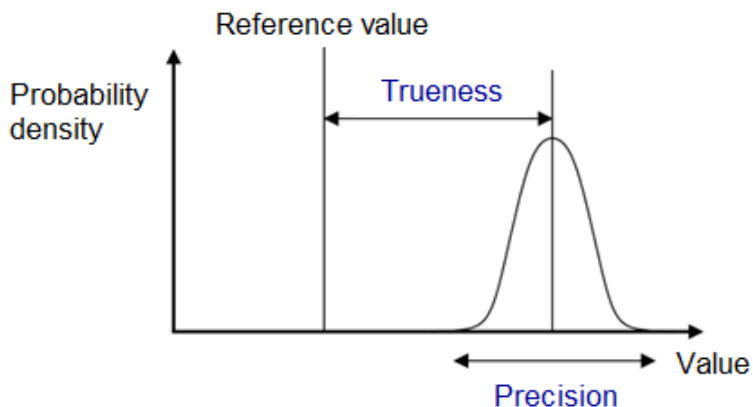


Figure 6.6: Accuracy according to ISO 5725-1:1994: a combination of ‘trueness’ and ‘precision’

The accuracy of the pseudo-static analysis results (i.e. the reduction factors) is expected to be good. The uncertainties in the (limited amount of) input parameters for the D-SHEET model that follow from lacking reference case data are mitigated by a physically explainable calibration. In addition the comparison with the more superior PLAXIS 2D model affirms the D-SHEET calibration and calculation results. These aspects indicate a good trueness. The precision is also expected to be good as close results for the sequential shake events are obtained (all reduction factors within the range of $r = 1.82$ to $r = 2.00$).

The accuracy of the permanent-displacement analysis strongly depends on the applied earthquake signals. Because six earthquake records are applied in the study as an approximation of the reference case record this means that both the trueness and the precision are affected. The -50%/+50% range for the permanent-displacement results was introduced to account for the low precision associated with the differences between the accelerograms. Within this range the permanent-displacement results still did not match the reference case target displacements though. This can be explained by a low trueness due to the approximation of the reference case record but possibly also as a result of the limited applicability of the sliding-block schematization on anchored sheet pile quay walls. As stated earlier more research is required on this topic. At this point the accuracy of the permanent-displacement analysis results is considered to be too low. The accuracy of the critical acceleration computations is expected to be good though, looking at the close results of the reference case, limit-equilibrium model and PLAXIS 2D model.

The accuracy of the PLAXIS 2D results is expected to be reasonable. The trueness of the PLAXIS 2D calculation results is affected by the interaction between computational limitations of PLAXIS 2D and the setup of the reference case experiment. The same holds for the higher complexity of the model, as it comprises more aspects (e.g. input parameters and modelling of damping) that can introduce uncertainty. Uncertainty with respect to the soil parameters is again reduced by a physically explainable calibration though. Looking at the calculation results the trueness is considered to be reasonable. The precision appears to be good, judging the close computation results of the six earthquake records.

6.6. The performance-based design principle in the present study

The results of the seismic analyses of the present study are in this section linked to the performance-based design principle. This is done by comparing reference case performance with the relationship between permanent displacement and observed damage of anchored sheet pile quay walls from (Kitajima & Uwabe, 1979). The earthquake /performance levels from PBD methodology as discussed in paragraph 2.3.2 are linked to the relationship of (Kitajima & Uwabe, 1979) as well. This is illustrated by Figure 6.7^{xvi}.

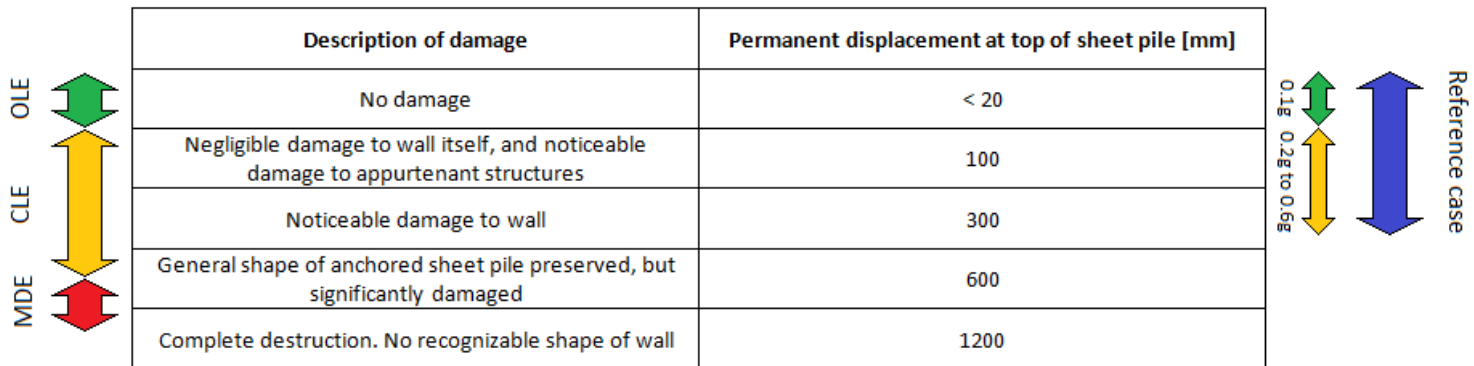


Figure 6.7: Relationship between permanent displacement and observed damage of anchored sheet pile walls, adapted from (Kitajima & Uwabe, 1979), linked to earthquake levels from PBD methodology and reference case performance

^{xvi} No clear insight concerning the influence of wall height within the relationship of (Kitajima & Uwabe, 1979) exists at this point. The height of the reference case wall is expected to be in the range of the 110 case histories investigated by (Kitajima & Uwabe, 1979).

Figure 6.7 shows that the Operating Level Earthquake (OLE), associated with serviceability performance of the structure, is linked to the amount of permanent displacement that relates to ‘no damage’ and thus ‘no noticeable damage to appurtenant structures’ (e.g. cranes). In other words the OLE is linked to the amount of permanent displacement which does not disrupt serviceability. This amount of permanent displacement (< 20 mm) corresponds with the CASE-100 (0.1g) shake event of the reference case. In the same manner the Contingency Level Earthquake (CLE), associated with damage control performance of the structure, is linked to the degrees of permanent displacement that relate to certain repairable amounts of damage (negligible – significant). The CASE-200 (0.2g), CASE-300 (0.3g) and CASE-600 (0.6g) displacements of the reference case are situated within this damage control range (100 mm to a maximum of 600 mm). The Maximum Design Earthquake (MDE), associated with collapse control performance, is linked to permanent displacement values of approximately 600 mm and larger.

When associating the conventional seismic design of a new sheet pile quay wall with a negligible amount of permanent displacement and therefore ‘no damage’, it can be deduced from Figure 6.7 that the reference case performance matches with the typical seismic demand of approximately 0.15g up to which sheet pile quay walls conventionally are applied in new design. When designing for higher seismic demands the dimensions of sheet pile wall and anchoring are increased significantly in conventional design to stay within the ‘no damage’ (OLE) range. With performance-based seismic design methodology one can design for higher seismic demands without such a significant increase of the anchored sheet pile dimensions by entering the ‘controllable damage’ (CLE) range. Based on the applied reference case and the seismic analyses performed in the present study approaches were proposed to investigate seismic design in the controllable damage range.

Extending the ‘0.15g seismic design boundary’

According to Figure 6.7 it is for the current reference case example possible to cross the ‘0.15g seismic design boundary’ without increase of dimensions but a certain amount of damage has to be accepted. From this observation the question arises whether it can be quantified to what extent the ‘0.15g-boundary’ can be crossed, based on literature and the present study results. To reflect on this question the earlier findings from literature and the present study are graphically combined in Figure 6.8.

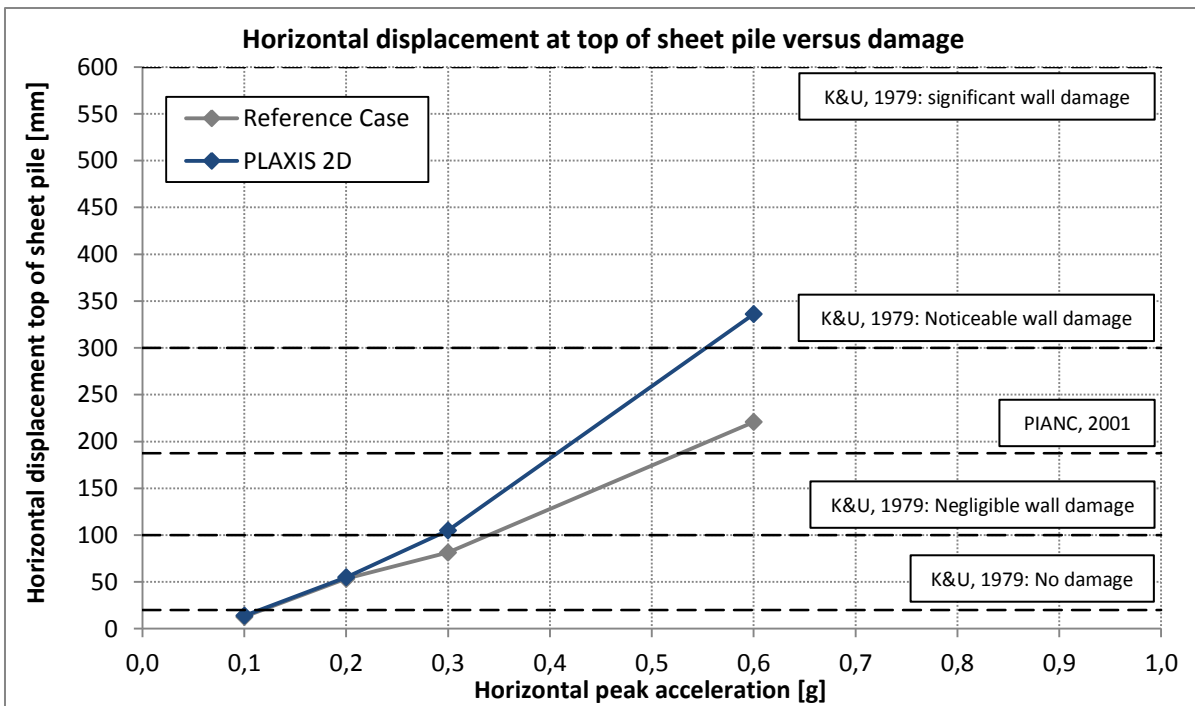


Figure 6.8: Findings from literature and the present study: horizontal displacement at top of sheet pile versus damage

Figure 6.8 shows the permanent displacements at the top of the sheet pile wall for the different shake events. Both the reference case and PLAXIS 2D top displacements are shown. The PLAXIS 2D top displacements are the averages of the six ground motions (see Figure 5.35). The reference case top displacements are estimated by multiplying the ratios between the PLAXIS 2D top and anchor displacements with the reference case anchor displacements. In addition the permanent-displacement values at top of sheet pile corresponding to different degrees of damage as reported by (Kitajima & Uwabe, 1979) are added. Also the permanent-displacement value at top of sheet pile as proposed by (PIANC, 2001) - i.e. 1.5% of the retaining height - is included.

Based on the present reference case measurements and corresponding PLAXIS 2D simulations it can be seen from Figure 6.8 that it would be possible (without increasing structure dimensions) to allow a 0.3g earthquake signal, when accepting negligible damage on the sheet pile wall, but noticeable damage on e.g. cranes on top of the quay. This is promising as ‘noticeable damage’ on the appurtenant structures probably only does disrupt serviceability for a short time or possibly does not disrupt it at all (when certain damage can be repaired during operation). And ‘negligible wall damage’ on the other hand does not indicate any disruption of serviceability.

The permanent-displacement value proposed by (PIANC, 2001) remarkably enough corresponds to serviceability performance, according to (PIANC, 2001). Compared to the values given by (Kitajima & Uwabe, 1979) this seems somewhat optimistic. By interpreting the displacement value by (PIANC, 2001) as a value which is a trade-off between serviceability and a reasonable amount of damage, and by interpreting the displacement value by (Kitajima & Uwabe, 1979) for ‘noticeable wall damage’ as a first upper boundary for acceptable damage, it is from Figure 6.8 deduced that earthquakes in the range of 0.4g to 0.6g can at maximum be allowed if the anchored sheet pile quay wall must remain repairable. Earthquakes that are more severe than that are expected to result in non-acceptable amounts of damage and eventually collapse.

Although this section provides an idea about the seismic performance limits of anchored sheet pile quay walls in quantitative terms it remains to a certain extent subject to speculation. First of all the whole performance-based design aspect is an economic trade-off (risk optimisation) in which amongst other the importance grade of the structure plays a role. Furthermore it is emphasized that the quantitative reflections in this section are based on the characteristics of the present reference case only. Therefore it is again stated that is desirable to create more seismic test cases of anchored sheet pile quay walls.

6.7. Reflection on PGA as the predominant seismic design parameter

To finish the evaluation of the research conducted in this study a short reflection is presented on the peak ground acceleration (PGA) as the predominant parameter in current seismic design of anchored sheet pile quay walls.

The use of PGA as the predominant seismic design parameter has gained wide acceptance due to the easy incorporation of the parameter into pseudo-static methodology. The use of PGA in pseudo-static approach is well-understood due to its physical simplicity and is associated with long experience in engineering practice. This is a big advantage of the pseudo-static PGA-approach.

Clearly the disadvantage of PGA as a single seismic design parameter is that it fails to account for other important aspects of seismic ground motion, i.e. duration and frequency content. Furthermore it has been stated frequently that the key design parameters for the performance of structures under seismic loading are stress states and deformations of soil and structure, rather than just a seismic design force (defined by mass times PGA).

The limited applicability of the PGA as the predominant seismic parameter is apparent in the present study. In simplified analysis a reduction factor on the pseudo-static load (PGA) was proposed. This is an improvement for realistically calculating structural forces in the sheet pile wall by indirectly taking into account energy absorption capacity due to deformation capability. Nonetheless, there is still no sense of actual displacement (which can be linked directly to damage and performance).

In methodologies that estimate displacements (permanent-displacement and FE analysis) the PGA is only one of the seismic design parameters. It is associated with the strength (amplitude) of the earthquake motion. It is evident from site-response analysis that amplitudes, duration and frequency content of an earthquake motion are all affected due to the interaction with the soil column. These three characteristics of the earthquake motion successively all influence the outcome of a permanent-displacement or FE analysis.

In the more sophisticated seismic analysis methodologies the importance of other parameters besides PGA is acknowledged while in simplified analysis PGA is the only seismic parameter. It is clear that the focus should not be on PGA alone. So what about pseudo-static analysis, which has the advantage of simplicity? Possibly alternatives can be developed for the use of PGA in pseudo-static methodology without increasing the complexity of the methodology.

One of the conservative factors in using the PGA in pseudo-static methodology is that it is assumed that the peak acceleration works as a constant value on the structure while there are a limited number of significant acceleration peaks in the earthquake signal. Therefore applying ‘impulse’ instead of ‘force’ in simplified analysis could possibly offer an alternative. Impulse is defined as the integral of a force F over the time interval t , during which it acts. Moreover impulse can be defined as ‘change in momentum Δp ($=mv_2-mv_1$) of the object to which the force F is applied during time interval t' . This line of reasoning yields that ‘velocity’ (during certain time intervals) would be a more appropriate seismic design parameter in simplified analysis than ‘acceleration’. Practically implementing the impulse-based approach in simplified analysis can be an interesting topic of further research.

In addition it is noted that applying PGA in pseudo-static methodology is even more conservative for induced earthquakes (pulse-like signals) than for tectonic earthquakes (for which simplified analysis approaches are originally developed). So for that matter an impulse-based approach is also expected to be more promising.

Concerning the limitation of simplified analysis to evaluate the amount of displacement (and therefore seismic performance of the structure) it might be a solution to develop an empirical relationship between peak ground displacement (PGD) of earthquake motion (obtained by double integration of an accelerogram) and residual displacement of anchored sheet pile walls.

7. Conclusions and recommendations

7.1. Conclusions

In the present research three levels of seismic analysis are performed on a case study of a typical anchored sheet pile quay wall. The general objective of the research is to obtain more insight in the seismic behaviour of anchored sheet pile quay walls and the performance of seismic analysis methods in order to give recommendations on the application of (simplified) seismic analysis methodology on this type of quay wall. For that purpose the following research question is answered in this section:

"Can (simplified) seismic design methodologies for anchored sheet pile quay walls be improved by considering deformation behaviour?"

Simplified methodology: deformation-based reduction factor

For simplified, i.e. pseudo-static, methodology a seismic load reduction is derived for structural forces in the sheet pile wall. This reduction is considered to be deformation-based mainly. The reduction is specified by the reduction factor r which is applied via the Mononobe-Okabe and Westergaard equations. For the reference case it is concluded that a reduction in the range of 45% to 50% (factor $r = 1.82$ to $r = 2.00$) is allowable. These results follow from a sound calibration with the reference case and a reasonable validation with PLAXIS 2D.

Simplified dynamic methodology: permanent-displacement analysis and new limit-equilibrium model

From permanent-displacement analysis it is concluded that more research effort is required to determine whether permanent-displacement analysis is suitable for anchored sheet pile quay walls. It is observed that both rigorous and empirical results do not match with the target displacements of the reference case. An explanation is that both the rigorous and empirical permanent-displacement analyses, which are originally developed for embankments / landslides, are not that suitable for anchored sheet pile quay walls. The validity of this explanation is questionable though, as the exact properties of the applied earthquake signals, which are an uncertainty in the present research, have a big influence on the permanent-displacement results.

From site-response analyses with SHAKE2000 and PLAXIS 2D it is concluded that for simplified dynamic and dynamic analysis of anchored sheet pile quay walls more extensive research on signal processing is needed. Uncertainty around the site-response analysis performance of SHAKE2000 with respect to physical reality exists and research concerning the frequency-independent material damping in dynamic calculations with the HSsmall model of PLAXIS 2D is desirable. In addition the development of peak accelerations and the possibility of maximum peak acceleration equilibria for soil columns with different properties are of interest.

In order to make traditional Newmark-sliding-block / permanent-displacement analysis more suitable for an anchored sheet pile quay wall a simple analytical limit-equilibrium model for the reference case is developed. From comparison with the reference case and validation with PLAXIS 2D it is concluded that the limit-equilibrium model is properly able to estimate the critical acceleration of the anchored sheet pile quay wall. In addition it is concluded from comparison with the reference case that the limit-equilibrium model is reasonably able to compute the structural forces in the sheet pile wall for the critical acceleration.

Dynamic methodology: 2D finite element analysis

Dynamic analysis is performed to validate simplified and simplified dynamic analysis results. It is concluded that PLAXIS 2D is able to compute the reference case failure behaviour reasonably well, despite some setbacks which are explained by an interaction between computational limitations of PLAXIS 2D and the setup of the reference case experiment. In addition PLAXIS 2D calculation results for the six different earthquake records confirm that the fitting of these records on frequency content (acceleration spectra) is a suitable procedure. Complementary is the conclusion that PLAXIS 2D pseudo-static approach proves to be suitable to determine the critical acceleration of an anchored sheet pile structure while pseudo-dynamic approach appears not very suitable for that matter.

The performance-based design principle for anchored sheet pile quay walls

In section 6.6 it is for the anchored sheet pile quay wall of the reference case concluded that it is possible to cross the '0.15g seismic design boundary' without increase of dimensions but that a certain amount of (controllable) damage has to be accepted. Clearly this is a structure-specific economic trade-off. Nonetheless an idea about the seismic performance limits of anchored sheet pile quay walls in quantitative terms is provided.

General answer to the research question

From the research findings in the present study it is concluded that improvement of the simplified seismic design methodologies for anchored sheet pile quay walls is possible by considering deformation behaviour. In the present study approaches are proposed to make existing (simplified) seismic analysis methods suitable for anchored sheet pile quay walls in a deformation-based manner.

7.2. Recommendations

From the evaluation of research results and the successive conclusions a number of recommendations on further research are deduced.

Present study

Concerning the present study results it is recommended to perform more extensive research on the ability of permanent-displacement analysis to evaluate the amount of sliding displacement of an anchored sheet pile quay wall. In line with this recommendation it has been stated that further research on seismic signal processing is definitely desirable for the application of simplified dynamic and dynamic analysis on anchored sheet pile quay walls. This concerns the site-response analysis performance of SHAKE2000 with respect to physical reality and possible improvements on the frequency-independent material damping in the HSsmall model of PLAXIS 2D for dynamic calculations.

Test cases

In general it is recommended to consider and create more seismic test cases of anchored sheet pile quay walls which e.g. include varying anchor configurations, soil setups and dimensions. In this way a broader validity can be obtained for the proposed improvements for simplified and simplified dynamic analysis and corresponding uncertainties can be decreased. Moreover the consideration of more seismic test cases is desirable as the current experimental reference case includes uncertainty and inaccuracy with respect to reality. It is suggested to create more seismic test cases of anchored sheet pile walls by setting up a research series for BSc. theses at the DUT Civil Engineering faculty during which (simple) seismic (shake table) scale tests are performed.

Seismic analysis of anchored sheet pile quay walls in the Netherlands

In line with the recommendation on researching more seismic test cases it is more specifically of interest to look into seismic analysis of anchored sheet pile quay walls in the Netherlands, i.e. in the Province of Groningen. Investigating the validity of the proposed improvements in simplified seismic design methodology for the Groningen setup (clayey soil, grout anchorage, seismic signals characterised by short pulses, liquefaction susceptibility) is from an actual point of view recommended.

Verification

In the present study the applied seismic analysis models are calibrated as much as possible with an experimental case in order to optimise the model coefficients so that model findings can be checked with physical test results. Furthermore the model outputs of the simplified models are validated with the model output of a more superior model. To make evidence for the proposed improvements stronger it is recommended to verify the model outputs with real field measurements (during actual earthquakes). This has not been done as such specific field measurements could not be obtained for the present study.

Availability of data

In line with the verification aspect it is recommended that instrumentation for seismic measurements is installed on new or existing anchored sheet pile quay walls in earthquake prone areas to increase real field measurement data. Moreover it is recommended that any data from seismic testing / measuring is made public as much as possible for the sake of research.

Alternatives for PGA as the predominant design parameter in simplified analysis

In the short reflection of section 6.7 ideas for further research are suggested on the use of PGA in simplified (pseudo-static) analysis. It is recommended to research the possibilities of applying the concept of Impulse in simplified analysis and in addition the development of an empirical relation between PGD and residual displacement of anchored sheet pile quay walls. For the latter the availability of (open-source) field measurement data is again important.

8. References

Ambraseys N.N. and Menu J.M., "Earthquake-induced ground displacements", Earthquake Engineering and Structural Dynamics 16, p985-1006: 1988

American Society of Civil Engineers (ASCE), 1998, "Seismic Guidelines for Ports", Ports Committee of the Technical Council on Lifeline Earthquake Engineering, Monograph No. 12, Edited by Werner S.D., ASCE: 1998

American Society of Civil Engineers (ASCE), "Seismic Design of Pile-Supported Piers and Wharves", Public Comment Response Version, ASCE: 2013

Anshan The Third Steel Rolling Co., Ltd., "Japanese Standard U-Shaped Steel Sheet Pile", Online Product List, URL: <http://cnsanzha.en.made-in-china.com/product/CouJmbSVfBYw/China-Japanese-Standard-U-Shaped-Steel-Sheet-Pile.html> (accessed: October 2014)

Benz T., "Small-strain stiffness of soils and its numerical consequences", Ph.d. thesis, Universität Stuttgart: 2006

Besseling F., "Soil-structure interaction modelling in performance-based seismic jetty design", MSc. Thesis, Delft University of Technology: 2012

Bolton M.D., "The strength and dilatancy of sands", Géotechnique 36, No.1, p65-78: 1986

Bray J.D. and Travasarou T., "Simplified Procedure for Estimating Earthquake-Induced Deviatoric Slope Displacements", Journal of Geotechnical and Geo-environmental Engineering 135, p1336-1340: 2007

Brinkgreve R.B.J., Kappert M.H. and Bonnier P.G., "Hysteretic damping in a small-strain stiffness model", Numerical Models in Geomechanics, NUMOG X, p737-742: 2007

Brinkgreve R.B.J., Engin E. and Engin H.K., "Validation of empirical formulas to derive model parameters for sands", Numerical Methods in Geotechnical Engineering: 2010

Caquot A. and Kerisel F., "Tables for the calculation of passive pressure, active pressure and bearing capacity of foundations", Gauthier-Villars, Paris: 1948

Conti R., Madabhushi G.S.P. and Viggiani G.M.B., "On the behaviour of flexible retaining walls under seismic actions", Géotechnique 62, No.12, p1081-1094: 2012

Coulomb C.A., "Essai sur une application des règles des maximis et minimis à quelques problèmes de statique relatifs à l'architecture", Mémoires de l'Academie Royale des Divers Savants, Vol.7: 1776

Culmann K., "Die Graphische Statik", Zürich: 1866

CROW Infrastructuur, "Handboek Zandboek", Artikelnummer 599: 2004

CUR Bouw & Infra, "Publicatie 166: Damwandconstructies", 6^e druk, delen 1 & 2: 2012

Deltares, "Groningse kades en dijken bij geïnduceerde aardbevingen - globale analyse van sterkte en benodigde maatregelen", Various Authors, Deltares: 2014b

Deltares systems, "D-Sheet Piling, Design of diaphragm and sheet pile walls, User Manual", Deltares: 2014

Dey A., Rainieri C., Fabbrocino G., Magistris, de F.S., "Fully instrumented full-scale embedded cantilever sheet pile retaining wall: PLAXIS FE modelling and interpretation", Proceedings of Indian Geotechnical Conference, Roorkee: 2013

Dost B., Kraaijpoel D. (KNMI), "Earthquakes and gas extraction", Lecture during the 'Knowledge Sharing Meeting on Earthquakes in Groningen' organised by Delft University of Technology and Groningen Seaports, Delft: September 22nd, 2014.

Earthquake Engineering Research Institute (EERI), "Photograph of tilted anchored bulkhead at Port of Hakodate due to the 1993 Hokkaido-Nansei-Oki earthquake", URL: <https://www.eeri.org/1993/06/hokkaido-nansei-oki/03-55/> (accessed: October 2014)

Ebeling R.M. and Morrison E.E., "The Seismic Design of Waterfront Retaining Structures", Technical Report ITL-92-11, NCEL TR-939, U.S. Naval Civil Engineering Laboratory, Port Hueneme, California: 1992

Electric Power Research Institute (EPRI), "Guidelines for Site Specific Ground Motions", Palo Alto, California, Electrical Power Research Institute, November, TR-102293: 1993

Elms D.G., "Refinements to the Newmark Sliding Block Model", 12th World Conference on Earthquake Engineering: 2000

Gijt de, J.G., Lecture notes "Port Infrastructure", Delft University of Technology: 2004

Hardin B.O. and Drnevich V.P., "Shear modulus and damping in soils: Design equations and curves", Proc. ASCE: Journal of the Soil Mechanics and Foundations Division, 98(SM7), p667-692: 1972

Higuchi S., Miki K. & Nakamura Y., Morikawa Y. & Sugano T., Kikuchi Y., Hoshino M. and Higashiyama K., "Evaluation of the Seismic Performance of Dual Anchored Sheet Pile Wall", 15th World Conference on Earthquake Engineering: 2012

Holthuijsen L.H., "Waves in Oceanic and Coastal Waters", Cambridge University Press: 2007

International Navigation Association (PIANC), "Seismic Design Guidelines for Port Structures", Working Group No. 34 of the Maritime Navigation Commission, A.A. Balkema Publishers: 2001.

ISO 5725-1:1994, "Accuracy (trueness and precision) of measurement methods and results", Part 1: General principles and definitions

Hiap Teck Venture Berhad (HTVB), "Steel Sheet Piles", Online (PDF) Catalogue, URL: http://www.htgrp.com.my/images/pdf/steel_trading/Steel%20Sheet%20Piles.pdf (accessed: October 2014)

Jaky J., "Minimum value of earth pressure", Proc. 2nd Int. Conf. Soil Mech. Found. Eng. I, Rotterdam: 1948

JFE Steel Corporation (JFESP), "JFE Steel Sheet Piles", Online (PDF) Catalogue, Cat.No.D1E-501-03, URL: <http://www.jfe-steel.co.jp/en/products/shapes/catalog/d1e-501.pdf> (accessed: October 2014)

Jibson R.W., "Predicting earthquake-induced landslide displacements using Newmark's sliding block analysis", Transportation Research Record 1411, p9-17: 1993

Jibson R.W., "Regression models for estimating co-seismic landslide displacement", *Engineering Geology* 91, p209-218: 2007

Jibson R.W., Methods for assessing the stability of slopes during earthquakes — a retrospective: *Engineering Geology*, v. 122, p. 43-50: 2011

Jibson R.W., Harp E.L. and Michael J.A., "A method for producing digital probabilistic seismic landslide hazard maps - An example from the Los Angeles, California, area", U.S. Geological Survey Open-File Report 98-113, 17 p, 2 pl:1998

Jibson, R.W., Harp, E.L. and Michael J.A., "A method for producing digital probabilistic seismic landslide hazard maps", *Engineering Geology* 58, p271-289: 2000

Kavazanjian E. Jr., "Evaluating the Seismic Coefficient for Slope Stability Analysis", Lecture, Ira A. Fulton School of Sustainable Engineering, Arizona State University: October 22nd, 2013

Kitajima S. and Uwabe T., "Analysis of seismic damage in anchored sheet-piling bulkheads", Report of the Japanese Port and Harbour Research Institute, Vol.18, No.1, p67-130 (in Japanese): 1979

Korff M. (Deltaires), "Effects of induced earthquakes on levees in Groningen", Guest lecture during the course Flood Defences at Delft University of Technology: June 2014

Kötter F., "Die Bestimmung des Druckes an gekrümmten Gleitflächen", *Sitzungsbericht Kön. Preu. Ak. d. Wissenschaften*, Berlin: 1903

Kramer S.L., "Geotechnical Earthquake Engineering", Prentice-Hall International Series in Civil Engineering and Engineering Mechanics, Prentice-Hall Inc., Upper Saddle River, New Jersey: 1996.

Kranz E., "Über die Verankerung von Spundwänden", Verlag Wilhelm Ernst & Sohn: 1953

Makdisi F.I. and Seed H.B., "Simplified Procedure for Estimating Dam and Embankment Earthquake-Induced Deformations", ASCE Journal of the Geotechnical Engineering Division 104, p849-867: 1978

Matsuzawa H., Ishibashi I. and Kawamura, M., "Dynamic soil and water pressures of submerged soils", *Journal of Geotechnical Engineering*, ASCE, Vol.111 No.10, p1161-1176: 1985

Mononobe N. and Matsuo H., "On the determination of earth pressures during earthquakes", Proceedings, World Engineering Congress: 1929

Müller-Breslau H, "Erddruck auf Stützmauern", Verlag Kröner, Stuttgart: 1906

National Cooperative Highway Research Program (NCHRP), "Seismic Analysis and Design of Retaining Walls, Buried Structures, Slopes and Embankments", Transportation Research Group of the National Academies, Report 611, Washington, D.C.: 2008

National Research Institute for Earth Science and Disaster Prevention (NIED), "Online database of the strong motion seismographic networks K-NET and KIK-NET", URL: http://www.kyoshin.bosai.go.jp/kyoshin/data/index_en.html (accessed: October 2014)

Neelakantan G., Budhu M. and Richards R., "Balanced seismic design of anchored retaining walls", J. Geotech. Engng 118, No.6, p873-888: 1992

NEN-EN1998-1:2005, "Design of structures for earthquake resistance", Part 1: General rules

NEN-EN1998-5:2005, "Design of structures for earthquake resistance", Part 5: Foundations, retaining structures and geotechnical aspects

NEN-9997-1:2011, "Geotechnisch ontwerp van constructies", Deel 1: Algemene regels

Newmark N.M., "A Method of Computation for Structural Dynamics", ASCE, Journal of the Engineering Mechanics Division, Vol.85 No.EM3: 1959

Newmark N.M., "Effects of earthquakes on dams and embankments", Geotechnique Vol.15 No.2, p139-160: 1965

Nippon Steel & Sumitomo Metal Corporation (NSSMC), "Steel Sheet Piles", Online (PFD) Catalogue, URL: http://www.nssmc.com/product/catalog_download/pdf/K007en.pdf (accessed: October 2014)

Nishimura S., Takahashi H., Morikawa Y., "Observations of dynamic and non-dynamic interactions between a quay wall and partially stabilised backfill", The Japanese Geotechnical Society, Soils and Foundations 52 (1), p81-98: 2012

Nozu A., "Current Status of Strong-motion Earthquake Observation in Japanese Ports", Journal of Japan Association for Earthquake Engineering, Vol.4, No.3 (Special Issue): 2004

Nozu A., Ichii K. and Sugano T., "Seismic Design of Port Structures", Journal of Japan Association for Earthquake Engineering, Vol.4, No.3 (Special Issue), p195-208: 2004

The Overseas Coastal Area Development Institute of Japan (OCDI), "Technical Standards and Commentaries for Port and Harbour Facilities in Japan", Ports and Harbours Bureau, Ministry of Land, Infrastructure, Transport and Tourism (MLIT), National Institute for Land and Infrastructure Management, MLIT, Port and Airport Research Institute, Tokyo: 2009

Okabe S., "General theory of earth pressures", Journal of the Japan Society of Civil Engineering, Vol.12, No.1: 1926

Ordóñez G.A., "SHAKE2000 - A Computer Program for the 1-D Analysis of Geotechnical Earthquake Engineering Problems", User's Manual, GeoMotions LLC: 2012

Plaxis bv, "PLAXIS 2D Anniversary Edition – 0 General Information", Delft: 2014

Plaxis bv, "PLAXIS 2D Anniversary Edition – 1 Tutorials Manual", Delft: 2014

Plaxis bv, "PLAXIS 2D Anniversary Edition – 2 Reference Manual", Delft: 2014

Plaxis bv, "PLAXIS 2D Anniversary Edition – 3 Material Models Manual", Delft: 2014

Plaxis bv, "PLAXIS 2D Anniversary Edition – 4 Scientific Manual", Delft: 2014

Port and Airport Research Institute (PARI), "Technical Note of the Port and Airport Research Institute No.1231", p8-30 (in Japanese): 2011

Port and Airport Research Institute (PARI), "Online database of strong earthquake motions recorded in Japanese ports (in Japanese)", URL: <http://www.eq.pari.go.jp/kyosin/> (accessed: November 2014)

Port of Long Beach (POLB), "Wharf Design Criteria", Version 2.0, Various Authors, Long Beach, California: 2009

Pscharis I.N., "Displacement-Based Seismic Design", Lecture, Laboratory for Earthquake Engineering, National Technical University of Athens

Rathje E.M. and Antonakos G., "A Unified Model for Predicting Earthquake-Induced Sliding Displacements of Rigid and Flexible Slopes," *Engineering Geology*, 122, p51-60: 2011

Rathje E.M. and Saygili G., "Probabilistic assessment of earthquake-induced sliding displacements of natural slopes", *Bulletin of the New Zealand Society of Earthquake Engineering* 41, p18-27: 2009

Rathje E.M. and Saygili G., "Estimating Fully Probabilistic Seismic Sliding Displacements of Slopes from a Pseudoprobabilistic Approach", *Journal of Geotechnical and Geo-environmental Engineering*, Vol.173 No.3, p208-217: 2011

Rankine W., "On the stability of loose earth", *Philosophical Transactions of the Royal Society of London*, Vol.147: 1857

Richards R. and Elms D.G., "Seismic passive resistance of tied-back walls", *J.Geotech.Engng* 118, No.7, p996-1011: 1992

Royal HaskoningDHV, "Capability Statement Earthquake Engineering", HaskoningDHV Nederland B.V.: 2014

Santos J.A. and Correia A.G., "Reference threshold shear strain of soil, its application to obtain a unique strain-dependent shear modulus curve for soil", In Proceedings 15th International Conference on Soil Mechanics and Geotechnical Engineering, Istanbul, Turkey, Volume 1, p267-270: 2001

Saygili G. and Rathje E.M., "Empirical predictive models for earthquake-induced sliding displacements of slopes", *Journal of Geotechnical and Geo-environmental Engineering* 134, p790-803: 2008

Seed H.B. and Idriss I.M., "Soil Moduli and Damping Factors for Dynamic Response Analysis", Report No. EERC 70-10, University of California, Berkeley: 1970

Seed H.B. and Whitman R.V., "Design of earth retaining structures for dynamic loads", Proceedings, ASCE Specialty Conference on Lateral Stresses in the Ground and Design of Earth Retaining Structures, p103-147: 1970

Spijkers J.M.J., Vrouwenvelder A.W.C.M. and Klaver E.C., "Dynamics of Structures – Part 1: Vibration of Structures", Lecture notes Dynamics of Structures, Delft University of Technology: 2006

Towhata I. and Islam M.S., "Prediction of lateral displacement of anchored bulkheads induced by seismic liquefaction", *Soils Found.* 27, No.4, p137-147: 1987

TNO, "Geïnduceerde aardtrillingen Groningen veld", TNO, Utrecht: 2009

US Army Corps of Engineers (USACE), "Response Spectra and Seismic Analysis for Concrete Hydraulic Structures", EM 1110-2-6050, Washington D.C.: 1999

US Army Corps of Engineers (USACE), "Time-History Dynamic Analysis of Concrete Hydraulic Structures", EM 1110-2-6051, Washington D.C.: 2003

US Army Corps of Engineers (USACE), "Earthquake Design and Evaluation of Concrete Hydraulic Structures", EM 1110-2-6053, Washington D.C.: 2007

Visone C., "Performance-Based Approach in Seismic Design of Embedded Retaining Walls", PhD Thesis, Università Degli Studi Di Napoli Federico II: 2008

Visone C. and Magistris, de F.S., "A review of design methods for retaining structures under seismic loadings", Structural and Geotechnical Dynamic Lab StreGa, University of Molise, Termoli (CB), Italy: 2008

Vrouwenvelder A.C.W.M., Besseling F., "Current situation structural design methods", Lecture during the 'Knowledge Sharing Meeting on Earthquakes in Groningen' organised by Delft University of Technology and Groningen Seaports, Delft: September 22nd, 2014.

Vrouwenvelder A.C.W.M. and Witteveen J., "Plasticity – The plastic behaviour and the calculation of plates subjected to bending", Lecture notes Plasticity, Delft University of Technology: 2003

Westergaard H., "Water pressure on dams during earthquakes", Transactions of ASCE, Paper No.1835, p418-433: 1931

Wood J., "Earthquake-induced soil pressures on structures", Report EERL 73-05, California Institute of Technology, Pasadena, California, 311 p: 1973

Zeng X. and Steedman R.S., "On the behaviour of quay walls in earthquakes", Géotechnique 43, No.3, p417-431: 1993

Appendix A: Soil pressure theories

An important aspect in seismic computations associated with retaining walls is the calculation of soil pressures. Lateral soil pressures, which develop during earthquake shaking, influence the behaviour of retaining walls. These soil pressures comprise static gravitational pressures (prior to earthquake) and transient dynamic pressures (during earthquake). Both are important for the seismic response of retaining walls. Different theories are available for calculating static and dynamic soil pressures. A brief overview is provided in the following paragraphs. A clarification of a number of symbols used in the soil pressure theories is provided by Figure A.1. (Ebeling & Morrison 1992, Kramer 1996, Visone 2008)

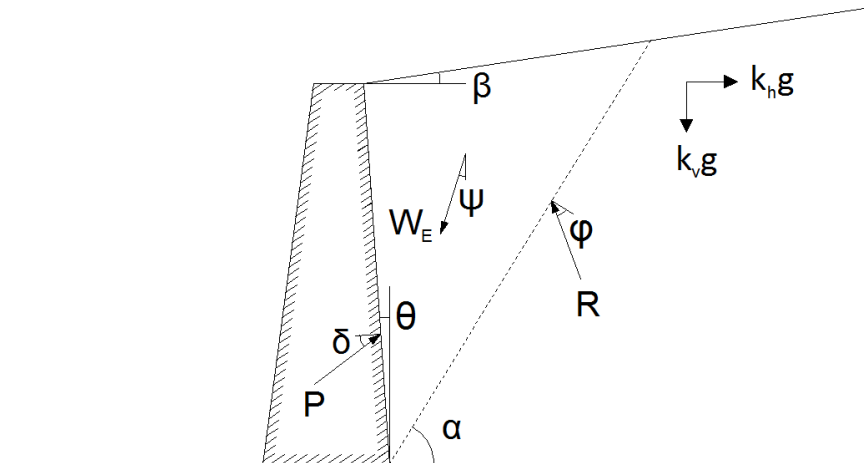


Figure A.1: Applied symbols in soil pressure theories, adapted from (Visone, 2008)

A more complete overview of the symbols used in soil pressure theories:

- α = angle of the planar failure surface with respect to the horizontal [°]
- β = inclination angle of the backfill with respect to the horizontal [°]
- γ_b = buoyant unit weight of soil [kN/m^3]
- γ_{dry} = dry unit weight of the soil [kN/m^3]
- γ_{sat} = saturated unit weight of the soil [kN/m^3]
- γ_w = unit weight water [kN/m^3]
- Δu = excess pore pressure [kN/m^2]
- δ = soil wall friction angle [°]
- θ = inclination angle of the wall interface with respect to the vertical [°]
- σ = total soil stress [kN/m^2]
- σ' = effective soil stress [kN/m^2]
- ϕ = friction angle of the soil [°]
- ψ = inclination angle of the seismic coefficient k with the vertical [°]
- a_h = horizontal acceleration [m/s^2]
- a_v = vertical acceleration [m/s^2]
- c = cohesion of the soil [kN/m^2]
- F_p = dynamic thrust factor [-]
- F_m = dynamic moment factor [-]
- H_{wall} = retaining height [m]
- h_w = water depth
- k_h = horizontal seismic coefficient [-]
- k_v = vertical seismic coefficient [-]
- $K_{A(E)}$ = active soil pressure coefficient [-]

- $K_{P(E)}$ = passive soil pressure coefficient [-]
- K_0 = neutral soil pressure coefficient [-]
- p_a = active soil pressure on the wall [kN/m^2]
- p_p = passive soil pressure on the wall [kN/m^2]
- $P_{A(E)}$ = active soil thrust on the wall [kN]
- $P_{P(E)}$ = passive soil thrust on the wall [kN]
- p_w = water pressure [kN/m^2]
- P_w = water thrust on the wall [kN]
- r_u = pore pressure ratio [-]

A.1. Static earth pressure theory

Static soil pressures acting on a retaining structure strongly depend on the deformation of soil and structure. Active soil pressures develop as a result of the structure moving away from the retained soil and passive soil pressure when moving towards the retained soil. Generally it can be said that active soil pressures develop in the retained soil behind the wall and passive soil pressure in the embedment in front of the wall. When the strength of the soil is fully mobilized minimum soil pressures act on the wall on the active side and maximum soil pressures on the passive side. In case of restrained lateral wall movement, which holds for anchored sheet pile walls, static soil pressures can be larger than the minimum active. It should be noted that even under static conditions the prediction of retaining wall forces and deformations is a complicated problem due to soil-structure interaction. The three main static earth pressure theories found in literature and engineering practice (i.e. Rankine, Coulomb and Log-spiral theory) are treated below (Ebeling & Morrison 1992, Kramer 1996, Visone 2008)

A.1.1. Rankine theory

The simplest procedure for calculating minimum active and maximum passive soil pressures was developed by Rankine (1857). In the procedure it is assumed that vertical soil stress at any depth in the ground can be computed by multiplying the depth with the unit weight of the overlying soil plus any surcharge at ground level and that successively the horizontal soil stress can be found by assuming full mobilization of shear resistance in the soil. According to Rankine the minimum active soil pressure and maximum passive soil pressure at any point behind the wall can be computed by the following expressions respectively (Ebeling & Morrison 1992, Kramer 1996):

$$p_a = K_A \sigma'_v - 2c\sqrt{K_A} \quad (\text{A1})$$

$$p_p = K_p \sigma'_v + 2c\sqrt{K_p} \quad (\text{A2})$$

In case of a smooth vertical wall retaining a horizontal backfill the coefficients of minimum active soil pressure K_A and maximum passive soil pressure K_p can be calculated by the following equations respectively:

$$K_A = \frac{1-\sin\varphi}{1+\sin\varphi} = \tan^2\left(45 - \frac{\varphi}{2}\right) \quad (\text{A3})$$

$$K_p = \frac{1+\sin\varphi}{1-\sin\varphi} = \tan^2\left(45 + \frac{\varphi}{2}\right) \quad (\text{A4})$$

There are also equations available for calculating Rankine active and passive soil coefficients that take into account inclination of the backfill surface, see e.g. (Ebeling & Morrison, 1992) and (Kramer, 1996). The minimum active and maximum passive soil thrusts acting at a height $H_{\text{wall}}/3$ on the wall can then be computed by:

$$P_A = \frac{1}{2} K_A \gamma H_{\text{wall}}^2 \quad (\text{A5})$$

$$P_P = \frac{1}{2} K_P \gamma H_{\text{wall}}^2 \quad (\text{A6})$$

A.1.2. Coulomb theory

The commonly applied soil pressure theory developed by Coulomb (1776) considers the equilibrium of forces acting on a soil wedge behind a retaining wall without regard to the state of stress within the soil. A planar failure surface is assumed, stretching from heel / toe of the wall to ground level, along which shear resistance is assumed to be fully mobilized. In contrast to Rankine theory, Coulomb theory considers wall-soil friction and it is applicable for calculating soil thrusts on walls with irregular backfill slopes, concentrated loads on the backfill surface and seepage forces. The active and passive soil thrusts acting at a height $H_{\text{wall}}/3$ on a wall retaining cohesionless soil can be computed by equations (A5) and (A6) respectively. The active and passive soil coefficients in these equations can be obtained by the following expressions (Ebeling & Morrison 1992, Kramer 1996):

$$K_A = \frac{\cos^2(\varphi-\theta)}{\cos^2\theta \cos(\delta+\theta) \left[1 + \sqrt{\frac{\sin(\delta+\varphi)\sin(\varphi-\beta)}{\cos(\delta+\theta)\cos(\beta-\theta)}} \right]^2} \quad (\text{A7})$$

$$K_P = \frac{\cos^2(\varphi+\theta)}{\cos^2\theta \cos(\delta-\theta) \left[1 - \sqrt{\frac{\sin(\delta+\varphi)\sin(\varphi+\beta)}{\cos(\delta+\theta)\cos(\beta-\theta)}} \right]^2} \quad (\text{A8})$$

The corresponding active and passive wedge failure surfaces are inclined under an angle with respect to the horizontal and can be calculated by the following equations respectively:

$$\alpha_A = \varphi + \tan^{-1} \left[\frac{\tan(\varphi-\beta) + \sqrt{\tan(\varphi-\beta)[\tan(\varphi-\beta)+\cot(\varphi-\theta)][1+\tan(\delta+\theta)\cot(\varphi-\theta)]}}{1 + \{\tan(\delta+\theta)[\tan(\varphi-\beta)+\cot(\varphi-\theta)]\}} \right] \quad (\text{A9})$$

$$\alpha_P = -\varphi + \tan^{-1} \left[\frac{\tan(\varphi+\beta) + \sqrt{\tan(\varphi+\beta)[\tan(\varphi+\beta)+\cot(\varphi+\theta)][1+\tan(\delta-\theta)\cot(\varphi+\theta)]}}{1 + \{\tan(\delta-\theta)[\tan(\varphi+\beta)+\cot(\varphi+\theta)]\}} \right] \quad (\text{A10})$$

D-SHEET PILING applies equations (A7) and (A8) in reduced form (horizontal backfill, vertical wall), known as the Müller-Breslau (1906) equations, for the calculation of the active and passive coefficients. For the corresponding inclination angle of the failure planes it is assumed that α equals $(\frac{\pi}{4} \pm \frac{\varphi}{2})$. D-SHEET PILING also determines the neutral soil pressure coefficient (soil at rest) for its calculations by using the Jáky (1948) formula. In case of non-horizontal soil surfaces D-SHEET PILING applies Culmann (1866) method for iteratively determining a planar critical failure surface and successively computing soil pressure coefficients in each point from top to toe of the sheet pile wall. (Deltaires Systems, 2014)

A.1.3. Logarithmic spiral theory

Multiple authors have developed relationships for active and passive soil pressure coefficients based on the (more physically realistic) assumption of a failure surface described by a logarithmic spiral function. This means that both the active as the passive failure surface consist of a curved section near the heel / toe of the wall and a linear section stretching from the curved part towards ground level. A tabulated set of active and passive coefficient values which is commonly used for this matter was developed by Coquet & Kerisel (1948). The tables of Coquet & Kerisel can be found in a number of publications, such as (Ebeling & Morrison, 1992),

(Kramer, 1996) and (Visone, 2008). For the calculations based on curved failure surfaces D-SHEET PILING applies the Kötter (1903) equations. These equations assume an unloaded horizontal surface, homogeneous soil with a volumetric weight of zero and a slip plane consisting of a logarithmic-spiral and a straight part. (Ebeling & Morrison 1992, Kramer 1996, Visone 2008, Deltares Systems 2014)

An impression of Coulomb-type failure surfaces and Log-spiral-type failure surfaces associated with an embedded retaining wall is presented in Figure A.2.

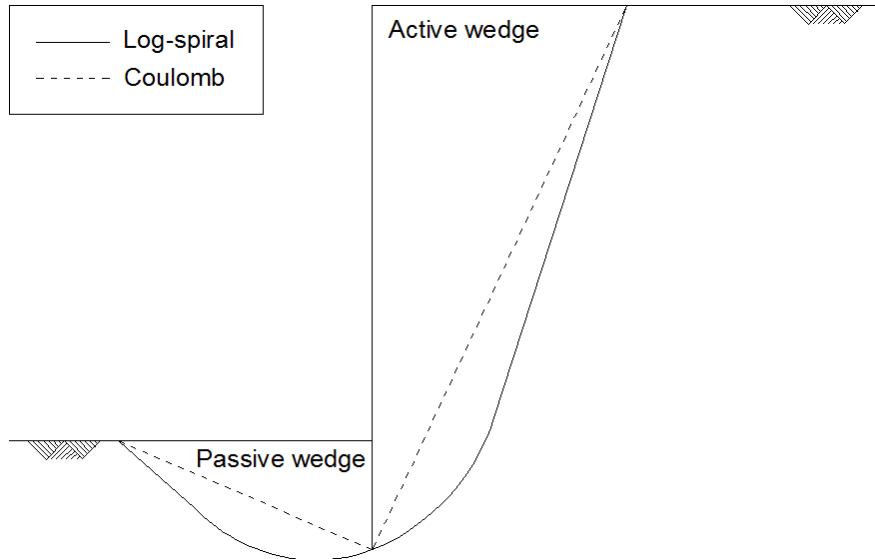


Figure A.2: Coulomb and log spiral type failure surfaces associated with an embedded retaining wall

In case that the wall-friction angle equals zero the Rankine, Coulomb and Log-spiral approach all three give similar results for the calculated active and passive thrust. In situations with a wall-friction angle larger than zero the Log-spiral method gives slightly more accurate results than the Coulomb method but because of the small difference the more convenient Coulomb equations are usually applied. The value of Log-spiral theory becomes more evident in the case of passive soil pressure. While Rankine theory underpredicts actual passive soil pressure, and is therefore rarely applied, Coulomb theory increasingly overpredicts actual passive soil pressure with increasing wall-friction angle. The latter can be explained by the fact that the failure surface becomes more curved with increasing wall-friction angle. For $\delta = \phi/2$ Coulomb approach overpredicts the passive soil pressure by approximately 11% and by 100% or more in case of $\delta = \phi$. Therefore Coulomb generally is not applied when $\delta > \phi/2$. (Ebeling & Morrison 1992, Kramer 1996)

A.2. Dynamic earth pressure theory

The approaches presented in this section for the calculation of dynamic soil pressures are applied in pseudo-static analysis. The ability of the retaining wall to yield / move relative to the soil, i.e. whether an active soil state can develop, determines which dynamic soil pressure theory should be used for calculations. In case of a yielding wall Mononobe-Okabe methodology can be applied. For non-yielding walls the approach developed by Wood can be used. (Ebeling & Morrison 1992, Kramer 1996)

A.2.1. Yielding walls: Mononobe-Okabe

The dynamic earth pressure theory known as the Mononobe-Okabe (M-O) method was developed by Okabe (1926) and Mononobe & Matsuo (1929). In this method pseudo-static accelerations are applied on an active (or passive) wedge as defined in static Coulomb theory. The pseudo-static soil thrust is subsequently obtained from force equilibrium of the wedge. So basically M-O methodology is an extension of static Coulomb theory.

The total active soil thrust on a wall retaining dry cohesionless soil can be computed by the following expression (Ebeling & Morrison 1992, Kramer 1996):

$$P_{AE} = \frac{1}{2} K_{AE} \gamma H_{wall}^2 (1 - k_v) \quad (A11)$$

The active dynamic soil pressure coefficient (K_{AE}) in equation (A11) can be obtained by:

$$K_{AE} = \frac{\cos^2(\varphi - \theta - \psi)}{\cos \psi \cos^2 \theta \cos(\delta + \theta + \psi) \left[1 + \sqrt{\frac{\sin(\delta + \varphi) \sin(\varphi - \beta - \psi)}{\cos(\delta + \theta + \psi) \cos(\beta - \theta)}} \right]^2} \quad (A12)$$

In equation (A12) it holds that $\phi - \beta \geq \psi$, $\gamma = \gamma_d$ and $\psi = \tan^{-1}[k_h/(1-k_v)]$. The corresponding M-O active wedge failure surface is inclined under a smaller angle with respect to the horizontal compared to the static case. It can be computed by:

$$\alpha_{AE} = \varphi - \psi + \tan^{-1} \left[\frac{-\tan(\varphi - \psi - \beta) + \sqrt{\tan(\varphi - \psi - \beta)[\tan(\varphi - \psi - \beta) + \cot(\varphi - \psi - \theta)][1 + \tan(\delta + \psi + \theta) \cot(\varphi - \psi - \theta)]}}{1 + \{\tan(\delta + \psi + \theta)[\tan(\varphi - \psi - \beta) + \cot(\varphi - \psi - \theta)]\}} \right] \quad (A13)$$

The total active soil thrust P_{AE} can be split up into a static part (P_A), acting at a height $H_{wall}/3$ on the wall, and a dynamic part (ΔP_{AE}) which is considered to act approximately at a height $0.6H_{wall}$ on the wall (according to the commonly adapted recommendation by (Seed & Whitman, 1970)). The height h at which the total active thrust P_{AE} acts on the wall can then be obtained by (Ebeling & Morrison 1992, Kramer 1996):

$$h = \frac{P_A H_{wall}/3 + \Delta P_{AE}(0.6H_{wall})}{P_{AE}} \quad (A14)$$

The total passive thrust on a wall retaining dry cohesionless soil and the corresponding passive dynamic soil pressure coefficient can be predicted by equations (A15) and (A16):

$$P_{PE} = \frac{1}{2} K_{PE} \gamma H_{wall}^2 (1 - k_v) \quad (A15)$$

$$K_{PE} = \frac{\cos^2(\varphi + \theta - \psi)}{\cos \psi \cos^2 \theta \cos(\delta - \theta + \psi) \left[1 - \sqrt{\frac{\sin(\delta + \varphi) \sin(\varphi + \beta - \psi)}{\cos(\delta - \theta + \psi) \cos(\beta - \theta)}} \right]^2} \quad (A16)$$

The inclination of the M-O passive wedge failure surface with respect to the horizontal can be found by equation (A17):

$$\alpha_{PE} = \psi - \varphi + \tan^{-1} \left[\frac{\tan(\varphi + \psi + \beta) + \sqrt{\tan(\varphi + \beta - \psi)[\tan(\varphi + \beta - \psi) + \cot(\varphi + \theta - \psi)][1 + \tan(\delta + \psi - \theta) \cot(\varphi + \theta - \psi)]}}{1 + \{\tan(\delta + \psi - \theta)[\tan(\varphi + \beta - \psi) + \cot(\varphi + \theta - \psi)]\}} \right] \quad (A17)$$

Computed M-O soil pressure coefficients can be manually inserted as input parameters in D-SHEET PILING. In this way pseudo-static calculations can be carried out by the program.

A.2.2. Non-yielding walls: Wood

The M-O methodology assumes that shear resistance of the soil can develop to full extent. This will not be the case for non-yielding wall structures, such as massive gravity walls founded on rock or basement walls braced at top and bottom. So in these situations one cannot perform calculations which are based on minimum active and maximum passive soil pressure conditions. Expressions commonly used in practice for the non-yielding wall

situation were developed by Wood (1973). He analysed the dynamic response of a homogeneous elastic soil trapped between two smooth rigid walls connected to a rigid base. For this soil-structure system a number of things were shown (Kramer, 1996):

- In case of sufficiently far spacing of the two walls (spacing $> 1.5H_{\text{wall}}$) the soil pressures on a wall will negligibly be influenced by the presence of the other wall;
- Dynamic amplification is negligible for motions at less than half the fundamental frequency of the unrestrained backfill soil $f_0 = V_s/4H_{\text{wall}}$ (these low-frequency motions apply to many practical problems);
- When subjected to a uniform, constant, low-frequency horizontal acceleration throughout the soil, the elastic solution yields the wall pressures.

Wood (1973) derived from this the following expressions for the dynamic soil thrust and dynamic soil overturning moment (about the base of the wall) respectively (Ebeling & Morrison 1992, Kramer 1996, NEN-EN1998-5):

$$\Delta P_{\text{eq}} = \gamma H_{\text{wall}}^2 \frac{a_h}{g} F_p \quad (\text{A18})$$

$$\Delta M_{\text{eq}} = \gamma H_{\text{wall}}^3 \frac{a_h}{g} F_m \quad (\text{A19})$$

The dimensionless dynamic thrust and moment factors F_p and F_m can be obtained from graphs which are e.g. provided in (Kramer, 1996). The dynamic thrust according to Wood acts on a height above the wall $\Delta M_{\text{eq}}/\Delta P_{\text{eq}}$ which typically approximately equals $0.63H_{\text{wall}}$.

A.2.3. Water pressure

All the basic soil pressure theory equations discussed above are valid for the dry backfill case. For water retaining quay walls this is however not the case. The presence of water in the backfill and outside the retaining structure is of importance because it significantly influences the seismic behaviour of the soil-structure system. The water level in the backfill is usually approximately equal to the outside water level as few quay walls are fully impermeable. In case of outside water level changes the backfill water level generally lags behind depending on the permeability of the wall and backfill and the rate of outside water level change. In absence of seepage within the backfill the total water pressures that act on a quay wall consist of two components, i.e. hydrostatic water pressure and hydrodynamic water pressure. Hydrostatic water pressure increases linearly with the depth and acts on the quay wall before, during and after earthquake shaking. Hydrodynamic water pressures result from the dynamic response of the water to earthquake shaking. (Kramer, 1996)

A.2.3.1. Outward water pressure

For computing the hydrodynamic water pressures outside of a quay wall the Westergaard (1931) procedure is generally applied. These pressures are superimposed on the hydrostatic water pressure distribution along the outer side of the wall. The outside hydrodynamic pressures destabilize the wall because they act in the opposite direction of the hydrostatic pressures (so away from the wall). Westergaard derived its expressions for the case of semi-infinite water reservoir retained by a vertical rigid dam subjected to a horizontal harmonic acceleration. The expressions for the amplitude of the hydrodynamic pressure amplitude p_w and the resultant hydrodynamic thrust P_w respectively:

$$p_w = \frac{7}{8} \frac{a_h}{g} \gamma_w \sqrt{z_w h_w} \quad (\text{A20})$$

$$P_w = \frac{7}{12} \frac{a_h}{g} \gamma_w h_w^2 \quad (\text{A21})$$

Equations (A20) and (A21) are valid in case that the applied frequency is lower than the fundamental frequency of the reservoir $f_0 = v_p/4h_w$ (with v_p the p-wave velocity of water, equal to approximately 1400 m/s). Validity of the equations is usually the case. Figure A.3 provides an illustration of the hydrostatic and Westergaard hydrodynamic pressure distributions and the corresponding resultant thrusts. The hydrostatic thrust P_H acts at a height $h_w/3$ above the wall and the Westergaard hydrodynamic thrust P_W at a height $0.4h_w$. (Ebeling & Morrison 1992, Kramer 1996, NEN-EN1998-5):

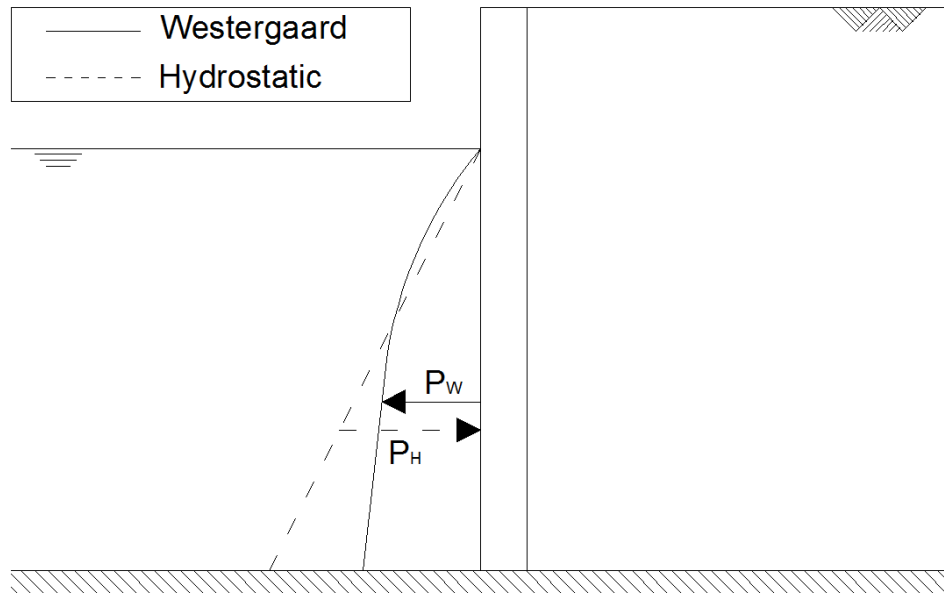


Figure A.3: Outward hydrostatic and Westergaard hydrodynamic pressures

A.2.3.2. Backfill water pressure

During earthquake shaking the water present in a backfill can affect the seismic loading on a quay wall in three different ways according to references (Ebeling & Morrison 1992, Kramer 1996, Visone 2008):

- Altering backfill inertial forces
- Adding hydrodynamic pressure forces
- Allowing development of excess pore pressures (possibly resulting in liquefaction)

The altering of the inertial backfill forces depends on the amount of possible relative movement between the backfill soil particles and the surrounding pore water. This amount of relative movement can be characterized by two opposite conditions, the restrained water condition and the free water condition. The restrained water condition corresponds to no relative movement between soil particles and pore water due to limited permeability (typically $k < 10^{-5}$ m/s), in which case the inertial forces will be proportional to the saturated unit weight of the soil. The free water condition corresponds to independent movement of soil particles through nearly stationary pore water due to high permeability (typically $k > 10^{-2}$ m/s), in which case the inertial forces will be proportional to the buoyant (submerged) unit weight of the soil. In these free water conditions hydrodynamic pressure forces can also develop. These hydrodynamic pressures can be calculated by the Westergaard equations (A20) and (A21) and must be added to the hydrostatic pressure distribution.

For the restrained water case, which appears to be in practice the usual case, a modification of the M-O method was proposed by (Matzusawa *et al.*, 1985) to account for the presence of pore water in the backfill and include excess pore water pressure (via the pore pressure ratio $r_u = \Delta u/\sigma'_v$). Equations (A11) and (A12) can be adapted by using the following expressions respectively:

$$\gamma = \gamma_b(1 - r_u) \quad (\text{A22})$$

$$\psi = \tan^{-1} \left[\frac{\gamma_{\text{sat}} k_h}{\gamma_b (1 - r_u) (1 - k_v)} \right] \quad (\text{A23})$$

In case of excess pore pressure the computed soil thrust must be added to an equivalent hydrostatic thrust which can be calculated in this case using $\gamma_{\text{eq}} = \gamma_w + r_u \gamma_b$, which reduces to $\gamma_{\text{eq}} = \gamma_{\text{sat}}$ in case that $r_u = 1$, i.e. when liquefaction occurs.

Closing of a complementary expression is available for computing dynamic soil thrusts in case of a partially submerged backfill. An average soil unit weight based on the relative volumes of dry and saturated soil in the active wedge behind the quay wall is applied in the M-O method:

$$\gamma_{\text{av}} = \lambda^2 \gamma_{\text{sat}} + (1 - \lambda^2) \gamma_{\text{dry}} \quad (\text{A24})$$

In which λ represents the ratio between the 'saturated height' and the total height of the retaining wall, i.e. $\lambda = H_{\text{sat}}/H_{\text{tot}}$.

Appendix B: Software

B.1. D-SHEET PILING

D-SHEET PILING is a software tool developed by Deltaris for the design of retaining walls (predominantly sheet piling) and single piles. In the D-SHEET PILING code the sheet pile wall is modelled as an elastic beam on a foundation of uncoupled elasto-plastic springs (representing the soil). In this modelling the assumption of Bernoulli is applied, which means that cross-sections of the beam are assumed to remain straight and perpendicular to the beam axis. The following well-known differential equation describes this behaviour:

$$b \cdot EI \frac{d^4 w}{dx^4} + N \frac{d^2 w}{dx^2} = b \cdot f_p(x, w) \quad (B1)$$

In which:

- w = horizontal displacement of the beam [m]
- x = coordinate along the axis of the beam [m]
- f_p = total pressure on the beam per running meter, including the reaction of the soil springs [kN/m]
- EI = flexural stiffness of the beam with E the Young's modulus and I the moment of inertia [kNm^2/m]
- N = normal force in the beam [kN]
- b = acting width of the beam [m]

D-SHEET PILING solves equation (B1) numerically by applying finite element method. The sheet pile wall is divided in a number of elements that are connected at the edges (nodes). At these nodes the displacements and rotations of adjacent elements are equal so that a continuous beam is created. The positions of the nodes are automatically determined by D-SHEET PILING. Nodes are always created at boundaries of soil layers, boundaries of water pressures, boundaries of wall segments with different properties and points with discontinuities. The length of an element is at maximum 1/20 of the total wall height and every element is in addition subdivided into five sections. For each section boundary bending moments, shear forces, displacements and horizontal soil and water pressures are determined.

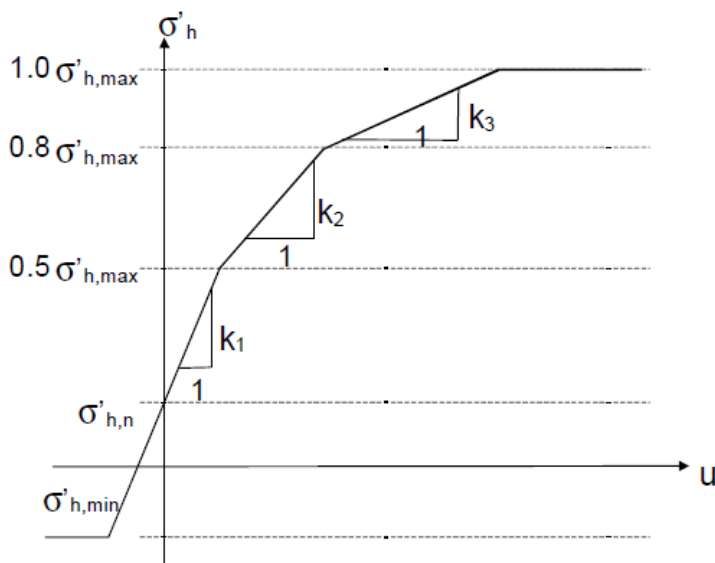


Figure B.1: Horizontal soil stress-displacement relationship applied in D-SHEET PILING

The uncoupled elasto-plastic soil spring modelling is an important characteristic of D-SHEET PILING. For the retaining wall modules the soil springs are considered to be tri-linear (the single pile module uses bi-linear soil springs). Basically the tri-linear soil-spring curve is a simplified schematization of a continuous nonlinear p-y curve. With such a curve the nonlinear character of the soil is taken into account, i.e. that the stiffness of the

soil decreases with increasing load. Figure B.1 shows the tri-linear soil-spring curve which embeds a schematization of the horizontal soil stress-displacement relationship. The minimum and maximum horizontal effective stresses in this curve are computed with the active (K_a) and passive (K_p) soil pressure coefficients respectively. The neutral horizontal effective soil stress, corresponding to zero displacement, is computed with the neutral soil pressure coefficient (K_0).

In D-SHEET PILING the k_1 , k_2 and k_3 values per soil layer can be selected from table 3.3 of CUR 166 (characteristic values per type of soil material) or manually defined. Concerning the soil pressure coefficients D-SHEET PILING offers a choice between two soil parameter models, the so-called K_A , K_0 and K_p basic model and c , ϕ , δ model. In the first model the option is provided to calculate them automatically by using Müller-Breslau equations or Kötter equations (see sections A.1.2 and A.1.3) or to define them manually. The soil pressure coefficient values are constant per soil layer in this model. In the second model the iterative Culmann method is used (see section A.1.2) which automatically determines soil pressure coefficients that vary within a soil layer.

Other input parameters per soil layer in both models are the internal friction angle, wall-friction angle, cohesion, shell factor, over-consolidation ratio, relative density and horizontal permeability. Other input for a D-SHEET PILING model in general are geometry, water properties, sheet pile properties, loads, supports and staging of the design conditions.

B.2. SHAKE2000 & SLAMMER

B.2.1 SHAKE2000

SHAKE2000 is a software tool of GeoMotions LCC which is developed for 1-D analysis of geotechnical earthquake engineering problems. More specifically SHAKE2000 computes the site response to a seismic shear wave travelling vertically in a soil system as described in paragraph 2.4.2. This is a soil system consisting of homogeneous visco-elastic horizontal layers extending infinitely in all lateral directions. The continuous (or steady-state) solution to the 1D shear wave equation in this Kelvin-Voigt solid, i.e. equation (1), adapted for use with transient motions through Fast Fourier Transformation (FFT) algorithm, is the basis for the program. For all the equations corresponding to the steady-state solution and transient algorithm one is referred to the SHAKE2000 manual (Ordóñez, 2012). The nonlinearity of the shear moduli and damping of the soil layers is accounted for by computing equivalent linear values compatible with the average effective strains in each layer by applying an iterative procedure.

In SHAKE2000 the material input consists of dynamic soil properties (i.e. shear modulus and damping curves) and soil column properties (i.e. thickness, density, damping ratio, density and shear wave velocity) per soil layer. So the program is able to handle soil systems with variation in both moduli and damping and furthermore it can take into account the effect of the base rock layer being elastic. The input values assigned per soil layer are all independent of frequency. Concerning the strong-motion record which is used for the analysis (the object motion), it can be scaled and assigned to any one layer in the system and new motions can be computed in any other layer. And computed motions can be scaled and assigned to any other soil column as well.

With SHAKE2000 the following output, which is relevant for the present study, can be generated:

- For every object motion:
 - Acceleration- velocity-, displacement- and energy time histories
 - RMS of acceleration time history, Arias intensity, bracketed durations and mean period
 - Acceleration spectrum (spectral acceleration as a function of period) and corresponding characteristic spectral periods (T_0 , T_p and T_{avg})
 - Fourier amplitude spectrum (Fourier amplitude as a function of frequency)

- Over the depth of the soil column:
 - Strain-compatible damping, shear moduli, maximum shear strain, maximum shear stress, shear wave velocity, peak acceleration and cyclic stress ratio
- At any soil layer:
 - Acceleration time histories
 - Shear stress and strain time histories
 - Response spectrum (spectral displacement as a function of period)
 - Fourier amplitude spectrum (acceleration amplitude as a function of frequency)
- Between any two soil layers:
 - Amplification spectrum (amplification ratio as a function of frequency)

Furthermore SHAKE2000 offers the possibility to perform four variants of permanent-displacement analysis:

- Newmark rigid-sliding-block analysis:
 - Similar to rigorous Newmark-sliding-block analysis in SLAMMER software (see B.2.2)
- Rathje & Saygili (2011) deterministic or pseudo-probabilistic simplified rigid-sliding-block analysis:
 - Applying empirical functions that estimate sliding displacements as functions of peak acceleration, peak velocity, moment magnitude, Arias intensity and mean period
 - Comparable with Rathje & Saygili (2008, 2009) methods in SLAMMER software (see B.2.2)
- Makdisi & Seed (1978) simplified decoupled flexible-sliding-block analysis:
 - Applying design charts through which displacements as a function of critical acceleration, ground motion and earthquake magnitude are iteratively estimated. This analysis is designed and calibrated for earth dams.
- Bray & Travasarou (2007) simplified coupled flexible-sliding-block analysis:
 - Same as in SLAMMER software (see B.2.2)

B.2.2 SLAMMER

SLAMMER (Seismic Landslide Movement Modelled using Earthquake Records) is a software tool developed by Jibson et al. (2013) from United States Geological Survey (USGS) for performing a variety of sliding-block (permanent-displacement) analyses in order to evaluate seismic slope performance, i.e. to estimate displacements of a soil body during a landslide. SLAMMER offers the possibility to carry out the following types of permanent-displacement analysis:

- Rigorous analyses
 - Newmark rigid-sliding-block
 - Decoupled flexible-sliding-block
 - Coupled flexible-sliding-block
- Empirical analyses
 - Rigid-sliding-block
 - Flexible-sliding-block (coupled)
 - Flexible/rigid-sliding-block (unified)

Rigorous analysis

Rigorous analysis calculates the displacement of a sliding soil mass by integrating the peaks of a strong-motion record over the threshold acceleration twice. This critical acceleration is an input parameter which can be defined as being constant or as varying over time. The strong-motion records can be obtained from the database which is implemented in the program. With only a few exceptions, the strong-motion records included in the imported program database were downloaded from the New Generation Attenuation (NGA) database, which is maintained by the Pacific Earthquake Engineering Research Center (PEER) at the University of California, Berkeley. The record library contains horizontal components only. Additional strong-motion records can be added to this database if wanted. In the analysis the records can be scaled to a desired PGA. In

case of rigid-block analysis a choice can be made between displacements in downslope only or both down- and upslope direction. For decoupled and coupled analyses some additional input parameters are necessary, i.e. the height of the soil mass, the shear wave velocities above and below the slip surface, the damping ratio and the soil model (linear elastic or equivalent linear).

Empirical analysis

These simplified variants of permanent-displacement analysis are based on empirical regression relationships which predict ground displacement based on ground motion parameters such as PGA and moment magnitude. In SLAMMER the following empirical relationships are implemented for simplified rigid-sliding-block analysis:

- The regression equation of Rathje and Saygili (2009) which estimates the Newmark displacement (D_n) as a function of critical acceleration (a_c), peak acceleration (a_{max}) and moment magnitude (M_w):

$$\ln D_n = 4.89 - 4.85 (a_c / a_{max}) - 19.64 (a_c / a_{max})^2 + 42.49 (a_c / a_{max})^3 - 29.06 (a_c / a_{max})^4 + 0.72 \ln a_{max} + 0.89 (M_w - 6) \quad (B2)$$

This equation was developed by conducting rigorous Newmark integrations on more than 2000 single-component strong-motion records for several discrete values of critical acceleration.

- The three regression equations of Saygili and Rathje (2008) which estimate the Newmark displacement (D_n) as functions of critical acceleration (a_c), peak acceleration (a_{max}), peak ground velocity (v_{max}) and Arias intensity (I_a):

$$\ln D_n = 5.52 - 4.43 (a_c / a_{max}) - 20.39 (a_c / a_{max})^2 + 42.61 (a_c / a_{max})^3 - 28.74 (a_c / a_{max})^4 + 0.72 \ln a_{max} \quad (B3)$$

$$\ln D_n = -1.56 - 4.58 (a_c / a_{max}) - 20.84 (a_c / a_{max})^2 + 44.75 (a_c / a_{max})^3 - 30.50 (a_c / a_{max})^4 - 0.64 \ln a_{max} + 1.55 \ln v_{max} \quad (B4)$$

$$\ln D_n = -0.74 - 4.93 (a_c / a_{max}) - 19.91 (a_c / a_{max})^2 + 43.75 (a_c / a_{max})^3 - 30.12 (a_c / a_{max})^4 - 1.30 \ln a_{max} + 1.04 \ln v_{max} + 0.67 \ln I_a \quad (B5)$$

These equations were developed by conducting rigorous Newmark integrations on 2383 strong-motion records for critical acceleration values between 0.05 and 0.30 g.

- The four regression equations of Jibson (2007) which estimate the Newmark displacement (D_n) as functions of critical acceleration (a_c), peak acceleration (a_{max}), moment magnitude (M_w) and Arias intensity (I_a):

$$\log D_n = 0.215 + \log [(1 - a_c / a_{max})^{2.341} (a_c / a_{max})^{-1.438}] \quad (B6)$$

$$\log D_n = -2.710 + \log [(1 - a_c / a_{max})^{2.335} (a_c / a_{max})^{-1.478}] + 0.424 M_w \quad (B7)$$

$$\log D_n = 2.401 \log I_a - 3.481 \log a_c - 3.230 \quad (B8)$$

$$\log D_n = 0.561 \log I_a - 3.833 \log (a_c / a_{max}) - 1.474 \quad (B9)$$

These equations were developed by conducting rigorous Newmark integrations on 2270 (first two) and 875 (last two) single-component strong-motion records from 30 earthquakes for several discrete values of critical acceleration.

- The regression equation of Jibson *et al.* (1998, 2000) which estimates the Newmark displacement (D_n) as a function of critical acceleration (a_c) and Arias intensity (I_a):

$$\log D_n = 1.521 \log I_a - 1.993 \log a_c - 1.546 \quad (B10)$$

This equation was developed by conducting rigorous Newmark integrations on 555 single-component strong-motion records from 13 earthquakes for several discrete values of critical acceleration.

- The regression equation of Jibson (1993) which estimates the Newmark displacement (D_n) as a function of critical acceleration (a_c) and Arias intensity (I_a):

$$\log D_n = 1.460 \log I_a - 6.642 a_c + 1.546 \quad (B11)$$

This equation was developed by conducting rigorous Newmark integrations on 11 single-component strong-motion records for several discrete values of critical acceleration.

- The regression equation of Ambraseys and Menu (1988) which estimates the Newmark displacement (D_n) as a function of critical acceleration (a_c) and peak acceleration (a_{max}):

$$\log D_n = 0.90 + \log[(1 - a_c / a_{max})^{2.53} (a_c / a_{max})^{-1.09}] \quad (B12)$$

This model is based on analysis of 50 strong-motion records from 11 earthquakes.

In SLAMMER the empirical relationship of Bray and Travasarou (2007) is implemented for simplified coupled flexible-sliding-block analysis:

$$\ln D = -1.10 - 2.83 \ln (k_{cr}) - 0.333 (\ln (k_{cr}))^2 + 0.566 \ln (k_{cr}) \ln (S_a (1.5 T_s)) + 3.04 \ln (S_a (1.5 T_s)) - 0.244 (\ln (S_a (1.5 T_s)))^2 + 1.50 T_s + 0.278 (M_w - 7) \quad (B13)$$

In this regression equation the displacement (D) is estimated as a function of the yield coefficient (k_{cr}), site period ($T_s = 4H_{soil} / V_s$), the spectral acceleration at 1.5 * the site period ($S_a(1.5T_s)$) and the moment magnitude (M_w). This model is based on analysis of 688 strong-motion records from 41 earthquakes.

Closing of an empirical unified model proposed by Rahtje and Antonakos (2011) is also implemented in SLAMMER. It is designed to give reliable results for a full range of period ratios representing both flexible and rigid conditions.

B.3. PLAXIS 2D

PLAXIS 2D is a two-dimensional finite element program for geotechnical engineering and design developed by the PLAXIS company (Plaxis bv). A large number of geotechnical problems can be analysed with the program concerning deformation, stability and groundwater flow. An important add-on module for the present study is the Dynamics module. It can be applied for analysing earthquake motions in the soil and their influence on nearby structures. Liquefaction is not included in this module.

In the following the relevant topics concerning the modelling of the reference case with PLAXIS 2D will be discussed. This concerns material models, structural elements and dynamics. For background information not treated in this section (e.g. the underlying mathematics, numerics and calculation schemes of the program) one is referred to the different PLAXIS 2D Manuals (Reference, Material Models, Scientific).

B.3.1. Soil material models

In PLAXIS material models are used to obtain a qualitative representation of soil behaviour and the corresponding model parameters to quantify the soil characteristics. The material model that will be applied in the present PLAXIS 2D calculations, both static and dynamic, is the Hardening Soil model with small-strain stiffness (HSsmall). Before elaborating on the key features of this model, underlying more simple models will shortly be discussed in advance for the sake of clarity. The PLAXIS Material Models Manual (Plaxis bv, 2014-3) is used as the main reference in this part. For more elaborate background information than treated in this section, one is referred to that manual.

B.3.1.1. Linear Elastic (LE) model

This most simple material model in PLAXIS 2D is based on Hooke's law of isotropic elasticity. It assumes that the considered material is linear elastic and has the same physical properties in all directions. Because soil behaviour is highly non-linear and irreversible this model can only be applied to model stiff elements in the soil

like concrete structures or bedrock formations and layers. Because stress states in this simple model are not limited (no plasticity considered) the model implicitly assumes unlimited strength of the material which obviously is not realistic. The characteristic input parameters for this model are the Young's Modulus E [kN/m^2] and the Poisson's ratio ν [-].

B.3.1.2. Mohr-Coulomb (MC) model

An improvement of the Linear Elastic material model is the Linear Elastic Perfectly Plastic model, which is generally referred to as the Mohr-Coulomb model. In this model a decomposition is made in a linear elastic part and a perfectly plastic part, as depicted in Figure B.2 (left). In the elastic part the material behaves according to Hooke's law and in the plastic part irreversible strains occur which lead to soil failure. The perfectly plastic part, or the Mohr-Coulomb failure criterion, is fully described by the parameters cohesion and friction angle, which means that it is fixed and not affected by (plastic) straining. This condition can be presented in the principal stress space as a fixed yield surface, as is depicted in Figure B.2 (right). Within this hexagonal cone the soil behaviour is purely elastic, at the cone surface fully plastic and outside the cone no description of material behaviour exists.

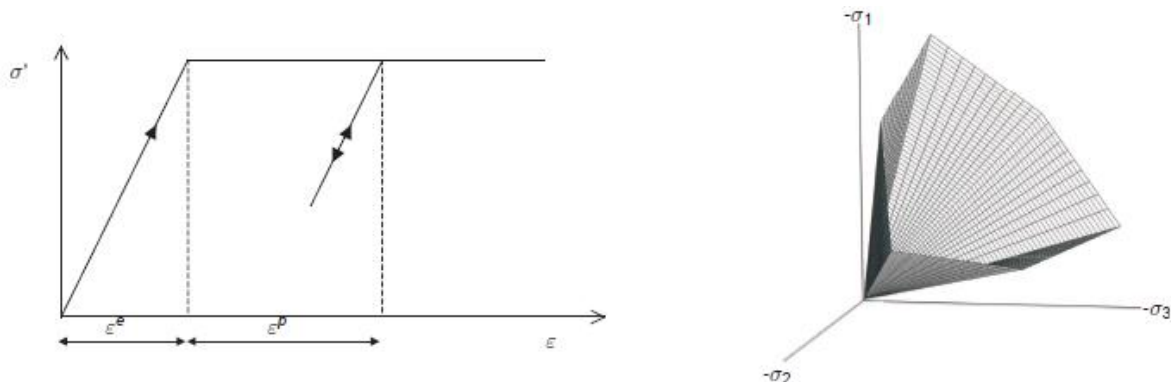


Figure B.2: Principle of linear elastic perfectly plastic model (left) and the associated Mohr-Coulomb yield surface (right), adapted from (Plaxis bv, 2014-3)

The characteristic input parameters for this model are Young's Modulus (E) and Poisson's ratio (ν) for the elastic part, cohesion c [kN/m^2] and friction angle φ [$^\circ$] for the plastic part and the angle of dilatancy ψ_{\max} [$^\circ$].

B.3.1.3. Hardening Soil (HS) model

The Hardening Soil model is more advanced than the MC model in describing soil behaviour. It does not consider a fixed yield surface in the principal stress space but a yield surface that can evolve due to plastic straining, a process which is referred to as hardening. Two types of hardening are distinguished (and both contained in PLAXIS code): shear hardening and compression hardening. Shear hardening is associated with primary deviatoric loading during which soil stiffness decreases and simultaneously irreversible strains develop. Compression hardening is associated with the development of irreversible strains during oedometer loading and isotropic loading. The evolving of the yield surface due to hardening is in PLAXIS limited by the Mohr-Coulomb yield criterion which represents the ultimate failure state. This is visualised in the two-dimensional stress plane by Figure B.3 (left).

Another improvement compared to the MC model, in line with the inclusion of shear and compression hardening, is that the soil stiffness depends on the stress/strain state and that it is described more accurately by applying three different stiffness moduli, instead of one Young's modulus. These stiffness parameters, corresponding to three typical loading types, are:

- E_{50}^{ref} = secant stiffness in standard drained triaxial test [kN/m^2]
- $E_{\text{oed}}^{\text{ref}}$ = tangent stiffness for primary oedometer loading [kN/m^2]
- $E_{\text{ur}}^{\text{ref}}$ = unloading-reloading stiffness (default: $E_{\text{ur}}^{\text{ref}} = 3E_{50}^{\text{ref}}$) [kN/m^2]

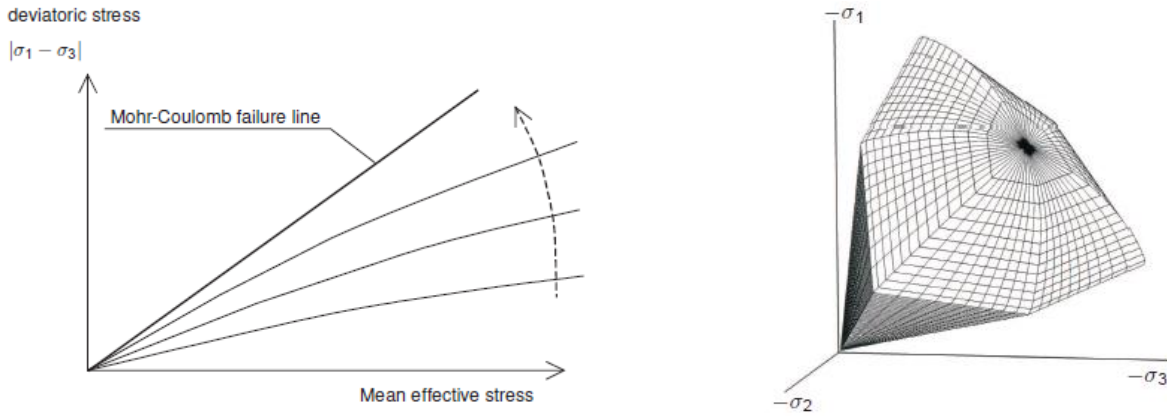


Figure B.3: Successive yield surfaces due to hardening limited by the Mohr-Coulomb ultimate failure state (left) and the associated yield cone including yield cap (right), adapted from (Plaxis bv, 2014-3)

The E_{ur}^{ref} modulus relates to elastic unloading and reloading within the hexagonal yield cone. The E_{50}^{ref} modulus corresponds to the shear type loading and therefore governs the development of the yield surface. This means that it largely controls the magnitude of the plastic strains that relate to the shear yield surface. Because this surface does not explain the plastic volume strain resulting from isotropic compression a second type of yield surface is therefore introduced to close the elastic region for compressive stress paths. This is the so called yield cap, which can be seen in Figure B.3 (right). The associated modulus E_{oed}^{ref} controls the cap yield surface, i.e. the magnitude of plastic strains that originate from the yield cap. The specific shape of the yield cap is determined via E_{oed}^{ref} and the parameter K_0^{nc} (Jaky neutral soil pressure coefficient).

The characteristic input parameters for this model are the three stiffness moduli (E_{50}^{ref} , E_{oed}^{ref} , E_{ur}^{ref}), cohesion (c), friction angle (φ), dilatancy angle (ψ_{\max}) and power (m). The latter defines the amount of stress-level dependency of the stiffness moduli (all stiffnesses increase with pressure). It is noted that this implies that all three input stiffnesses relate to a reference stress (p_{ref}). In PLAXIS 2D a default value of 100 kPa is assigned to p_{ref} .

B.3.1.4. Hardening Soil model with small-strain stiffness (HSsmall)

Now that the background of the HS model is known, the HSsmall model can be discussed. The HSsmall model is a modification of the HS model which accounts for increased stiffness of soil at small strains. In the HS model it is assumed that within the yield cone the soil response is purely linear elastic while it is typical for soils that a low strain level accompanies a higher stiffness than an engineering strain level and that this stiffness varies non-linearly with strain (as e.g. can be seen in the shear modulus curves in Figure 5.14). Two additional input parameters are used in the HSsmall model to describe this relation between stiffness and strain:

- The initial or very small-strain shear modulus G_0 [kN/m²]
- The shear strain level $\gamma_{0.7}$ [-] at which the secant shear modulus G_s [kN/m²] is reduced to 72.2% of G_0

Regarding these additional parameters, the following relationship by Hardin & Drnevich (1972), modified by Santos & Correia (2001), is used for the HSsmall model:

$$\frac{G_s}{G_0} = \frac{1}{1 + 0.385 \left| \frac{\gamma}{\gamma_{0.7}} \right|} \quad (\text{B14})$$

Because relationship (B14) is used in the HS model for improving the elastic domain within the yield cone (i.e. the unloading-reloading domain), it needs an extension which accounts for (un- and re-) loading history. Such a strain history dependent, multi-axial extension of the modified Hardin-Drnevich relationship was proposed by Benz (2006) and implemented in PLAXIS. An example of a resulting small-strain stiffness reduction curve as applied in the HSsmall model is shown in Figure B.4.

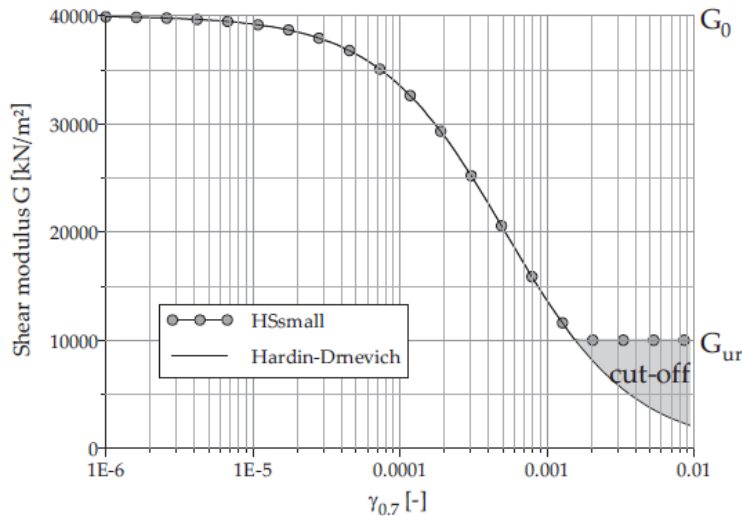


Figure B.4: Small-strain stiffness reduction curve with lower cut-off (Plaxis bv, 2014-3)

Because the curve reaches far into the plastic material domain, i.e. into the domain where stiffness degradation is accounted for through strain hardening, the curve has to be bounded. This results in the lower cut-off which can be seen in Figure B.4. This lower limit can be determined by conventional laboratory tests.

So the characteristic input parameters for HSsmall model are the three stiffness moduli (E_{50}^{ref} , $E_{\text{oed}}^{\text{ref}}$, $E_{\text{ur}}^{\text{ref}}$), initial shear modulus (G_0^{ref}), shear strain level $\gamma_{0,7}$, cohesion (c), friction angle (ϕ), dilatancy angle (ψ_{\max}) and power (m). A first estimation of the HSsmall parameters for quartz sand based on the relative density (RD) is given in (Brinkgreve *et al.*, 2010). It is noted that this paper is useful for translating the reference case soil setup into PLAXIS 2D material parameters.

B.3.1.5. Dynamics with the HSsmall model

It can be deduced from the above that the HSsmall model compared to the HS model has advanced features in the working load domain and therefore computes more reliable displacements. Another advancement of the HSsmall model becomes apparent when using the Dynamics module because it then also introduces hysteretic material damping to the model. The typical hysteretic behaviour that the HSsmall model shows under cyclic shear (i.e. seismic) loading is presented in Figure B.5: a loop in the shear stress-(cyclic) shear strain plane.

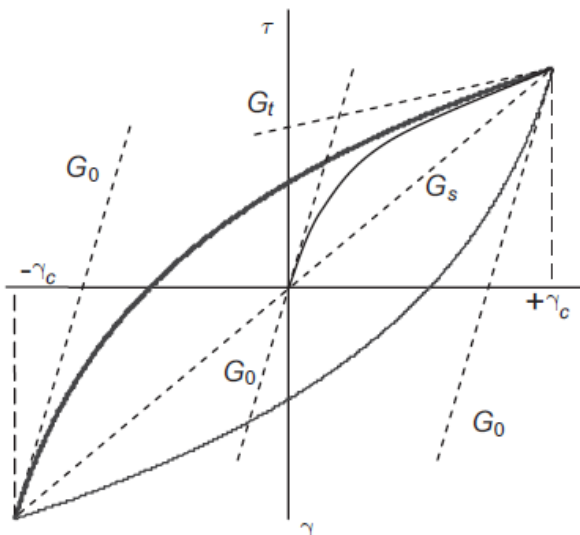


Figure B.5: Hysteretic behaviour in the HSsmall model (Brinkgreve *et al.*, 2007)

Starting from the small-strain shear stiffness (G_0), it can be seen in the figure that the actual stiffness will decrease with increasing shear strain (according to expression B14). Upon load reversal the stiffness will restart from G_0 and will decrease again until the next load reversal. The area within the closed loop is the equivalent of the energy dissipated during one load cycle (E_D). By dividing this by the energy stored (E_S) at maximum strain (γ_c) the local hysteretic damping ratio ξ can be obtained:

$$\xi = \frac{E_D}{4\pi E_S} \quad (B15)$$

This hysteretic damping is frequency independent because it is only derived from the stress-strain relationship in Figure B.5. Furthermore expression (B15) solely applies if the shear modulus decreases according to the small-strain reduction relationship. And in the same way that the small-strain reduction curve only applies until the cut-off, the damping ratio computed with (B15) only applies within this same elastic domain. As soon as G_{ur} is reached hysteretic damping does not further increase while subsequently increasing damping can be observed due to plasticity hardening.

In (Brinkgreve *et al.*, 2007) it is shown that PLAXIS HSsmall calculation results match expression (B15) well in case of constant load cycles. In case of free vibration PLAXIS outputs lower damping values than expression (B15) at low strain levels while at higher strain levels analytical and numerical results match reasonably well. From a comparison of PLAXIS results with empirical data it appears that to simulate damping even more realistically with the HSsmall model some viscous damping, which is strain-independent, should be added to account for a small amount of additional damping at small strain levels. In PLAXIS 2D this can be done by applying Rayleigh damping in the model. It is noted that Rayleigh damping cannot be used as an alternative for hysteretic damping though.

When specifying Rayleigh damping a damping matrix \mathbf{C} is composed by adding a portion (α_R) of the mass matrix \mathbf{M} and a portion (β_R) of the stiffness matrix \mathbf{K} . In formula:

$$\mathbf{C} = \alpha_R \mathbf{M} + \beta_R \mathbf{K} \quad (B16)$$

The parameters α_R [-] and β_R [-] are the so called Rayleigh coefficients which can be defined per material in PLAXIS. For the α_R -coefficient it holds that it determines the influence of the material mass in the damping of the system and that with increasing α_R , the lower frequencies are damped to a greater extent. For the β_R -coefficient it holds that it defines the influence of the material stiffness in the damping of the system and that with increasing β_R , the higher frequencies are damped to a greater extent. From the latter it can be seen that Rayleigh damping is frequency dependent. The relationship between damping ratio, frequency and Rayleigh coefficients:

$$\alpha_R + \beta_R \omega^2 = 2\omega\xi, \text{ with } \omega = 2\pi f \quad (B17)$$

In equation (B17) ω is the angular frequency [rad/s] and f the frequency [Hz]. Solving (B17) for two different target frequencies f_1 and f_2 , gives the following expressions:

$$\alpha_R = 2\omega_1\omega_2 \frac{\omega_1\xi_2 - \omega_2\xi_1}{\omega_1^2 - \omega_2^2} \quad (B18)$$

$$\beta_R = 2 \frac{\omega_1\xi_1 - \omega_2\xi_2}{\omega_1^2 - \omega_2^2} \quad (B19)$$

In PLAXIS 2D the target frequencies and damping ratio can be specified after which the Rayleigh coefficients are automatically calculated through equations (B18) and (B19). At the target frequencies the damping equals the

desired target damping (e.g. $\xi = 0.05$). Within the target frequency range the damping is lower than the target damping and outside the range the damping is higher than the target damping. An example of a resulting Rayleigh curve (for $\xi = 5\%$, $f_1 = 1.00$ Hz, and $f_2 = 10.00$ Hz) is shown in Figure B.6. The calculated values of the Rayleigh coefficients are in this case $\alpha_R = 0.5712$ and $\beta_R = 0.001447$.

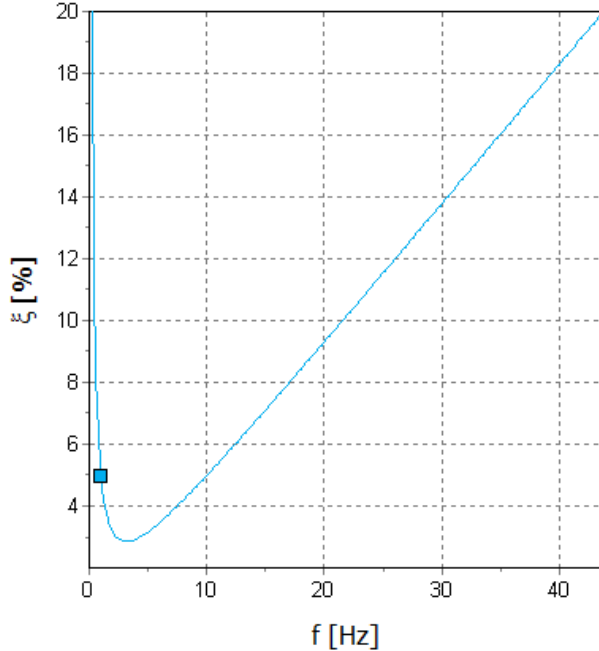


Figure B.6: Example Rayleigh damping curve in PLAXIS 2D

B.3.1.6. Dynamic boundary conditions

An important aspect in PLAXIS dynamic calculations (for any soil material model) concerns the dynamic boundary conditions. For static calculations standard fixities at the boundaries of the model are sufficient. For dynamic calculations other boundaries are required though in order to absorb incoming waves so that spurious reflection of these waves back into the model is prevented. The boundary condition options which are available in PLAXIS 2D:

- x-boundaries: None (standard fixities), Viscous, Free-field and Tied degrees of freedom
- y-boundaries: None (standard fixities), Viscous and Compliant base (only for y_{min})

The following elaborates specifically on the different dynamic boundary condition options.

Viscous

At the boundaries of the model viscous dampers are applied. These dampers absorb normal and shear stress components of incoming (seismic) waves. For a damper in x-direction it holds that:

$$\sigma_n = -C_1 \rho V_p \dot{u}_x \quad (B20)$$

$$\tau = -C_2 \rho V_s \dot{u}_y \quad (B21)$$

In equations (B20) and (B21), ρ [kg/m^3] is the density of the soil material and \dot{u}_x [m/s] and \dot{u}_y [m/s] are the (seismic) wave velocities in x- and y-direction respectively. V_p [m/s] and V_s [m/s] are the soil material's compression and shear wave velocities respectively. These are calculated with the following equations:

$$V_p = \sqrt{\frac{E_{oed}}{\rho}} \quad \text{where} \quad E_{oed} = \frac{(1-v)E}{(1+v)(1-2v)} \quad \text{and} \quad \rho = \frac{\gamma_{unsat}}{g} \quad (B22)$$

$$V_s = \sqrt{\frac{G}{\rho}} \quad \text{where} \quad G = \frac{E}{2(1+v)} \quad \text{and} \quad \rho = \frac{\gamma_{unsat}}{g} \quad (B23)$$

The coefficients C_1 [-] and C_2 [-] are the so-called relaxation coefficients. These parameters, which have to be specified by the user in PLAXIS 2D, are introduced in order to improve the absorption effect of the applied viscous boundaries. The default setting of the relaxation coefficients is $C_1 = C_2 = 1$, which means that no relaxation is taken into account. For pressure waves striking the boundaries perpendicular only, the default setting is applicable. For shear waves it holds that the damping effect of the viscous boundaries is not sufficient without relaxation. Particularly the adaption of C_2 improves the damping effect. Experience until now has learned that the setting $C_1 = 1$ and $C_2 = 0.25$ results in a reasonable absorption of shear waves to such an extent that it is considered sufficient for practical applications. Full absorption of shear waves is not possible though.

Free-field

Free-field boundary conditions, applicable at the x_{min} and x_{max} model boundaries, simulate the continuation of waves into the far field with only a small amount of reflection. It requires user-defined interface elements along the full length of the vertical model boundaries.

Compliant base

The compliant base boundary condition, applicable at the y_{min} model boundary, simulates the continuation of waves into the deep soil with only a small amount of reflection. It again requires user-defined interface elements along the full length of the lower horizontal modal boundary.

Tied degrees of freedom

With this special type of boundary the nodes at the x_{min} and x_{max} model boundaries will be connected so that the matching nodes will undergo exactly the same displacements. This boundary option is suitable for site-response analysis within a 1D shear column.

B.3.2. Structural elements

In this part the PLAXIS 2D structural elements, relevant for the present study, will be discussed. These are the node-to-node anchor, the 2D plate and the 2D embedded pile row. Again (Plaxis bv, 2014-3) is used as the main reference in this part.

B.3.2.1. Anchors

The behaviour of the 1D node-to-node anchor element in PLAXIS 2D is described by the following (elastic) relationship between axial force N [kN] and displacement, or elongation, Δx [m]:

$$N = \frac{EA}{l} \Delta x \quad (B24)$$

The axial anchor stiffness EA [kN] and anchor spacing l [m] have to be specified by the user. When considering elastoplastic material behaviour, tension ($F_{max,tens}$) and compression ($F_{max,comp}$) force boundaries must be inputted as well.

B.3.2.2. 2D Plates

The behaviour of the 2D Plate element in PLAXIS 2D is described by the following relationship between stresses (normal σ_N , out of plane σ_2 , shear τ) [kN/m^2] and strains (normal ϵ_N , out of plane ϵ_2 , shear γ) [-]:

$$\begin{bmatrix} \sigma_N \\ \sigma_2 \\ \tau \end{bmatrix} = \begin{bmatrix} \frac{2G}{(1-v)} & \frac{2G}{(1-v)} & 0 \\ \frac{2G}{(1-v)} & \frac{2G}{(1-v)} & 0 \\ 0 & 0 & k_s G \end{bmatrix} \begin{bmatrix} \varepsilon_N \\ \varepsilon_2 \\ \gamma \end{bmatrix} \quad (B25)$$

In equation (B25) the shear modulus G [kN/m^2] is, in case of isotropic material ($E_1 = E_2$), defined as:

$$G = \frac{E_1}{2(1+v)} \quad (B26)$$

The corresponding relationships between structural forces (normal N , out of plane H , shear Q) [kN/m] and strains:

$$N = EA_1 \varepsilon_N \quad (B27)$$

$$H = EA_2 \varepsilon_2 \quad (B28)$$

$$Q = \frac{k_s EA}{2(1+v)} \gamma^* \quad (B29)$$

$$M = EI \kappa \quad (B30)$$

Concerning the elastic behaviour, the normal stiffness EA_1 [kN/m], out of plane stiffness EA_2 ($=EA_1$ when isotropic) [kN/m], bending stiffness EI [kNm^2/m] and Poisson's ratio v [-] are to be specified by the user. In case of sheet pile walls (relatively flexible in the out of plane direction) it is advised to set v to zero. The shear correction factor k_s [-] in (B25) and (B29) is by default set to 5/6, which implies that the shear stiffness is determined from the assumption that the plate has a rectangular cross-section. This will be correct when modelling a solid wall but for e.g. a sheet pile wall the computed shear deformation may be too large. The validity of the default k -value can be tested by checking if d_{eq} ($=\sqrt{12EI/EA}$) $\leq L_{plate}/10$ to ensure negligible shear deformations. The modified shear strain γ^* is computed from the shear strain γ and "some additional terms" so that the calculation result is more accurate.

Concerning plastic behaviour, the maximum (plastic) bending moment M_p [kNm/m] and maximum (plastic) normal force N_p [kN/m] must be specified by the user as well. In case of dynamic calculations Rayleigh damping can be defined for the structural material in the same way as for the soil material.

B.3.2.3. 2D Embedded Pile Rows

An embedded pile in PLAXIS 2D consists of plate elements with embedded interface elements. The function of the embedded interface elements (springs) is to describe the interaction of the pile skin and pile foot with the soil. The 2D embedded pile row is e.g. used for modelling a grout body at the end of a ground anchor. Caution is required though. It is only possible with this element to estimate the stress distribution, the deformation and the stability of the structure on a global level, assuming that the grout body does not slip relative to the soil. With this model it is certainly not possible to evaluate the pull-out force of a ground anchor (which is associated with a complex 3D problem). So it is not advisable to use these elements in a situation where an anchored sheet pile wall is loaded up to failure, as is the case in the present study.

Appendix C: D-SHEET PILING reports

C.1. CASE-000

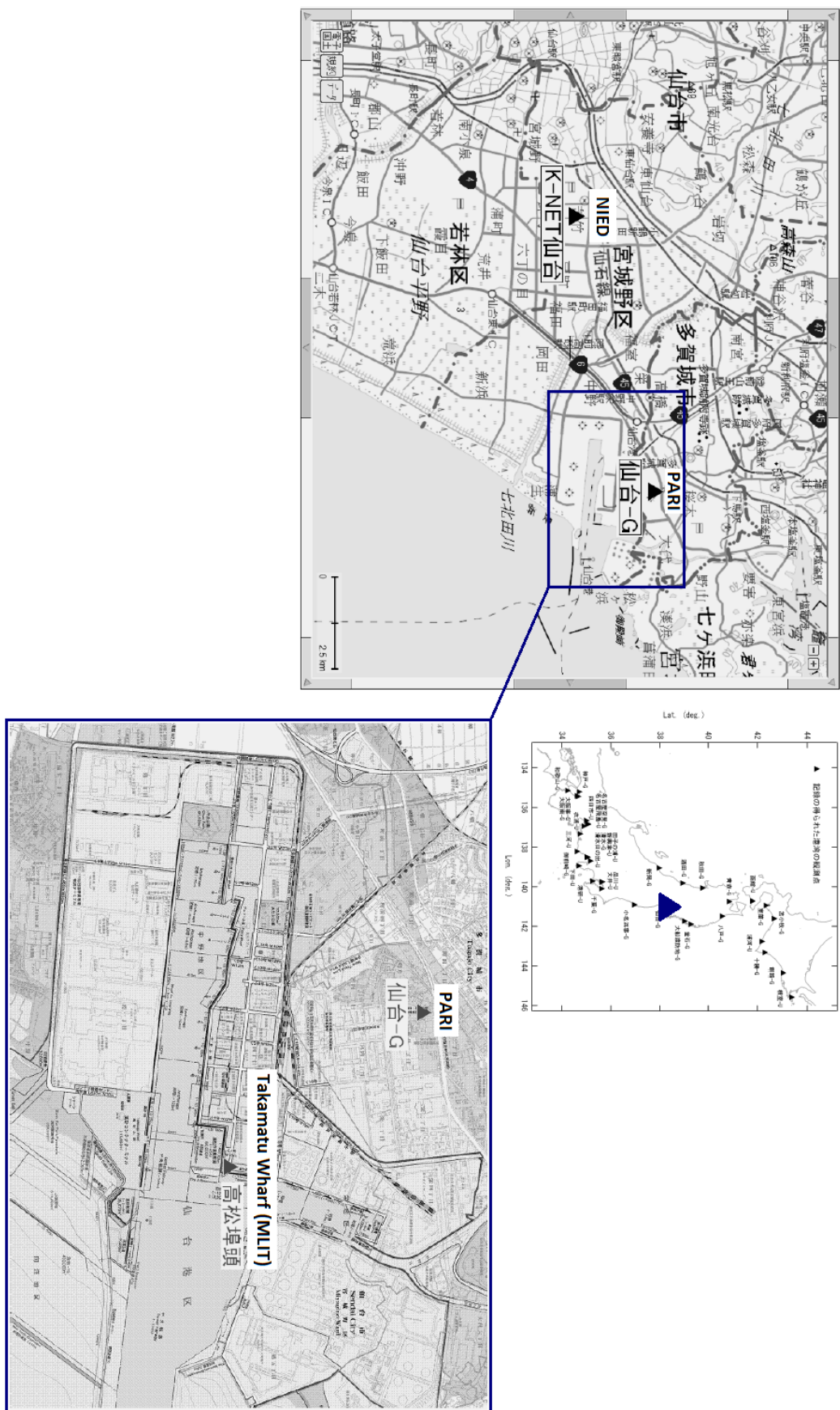
C.2. CASE-100

C.3. CASE-200

C.4. CASE-300

C.5. CASE-600

Appendix D: Earthquake recorders at Port of Sendai



Appendix E: Expressions in the limit-equilibrium model

The expressions of the forces in the newly derived limit equilibrium model and corresponding seismic translation mechanism of paragraph 5.2.2 (see Figure E.1) are listed in this appendix.

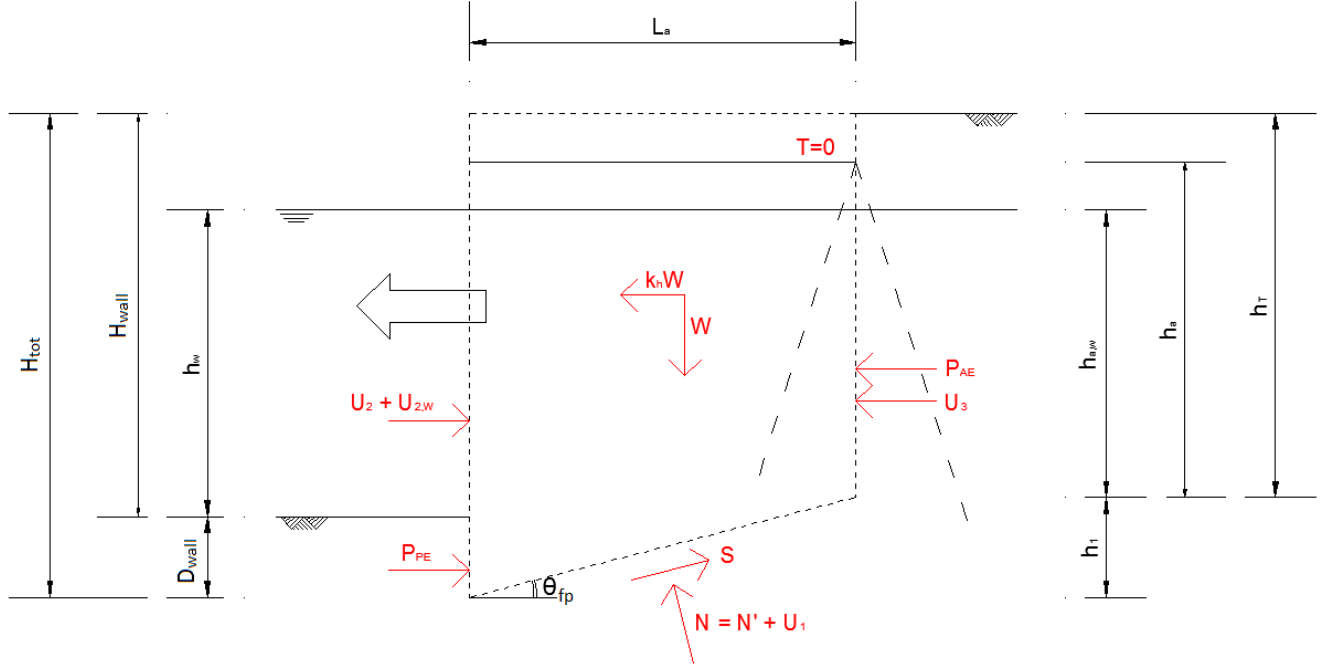


Figure E.1: Seismic translation failure mechanism of anchored sheet pile quay wall with batter pile anchor - based on Kranz (1953) and Towhata & Islam (1987) limit equilibrium models

Effective component of normal force in the failure plane beneath the sliding mass

$$N' = [\gamma_{dry}(H - h_w)L_a + \gamma_b(h_{a,w}L_a + 0.5h_1L_a)]/\cos\theta \quad (E1)$$

Dynamic active soil thrust behind the vertical failure plane

$$P_{AE} = 0.5\gamma_{av}h_T^2 * K_{AE} \quad (E2)$$

Dynamic passive soil thrust in front of the sheet pile

$$P_{PE} = 0.5\gamma_bD^2 * K_{PE} \quad (E3)$$

Shear force along the failure plane beneath the sliding mass

$$S = N'\tan\phi \quad (E4)$$

Limit equilibrium force in anchor tie

$$T = 0 \quad (E5)$$

Hydrostatic force 1, in the failure plane beneath the sliding mass

$$U_1 = \gamma_w[h_1(h_a + 0.5h_1)]/\sin\theta \quad (E6)$$

Hydrostatic force 2, in front of the sheet pile

$$U_2 = 0.5\gamma_w(h_w + D)^2 \quad (E7)$$

Westergaard hydrodynamic force over the water depth in front of the sheet pile

$$U_{2,w} = -\frac{7}{12}\gamma_w h_w^2 k_h \quad (\text{E8})$$

Hydrostatic force 3, behind the vertical failure plane

$$U_3 = 0.5\gamma_w h_a^2 \quad (\text{E9})$$

Weight of sliding soil body

$$W = \gamma_{\text{dry}}(H - h_w)L_a + \gamma_{\text{sat}}(h_{a,w}L_a + 0.5h_1L_a) \quad (\text{E10})$$

Yield or critical seismic coefficient iteratively computed from horizontal and vertical equilibrium

$$k_{cr} = \frac{P_{PE} + U_2 + U_{2,w} + S \cos \theta - U_1 \sin \theta - N' \sin \theta - P_{AE} - U_3}{U_1 \cos \theta + N' \cos \theta + S \sin \theta} \quad (\text{E11})$$

The above force expressions of the limit equilibrium contain a number of symbols which are listed below:

- γ_{av} = average unit weight over height $h(T)$ [kN/m^3]
- γ_b = buoyant unit weight of soil [kN/m^3]
- γ_{dry} = dry unit weight of the soil [kN/m^3]
- γ_{sat} = saturated unit weight of the soil [kN/m^3]
- γ_w = unit weight water [kN/m^3]
- θ_{fp} = inclination angle of the lower failure plane with respect to the horizontal [°]
- φ = internal friction angle of the soil [°]
- D_{wall} = embedment depth of sheet pile wall [m]
- H_{wall} = retaining height [m]
- h_a = height schematized anchor pile [m]
- $h_{a,w}$ = height water table with respect to toe of anchor pile [m]
- h_T = height vertical failure plane [m]
- h_w = water depth in front of the sheet pile wall [m]
- h_1 = vertical height of the lower failure plane [m]
- k_h = horizontal seismic coefficient [-]
- K_{AE} = active soil pressure coefficient obtained with M-O methodology [-]
- K_{AE} = passive soil pressure coefficient obtained with M-O methodology [-]
- H_{tot} = total height of sheet pile wall [m]
- L_a = length anchor tie, i.e. length of sliding soil body [m]

Appendix F: SHAKE2000 input files

F.1. PARI Sendai-G column

SHAKE2000 - Input File Information

Option 1 - Dynamic Soil Properties at Sendai-G

```

1
2
9   Sand Avg.   G/Gmax - SAND, Average (Seed & Idriss 1970)
.0001   .0003   .001   .003   .01   .03   .1   .3
1
1   .98   .95   .89   .73   .52   .29   .14
.06
9   Sand Avg.   Damping for SAND, Average (Seed & Idriss 1970)
.0001   .0003   .001   .003   .01   .03   .1   .3
1
.5   .8   1.7   3.45   6.5   10.7   16.5   21.9
25.7
10  EPRI Rock 2 G/Gmax for Rock - 21 to 50 feet (EPRI, 1993)
.0001   .000316   .001   .00316   .0101   .0316   .1   .316
1   3.16
1   1   1   1   .92   .75   .48   .255
.105   .035
10  EPRI Rock 2 Damping for Rock - 21 to 50 feet (EPRI, 1993)
.0001   .000316   .001   .00316   .0101   .0316   .1   .316
1   3.16
3   3.43   3.865   5.25   8.75   13.75   20.25   26
30.25   32.25
2   1   2

```

Option 2 - Column 1 - Sendai-G

```

2
1   7   Sendai-G           9.842
1   1   3.2808   .05   .111   427
2   1   3.2808   .05   .111   427
3   1   3.2808   .05   .111   427
4   1   3.2808   .05   .118   591
5   1   3.2808   .05   .118   591
6   1   4.9212   .05   .118   591
7   2                   .02   .153   2690

```

Option 3 - Representative Motion

```

3
6000 8192   .01   (8F9.6)   F2660NS
C:\Users\906148\Desktop\Graduation Thesis\Phase 3 - Research Part 2\SHAKE2000\PARI-
F2660SMA-North-SHAKE.eq
1   25   4   8

```

Option 4 - Input Motion at Layer 1

```

4
1   1

```

Option 5 - Number of Iterations: 10 - Strain Ratio: 0.59 - Mw: 6.9

```

5
10   .59

```

Option 6 - Column 1 - Layers 1 to 7

```

6
1   2   3   4   5   6   7
0   1   1   1   1   1   1
1   1   1   1   1   1   1

```

Option 7 - Stress & Strain Time Histories for Layer 2

```

7
2   1   1   2048   Stress History Layer No.2

```

```

2   0   1      2048      Strain History Layer No. 2

Option 7 - Stress & Strain Time Histories for Layer 4
7
4   1   1      2048      Stress History Layer No.4
4   0   1      2048      Strain History Layer No.4

Option 7 - Stress & Strain Time Histories for Layer 6
7
6   1   1      2048      Stress History Layer No.6
6   0   1      2048      Strain History Layer No.6

Option 9 - Response Spectrum at Surface
9
1   0
6   0      32.2
.01     .025      .05       .1        .15       .2

Option 9 - Response Spectrum at Layer 6
9
6   1
6   0      32.2
.01     .025      .05       .1        .15       .2

Option 10 - Amplification Spectrum - Layers 7-1
10
7   1   1   0      .125Amplification Layers 7-1

Option 11 - Fourier Spectrum at Layers 1 & 7
11
1   0   2   3 2048
7   1   2   3 2048

```

Execution will stop when program encounters 0
0

F.2. Reference case column

SHAKE2000 - Input File Information

```

Option 1 - Dynamic Soil Properties Set No. 1
1
2
9   Sand CASE   G/Gmax - SAND, Average (Seed & Idriss 1970)
.0001    .0003    .001    .003    .01    .03    .1    .3
1
1   .98      .95      .89      .73      .52      .29      .14
.06
9   Sand CASE   Damping for SAND, Average (Seed & Idriss 1970)
.0001    .0003    .001    .003    .01    .03    .1    .3
1
.5   .8       1.7      3.45      6.5      10.7     16.5     21.9
25.7
10  B-Rock CASE G/Gmax for Rock - 51 to 120 feet (EPRI, 1993)
.0001    .000316   .001    .00316   .0101    .0316   .1    .316
1
1   3.16
1
.08   .03
10  B-Rock CASE Damping for Rock - 51 to 120 feet (EPRI, 1993)
.0001    .000316   .001    .00316   .0101    .0316   .1    .316
1
3   3.16
3
3   3.36      3.73      5       8       12.5     19      24.75
29.5   32
2   1   2

```

Option 2 - Column 1 - CASE

2	15	Case Study Soil Profile	9.842		
1	1	3.2808	.05	.127	820
2	1	3.2808	.05	.127	820
3	1	3.2808	.05	.127	820
4	1	3.2808	.05	.14	820
5	1	3.2808	.05	.14	820
6	1	3.2808	.05	.14	820
7	1	3.2808	.05	.14	820
8	1	3.2808	.05	.14	820
9	1	3.2808	.05	.14	820
10	1	3.2808	.05	.14	820
11	1	6.5616	.05	.14	820
12	1	8.202	.05	.14	820
13	1	8.202	.05	.14	820
14	1	8.202	.05	.14	820
15	2		.02	.153	2690

Option 3 - Motion: Bedrock Motion

3	819216384	.01	(8F15.6)	F2660NS
C:\Users\906148\Desktop\Graduation Thesis\Phase 3 - Research Part	2\SHAKE2000\Output\Sendai-Gmul-L7A1D1-7-Sendai-G-F2660NS.ahl			
1		25	3	8

Option 4 - Input Motion at Layer 15

4	15	1
---	----	---

Option 5 - Number of Iterations: 10 - Strain Ratio: 0.59 - Mw: 6.9

5	10	.59
---	----	-----

Option 6 - Column 1 - Short Course - Layers 1 to 15

6	1	2	3	4	5	6	7	8	9	10	11	12	13	14	15
0	1	1	1	1	1	1	1	1	1	1	1	1	1	1	1
1	1	1	1	1	1	1	1	1	1	1	1	1	1	1	1

Option 7 - Stress & Strain Time Histories for Layer 3

7	3	1	1	6000	Stress History Layer No.3
3	0	1	6000	Strain History Layer No.3	

Option 7 - Stress & Strain Time Histories for Layer 6

7	6	1	1	6000	Stress History Layer No.6
6	0	1	6000	Strain History Layer No.6	

Option 7 - Stress & Strain Time Histories for Layer 9

7	9	1	1	6000	Stress History Layer No.9
9	0	1	6000	Strain History Layer No.9	

Option 7 - Stress & Strain Time Histories for Layer 12

7	12	1	1	6000	Stress History at Layer No.12
12	0	1	6000	Strain History at Layer No.12	

Option 9 - Response Spectrum at Surface - Damping 1, 2.5, 5, 10, 15, 20%

9	1	0			
6	0	32.2			
.01	.025	.05	.1	.15	.2

Option 9 - Response Spectrum at Layer No.7 - Damping 1, 2.5, 5, 10, 15, 20%

9						
7	1					
6	0	32.2				
.01		.025	.05	.1	.15	.2

Option 10 - Amplification Spectrum - Layers 15-1

10						
15	1	1	0	.125	Amplification	spectrum 15-1

Option 10 - Amplification Spectrum - Layers 15-7

10						
15	1	7	1	.125	Amplification	Spectrum Layers 15-7

Option 11 - Fourier Spectrum at Layers 1 & 5

11						
1	0	2	3	2048		
5	1	2	3	2048		

Option 11 - Fourier Spectrum at Layers 10 & 15

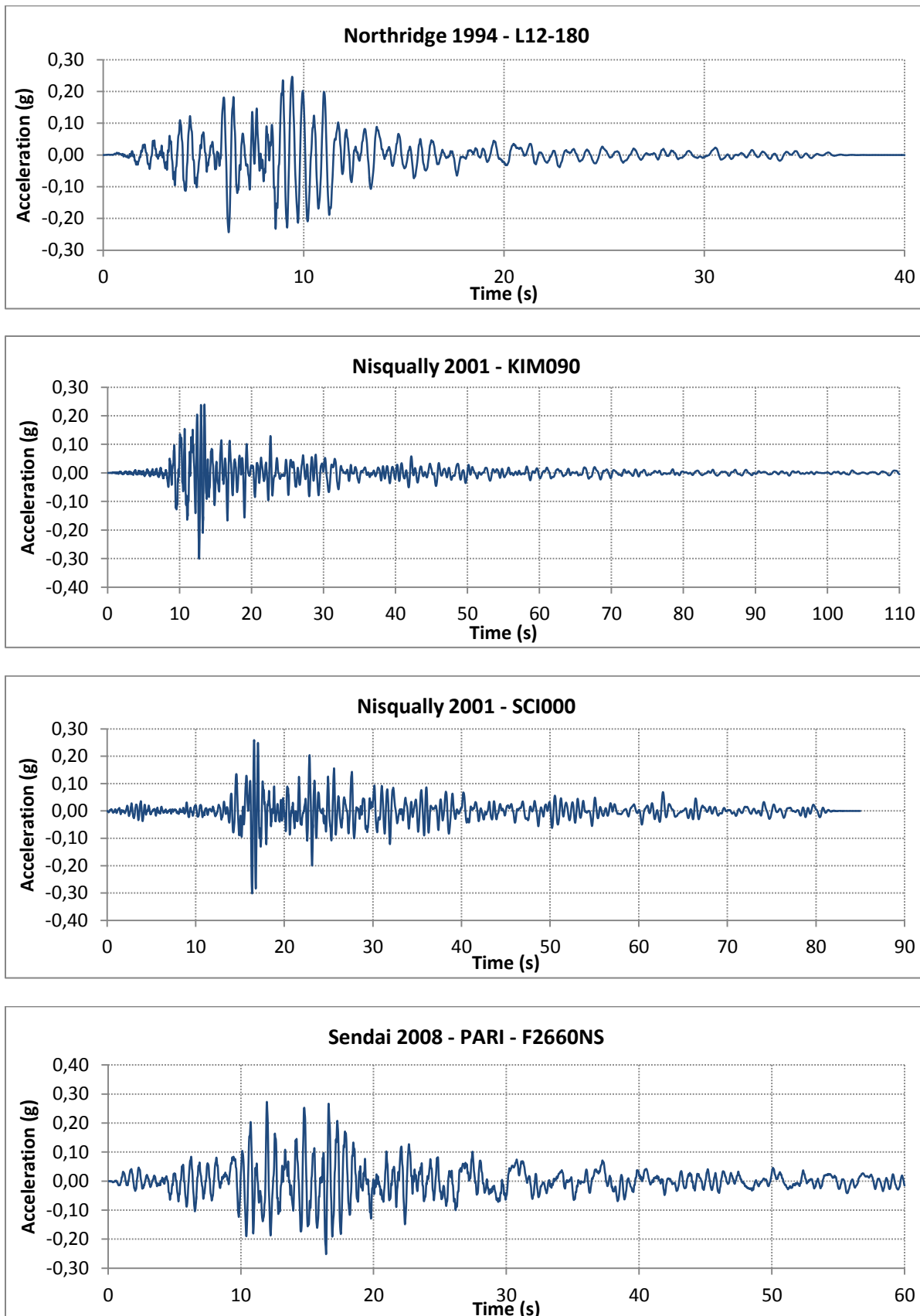
11						
10	1	2	3	2048		
15	1	2	3	2048		

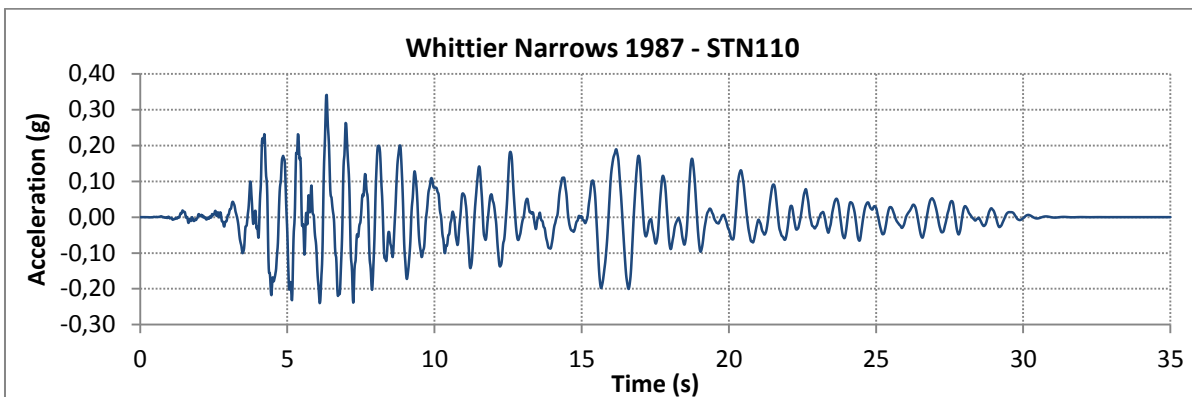
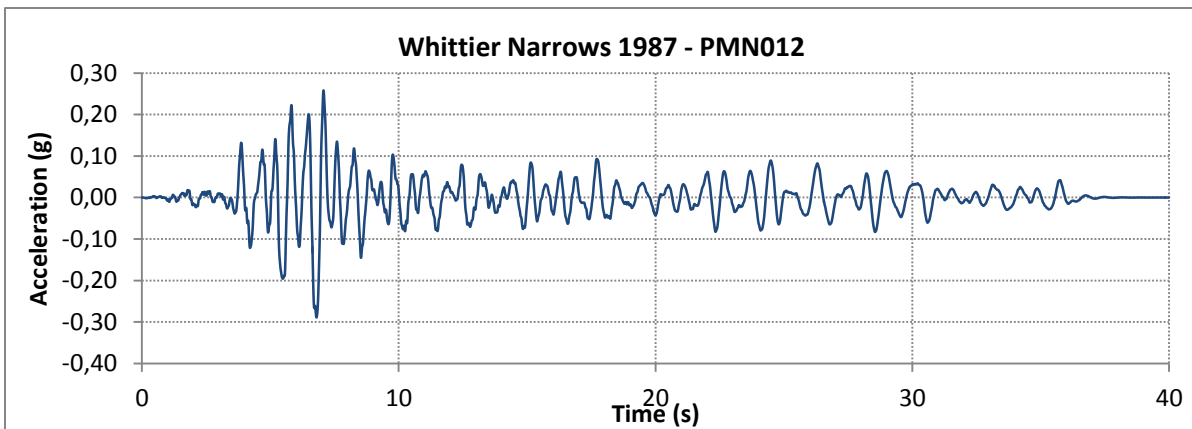
Execution will stop when program encounters 0

0

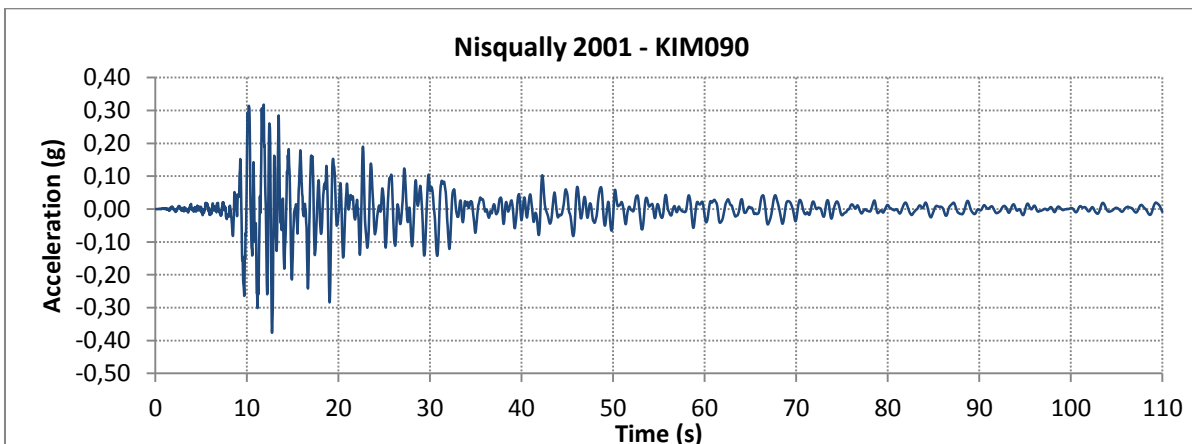
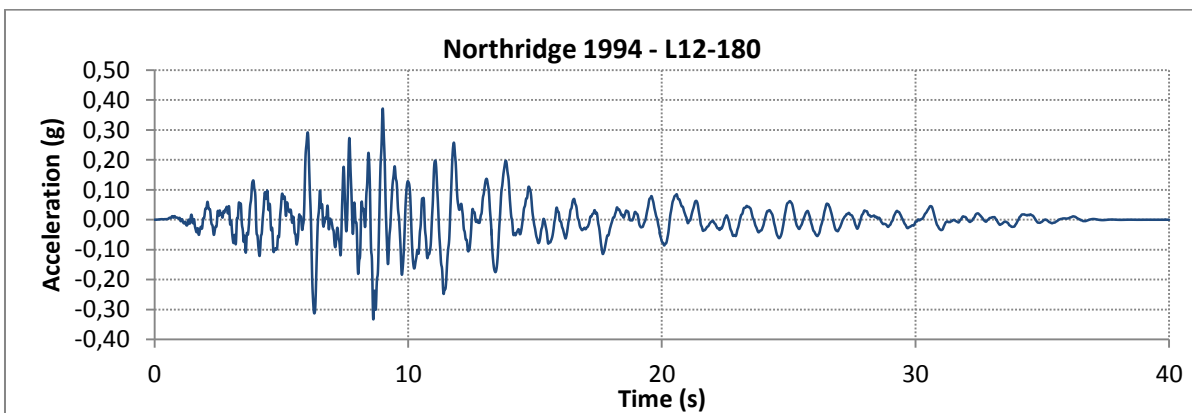
Appendix G: SHAKE2000 site-response analysis results (SLAMMER input)

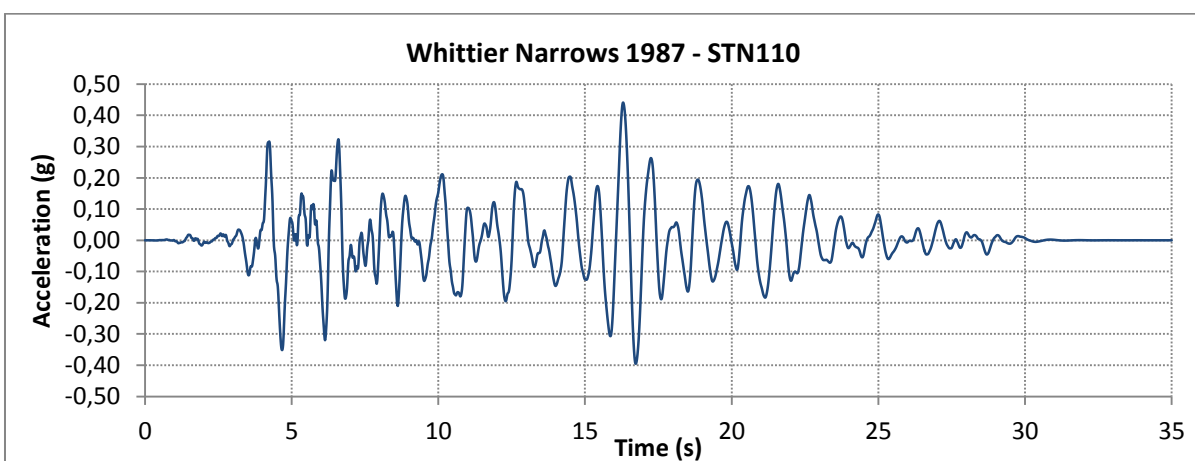
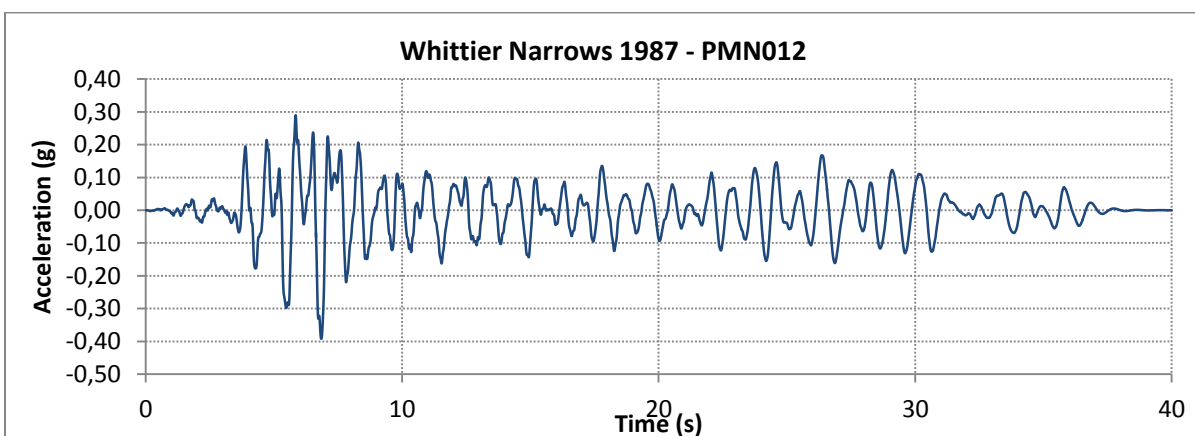
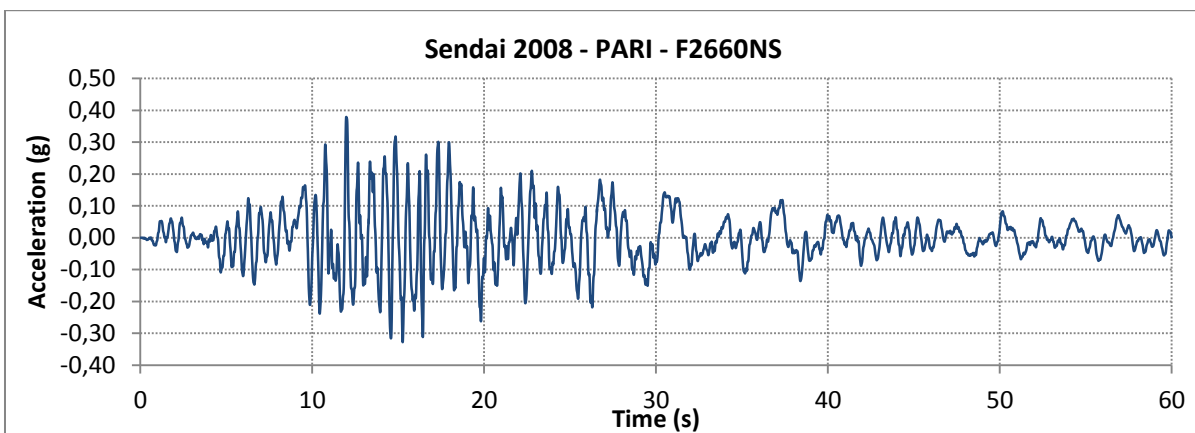
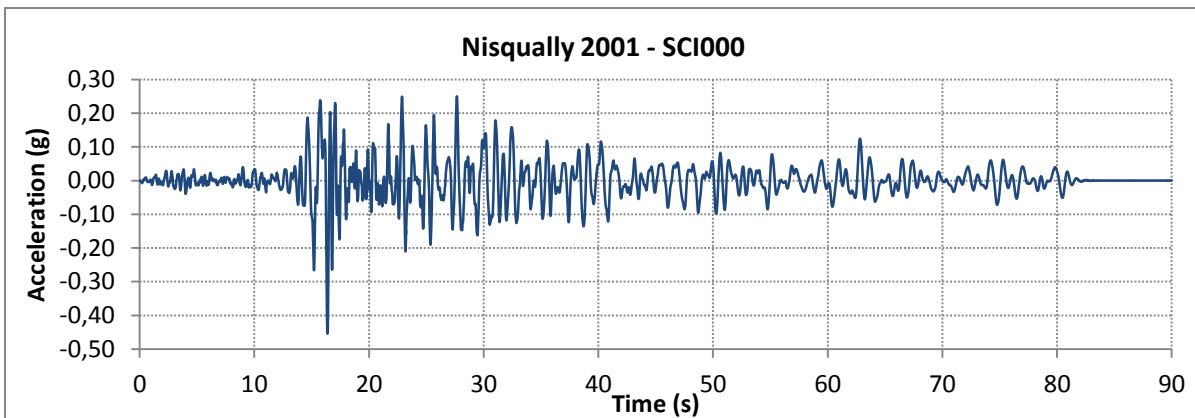
G.1. CASE300 - Ground motions at centre of gravity of soil-structure system





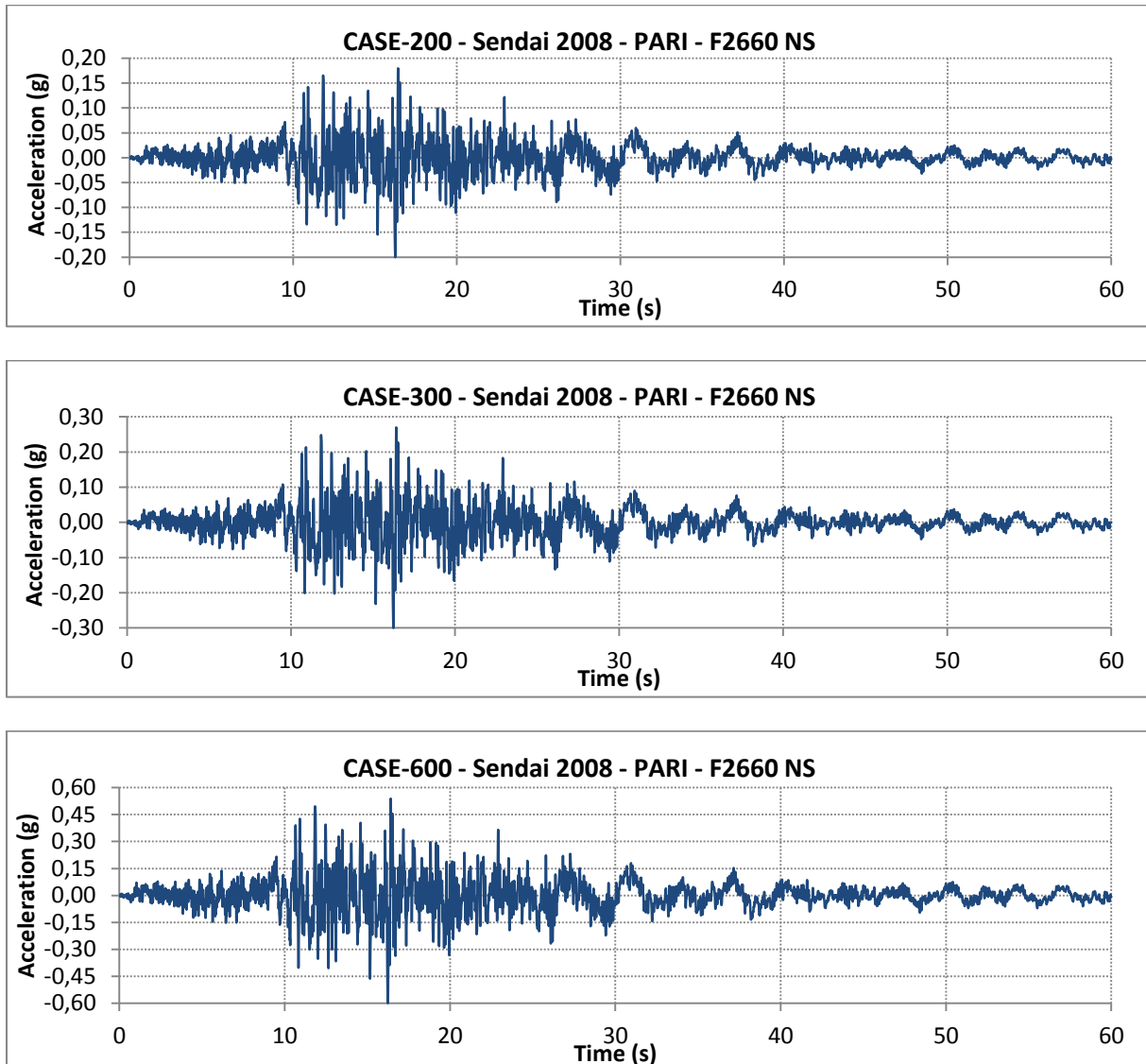
G.2. CASE600 - Ground motions at centre of gravity of soil-structure system





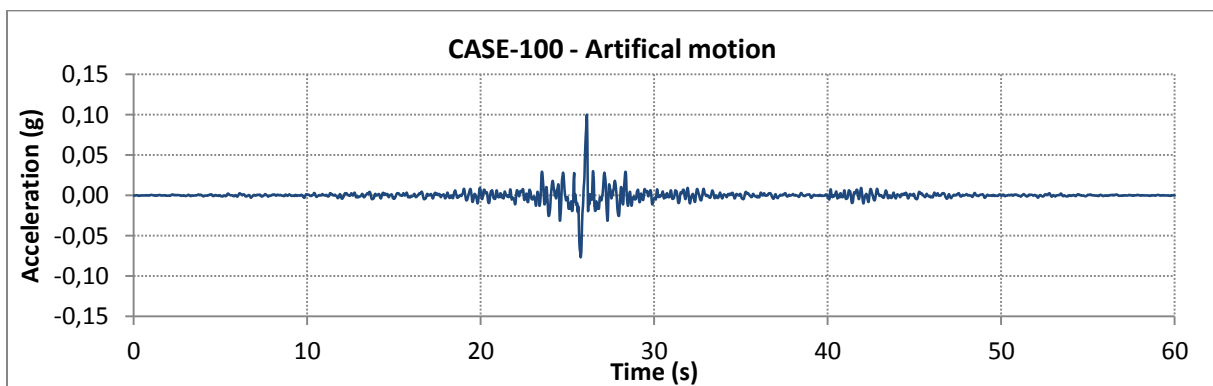
Appendix H: PLAXIS 2D input motions at bedrock level

H.1. Site-response analysis

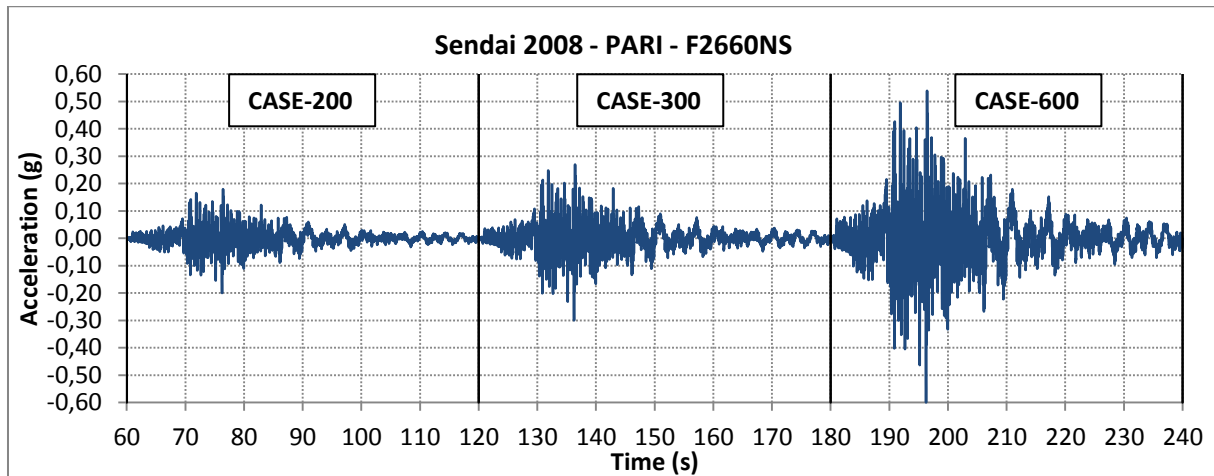


H.2. Dynamic calculations

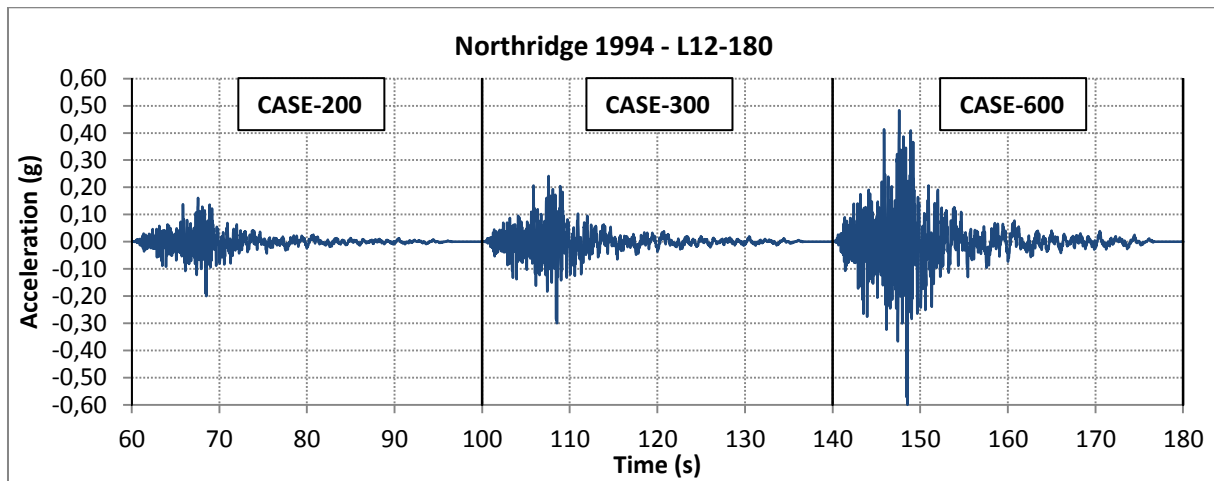
H.2.1. CASE-100: Artificial motion



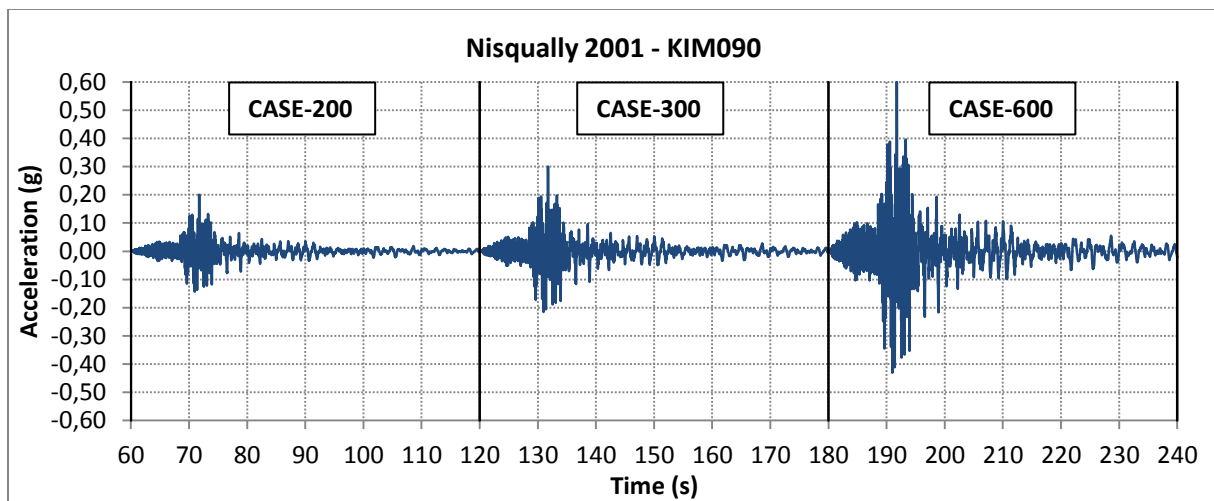
H.2.2. CASE-200, CASE-300 and CASE-600: Recorded motion - S2008-PARI-F2660NS



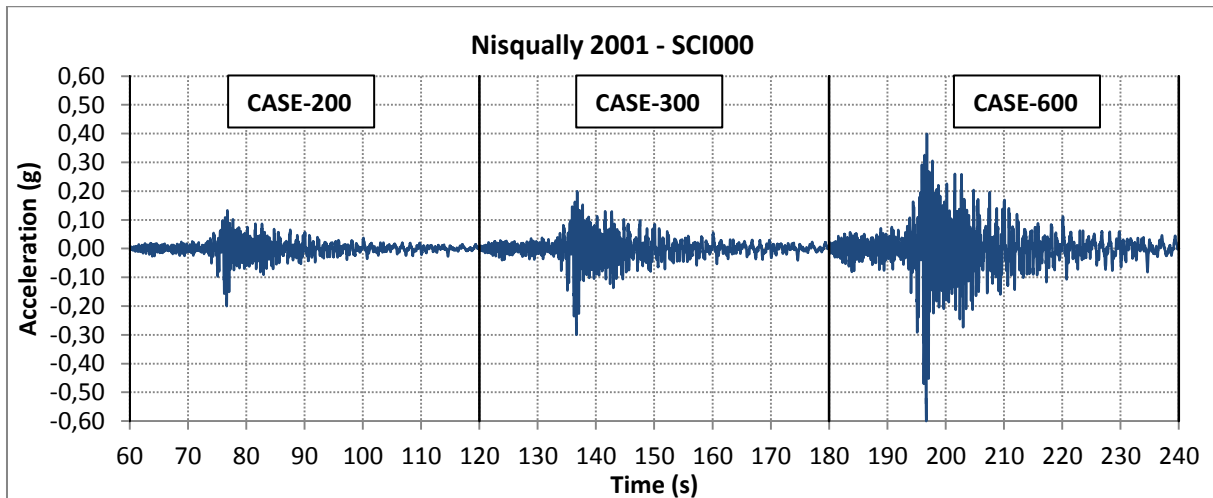
H.2.3. CASE-200, CASE-300 and CASE-600: Recorded motion – N1994-L12-180



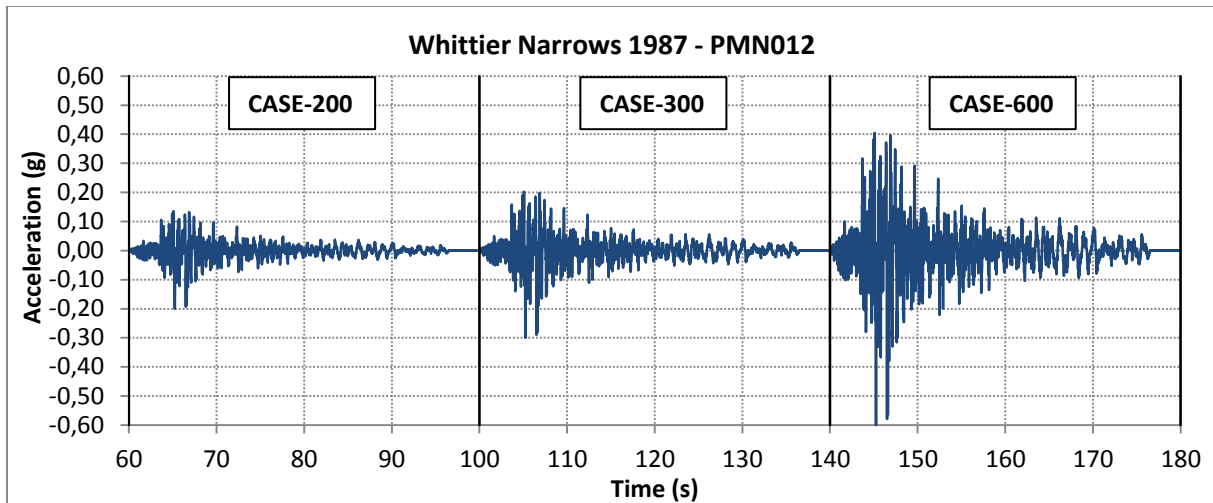
H.2.4. CASE-200, CASE-300 and CASE-600: Recorded motion - N2001-KIM090



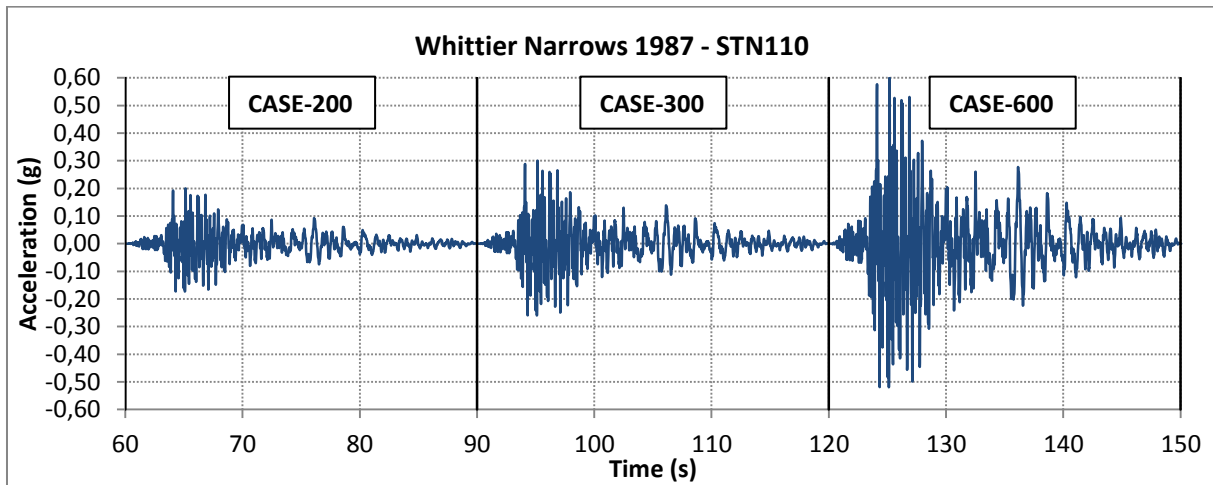
H.2.5. CASE-200, CASE-300 and CASE-600: Recorded motion - N2001-SCI000



H.2.6. CASE-200, CASE-300 and CASE-600: Recorded motion - WN1987-PMN012



H.2.7. CASE-200, CASE-300 and CASE-600: Recorded motion - WN1987-STN110



Appendix I: Lists of figures and tables

I.1. List of figures

Figure 2.1: Types of plate boundaries (Kramer, 1996).....	2
Figure 2.2: Fault types, adapted from (ASCE, 1998)	3
Figure 2.3: Orientation earthquake magnitudes and faults (red lines) experiencing differential compaction at the location of the Groningen gas field (grey marking), adapted from (TNO, 2009).....	3
Figure 2.4: Body waves: p-waves (top) and s-waves (bottom), adapted from (Kramer, 1996)	4
Figure 2.5: Surface waves: Rayleigh waves (top) and Love waves (bottom), adapted from (Kramer, 1996)	5
Figure 2.6: Overview seismic hazards affecting port structures, adapted from (PIANC, 2001).....	6
Figure 2.7: Accelerogram associated with tectonic activity and corresponding PGA (from lecture at DUT by Deltares, 2014).....	6
Figure 2.8: Schematic of (one dimensional) site-response analysis, adapted from (USACE, 1999).....	7
Figure 2.9: Typical quay wall structures, adapted from (PIANC, 2001) and (de Gijt, 2004).....	9
Figure 2.10: Typical failure modes of gravity-based quay walls, adapted from (ASCE, 1998) and (PIANC, 2001)	10
Figure 2.11: Typical failure modes of sheet pile quay walls, adapted from (EERI, 1993) and (PIANC, 2001)	10
Figure 2.12: Typical failure modes of pile-deck structures, adapted from (ASCE, 1998) and (PIANC, 2001).....	11
Figure 2.13: Example flowchart Performance-Based Design Methodology, adapted from (PIANC, 2001)	12
Figure 2.14: Example design requirements for pile-supported piers and wharves (ASCE 2013).....	14
Figure 2.15: Preferred yield sequence of an anchored sheet pile wall (PIANC 2001, Visone 2008)	15
Figure 2.16: Preferred yield sequence of a pile-deck structure (PIANC, 2001).....	16
Figure 2.17: Displacement reduction factors according to NEN-EN1998-5 ^{iii, iv, v}	19
Figure 2.18: The elastic response spectrum obtained by plotting the spectral accelerations against the periods of vibrations of the SDOF system (Kramer, 1996)	20
Figure 2.19: Elastic response spectra for different soil classifications according to NEN-EN1998-1	20
Figure 2.20: Newmark analysis procedure, adapted from (Jibson, 2011)	21
Figure 2.21: Pushover curve and plastic hinge sequence of a pile-deck structure (POLB, 2009)	22
Figure 2.22: Bilinear capacity spectrum and response spectra plot for determining structural performance, adapted from (RHDHV, 2014)	23
Figure 2.23: The principle of uncoupled DA accounting for SSI (USACE, 2007)	24
Figure 3.1: Typical limit design PGA's corresponding to different quay structure types (derived from conversations with D.J. Peters and A. Wiggers of RHDHV)	26
Figure 3.2: Flowchart of the research methodology.....	28
Figure 4.1: Step 1 of the research methodology: selecting a reference case	31
Figure 4.2: Conceptual overview of the single anchored sheet pile quay wall model, showing both field and centrifuge (scale) model geometry, adapted from (Higuchi <i>et al.</i> , 2012).....	32
Figure 4.3: Photo of the centrifuge model during preparation, adapted from (Higuchi <i>et al.</i> , 2012)	33
Figure 4.4: Outline centrifuge testing procedure (Higuchi <i>et al.</i> , 2012)	33
Figure 4.5: Input motions: artificial accelerogram (top) and 2008 Iwate-Miyagi inland earthquake record (bottom), adapted from (Higuchi <i>et al.</i> , 2012).....	34
Figure 4.6: Measured bending moments in the sheet pile per load case (field model values), from (Higuchi <i>et al.</i> , 2012)	35
Figure 4.7: Push-up of soil wedge due to wall displacement after passive failure (applying conservation of soil mass)	36
Figure 5.1: Step 2 of the research methodology: calibrated simplified analysis	37
Figure 5.2: Layout of the D-SHEET PILING model.....	40
Figure 5.3: Fit of calculated structural forces with CASE-000 measurements after static calibration of the D-SHEET PILING model.....	42
Figure 5.4: Computed active failure plane angles (α_{AE}) and corresponding Coulomb and M-O failure planes	45

Figure 5.5: Bending moment line fits between D-SHEET PILING pseudo-static results and reference seismic load cases	46
Figure 5.6: Shear force line fits between D-SHEET PILING pseudo-static results and reference seismic load cases	47
Figure 5.7: Resulting soil stress fits between D-SHEET PILING pseudo-static results and reference seismic load cases	48
Figure 5.8: Step 3 of the research methodology: calibrated simplified dynamic analysis	49
Figure 5.9: Towhata & Islam (1987) and Kranz (1953) limit equilibrium models corresponding to sliding along assumed failure planes, adapted from (Towhata & Islam 1987) and (CUR 166) respectively	50
Figure 5.10: Seismic translation failure mechanism of anchored sheet pile quay wall with batter pile anchor - based on Kranz (1953) and Towhata & Islam (1987) limit equilibrium models	51
Figure 5.11: Sub-equilibria of forces in the limit-equilibrium model in order to compute shear forces in sheet pile wall	52
Figure 5.12: Shear force line (left) and bending moment line (right) computed with the limit-equilibrium model and compared with CASE-300 measurements	53
Figure 5.13: SHAKE2000 site-response analysis procedure	54
Figure 5.14: Dynamic soil properties: G/G_{\max} and Damping curves for average sand (Seed & Idriss, 1970), 20-50ft rock (EPRI, 1993) and 51-120ft rock (EPRI, 1993) respectively	54
Figure 5.15: Accelerogram N-S component of the PARI F2660 motion, recorded at Port of Sendai in 2008	55
Figure 5.16: Acceleration spectra of earthquake motions at ground level, compared to the PARI-F2660NS ground motion	55
Figure 5.17: Centre of gravity of the schematized failure wedge (sliding mass) of the anchored sheet pile quay wall	56
Figure 5.18: Site-response (peak acceleration vs depth) for the S2008-PARI-F2660 record, computed with SHAKE2000	57
Figure 5.19: Step 4 of the research methodology: calibrated dynamic analysis	62
Figure 5.20: Layout PLAXIS 2D model	63
Figure 5.21: Bending moment and shear force line fits between PLAXIS 2D and reference case results	65
Figure 5.22: Failure plane (incremental deviatoric strain $\Delta\gamma_s$) corresponding to the pseudo-static critical acceleration and the soil parameter setup for a relative density of 80%	66
Figure 5.23: Failure plane (incremental deviatoric strain $\Delta\gamma_s$) corresponding to the pseudo-static critical acceleration and the soil parameter setup for a relative density of 100%	67
Figure 5.24: Linearly increasing acceleration signals applied in pseudo-dynamic analysis	67
Figure 5.25: Failure plane (horizontal accelerations in g's) corresponding to the pseudo-dynamic critical acceleration and the soil parameter setup for a relative density of 80%	68
Figure 5.26: Failure plane (horizontal accelerations in g's) corresponding to the pseudo-dynamic critical acceleration and the soil parameter setup for a relative density of 100%	68
Figure 5.27: 1D soil column model in PLAXIS 2D for site-response analysis	69
Figure 5.28: PLAXIS 2D site-response analysis result for the CASE-200 event, compared with SHAKE2000 result	71
Figure 5.29: PLAXIS 2D site-response analysis result for the CASE-300 event, compared with SHAKE2000 result	72
Figure 5.30: PLAXIS 2D site-response analysis result for the CASE-600 event, compared with SHAKE2000 result	73
Figure 5.31: PLAXIS 2D bending moment and shear force line results for CASE-100, compared to reference case results	75
Figure 5.32: PLAXIS 2D bending moment and shear force line results for CASE-200, compared to reference case results	76
Figure 5.33: PLAXIS 2D bending moment and shear force line results for CASE-300, compared to reference case results	77

Figure 5.34: PLAXIS 2D bending moment and shear force line results for CASE-600, compared to reference case results.....	78
Figure 5.35: PLAXIS 2D dynamic displacement results, compared to reference case results.....	79
Figure 5.36: PLAXIS 2D dynamic displacement results: Example of horizontal displacement contours for the CASE-300 S2008-PARI-F2660NS motion	80
Figure 6.1: Step 5 of the research methodology: evaluation of the analysis results	82
Figure 6.2: Pseudo-static model.....	83
Figure 6.3: Limit-equilibrium model.....	85
Figure 6.4: Finite element model	86
Figure 6.5: Larger push-up of seabed at sliding of sheet pile due to presence of steel container – a combination of a lower bound failure mechanism (strut - left side) and upper bound failure mechanism (plastic failure plane - right side)	87
Figure 6.6: Accuracy according to ISO 5725-1:1994: a combination of ‘trueness’ and ‘precision’	89
Figure 6.7: Relationship between permanent displacement and observed damage of anchored sheet pile walls, adapted from (Kitajima & Uwabe, 1979), linked to earthquake levels from PBD methodology and reference case performance	90
Figure 6.8: Findings from literature and the present study: horizontal displacement at top of sheet pile versus damage.....	91
Figure A.1: Applied symbols in soil pressure theories, adapted from (Visone, 2008)	102
Figure A.2: Coulomb and log spiral type failure surfaces associated with an embedded retaining wall	105
Figure A.3: Outward hydrostatic and Westergaard hydrodynamic pressures	108
Figure B.1: Horizontal soil stress-displacement relationship applied in D-SHEET PILING	110
Figure B.2: Principle of linear elastic perfectly plastic model (left) and the associated Mohr-Coulomb yield surface (right), adapted from (Plaxis bv, 2014-3)	115
Figure B.3: Successive yield surfaces due to hardening limited by the Mohr-Coulomb ultimate failure state (left) and the associated yield cone including yield cap (right), adapted from (Plaxis bv, 2014-3)	116
Figure B.4: Small-strain stiffness reduction curve with lower cut-off (Plaxis bv, 2014-3).....	117
Figure B.5: Hysteretic behaviour in the HSsmall model (Brinkgreve et al., 2007)	117
Figure B.6: Example Rayleigh damping curve in PLAXIS 2D	119
Figure E.1: Seismic translation failure mechanism of anchored sheet pile quay wall with batter pile anchor - based on Kranz (1953) and Towhata & Islam (1987) limit equilibrium models	124

I.2. List of tables

Table 4.1: Summary of modelling structural elements, adapted from (Higuchi <i>et al.</i> , 2012).....	32
Table 4.2: Similitude of the centrifuge (30g), adapted from (Higuchi <i>et al.</i> , 2012)	32
Table 4.3: Reference case test results (field model values), from (Higuchi <i>et al.</i> , 2012).....	36
Table 5.1: VL Sheet piling properties relevant for D-SHEET PILING input.....	38
Table 5.2: Soil material properties relevant for D-SHEET PILING input	39
Table 5.3: Anchor properties relevant for D-SHEET PILING input	40
Table 5.4: Calibrated pseudo-static input parameters	44
Table 5.5: Obtained reduction factors on seismic loading resulting from calibrated pseudo-static calculations	45
Table 5.6: Critical seismic coefficients computed with the limit equilibrium model, derived for the reference case	51
Table 5.7: Soil column beneath PARI Sendai-G recorder	55
Table 5.8: Soil column at reference case	55
Table 5.9: Rigorous decoupled / coupled permanent-displacement analysis parameters.....	58
Table 5.10: Input parameters of the different CASE-300 and CASE-600 earthquake signals for the empirical Newmark rigid-sliding-block analyses.....	59
Table 5.11: Target displacements and corresponding acceptance ranges	59

Table 5.12: SLAMMER rigorous permanent-displacement analysis results	60
Table 5.13: SLAMMER empirical permanent-displacement analysis results	60
Table 5.14: HSsmall model input parameters based on RD, derived from (Brinkgreve <i>et al.</i> , 2010)	63
Table 5.15: 2D Plate (sheet pile) input parameters	64
Table 5.16: 2D Plate (batter H-pile) input parameters	64
Table 5.17: Node-to-node anchor (tie rod) input parameters	64
Table 5.18: PLAXIS 2D static calibration results	66
Table 5.19: Critical accelerations obtained with the limit-equilibrium and the PLAXIS 2D model	69
Table 5.20: Rayleigh damping properties	70
Table 5.21: Accelerograms applied in PLAXIS 2D dynamic calculations.....	74
Table 5.22: PLAXIS 2D dynamic calculation results for CASE-100 (artificial motion), compared to reference case results.....	75
Table 5.23: PLAXIS 2D dynamic calculation results for CASE-200 (multiple motions), compared to reference case results.....	76
Table 5.24: PLAXIS 2D dynamic calculation results for CASE-300 (multiple motions), compared to reference case results.....	77
Table 5.25: PLAXIS 2D dynamic calculation results for CASE-600 (multiple motions), compared to reference case results.....	78
Table 5.26: PLAXIS 2D dynamic calculation results: displacements at the centre of gravity of the schematized failure wedge (sliding mass) of the anchored sheet pile quay wall	81